University of Salford MANCHESTER

Risk of Radiation-Induced Cancer from Screening Mammography

Raed Mohammed Kadhim M. Ali

School of Health Sciences

UNIVERSITY OF SALFORD, SALFORD, UK

Submitted in Partial Fulfillment of the Requirements of the

Degree of Doctor of Philosophy, November 2016

(Medical Physics)

Table of Contents

List of Figures

List of Tables

List of Publications, Conference Presentations and Seminars	
Title	Note
A method for calculating effective lifetime risk of radiation-induced cancer from screening mammography; R M. Ali, A England, M.F McEntee, P Hogg. Radiography. 2015;21(4):298-303.	Journal article
Lifetime risk of radiation-induced cancer from screening Mammography; R M.Ali, A England, P Hogg; presented in the European Congress of Radiology; Vienna 2015	E-Poster
Lifetime risk of radiation-induced cancer from screening mammography; R M.Ali, A England, P Hogg; presented in the United Kingdom Radiological Congress; Liverpool 2015.	Poster
Radiation risk from screening mammography; R M.Ali, A England, A Tootell, P Hogg; presented in the European Congress of Radiology; Vienna 2016.	Conference paper
Radiation risk from screening mammography; R M.Ali, A England, A Tootell, C Mercer, P Hogg; presented in the United Kingdom Radiological Congress; Liverpool 2016	Poster
Mathematical modelling of radiation-induced cancer from screening mammography; R M.Ali, A England, A Tootell, C Mercer, P Hogg; presented in the European Congress of Radiology; Vienna 2017.	Conference paper
The effect of Mean Glandular Dose variations on effective risk from Full Field Digital Mammography in screening; R M.Ali, A England, A Tootell, C Mercer, P Hogg; presented in the European Congress of Radiology; Vienna 2017.	Conference paper
Methods for direct measurement of radiation dose: TLD and MOSFET. In P Hogg, R H Thompson, C Buissink (Eds.), *OPTIMAX 2016*; R M.Ali, M Alrowily, M Benhalim, A Tootell; 2017.	Book chapter
Radiation risk from screening mammography; R M.Ali, A England, P Hogg; School of Health Sciences Research Seminar Series - Mammography on 08-12-2014	Research seminar
Effective lifetime risk from screening mammography; R M.Ali, A England, A Tootell, C Mercer, P Hogg; School of Health Sciences Research Seminar Series – Controversial issues in breast cancer diagnosis using FFDM on 10-02-2016.	Research seminar
How to make TLD X-radiation dose measurements in phantoms; R M.Ali; School of Health Sciences Research Seminar Series – Direct X-radiation dose measurements in human phantoms on 01-04-2016.	Research seminar

How to calculate organ dose and effective dose from TLD/MOSFET data; R M.Ali; School of Health Sciences Research Seminar Series – Direct X-radiation dose measurements in human phantoms on 01-04-2016.	Research seminar
How to calculate lifetime effective risk/ attributable risk from TLD/MOSFET data; R M.Ali; School of Health Sciences Research Seminar Series – Direct X-radiation dose measurements in human phantoms on 01-04-2016.	Research seminar
FFDM breast cancer screening and effective risk / lifetime attributable risk; R M.Ali; School of Health Sciences Research Seminar Series – Direct X-radiation dose measurements in human phantoms on 01-04-2016.	Research seminar

List of Training Sessions

Session name	Date
Introduction to Endnote x7	30-01-2014
PGR induction program	03-02-2014
Completing a learning agreement and PhD progression points	06-02-2014
Doing literature review	19-02-2014
Critical thinking and critical writing at doctoral level	19-03-2014
Electronic resources for researcher	26-03-2014
Wordscop workshop	10-04-2014 to 12-06-2014 weekly session
Introduction to SPSS with Statistics - Day 1	16-04-2014
Introduction to SPSS with Statistics - Day 2	17-04-2014
Structuring your research	30-04-2014
Guide to getting published	14-05-2014
Research data management	07-10-2015
Quantitative research method (3days session)	13 to 15-01-2016
Advanced SPSS session	18-01-2016
Planning and writing a thesis	17-03-2016
Open access publication	04-05-2016

Acknowledgements

My PhD journey would not been possible without the support, assistance and co-operation of many people. During my journey I met many people who helped me a lot and I would like to take this opportunity to thank them.

To begin with, I would like to express my profound gratitude to my main supervisors, Professor Peter Hogg and Dr. Andrew England, and to my other supervisory team members Dr. Claire Mercer and Mr. Andrew Tootell. All of them have been an inspiration to me and they have motivated throughout my journey. Without their advice, feedback, support and guidance, this thesis would not be what it is. I should also like to offer a particular thank you for Professor Peter Hogg and Dr. Andrew England for their help with data collection. I would like also to thank Dr. John Thompson for his kind help with data collection. I am grateful to Mrs. Katy Szczepura for her valuable advice and for sharing her expertise. I would also like to offer a special thank you to all the mammography practitioners who gave up their time to help with data collection.

I also offer great thanks to my father for his persistent support and encouragement. My deepest gratitude goes to my beloved wife for her unfailing support and endless patience throughout my long journey. Many thanks also go to my brother in law and close friend Dr. Hussien Mraity for his continuous support and endless help. Also, I would like to say thank you to my children, siblings, friends and colleagues for their encouragement during this challenging time.

Finally, I would like to express my upmost gratitude to the Higher Committee for Education Development in Iraq for their financial support and to Kufa University who gave me study leave.

Terminology

Term	Definition
Practitioner	Refers to radiographer or radiologic technologist working in mammography (mammographer).
Dose	Radiation dose.
mAs	Tube current (milliamperes) multiplied by exposure time (seconds).
High risk women	Refers to a group of women who have high risk to develop breast cancer.
Average risk women	Refers to the women with average risk of breast cancer development.

List of Abbreviations

Acronym	Definition
AAFP	American Academy of Family Physicians
ACA	American Cancer Association
ACOG	The American Congress of Obstetricians and Gynaecologists
ACR	American College of Radiology
ACS	American Cancer Society
Ag	Silver
Al	Aluminium
BCT	Breast Computed Tomography
BI-RADS	Breast Imaging-Reporting and Data System
BM	Bone Marrow
CC	Cranio-caudal projection
cm	centi-metre
CR	Computed Radiography
C-spine	Cervical spine
CV	Coefficient of Variance
DBT	Digital Breast Tomosynthesis
DM	Digital Mammography
DR	Digital Radiography
ESD	Entrance Skin Dose
FDA	Food and Drug Administration
FFDM	Full Field Digital Mammography
FSM	Film-Screen Mammography
HVL	Half-value Layer
IAEA	International Atomic Energy Agency
ICC	Intra-Class Correlation
ICRP	International Agency for Research on Cancer
ICSN	International Cancer Screening Network
IPEM	Institute of Physics and Engineering in Medicine

kV	kilo-Voltage
LAR	Lifetime Attributable Risk
mA	milliampere
MGD	Mean Glandular Dose
mGy	milli-Gray
MLO	Medio-lateral Oblique projection
mm	milli-metre
Mo	Molybdenum
MOSFET	Metal Oxide Semiconductor Field Effect Transistors
MRI	Magnetic Resonance Imaging
mSv	milli-Sievert
nC	nano - Coulomb
NCCN	National Cancer Comprehensive Network
NCI	National Cancer Institute
NHSBSP	National Health Service Breast Screening Programme
PE	Polyethylene
PMMA	Poly(Methyl Methacrylate)
Rh	Rhodium
T/L spine	Thoracic-Lumbar spine
TLD(s)	Thermo-Luminescence Dosimeter (s)
UK	United Kingdom
UNSCEAR	United Nations Scientific Committee on the Effects of Atomic Radiation
US	United States
USPSTF	United States Preventive Services Task Force
W	Tungsten

Abstract

Background and Objectives: When the benefits and risks of mammography are considered, the risk of radiation-induced cancer is calculated only for the breast using the mean glandular dose (MGD). Whilst MGD is a useful concept, it has many limitations. This thesis aims to establish a novel method to determine and convey radiation risk from full field digital mammography (FFDM) screening using lifetime effective risk.

Method: For effective risk calculations, organ doses as well as examined breast MGD are required. Screening mammography was simulated by exposing a breast phantom for cranio-caudal and medio-lateral oblique for each breast using 16 FFDM machines. An anthropomorphic dosimetry phantom loaded with thermo-luminescent detectors (TLDs) was positioned in contact with the breast phantom to simulate the client's body. Once the risk per individual was calculated, total effective lifetime risk across 48 worldwide screening programmes was calculated. The total effective risk data sets were analysed to establish a regression model to predict the effective risk of any screening programme. Graphs were generated to extrapolate the total effective risk of any screening programme of specific screening commencement age and frequency considering the MGD differences of different FFDM machines. Since the highest radiation dose after examined breast was received by contralateral breast, the effect of a contralateral breast lead shield on effective risk was also investigated.

Results: Large differences in the effective lifetime risk exist between worldwide screening programmes. The effective lifetime risk varied from approximately 50 cases/10^6 to more than 1000 cases/10^6. These differences were mainly attributed to the commencement age and frequency of screening. Since tissue radio-sensitivity reduces with age, the cessation age of screening mammography does not result in a noteworthy effect on the total effective risk. The use of contralateral breast shield reduces the total effective risk by about 1.5% for most worldwide screening programmes.

Conclusion: A novel method has been proposed to assess radiation-induced cancer risk from FFDM screening which considers the radiation dose received by all body tissues in addition to the examined breast. Using effective risk, the data is more likely to be understandable by screening clients and referring clinicians, unlike MGD which is not readily available or understandable by the general populace. This novel method and the data are compatible with the incoming European Commission legislation about giving the patient information on radiation risk.

Chapter One
Introduction and Thesis Outline

1.1 Introduction

Diagnostic procedures that use X-radiation are one of the most common and useful tools in medicine. It is used in hospitals and clinics to non-invasively diagnose, stage and monitor progression of disease within the body (Brady, 2012). However, medical X-rays are the largest source of man-made ionising radiation to which humans are exposed in many developed countries (European Commission, 2008). The link between patient radiation dose in X-ray examinations and cancer incidence, makes dosimetry an area of great importance in diagnostic radiology (Meghzifene, Dance, McLean, & Kramer, 2010). This is particularly true for screening practices because healthy individuals are exposed to potentially harmful ionising radiation (Sechopoulos, Bliznakova, Qin, Fei, & Feng, 2012).

Mammography is the most important screening test for the investigation of breast cancer in asymptomatic women; it is used to detect breast cancer in its early stages (Aznar et al., 2005). Mean glandular dose (MGD) is the recommended dosimetric quantity used to express the radiation risk in screening mammography (European Commission, 2013; IAEA, 2011). However, some limitations have been identified with the use of this measurement. First, MGD only includes the radiation dose of the examined breast, ignoring the radiation dose received by body tissues due to scattered radiation. Second, the individual's age, which affects tissue's radio-sensitivity, is not considered in MGD calculations. Third, MGD generated data (mGy), is highly technical, and cannot be easily understood by the general public (screening clients). Therefore in this thesis a new dosimetric method for radiation risk assessment from screening mammography has been established - effective risk. Effective risk is a measure of radiation-induced cancer from screening mammography.

1.2 Rationale, Aim and Objectives

New European Commission legislation outlines the patient's right to have information about the risk of X-radiation associated with radiological examinations. This is particularly important for screening practices in which healthy individuals are examined. Mammography

is one of the most common screening procedures using X-ray. Many countries have a national organised screening mammography programme with different recommendations. The radiation risk from screening mammography is an essential point to screening justification. Presently no method exists to give risk estimates from screening mammography; equally no data which could be easily understood by patients exist. Therefore, this thesis aims to propose a novel method to assess and convey the risk of radiation-induced cancer from screening mammography.

The Objectives:

- Determine a novel method to assess radiation risk from screening mammography.
- Use the method to estimate the radiation risk (cancers induced per million people screened) for different screening scenarios.
- Use the method to compare radiation risk for different countries' screening programmes.
- Use the method to determine whether a contralateral breast secondary radiation shield has value in reducing the radiation risk.

1.3 Thesis Structure

This thesis comprises of eight chapters, which are summarised in **Figure (1-1)**, as follows:

Chapter 1: "Introduction and Thesis Outline" - Includes a brief introduction, thesis rationale, aim and objectives and a description of the thesis layout.

Chpater 2: "Breast Anatomy, Cancer and Imaging Modalities" - In this chapter background information about the female breast is addressed. This information helps to understand the effect of normal breast anatomy variations, particularly the breast density and size, on breast radiation dosimetry. Within this chapter the information will be presented in five main sections: Firstly, a breast anatomy section, comprising of the macroscopic and microscopic anatomical characteristics of the female breast. Secondly, the breast density definition, importance, and different scales used for breast density classifications will be explained. Thirdly, breast cancer and breast cancer risk factors will be presented. Fourthly, different breast imaging modalities used to investigate and diagnose breast cancer will be examined. Fifthly, the breast cancer screening modalities will be displayed.

Chapter 3: "Mammography: Development, Physics and Clinical Aspects" - This chapter commences with information about the origin and most prominent historical development points in mammography. The mammography dosimetric aspects during those periods are also explained. Next the physical aspects of digital mammography are explained. The physics and instrumentation of FFDM and DBT will then be reported. Following this, the anatomical characteristics of breast tissue in standard mammograms (CC and MLO projections images) and in supplementary projections will be presented. Finally, the last section of this chapter will be focused on screening mammography justification with regard to its advantages (breast cancer mortality reduction) and disadvantages (radiation risk, over diagnosis, false negative and false positive).

Chapter 4: "Mammography Dosimetry" - This chapter commences with an explanation of the risk of low radiation doses likely to be received from screening mammography. Following this, a comprehensive literature review of mammography dosimetry will be included. In this context the studies investigating the radiation dose to breast tissue and other body tissue from mammography will be considered. The mammography dosimetric methods including dose modelling by Monte Carlo and dose measurement instruments will be considered. In the last section of this chapter, breast tissue equivalent materials will be reviewed as mammographic dosimetry tools.

Chapter 5: "Materials and Methods" - This chapter commences with the methodology used for organ dose measurement, this includes a detailed explanation of the organ dose measurement process using the TLDs and the examined breast MGD calculation. Next, the method of how the generated organ dose data can be used for the calculation of effective risk and total effective risk of 48 worldwide screening programmes will be described. However some of the programmes have same recommendations resulting in 22 different programmes. Following this, the three methods of total effective risk modelling will be considered. Finally the design and use of a contralateral breast lead shield will be explained comprehensively in the last section of the chapter.

Chapter 6: "Results" - This chapter commences with an outline of the data amassed using the method. The data is organised into four sections: The first contains data of the measured organ radiation dose from complete screening exposures for 16 FFDM machines. The second shows the total effective risk of the 48 worldwide screening programmes. The third shows

the total effective risk modelling data and graphs. The fourth shows the organ radiation dose data and total effective risk of the 48 worldwide screening programmes for four FFDM machines with the use of the contralateral breast shield.

Chapter 7: "Discussion" - The data presented in the sixth chapter (results chapter) is discussed and links between the existing body of evidence are made. This chapter is set out in the same manner as the results chapter, where the data from each section is discussed separately. The final component of this chapter considers the limitations of the work presented in this thesis and what might be undertaken to address these limitations in future work.

Chapter 8: "Conclusions" - This chapter summarises the findings of the thesis in a concise manner.

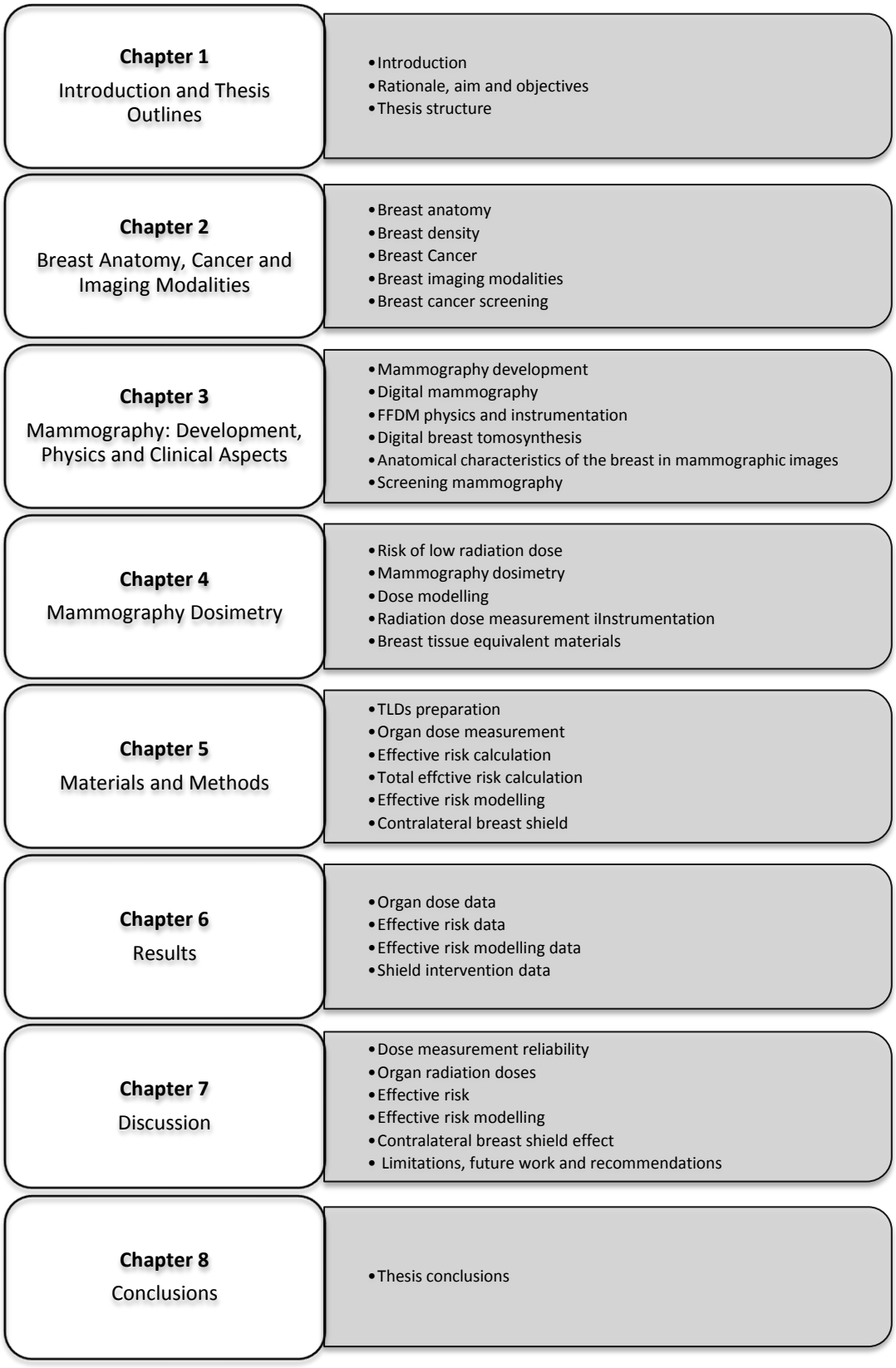

Figure (1-1) A flowchart illustrating the outline of this PhD thesis.

Chapter Two

Breast Anatomy, Cancer and Imaging Modalities

2.1 Chapter Overview

This chapter comprises of background information about normal breast anatomy and breast cancer. Since the breast density is the second most important breast cancer risk factor, breast density and breast classification methods have been considered along with the other risk factors. The physical principle of breast imaging modalities, including mammography, breast computed tomography (CT), breast ultrasound and magnetic resonance imaging (MRI), have been reviewed in later sections. The last section of this chapter focuses on the breast cancer screening techniques and the feasibility of each one in reference to breast cancer mortality reduction and their cost-effectiveness. These techniques are breast self-examination and why it is recommended to be replaced by breast self-awareness, clinical breast examination, mammography, breast ultrasound and breast MRI.

2.2 Breast Anatomy

The mature female breast is ‘tear drop’ shaped and is located on the anterior chest wall (Darlington, 2015). The base of the breast extends from the level of the second to the sixth ribs longitudinally, and between the boundary of the sternum and the mid-axillary line transversely, **Figure (2-1)**. The majority of breast tissue is usually located in its upper lateral quadrant (Ellis, 2004; Pandya & Moore, 2011). The internal structure of the breast is similar for all females. However, its size and shape differs in relation to many factors: race, diet, age, status of female parity and menopausal status (Standring & Gray, 2008).

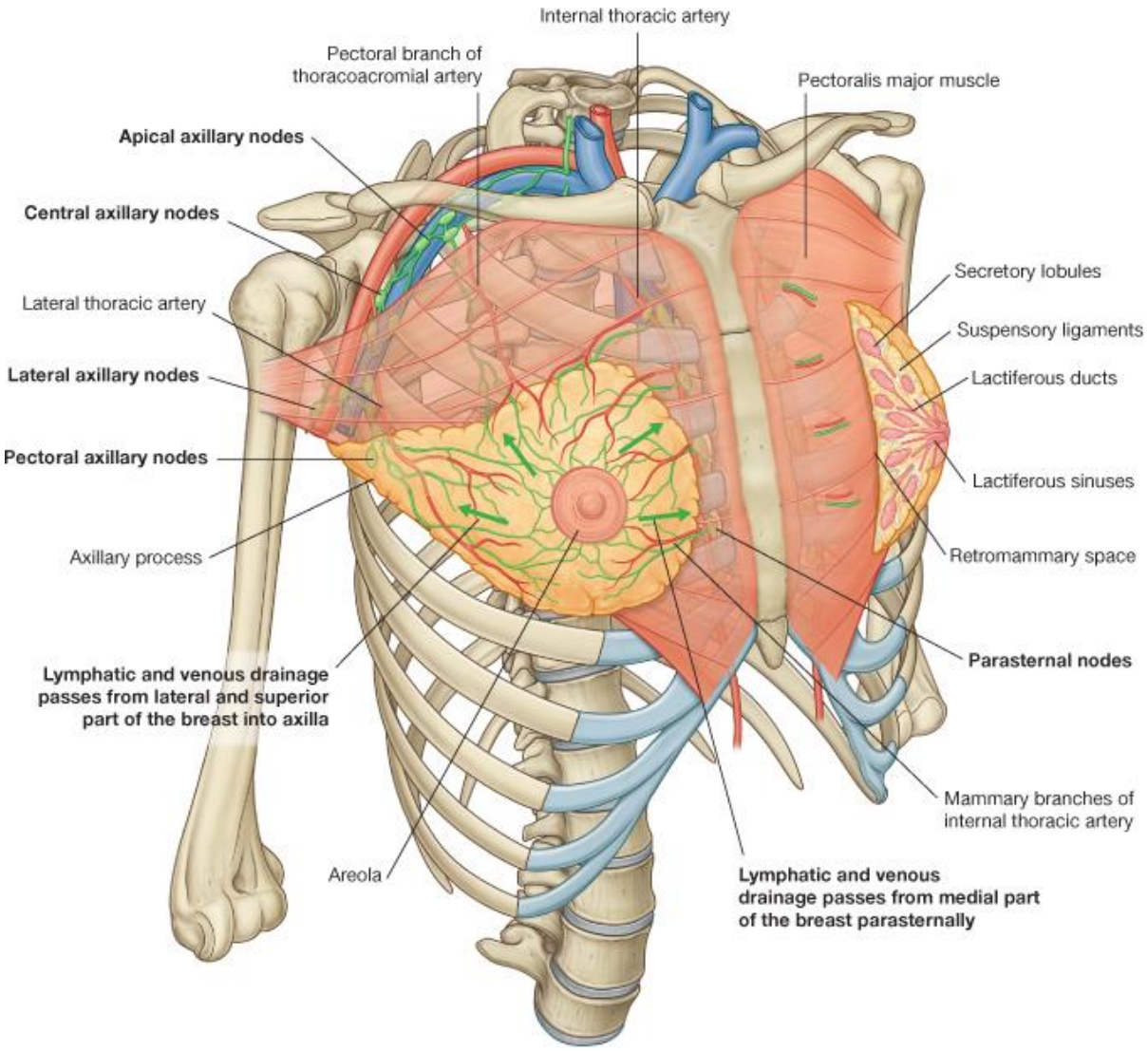

Figure (2-1) Shows the breast relations (Drake, Vogl, & Mitchell, 2015).

The female breast is fundamentally composed of fat, connective tissue and glandular tissue; the latter being the functional part of the breast tissue. Glandular tissue is a type of highly modified and specialised sweat gland (Brandt, Karemore, Karssemeijer, & Nielsen, 2011; Pandya & Moore, 2011). It changes with age as a response to body hormones (Allen, 2012). Early in childhood, the adipose tissue constitutes the majority of breast tissue. However, the glandular tissue begins to develop at puberty and continues until maturity when it progressively changes to adipose tissue (Dance, Skinner, & Carlsson, 1999). The glandular tissue in each breast is divided into 15-20 lobes, each with tree shape tubular structures branching out from the nipple. Each lobe includes 10-100 lobules which have a number of

acini, where the milk and hormones are produced (Darlington, 2015; Diffey, 2012). The functional unit of the breast is known as the terminal ductal lobular unit (TDLU) which is made up an acini, an intralobular terminal duct and an extralobular duct, **Figure (2-2)**. Both the acini and the ducts are formed of a one cell thick epithelial layer surrounded by myoepithelial layer and basement membrane (Darlington, 2015). The fraction of glandular tissue in the breast is known as breast density (Vachon et al., 2007).

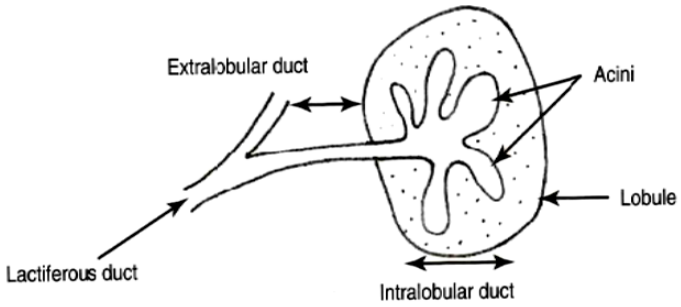

Figure (2-2) Illustrates the Terminal Ductal Lobular Unit (TDLU) (Darlington, 2015).

Connective and fat tissues can be considered as supportive tissues in the breast. Two different types of connective tissues can be identified within the breast: Interlobular connective tissue holds the breast tissue together and is spread between the lobules; Intralobular connective tissue is a specialised type of connective tissue found around the terminal ductal lobular unit. Breast fat tissue is present between the mammary glands (Kopans 2007). Externally the whole breast is covered by 0.5–2.0 mm of skin except the area directly surrounding the nipple where the skin becomes thicker, as it contains sweat glands, sebaceous glands and hair follicles, to form the areola. Just beneath the skin there is a 2–2.5 cm thick layer of subcutaneous fat covering the breast. At the breast level, the superficial layer of fascia divides into two layers. The superficial layer surrounds the breast under the subcutaneous fat and the deep layer surrounds the posterior aspect of the breast lying on the fascia of the pectoralis major muscle. Between these two layers of fascia a retro-mammary space is formed which is filled by fat tissue (Darlington, 2015).

The determination of breast size or volume can be achieved by physical procedures, either by molding the breast in plastic or by submerging the breast in water and determining its volume by measuring the volume of displaced water according to Archimedes' principle. Accurate

determination of breast volume is not easy and can be carried out by digital methods (Veitch, Burford, Dench, Dean, & Griffin, 2012). Alonzo-Proulx, Jong, and Yaffe (2012) used digital mammography to study some breast characteristics, such as the breast volume, for 55087 digital mammograms from 15351 Canadian women. They found that the mean breast volume for all studied women was 687cm^3 with slight differences in different age groups. For example, it was 703cm^3 and 736cm^3 for 50-55 year and 55-65 year age groups. These variations are due to the change of female breast volume with age. A greater mean breast volume around 820cm^3 has been found for British women by Diffey (2012). Wang et al. (2013) utilised ultrasound system to measure female breast volume and stated that the breast volume for around 57% of 306 adult Chinese females was between 400-800 cm^3.

2.3 Breast Density

Breast density is a measure of breast composition. It reflects the percentage of glandular tissue in the breast. Since it is basically assessed by mammography, it is expressed as mammographic density (Boyd, Martin, Yaffe, & Minkin, 2011). Mammographic density was first described in 1976 by Wolf as an independent risk factor for breast cancer (Ding & Molloi, 2012). Generally, younger women have denser breast than older women, and after the age of 40 the mammographic density progressively reduces with age due to hormonal changes (ACS, 2015b). However, Chelliah, Voon, and Ahamad (2013) reported that this process is slower in Chinese women compared to Malay and Indian women. They also reported that there is an inverse relationship between the mammographic density and body mass index (BMI) for the studied population (Chelliah et al., 2013). Breast density is either estimated qualitatively by a clinician or quantitatively by computer-assisted methods (Tagliafico et al., 2013). The film-screen mammographic images were formally digitised for computer-assisted breast density measurements. Presently, two dimensional or three dimensional breast images from different imaging modalities (FFDM, DBT, CT, MRI and US) are utilised (Alonzo-Proulx et al., 2012; Ekpo & McEntee, 2014; Salvatore et al., 2014; Tagliafico et al., 2013).

Sometimes the mammographic density is measured by two-dimensional means and expressed as the ratio of the area of dense glandular tissue to that of the whole breast (Stone, Ding, Warren, Duffy, & Hopper, 2010). In the general population, 26% - 32% of women

have high breast density which is 50% or greater (Vachon et al., 2007). A more logical method for breast density estimation can be utilised and is based on volume, here the breast density is expressed as volumetric breast density (VBD) (Alonzo-Proulx et al., 2010). According to Alonzo-Proulx et al. (2012), the mean value of VBD for 15351 women was 30.5%. Alonzo-Proulx et al. also demonstrated that VBD reduces by 2% per year on average as the age increases from 35 to 75 years. On average, the breasts of Asian women are thinner and denser than those of European and North American women, and in European women they are thinner and less dense than in North American women (Geeraert, Klausz, Muller, Bloch, & Bosmans, 2012).

Different methods have been used to classified female breasts according to their densities:

2.3.1 Wolf Classification

Wolf semi-quantitatively classified the female breast density into four categories: N1, mostly fatty breast; P1, less than one-third of the ductal structures are prominent; P2, more than one-third of the ductal structures are prominent; DY, extensively dense breast (dysplasia) (Boyd et al., 2010).

2.3.2 Tabar Classification

A semi-quantitative five level classification system developed by Gram, Funkhouser, and Tabar (1997), who classified the breast density depending on a parenchymal pattern as follows:

Category I: the mammogram has scalloped contours with fatty lucent areas and 1-2 mm evenly distributed nodular densities.
Category II: the mammogram has entirely lucent fatty areas and 1-2 mm evenly distributed nodular densities.
Category III: the mammogram's retroareolar area ductal structures are prominent.
Category IV: the mammogram has large nodular and linear densities.
Category V: the mammogram is homogeneous with the ground glass shape pattern.

2.3.3 BI-RADS Classification

The American College of Radiology developed the Breast Imaging Reporting and Data System (BI-RADS) which places breasts into four density categories: fatty breast with less

than 25% density, scattered fibroglandular with 25%-50% density, heterogeneous with 51%-75% density, and dense breast with more than 75% density (D'Orsi et al., 2013). BI-RADS' classification is the most accepted breast density classification and is the most commonly used (Ekpo, Hogg, Highnam, & McEntee, 2015).

2.3.4 Boyd Classification

Boyd used six categories to express breast density depending on the clinician's assessment and computer assessed measurements. These categories are 0, < 10%, 10% to < 25%, 25% to < 50%, 50% to < 75% and 75-100% (Boyd, Jensen, Cooke, & Han, 1992).

2.3.5 Summary

The importance of breast density appears in three areas: first, it affects the sensitivity of mammography - the denser the breast the lower the sensitivity for cancer detection because small lesions can be obscured by dense glandular tissue (Ford, Marcus, & Lum, 1999; Helvie & Rosen, 2011); second, breast cancer risk assessment - many researchers studied the relationship between breast density and breast cancer incidence, and they indicated mammographic breast density as the second substantial risk factor for breast cancer after age (Kontos et al., 2011); third, estimation of breast radiation dose - the validity of breast dose estimation could be improved by accurate measurement of breast density because the breast composition is an essential factor in breast dosimetry (Alonzo-Proulx et al., 2010). Overall, dense breasts indubitably absorb more radiation dose than fatty breasts; dense breasts are also associated with a reduction in mammography cancer detection accuracy (ACOG, 2015).

2.4 Breast Cancer

2.4.1 Breast Cancer Types

Breast cancer is an uncontrolled change in growth of breast tissue which mostly results in lump formation. This lump is known as a breast tumor (NHSBSP, 2013a). Depending on the place where the cancer develops, breast cancers are classified into ductal carcinoma, constituting about 90% of breast cancers, and lobular carcinoma, constituting up to 10% of breast cancers (Peart, 2005). The majority of breast cancers are invasive or infiltrating cancers which are formed in breast lobules or ducts and invade the surrounding breast tissues (ACS, 2011a). Another type of breast cancer, known as in situ carcinoma, proliferates in

epithelial cells of the duct wall but does not invade the basement membrane (Wentz & Parsons, 1997).

2.4.2 Breast Cancer Risk Factors

An individual's probability of developing breast cancer is called the breast cancer risk, sometimes referred to as the breast cancer lifetime risk. It is controlled by a large number of factors, but unfortunately a full explanation for the mechanism of how these factors affect cells cannot be given as it is not known (Hackney, 2015). The importance of breast cancer risk factor assessment has increased progressively over time in screening recommendations and preventive strategies (Kontos et al., 2011).

2.4.2.1 Unchangeable Risk Factors (Gender and Age)

The main two unchangeable risk factors are gender and age. More than 99% of breast cancer cases are in females (Anderson, Jatoi, Tse, & Rosenberg, 2010; Kopans 2007). Under the age of twenty years, breast cancer is very rare and only about 0.3% of breast cancer cases occur in females within their third decade (Finkel, 2005). However, about half of the breast cancer cases occur between 50-69 years (Hackney, 2015).

2.4.2.2 Relationship of Cancer with Breast Density

Since the identification of mammographic density as a breast cancer risk factor by Dr. Wolf, who found a 22-fold increase in breast cancer risk for women with DY category breast compared to those with N1 category breast, it has become an area of great interest for many researchers (Shepherd et al., 2011). Studies have revealed that for women with high breast density, the cancer risk may be between 4-6 times more than for women with lower breast density (Brandt et al., 2011). In 2007, Boyd et al. (2007) introduced a breast cancer risk model based on data from 1112 women. This model quantified the relative breast cancer risk for each breast density category as in **Table (2-1)** (Kontos et al., 2011).

Table (2-1) Breast cancer relative risk of different breast densities according to Boyd's model.	
Breast density (%)	Breast cancer relative risk
Less than 10	1.2
10 to < 25	2.2
25 to < 50	2.4
50 to < 75	3.4
75-100	5.3

More recently, in 2015, ACOG (2015) published their report number 625 in which they tabulated the relative risk of breast cancer for BI-RADS categories 3 and 4 as 1.2 and 2.1, respectively. Overall, they concluded that a dense breast is more liable to develop breast cancer than a fatty breast.

2.4.2.3 Genetic Factors

About 10-15% of the women with breast cancer have a breast cancer family history (Vetto, Luoh, & Naik, 2009). Women with one first degree relative (sister, mother, daughter) diagnosed with breast cancer have a 1.8 times more risk of developing breast cancer risk than those with no family history of it. This breast cancer risk is increased to 3 and 4 times as the number of first degree relatives, diagnosed with breast cancer, increases to 2 and 3 women (ACS, 2013a).

Moreover, it has been found that between 5-10% of breast cancer cases are due to mutations, which occur in less than 1% of general population, in the inherited breast cancer susceptibility genes BRCA1 and BRCA2. These inherited genes increase breast cancer risk 10 fold. Other rare inherited genes, such as Tumour Protein 53 (TP53), also contribute to increased breast cancer risk (ACS, 2013a; Hackney, 2015).

2.4.2.4 Other Factors

Other factors include personal history of breast cancer. Women with previous history of breast cancer are at 3-5 times more risk of developing an additional breast cancer than others. Socio-economic status is also an important factor; recent studies have reported that about 53% of breast cancer cases occur in developed countries. The use of hormonal therapy leads to an increased breast cancer incidence. Finally lifestyle factors, including a lack of physical

activity, smoking, incorrect diet, and alcohol consumption also raise the risk of developing breast cancer (ACS, 2015c; Kopans, 2007).

2.4.3 Breast Cancer Statistics

Breast cancer is a major public health problem and is the fifth most common cause of cancer deaths worldwide (Ferlay et al., 2013). It is reported to be the most frequently detected cancer among women in many countries. In 2012, breast cancer constituted 25% of new cancer cases in women when about 1.7 million new breast cancer cases were recorded worldwide (ACS, 2015c). Breast cancer morbidity differs significantly between regions: it is at least two to three times more common in America and Western Europe than in East Asian nations, where the latter show lower rates than African nations (UNSCEAR, 2008). The figures of breast cancer incidence range from 270 per million in Middle Africa and Eastern Asia to 920 per million in Northern America (Ferlay et al., 2013). In the US, breast cancer incidence showed a noticeable reduction (~7%) between 2002 and 2003. This reduction may be due to a reduction of menopausal hormone therapies (ACS, 2011b). In the UK, however, the smaller number of pregnancies, utilisation of hormones as contraceptives and obesity have attributed to an increase in breast cancer incidence between 1975 and 2003 (HPA, 2011).

With regard to breast cancer mortality, its rates have steadily decreased in developed countries. For instance, in England it has reduced by 37% between 1971 and 2011 (ONS, 2012). In the same way, a 5.2% per year reduction can be seen in the US between 1990 and 2011 (ACS, 2011b). These reductions in mortality rates are primarily due to prevention of breast cancer (cancer incidence reduction), early detection of breast cancer by screening, and the improvement of cancer treatment methods (ACS, 2011b; Säbel & Aichinger, 1996). In spite of this decline in breast cancer mortality in developed countries, breast cancer still has the second highest cancer mortality rate, after lung cancer (ACS, 2015c; Dellie, Rao, Admassie, & Meshesha, 2013; ONS, 2012). However, in developing countries the leading cause of cancer death was the breast cancer - about 44% of breast cancer deaths in the world occurred in Asian countries and 12%, 8% in African and Latin American countries (ACS, 2015c).

2.5 Breast Imaging Modalities

2.5.1 Mammography

The production of low contrast, fine detail, two-dimensional breast images using X-ray is known as mammography (Law, 2006). Unlike screening mammograms, which are undertaken on healthy asymptomatic women, diagnostic mammograms are utilised to investigate breast tissue abnormalities in women with either breast symptoms or abnormal findings resulting from a screening mammogram (ACS, 2015a). To date, there are two technologies for mammography - conventional film-screen mammography or digital mammography, which has progressively replaced film-screen techniques (Schueller et al., 2008). The main advantages of digital mammography over film-screen are that it is more sensitive in cancer detection within dense breasts and has a lower associated radiation dose (Pagliari et al., 2012). However, some film-screen systems can produce images with spatial resolution three times better than those of digital detectors (Obenauer, Hermann, & Grabbe, 2003). Overall, studies such as the Digital Mammographic Imaging Screening Trial (DMIST) have illustrated that for a screening population (50-69 years old) both film-screen and digital mammography are equal in diagnostic accuracy. Nevertheless, the use of digital mammography improves diagnostic accuracy for younger population with dense heterogeneous breast (Pagliari et al., 2012; Pisano et al., 2005; Thierens et al., 2009).

Despite the reported superiority of digital mammography in breast cancer detection, it has been found that 20% - 30% of breast cancers cannot be detected by two-dimensional mammograms due to the superimposition of dense breast tissue with cancers (Rafferty et al., 2013). To overcome the mammographic ‘anatomical noise’, Digital Breast Tomosynthesis (DBT) is used to produce three-dimensional images by reconstructing low dose, two-dimensional, thin slice images of breast volume (Svahn et al., 2012). This is achieved, as in conventional tomography, by the movement of the X-ray tube across an arc or linearly above the breast in order to expose the breast at different small angles (Williams, Judy, Gunn, & Majewski, 2010). Consequently, each plane of the breast can be clearly seen with less tissue overlap, thereby improving the lesion detectability (Young, 2006).

2.5.2 Breast Computed Tomography (BCT)

Compared to DBT, dedicated BCT allows the acquisition of high resolution volumetric breast image data (Sechopoulos, Bliznakova, Qin, Fei, & Feng, 2012). Accordingly, BCT can overcome the problem of tissue overlap resulting in accurate detection of breast cancers whilst at the same time obtaining more detailed information about the shape, location, and size of any lesion (Shen et al., 2014). Dedicated BCT consists of a gantry, which encloses the X-ray tube and detector assembly, that rotates around the breast during imaging. To avoid unnecessary radiation to the woman's chest, the breast is protruded downward through an opening in the patients' table while the woman is lying in prone position; see **Figure (2-3)** (Shaw & Whitman, 2013). Breast compression is not required during BCT making the technique more comfortable than the conventional mammographic procedure (Shen et al., 2014). The potential cost of BCT comes from the complex processes associated with data acquisition, analysis, visualisation, and interpretation (Russo, Coppola, Mettivier, Montesi, & Lauria, 2009). Although the reduced dose in dedicated BCT when compared to conventional chest CT, dedicated BCT exposes breast tissue to a higher radiation dose than mammography (Sechopoulos et al., 2012).

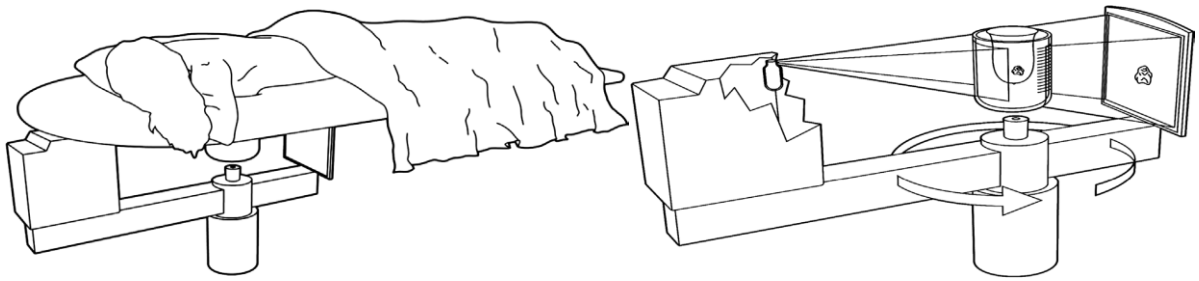

(a) **(b)**

Figure (2-3) Shows a diagram for dedicated breast CT **(a)** Woman positioning and **(b)** Gantry design with examined breast (Shaw & Whitman, 2013).

2.5.3 Breast Ultrasound

Breast ultrasound is one of the most common tools used for breast cancer detection. Since ultrasonography has lower specificity for breast cancer detection than mammography, it is primarily used as a diagnostic tool within a triple assessment process (Jan, Mattoo, Salroo, & Ahangar, 2010; Silverstein et al., 2009). The lower cost of ultrasound compared to

mammography is the main advantage of breast ultrasonography over mammography. Also, more detailed information about lesion size, boundary and blood circulation can be obtained by ultrasound (Wang et al., 2013). However, the high false-positive rate and the time required for ultrasonic examinations make breast ultrasonography unlikely to be a cost-effective screening technique. Therefore, it is used as a supplementary screening tool for intermediate cancer risk women and for those with dense breasts (Kopans, 2007).

Breast ultrasound depends on the production of longitudinal mechanical waves with frequencies higher than the audible range (20 - 20000 Hz). For medical imaging 1 - 15 MHz frequencies are used. In general, higher frequencies result in better resolution within the ultrasonic image so that more than 10 MHz frequency is often required for mammography. The scan head of an ultrasound system contains a number of piezoelectric crystals (transducers) which emit the ultrasound wave; they then receive the reflected back waves from the tissue. The reflected portion is used to determine the [acoustic] properties of the tissue. Then, the reflected ultrasonic waves are recorded over time to produce a two-dimensional image called a B-mode image. Colour and power Doppler techniques are additional tools of diagnostic ultrasound. Both of them are of great importance in breast cancer detection because they give information about a lesion's vascularity. The principle of work for both is similar and depends on ultrasound frequency shift due to blood motion. Colour Doppler ultrasound gives information about the speed and direction of motion. Power Doppler ultrasound is more flow sensitive than colour Doppler but it does not give information about flow direction (Kopans, 2007; Whitman, Khisty, & Stafford, 2013).

2.5.4 Breast Magnetic Resonance Imaging (MRI)

Clinical MRI utilises a strong magnetic field to polarize the magnetic moment of water molecule protons in the body. Next, an oscillating magnetic field, within the radiofrequency range, is applied to rotate the magnetisation vector into a transverse plane to the magnetic field. This oscillating magnetisation is measured by a radiofrequency coil which gives the primary MRI signal (Lane, Stafford, & Whitman, 2013). The MRI signal produces high contrast cross-sectional images of breast tissue (Saslow et al., 2007). Similar to breast CT, in MRI procedures women should lie prone with their breast protruding in a specially designed platform. No breast compression is required. However, the MRI scan time is long, often up to

an hour, as in most cases contrast enhancement is required (ACS, 2015a). Breast MRI is widely used for screening high risk women and for pre/post-operative evaluation of breast cancers (Lane et al., 2013).

2.6 Breast Cancer Screening

Screening is an examination or test used to investigate the presence of a certain disease, such as cancer, in a group of healthy asymptomatic people (ACS, 2014). It may also be used to determine the people at high risk of a disease before they have it (Gøtzsche, Hartling, Nielsen, & Brodersen, 2012). The performance of any screening test is assessed by a study known as a screening trial which investigates whether the screening practice achieves its aims or not. The main purpose of screening is to reduce disease mortality in a screened population compared to that in an unscreened population (control group). This can be achieved by the early detection of the disease when recovery is still possible (Boyle, 2003). The biological onset of some diseases may precede its symptoms by months or even years. Breast cancer is considered one of these progressively developed diseases. It is believed that breast cancer starts with one malignant cell which proliferates to form the tumour (Finkel, 2005). Symptomatic breast cancer is usually large and already metastatic. However, breast cancers detected by screening are mostly small and restricted within the breast (ACS, 2014). Accordingly, the early detection of breast cancer is undoubtedly useful (Baines, 2011; Gilbert et al., 2015). For the early detection of breast cancer many screening tests are used such as breast self-examination (BSE), clinical breast examination (CBE), mammography, MRI and breast ultrasound.

2.6.1 Breast Self-Examination (BSE)

Breast self-examination was first recommended in the 1930s as a breast cancer screening method (Ford et al., 1999). The Finnish study, based on Mama programme data, was the only study that reported breast cancer mortality reduction due to breast self-examination (Ford et al., 1999; Gastrin et al., 1994). However, all other randomised trials which have investigated breast cancer mortality reduction by breast self-examination concluded that there was no noteworthy reduction in breast cancer mortality. It may even increase the false-positive rate (Tirona, 2013). Therefore, most health organisations recommend against BSE, except the American Cancer Society (ACS) which recommended it optionally for women older than 20

years (Nelson et al., 2016). Some organisations recommend breast self-awareness (BSA) instead of BSE (Tirona, 2013). The aim of BSA is to teach the women, older than 20 years, about the normal look of their breast and encourage them to report any suspicious changes in their breast to health professionals as quickly as possible (ACS, 2014).

2.6.2 Clinical Breast Examination (CBE)

Clinical breast examination is usually done by experienced health professionals (ACS, 2014). In screening trials it has been found that CBE helps to reduce breast cancer mortality (Smith et al., 2003). The sensitivity of CBE for cancer detection is 54%, while its specificity is 94% (Tirona, 2013). CBE is recommended once every three years for women ages 20-40 who have an average risk of developing breast cancer, and annually for women older than 40 years (ACS, 2013a). The clinical performance of CBE can also be evidenced by screening trial which took place in rural area of Sudan wherein 10309 women were screened by trained volunteers. This study reported that 12 women became disease-free after treatment. Accordingly, they concluded that CBE is a useful screening tool in low-income communities where other screening modalities are unavailable (Abuidris et al., 2013).

2.6.3 Mammography Screening

Mammography is the most important breast cancer screening modality. It is recommended by organisations in more than 35 countries worldwide. The recommendations of screening mammography are different in various countries. These differences are attributed to the age of breast cancer incidence in each population and to the results of screening trials upon which the programme's recommendations are designed (ICSN, 2015; Nelson et al., 2016; TOP, 2013).

The effect of adding three-dimensional DBT imaging to the screening process and its efficacy is the focus of many researchers (Ciatto et al., 2013). In some instances researchers have assessed DBT as a screening modality with a view to replacing the two-dimensional mammogram (Lang et al., 2016). More details about screening mammography including the screening starting age, frequency, justification and controversies will be discussed in section 3.7 (page 53).

2.6.4 Magnetic Resonance Imaging (MRI) Screening

In some countries MRI screening is recommended annually along with mammography for high breast cancer risk women because it has higher sensitivity for cancer detection than mammography (ACS, 2014). Nevertheless, it cannot replace mammography screening because of the lack of standards for MRI screening imaging procedures, interpretation and performance (whether it is cost-effective or not). Also, it is a very high cost procedure and requires a long examination time (Tirona, 2013).

2.6.5 Ultrasound Screening

Despite the high sensitivity of ultrasound for breast cancer detection, it is not recommended as a screening tool. This is because of the long examination time, its high false-positive rate and its image quality, which is variable depending on the examiner's skill (ACS, 2014; Nelson et al., 2016). The feasibility of using ultrasound for breast cancer screenings was investigated by Wang et al. (2013) in a rural area of China. They concluded that ultrasound is more sensitive than mammography for breast cancer detection in Chinese women younger than 55 years old, with lower cost and more convenience for breast screening in such areas (Wang et al., 2013).

2.7 Chapter Summary

In addition to mammography, there are many breast imaging modalities including CT, ultrasound and MRI. In regard to cost-effectiveness, none of these techniques can replace mammography as a screening tool but can be supplementary to it. Breast self-examination is no longer being recommended by many breast cancer care organisations, with self-breast awareness being recommended instead. Clinical breast examination is a useful method for the early detection of breast cancer but its feasibility is still limited when compared to mammography. Overall, until now mammography has been considered the gold standard in breast cancer screening.

Chapter Three

Mammography: Development, Physics and Clinical Aspects

3.1 Chapter Overview

Mammographic technique is the main focus of this chapter. To begin with, the historic development of mammography, ranging from the production of early mammographic images to the development of the first dedicated mammographic machine will be reviewed. The radiation dose reduction achieved through the introduction of the mammography machine will also be highlighted. In general the radiation dose associated with mammography has reduced from approximately 150 mGy for early industrial non-screen film systems to less than 2 mGy for present day full field digital mammography (FFDM). In dedicated mammography machines, the use of a molybdenum anode X-ray tube has helped to improve image quality and reduce the radiation dose. Anti-scatter grids have also allowed an improvement in mammographic image quality but at the cost of an increased radiation dose. Beam collimators and breast compression further reduce the radiation dose and increase image quality.

This chapter will also discuss the physical principles of the different digital image receptor types (e.g. direct and indirect conversion detectors), along with that of the FFDM machine. Improved breast cancer detectability at a lower radiation dose has been reported in the majority of screening performance trials for FFDM, when compared to film-screen mammography. The physical principle, instrumentation and clinical performance of digital breast tomosynthesis (DBT), which is the new generation of digital mammography, will also be considered. The addition of 3D tomographic images to 2D FFDM imaging has resulted in improved breast cancer detectability but with an increase in radiation dose.

The last two sections of this chapter comprise of a comprehensive review of breast tissue appearances in mammographic standard images and screening mammography performance. Screening mammography trials used breast cancer mortality reduction as a measure of performance. A 20-30% reduction in breast cancer mortality has been reported by most screening trials. However, other researchers documented that the results of such screening

trials have been exaggerated. These results, alongside reports of over-diagnosis, have limited the net benefit from screening mammography. Despite the screening mammography controversy, many countries worldwide have organised screening programme since there is no strong evidence against screening mammography. The overall risk of radiation-induced cancer from screening mammography is reported to be small and as a result is not considered in the evaluation of breast cancer screening programmes.

3.2 The Origins of Mammography Imaging – Equipment and Rudiments of Technique

Concerns about breast disease were reported long before the discovery of X-rays (Wentz & Parsons, 1997). The first reported attempt to use X-rays for breast tissue imaging was by Salamon, a German surgeon, in 1913. He imaged 3000 mastectomy specimens observing the close correlation between the radiographic and pathologic abnormalities of breast tissue under investigation. He also described the radiographic appearance of malignant breast lesions. However, mammography only began being performed on patients from the mid to late 1920s in Europe, the United States, and South America where it helped to explain many breast abnormalities (Vyborny & Schmidt, 1989). The radiographic appearance of benign breast lesions and their distinctive features over breast carcinomas were reported by Walter Vogel (1931, as cited in Gold, Bassett, & Widoff, 1990). In the same year, Seabold (1931) documented his findings about breast disease detected by radiography. Work by Gershon-Cohen and Strickler (1938) described the normal radiographic appearances of breast tissue at different ages and across a range of menstrual conditions. The diagnostic information available from early mammograms was restricted due to technical limitations of the mammography equipment available in this period. This compelled many researchers to use different contrast agents such as gases for pneumocystography or iodinated compounds for ductography. Many studies reported the adverse effects of such contrast agents (Romano & McFetridge, 1938). Therefore, to address these mammographic limitations, developments in mammography technologies were required (Vyborny & Schmidt, 1989).

Early mammograms were performed using conventional radiography machines with tungsten anode tubes. Most of these tubes had a minimum energy level of 50 kVp, with some of them going down to 40 kVp (Law, 2006). Warren (1930) developed a stereoscopic system for *in*

vivo breast tumour identification. He utilised double sided emulsion film and dual high speed intensifying screens. Exposure factors of 60 kVp, 70 mA, and a 2.5s exposure time were used. Using his system, Warren (1930) investigated breast cancer in 119 preoperative patients and found that the mammographic false positives and false negatives were evident in 6.7% of the examined patients. Following on from this work, many investigators started to develop mammographic techniques to improve the quality of the images.

The correlation between radiographic calcification and breast cancer was first documented in a Spanish article by Leborgne in 1949 (as cited in Gold, Bassett, & Widoff, 1990). The same report also highlighted the importance of breast compression for calcification visibility in mammograms. Another study published by Leborgne (1951) investigated the radiographic appearance of palpable breast cancers. He confirmed that the use of slight compression by a cotton pad placed between the breast and the cone, a conical tool made of copper and extended from the X-ray tube window down to the breast to collimate the X-ray bream, improved mammographic image quality. The different radiographic appearances of benign and malignant breast calcifications were also described by Leborgne (1951). In this study, Leborgne (1951) utilised 30 kV X-rays, non-screen films, a 60 cm focal-film distance, and 5 mAs for each 1 cm of breast thickness. Breast compression, together with good collimation and the use of non-screen films, were further advocated by Ingleby and Gershon-Cohen (1960) as means by which to generate high contrast images. Gershon-Cohen also suggested the simultaneous exposure of two non-screens films with 0.5mm aluminium layer between them to overcome breast thickness non-uniformity. The aluminium attenuates the X-ray photons reaching the lower film and consequently the upper film which receives higher exposure will demonstrate the thicker juxtathoracic portion of the breast, and the thinner peripheral portion will be demonstrated by the lower (less) exposed film (Gold, Bassett, & Widoff, 1990).

3.2.1 Early Developments of Image Receptor

High quality breast images were produced by Egan (1960) who used high resolution industrial films (without an intensifying screen) with high current (300 mA), 6 seconds time and 26-28 kV X-ray. Egan (1960) also placed a lead shield under the film holder to protect the gonads from possible radiation. The industrial films were supplied in envelopes rather

than cassettes. The main advantage of these industrial non-screen films were that they produce fine detail with relatively lower patient exposure at the breast surface compared to conventional film-screen. The processing of industrial films was achieved by conventional wet (manual) techniques. In order to obtain more detailed mammograms, some centres used two films of different speeds in the same envelope. The low speed film was to demonstrate information within radiolucent areas, while the high speed film was to demonstrate information within denser areas (Law, 2006).

Higher quality breast images, achieved due to edge enhancement, were produced in the 1960s by using xeromammography. Gould, Ruzicka, Sanchez-Ubeda, and Perez (1960) reported the superiority of xeromammography over industrial non-screen film with regard to mammographic image quality (Gold et al., 1990; Odle, 2004). In xeromammography a thin sheet of photoconducting amorphous selenium contained within a lightproof cassette was used for image recording. After exposure, the breast image information was recorded on a charged selenium plate forming the latent image which becomes visible after it is dusted with thermoplastic powder. Next, plastic coated papers were used for the permanent recording of the image (Assiamah, 2004). The main advantage of xeromammography over direct film mammography was the possibility of obtaining more acceptable images using conventional radiography tubes with tungsten/aluminium targets/filters and at conventional kilo-voltages (~50 kVp) (Huda, Nickoloff, & Boone, 2008; Vyborny & Schmidt, 1989). In addition to its use with conventional radiography machines, xeromammography can also be used with dedicated mammographic machines that use molybdenum/aluminium target/filter combinations. However, xeromammography was replaced by the more efficient film-screen mammography in 1990 (Odle, 2004).

Double-sided emulsion films with dual intensifying screens have been used in conventional radiography to record the image. In such systems the X-ray photons are more efficiently absorbed by the intensifying screen than by film, and are then converted into light photons which produce the image on the film (Vyborny & Schmidt, 1989). This process has the advantage of reducing patient dose by about 8 times, but it has the disadvantage of increasing image unsharpness (Huda et al., 2008). In order to reduce image unsharpness in mammography, single-sided emulsion film with a single thin intensifying screen is used,

because a thinner intensifying phosphor layer screen produces less image unsharpness. In the mammographic energy range the photoelectric cross-sections of intensifying screen phosphor are very high and result in efficient X-ray photon recording, even with the thin phosphor layer (Vyborny & Schmidt, 1989). Since each screen emits a narrow wavelength of light, the film had to be sensitive to that wavelength. Both the screen and wavelength-specific film were manually placed inside black plastic bags or envelopes in a darkroom. To achieve firm contact between them, the bag or envelope must be a sealed vacuum. This evacuation process was performed either manually or automatically. Manual evacuation was achieved through an opening supplied with a nozzle in one corner of the bag and a special hand pump - in this case the bags were reusable. Automatic evacuation was performed via a box which heat sealed the envelope after the evacuation of the air. For the latter, the bags could be reused 3-5 times. This process was used until the late 1980s wherein the mammography cassettes were introduced (Law, 2006).

3.2.2 Dedicated Mammography Machine Development

Throughout the development of mammography, the key to producing the required high quality mammograms with an acceptable radiation dose was through the introduction of dedicated mammography machines (Odle, 2004). The earliest dedicated mammography machine was the Senograph. It was developed and tested in 1965 by Charles Gros in collaboration with Compagnie Generale de Radiographie (CGR) (Steen & Tiggelen, 2007). Senograph was subsequently marketed by CGR from 1967 (Nass, Henderson, & Lashof, 2001). It was the first commercial mammography system with molybdenum/molybdenum target/filter combinations (Vyborny & Schmidt, 1989). For mammographic imaging, the useful part of the molybdenum X-ray beam is the characteristic radiation of molybdenum, because the energy of its K-edge characteristic radiation is approximately 20 keV, where the majority of its other characteristic radiations have energies around 19 keV. For a tungsten anode, the continuous X-ray beam with 10-20 keV is the useful portion for breast imaging because the characteristic radiations of tungsten have energies 69 keV and around 9 keV for the K and L edges (Law, 2006). The use of molybdenum target tubes resulted in the production of lower energy radiation with a more limited energy range than that produced by conventional radiography tubes. This resulted in optimum image contrast (Vyborny & Schmidt, 1989).

The nominal focal spot size of the Senograph tube was 0.7 mm. This focal spot size reduced geometric unsharpness, which in turn improved the mammographic image quality by increasing the contrast between the glandular tissue, fat tissue, and calcification (Gold et al., 1990). The X-ray tube stand and film holder of the Senograph were designed to facilitate optimum patient positioning during the examination (Vyborny & Schmidt, 1989). Moreover, a copper cone extending from the X-ray tube down to the breast was provided with Senograph. This cone offered advantages in scatter radiation reduction; it also helped in breast localisation. Cones of different shapes and sizes, semicircular and elliptical, were available to accommodate different breast sizes and shapes. In later generations of dedicated mammography machines both the collimation and compression devices were built in. In early dedicated mammography machines the compression device was an inflatable balloon within the cone and was pumped up after patient positioning (Law, 2006).

3.2.3 Mammography Developments during the 1980s and 1990s

During the 1980s and 1990s mammographic equipment improved greatly. For instance, the nominal focal spot size decreased to 0.2 mm and 0.5 mm for small and large foci (Law, 2006). This reduction in focal spot size increased breast image sharpness by minimising geometrical unsharpness (Säbel & Aichinger, 1996). However, the use of such a focal spot size increases the tube thermal loading, resulting in potential for damage to the anode. Prolonged exposure times may reduce thermal loading but this brings with it an added risk of patient movement. In order to reduce this risk, rotating anode tubes were developed (Bushong, 2013). For additional image quality enhancement, mammography machines employed grids in order to reduce the scattered radiation which reached the film. However, these grids increased the patient radiation dose by 3 times or more. For mammographic purposes, the grids had 32 lines per inch with 5:1 grid ratios (Law, 2006). The air gap technique was developed as an alternative to the grid but had the same disadvantage with regards to patient dose, again increasing it by 25-30% (Jacobson, 2001). The later development of the magnification technique helped to clarify suspicious areas and microcalcifications without the need for the air gap technique (Säbel & Aichinger, 1996).

Since the molybdenum/molybdenum target/filter combination was suitable for average breasts only, other target/filter combinations were introduced such as molybdenum/rhodium

(Mo/Rh), (rhodium/rhodium (Rh/Rh), and tungsten/rhodium (W/Rh). The target/filter combination is determined by compressed breast thickness and breast composition (density) (Law, 2006). Also, tubes with dual track anodes have been produced. One of these tracks was molybdenum and the other was either rhodium or tungsten. Filters are automatically selected depending on the track material. Automatic exposure control (AEC) was introduced to obtain a constant mean optical density regardless of breast thickness, breast composition and exposure factors. However, this was changed with the introduction of film-screen because mammographic image quality depends on the X-ray beam (Säbel & Aichinger, 1996). Ionisation chambers or other electronic X-ray detectors were connected within the exposure time control circuit; these were placed beneath the film cassette. When the required amount of radiation is reached the exposure is terminated automatically. Later, post exposure mAs meters were also added to the AEC (Law, 2006).

Different film screen assemblies were then introduced with different film speeds (Law, 2006). The sensitivity of the film-screen combination system is defined by a quantity called system dose. This represents the required air kerma to produce the receptor-specific exposure (Säbel & Aichinger, 1996). Since the required tube kVp for mammography is low (25-35 kVp) when compared to general radiographic procedures, dedicated X-ray generators for mammography were introduced with tube voltages down to around 25 kVp in steps of 1 kV. Finally, in order to achieve more patient comfort and better image quality with less radiation dose, collimation and compression devices were developed. Motorised compression devices were introduced, and diaphragms, which are two pairs of adjustable lead hemistiches mounted within the X-ray tube behind the tube window with a light source to illuminate the X-ray field, were utilised instead of copper cones (Law, 2006; Statkiewicz-Sherer, Visconti, & Ritenour, 2010).

3.3 Digital Mammography

Currently there are two different types of digital mammography technologies (computed radiography and digital radiography) as well as conventional film-screen (Pagliari et al., 2012). In regards to digital technologies, the image receptor replaces film-screen with the introduction of digital detectors (Ongeval, 2007). The digital detectors were initially used for general radiography but rapidly became integrated into mammography machine design

(Schueller et al., 2008). The changeover to digital radiography was not an easy process, as many issues had first to be considered; these included technical factors, patient management and image quality. Patient radiation dose was a concern during the changeover period because the dynamic range of digital detectors, which was wider than that of film-screen, result in an increase in patient radiation dose by as much as 40-103% (Lança & Silva, 2009a). However, this wide dynamic range helped to improve the radiographic image quality (Uffmann & Schaefer-Prokop, 2009).

The term full field digital mammography (FFDM) is used in literature with reference to both digital mammographic technologies. However, the term small field digital mammography (SFDM) is utilised to indicate breast imaging with stereoscopic biopsy (Pagliari et al., 2012). The first FFDM machine was approved for clinical use in 2000 by the Food and Drug Administration (FDA) in the USA (Mekasut, 2011).

3.3.1 Types of Digital Mammography Detectors

With regard to digital detector types, digital mammography systems are classified into two subsections: computed radiography (CR) systems; and digital radiography (DR) systems. The latter is subdivided into indirect and direct digital radiography (Lança & Silva, 2009a). However, other researchers who classified digital systems into direct digital radiography (DR) and indirect digital radiography systems which also include computed radiography (CR) (Mothiram, Brennan, Lewis, Moran, & Robinson, 2014).

3.3.1.1 Computed Radiography (CR)

CR was first introduced in the early 1980s (Lança & Silva, 2009a). This was the earliest digital technology employed for mammography (James, 2004). Here the photostimulable phosphor detectors, known as storage phosphor screens (SPS), were used instead of traditional films inside special cassettes. They were still standard size of film-screen cassettes (Lança & Silva, 2009a). These image detectors could be thus used with conventional X-ray systems (Testagrossa et al., 2012). Exposing SPS to X-rays resulted in an excitation process through the movement of valence band electrons to the conduction band, thereby forming the latent image as an electronic signal. The SPS was then scanned with a laser in the reader; this converted the latent image to blue light which was proportional to the amount of incident X-ray on the SPS. Finally, a photomultiplier system in the reader converted the blue light to an

electronic signal which was then available as a digital dataset. To ensure that the SPS was free from any residual charge, it was then scanned with high intensity white light. Typically 25% of the latent image was lost from the SPS within 10 minutes to 8 hours (James, 2004; Lança & Silva, 2009a). The main disadvantage of this type of digital detector is the lack of spatial resolution due to light scattering. Thicker phosphor layer detectors are more sensitive to radiation but more light scattering is produced (Testagrossa et al., 2012).

3.3.1.2 Indirect Digital Mammography

The initial digital mammography (DM) systems utilised indirect conversion detectors. In this type of detector the image capturing process was achieved in two steps, using charge couple devices (CCD). The first step includes the X-ray energy to light photon conversion, which is then converted to an electronic signal in the second step (Smith, 2005). The CCD technology involves the use of phosphor, and millions of optic fibers on coupling plates. The main function of the optic fibers is to transfer light from the phosphor to the CCD. This is then digitised (Pisano & Yaffe, 2005). The early CCD was limited to a small field size of 5 cm X 5 cm. The success of these limited field size systems in digital spot mammography, for stereoscopic needle biopsy, led to the development of this technology in larger field sizes of 1cm X 22 cm, using an array of four phosphor-CCD assemblies. These detectors were synchronised with a slit collimated X-ray beam to scan the breast perpendicularly to a patient's body producing 22 cm X 30 cm images (James, 2004). The required image acquisition time was about 6 seconds longer than that required by large area detectors. Due to slit collimation, the scattered radiation was reduced significantly thereby eliminating the need for a grid (Pisano & Yaffe, 2005).

Amorphous silicon flat-panel detectors, commonly known as large area detectors, are another form of indirect digital radiography detectors. They were introduced to clinical use in the late 1990s (Lança & Silva, 2009a). They were made of a thallium activated caesium iodide (CsI:Tl) phosphor layer acting as an X-ray absorber, and a light sensitive two-dimensional (rectangular) array of photo-diodes. The incident X-ray beam on the detector is absorbed by the CsI:Tl layer releasing light photons. This light is then converted into an electronic signal by the photo-diodes. The electronic signal is then finally captured by thin film transistors (TFTs). Since the CsI:Tl crystals are designed in needle like channels and both the Cs and I

have high atomic numbers (for Cs Z=55 and for I Z=53), this technique exhibits high efficiency for X-ray absorption (80-90%). CsI:Tl light is in the green area of the light spectrum where the photo-diodes have relatively high absorption efficiency (approximately 80%) (Cowen, Kengyelics, & Davies, 2008). The principle advantage of this detector type is that it can be used for radiographic procedures which require rapid sequence imaging. However, its main limitations are the high cost, that format changing is difficult, and that the detector's element size cannot be easily reduced (Pisano & Yaffe, 2005).

3.3.1.3 Direct Digital Mammography

Amorphous selenium-based detectors avoid multiple conversions of X-ray photon energy, from light photons to an electronic signal, via direct X-ray conversion (James, 2004). This conversion process eliminates the light scattering problem associated with indirect conversion detectors. Direct conversion digital detectors are made from a layer of amorphous selenium (a-Se) mounted on the top of the image plate which consists of a regular matrix of storage capacitors and thin film transistors (Cowen et al., 2008). Before exposing the a-Se to X-ray, its surface is charged with a uniform positive charge. The uniform surface charge pattern is partially discharged when the X-rays are absorbed by the a-Se. The amount of discharge is proportional to the energy of the absorbed X-ray photons. This charge distribution forms the latent image as an electronic signal (James, 2004). This electronic signal is read by the thin film transistor array (NHSBSP, 2009). This type of detector is exemplary for use in digital mammography because its absorption efficiency is high, it produces high resolution images, and its dose efficiency is good (Qian, 2013).

3.3.2 FFDM Performance

Important features of digital mammography are the wide dynamic range, which is about 400 fold compared to that of a film-screen system, and the linear relationship between the radiation dose reaching the detector and the signal intensity produced. Also, the inverse relationship between the radiation dose at the detector and the image contrast is eliminated because both image contrast and brightness can be separately optimised after image acquisition (Obenauer, Hermann, & Grabbe, 2003; Uffmann & Schaefer-Prokop, 2009). Also there are additional benefits of FFDM including easier archiving and easy-to-share image data (Silverstein et al., 2009).

In FFDM, the overall image quality is determined by spatial resolution, image contrast, signal-to-noise ratio, and dose efficiency (Smith, 2005). Since the image acquisition, display and storage are achieved separately in FFDM, the image optimisation process is different from that in film-screen (Park, Kim, Choi, Oh, & Kim, 2011). Accordingly, the FFDM allows the optimisation of image acquisition, display, and storage processes separately (Pisano & Yaffe, 2005). The optimisation of image acquisition is dependent on digital detector optimisation, selected X-ray spectrum (target/filter combination) and exposure factors (Park et al., 2011). Digital detector characteristics that control the image acquisition process are field and pixel sizes, dynamic range, sensitivity, internal noise and readout (Lança & Silva, 2009b). National and European standards determine the required contrast resolution and the accepted radiation dose (European Commission, 2006; IAEA, 2011). They also proposed 100 μm as the maximum accepted pixel size and 18 ± 1cm X 24 ± 1cm as the minimum detector size to accommodate large breasts (Schulz-Wendtland, Fuchsjager, Wacker, & Hermann, 2009). For soft copy image display, two high resolution monitors (5 megapixels) should be used (IAEA, 2011). This 'reporting-grade' workstation should include software with a wide range of processing tools which enable image manipulation, such as image gray scale invert, window level and width change, zooming, edge enhancement, and measuring tools. Finally, the use of a picture archiving and communication systems (PACS) facilitates better digital archiving and sharing with others (teleradiology) (James, 2004; NHSBSP, 2009).

It has been reported that digital mammography provides better contrast resolution with lower patient dose than film-screen systems (NHSBSP, 2009; Smith, 2005). The superiority of digital mammography has been investigated by many researchers. Work by Gennaro and di Maggio (2006) compared the mean glandular dose (MGD) of 300 film-screen cranio-caudal mammograms with 296 FFDM cranio-caudal mammograms. They found that the use of FFDM reduces MGD by about 15% for thin breast and 30-40% for thick breast. The main limitation of Gennaro and di Maggio's (2006) work was that they compared the MGD of images taken by one film-screen system with that of images taken by one FFDM machine; MGD variations of different systems were not considered. More recently, Hendrick et al. (2010) evaluated the technical performance of both film-screen and FFDM systems for 4366

women who underwent screening mammography by both techniques. They reported a 22% reduction in breast MGD with the use of FFDM.

With regard to FFDM image quality evaluation, most researchers used breast cancer detectability as a means to investigate the performance of FFDM compared to film-screen, see **Table (3-1)**. All of the studies in **Table (3-1)** concluded that the cancer detectability of FFDM was equal or better than that of film-screen. The mammographic image quality of FFDM was compared with that of film-screen for 200 women wherein one of their breasts was examined by FFDM and the other one by film-screen. The results of this work indicate equal accuracy for both FFDM and film-screen in some studied criteria, while the FFDM was more accurate in other criteria (Fischmann, Siegmann, Wersebe, Claussen, & Muller-Schimpfle, 2005).

Table (3-1) A summary of the main screening trials which investigated the superiority of FFDM over FSM in breast cancer detection.

Study Author	Participants number	Study results
Chiarelli et al. (2013)	220520 women by DR, 64210 by CR and 403688 women by FSM	DR and FSM are equivalent, CR showed lower cancer detectability.
Hambly et al. (2009) (INBSP* Study)	35204 women by FFDM and 153619 women by FSM	FFDM has significantly higher cancer detectability and recall rate.
Vigeland, Klaasen, Klingen, Hofvind, and Skaane (2008) (Vestfold Study)	18239 women by FFDM and 324763 women by FSM	FFDM has statistically significant higher cancer detection with fewer recalls due to technical issues.
Heddson, Ronnow, Olsson, and Miller (2007)	52172 two-view examinations of 24,875 women. 25901 by FSM, 9841 by photon counting DR, and 16430 by CR.	DR has higher cancer detectability than FSM but this is statistically non-significant and significant lower recall rate and MGD.
Del Turco et al. (2007)	14385 women by FFDM and 14385 women by FSM	FFDM has greater detection rate but higher recall rate than FSM.
Skaane , Hofvind, and Skjennald (2007) (follow up of Oslo II)	16985 women by FSM and 6944 women by FFDM	FFDM has significantly higher cancer detection rate.
Pisano et al. (2005) (DMIST** trial)	42760 women screened by both FFDM and SFM	Both have equivalent detectability. FFDM more accurate for dense breast and (>50 years) women
Skaane and Skjennald (2004) (Oslo II trial)	18054 women by FSM and 7209 women by FFDM	FFDM showed higher but non-significant cancer detection rate.
Skaane, Young, and Skjennald (2003) (Oslo I trial)	3683 women underwent both SFM and FFDM (two view for each breast)	Both FFDM and FSM showed comparable cancer detection rate.
Lewin et al. (2002)	6736 women underwent both FSM and FFDM	No statistical difference between them and fewer recall rate with FFDM.

**Irish National Breast Screening Programme.*
***Digital Mammographic Imaging Screening Trial.*

3.4 FFDM Physics and Instrumentation

Mammography constitutes a real challenge for medical physics. It has to differentiate the attenuation coefficient of fat and glandular tissues with the lowest possible radiation dose. Accordingly, mammographic images have inherently low contrast and extremely high image resolution; about 15 lines pairs per mm is required (Hobbie & Roth, 2007). The conventional X-ray unit is not suitable to address these challenges, and specially designed dedicated mammography machines are required (Bushong, 2013). An example of a dedicated FFDM machine is shown in **Figure (3-1)**. It has a 'C' shaped assembly with changeable height and angular orientation to facilitate different mammographic positions. The upper arm of the assembly is where the X-ray tube is mounted, while the lower arm is where the breast support / X-ray image receptor is located. The distance between the X-ray tube focus and breast support is generally about 60 cm (Kotre & Reis, 2015).

Figure (3-1) Shows the FFDM machine.

3.4.1 X-ray Tube

The X-ray tube is composed of a source of electrons (cathode) and a target (anode) where the electrons interact and convert their kinetic energy to electromagnetic radiation (X-ray). The electrons, before interacting with anode, are accelerated by high potential difference inside an evacuated tube (Bushberg, Seibert, Leidholdt, & Boone, 2002). X-ray photons generated by electron deceleration at the anode and are classified into two types - Bremsstrahlung X-ray

photons and characteristic radiation **Figure (3-2)**. The former type (Bremsstrahlung) is produced when the electrons slow down and their energy is partly or wholly converted to [Bremsstrahlung] X-ray photons. Characteristic radiation is emitted when an electron interacts with an atomic electron within the anode and ejects it from its shell. Then the ejected electron vacancy is filled by an outer shell electron emitting X-ray photon whose energy is equal to the binding energy difference between the two shells (Montesdeoca, 2013).

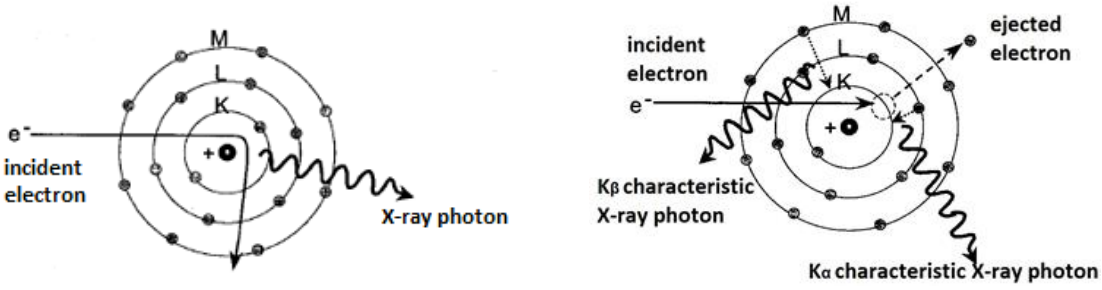

(a) **(b)**

Figure (3-2) Illustrates the X-ray production **(a)** Bremsstrahlung X-ray **(b)** Characteristic X-ray.

The anode of the mammographic X-ray tube can be made of tungsten (W), molybdenum (Mo), or rhodium (Rh) (Kotre & Reis, 2015). At energies required for mammographic imaging, the W X-ray spectrum is predominantly composed of Bremsstrahlung X-ray photons as well as L-shell 12-keV characteristic X-rays, which are not useful for imaging. The bremsstrahlung X-ray photons below 17 keV and above 24 keV are not particularly useful. However, the characteristic X-rays are the prominent portion of both Mo and Rh spectra (Bushong, 2013). The X-ray spectrum of the mammographic tube anode is optimised by adding filters which absorb the low energy photons, thus reducing the total number of photons but increasing the photons' average energy (Hendee & Ritenour, 2002). Mammography machines are therefore typically equipped with more than one target/filter combination to accommodate different breast thicknesses and densities (Bushong, 2013; Cunha, Tomal, & Poletti, 2012). Mo/Mo was the first target/filter combination used in dedicated mammography units; as time progressed other combinations were introduced such as Mo/Rh, Rh/Rh, W/Al, and W/Ag (Kotre & Reis, 2015).

The rotating anode design, with a small anode angulation, is employed in FFDM machines. This small angulation helps to reduce geometric image unsharpness by reducing the focal spot size (nominal focal spot) (Yaffe & Maidment, 2014). The typical nominal focal spot size of a mammographic X-ray tube is 0.3 mm and 0.1 mm for large and small foci (Bushong, 2013). The large focus is usually used for conventional mammographic imaging, while the small one is utilised for magnified views (Kotre & Reis, 2015). Since less focal-object distance is used in magnification mammography, the geometric focal spot unsharpness is increased. To overcome this unsharpness, a smaller focal spot is required. However, the use of small focal spot increases the tube thermal load which is accounted for by the use of longer exposure time. This consequently increases the possibility of patient movement blur.

Unlike the [helical] filament of a conventional imaging tube, the FFDM cathode filament is flat. The filament design results in a more focused electron beam to coincide with the required focus size (Smith & Webb, 2011). In order to exploit the anode-heel effect, the X-ray tube is positioned with the cathode toward the woman's chest wall so that the high intensity of the X-ray beam exposes the thicker side of the breast, while the thinner nipple side of the breast is exposed by the low intensity aspect of the beam (Yaffe & Maidment, 2014). The X-ray tube is often tilted within the housing making the central ray parallel to the patient's chest wall. Such tilting helps to achieve an even smaller focal spot size and superior X-ray distribution, matching the different thicknesses of the breast regions, see **Figure (3-3)** (Bushong, 2013). In order to avoid excessive attenuation of the low energy X-ray beam, the glass exit window of the conventional imaging X-ray tube is replaced with beryllium. The beryllium window separates the evacuated area of the tube from the outer atmosphere directly; there is no oil or glass in the beam path (Yaffe & Maidment, 2014).

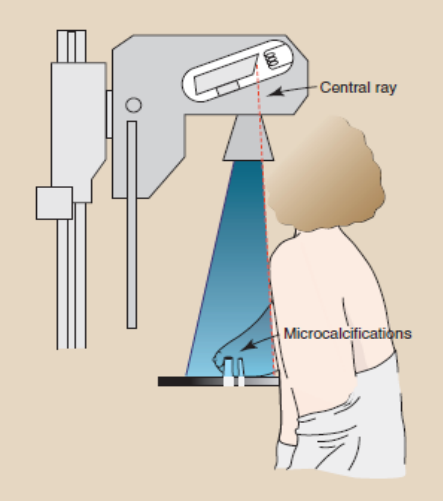

Figure (3-3) Shows the effect of the X-ray tube tilting inside the tube assembly (Bushong, 2013).

3.4.2 Breast Compression Device

Compression serves many purposes in conventional radiography and is extremely important in mammography (Bushong, 2013). The main purpose of breast compression in mammographic examination is to reduce breast thickness (Mercer, Hogg, Lawson, Diffey, & Denton, 2013). Reducing breast thickness has several advantages. Firstly, the image spatial resolution is improved by bringing the tissue closer to the image receptor, minimising magnification and maximising the impact of the focal spot size; both of which limit geometrical unsharpness (Bushong, 2013). Secondly, the reduced breast thickness results in less scattered radiation, this results in better image contrast through the reduction of scattered radiation (noise) (Yaffe & Maidment, 2014). Thirdly, the reduction of breast thickness helps to improve image contrast by making the low energy photons, which are sometimes scattered when dealing with thick breast tissue, useful in the mammographic image formation process (Kotre & Reis, 2015). Finally, reducing breast thickness decreases the breast radiation absorbed dose because less radiation is required to penetrate thinner breasts. More image quality refinement can be obtained through breast compression due to better image uniformity, via uniform breast tissue distribution, and lessened motion blur by minimising the woman's movement during exposure (Bushberg et al., 2002). Also, as mentioned by Hogg, Szczepura, Darlington, & Maxwell (2013), the breast compression ameliorates the image contrast by spreading the breast tissue which in turn reduces the tissue superimposition.

Compression is not without its problems. Work by Mercer, Hogg, Lawson, et al. (2013) investigated the compression magnitude applied for 488 women by 14 practitioners. Mercer, Hogg, Lawson, et al. (2013) found that, for individual practitioner the applied compression magnitude may be affected by breast density, less compression was used for higher BI-RADS women, and breast volume, wherein more compression is needed for large breasts. However, practitioners do not utilise the same mean breast compression. This variability in breast compression magnitude between practitioners was further confirmed by Mercer, Hogg, Szczepura, & Denton (2013) who assessed the compression force for 500 screening clients across three successive screening visits. It has been reported that for a client's three visits, the variation in compression force applied by same practitioner was not statistically significant. However, significantly different compression force was applied by different practitioners for the same client (Mercer, Hogg, Szczepura, & Denton, 2013). More extensively Mercer et al. (2015) analysed the compression force applied in three screening sites within the UK. Mercer et al. (2015) concluded that, with regard to applied breast compression the practitioner behavior was different within and between centres.

Since compression force variations affect the breast thickness of the client, the MGD is also different. According to Brnic and Hebrang (2001), the analysis of required mAs in relation to different breast thicknesses in MLO projection showed that when the average breast thickness for 52 women decreased, through compression, from 50.3 mm to 47.0 mm, the average required mAs reduced from 49.5 to 44.1. This reduction in required mAs will reduce breast MGD. The effect of mAs on MGD will be further discussed in section 7.3.1 (page 182). Overall, until now there has been no exact magnitude for the required breast compression, but it has been reported that the greater the compression, the better the image quality and lower patient dose. However, this can result in patient discomfort (Bushong, 2013).

All dedicated mammographic machines are supplied with a breast compression device, a rigid plate of radiolucent material driven by a motor. The compressed breast should be as uniform as possible. At the chest wall the compression plate edge should be horizontal and adjusted with both X-ray tube focal spot and image receptor (Yaffe & Maidment, 2014). The mammographic machine is usually supplied with a range of compression paddles. Each

paddle is designed for a specific purpose. The basic compression paddle is flat and rigid. This paddle is parallel to the image receptor so it can apply uniform force to the whole breast. A tilting paddle, also known as a flexible paddle, applies more compression at the chest wall side resulting in better breast fixation in mammographic position. For small breast imaging, a sliding compression paddle is suitable. This paddle has a smaller size than the image receptor and can be moved from one side to another. Smaller compression paddles are used for both spot views and magnification examinations. Finally, a biopsy compression paddle has an aperture for a biopsy needle (Kotre & Reis, 2015).

Breast thickness is nonuniform. It is thicker closer to the chest wall than when compared to the nipple side. In order to compensate for this the compression paddle is usually tilted during breast compression. Paddle tilting results in variations in the breast thickness readout accuracy for fixed and flexible paddles. For fixed paddles, the readout variations for 20 women for both CC and MLO projections, along with the variations' effect on breast density assessment, were determined by Diffey et al. (2008). A maximum readout variation of 21.2 mm was reported by Diffey et al. (2008). On average the use of indicated breast thickness resulted in underestimation of 10.5% in breast volume and this affects the accuracy of volumetric breast density calculation.

However, Hauge et al., (2012) extended their work to consider the readout variations across the paddle area of both fixed and flexible paddles of different sizes (18 X 24 cm and 24 X 30 cm) for 8 mammographic machines (3 FSM and 5 FFDM). For these eight machines, Hauge et al. (2012) found that the flexible paddle resulted in greater readout variations (16 mm and 10 mm for small and large paddles) across the paddle area than fixed paddle (5mm and 5.3 mm for small and large paddles). Overall, the maximum thickness readout variation reported by Hauge et al. (2012) was 13 mm. These variations were different for each of the studied machines, both between and within different equipment brands. In the work by Hauge et al. (2012) the effect of thickness readout variations on MGD was also discussed. They found that breast thickness readout variation may result in up to 20% difference in calculated MGD. More variations in MGD may be introduced if the thickness readout variation leads to a different target/filter combination selection.

3.4.3 Grid

In mammography not all of the X-ray photons which pass through the breast carry anatomical information about the breast. Some of the photons escape the breast without interaction and others scatter within the breast tissue and emerge from the breast at different angles to their entry. The latter photons possess a range of energies. It has been found that, at the kVp values used in mammography, about 40% of the photons which leave the breast are scattered radiation (Yaffe, 2010). The ratio of scatter to primary radiation determines the reduction amount in both image contrast and sharpness. The best method to minimise the effect of scatter is by using anti-scatter grids which absorb them (Qian, 2013). However, the use of anti-scatter grids has the disadvantage of increasing radiation dose because they also attenuate the primary beam (Bushberg et al., 2002). In FFDM machines the grid is integrated within the breast support above the image receptor. Most FFDM machines have a focused moving grid with 4:1 to 5:1 grid ratio. Grid ratio refers to the height of the lead strips relative to the width of the interspace between two strips. Grid movement during exposure is necessary to blur the lead strips image out of the mammogram. A 40 lines/cm is the typical grid frequency for mammography (Bushong, 2013; Yaffe & Maidment, 2014).

3.4.4 Automatic Exposure Control (AEC)

In mammography, precise estimation of the required exposure factors is not easy. This has led to the development of AECs, also known as photo-timers (Bushong, 2013; Yaffe & Maidment, 2014). In FFDM the aim of using AECs is to optimise the mammographic image quality (image contrast and noise) and patient radiation dose. The photo-timer is composed of one or more radiation detectors, ionisation chambers or solid state detectors, positioned just after the image receptor to detect the amount of radiation passing through the receptor. When they reach the required level, the exposure is terminated (Bushberg et al., 2002). Beam quality is determined by tube voltage and target/filter combination. The algorithm for this uses compressed breast thickness and transmitted exposure rate. The latter can be determined by very short exposure called pre-exposure. In modern mammographic machines, the digital image receptor itself works as an AEC depending on the information obtained by short low dose pre-exposure (Kotre & Reis, 2015; Qian, 2013). Although the radiation dose of this small pre-exposure increases the overall radiation dose, the image acquired from this pre-exposure may not be incorporated in the final mammographic image (IAEA, 2011).

The performance of AEC, with regard to mammographic image quality and MGD, was investigated by Young, Ramsdale, Rust, & Cooke (1997) and Young, Ramsdale, & Rust (1996). Young et al. (1997) compared the mammographic image quality and MGD of standard 28 kV with automatically selected kV for Mo/Mo target/filter combination of Philips MammoDiagnost 3000 mammographic machine within NHSBSP service. They concluded that the automatic kV selection resulted in slightly better image quality with a slight increment in MGD. However, Young, Ramsdale, & Rust's (1996) work compared the mammographic image quality and MGD of the standard 28kV with automatically selected kV of different target/filter combination (Mo/Mo, Mo/Rh, and W/Rh), using a Siemens Mammomat 3000 machine. They found that the automatic kV selection showed approximately comparable image quality and MGD for thin breasted clients. For thick breasted clients (60 mm and more), however, the use of AEC reduced the average MGD from 2.9 mGy to 1.87 mGy with a small reduction in image quality (Young, Ramsdale, & Rust, 1996). Currently, the European Commission (2013) documents that the mammographic machine should be equipped with full AEC, thus neither the systems with only manual or semi-AEC, which select the target/filter combination and kV value only, are permitted.

3.4.5 Generator

High frequency generators are typically used for FFDM. This type of generator is characterised by its small size, fast response, stability and lack of voltage ripples (Bushberg et al., 2002). It is a single-phase system which rectifies the AC input into DC voltage, which is then fed to a special circuit where it is changed to a high frequency (5-10 kHz). The resulting ripple in tube voltage is about 1%. Mammographic generators are usually designed to produce a maximum of 600 mAs in order to avoid the excessive radiation dose to the patient (Bushong, 2013).

3.4.6 Digital Mammographic Viewing Workstations

The final stage of the digital mammographic examination is image display and interpretation (Wang & Geiser, 2013). The FFDM unit is supplied with two different types of viewing workstations. The first is the acquisition workstation, and the second is the reporting workstation. The acquisition workstation display is of lower quality (e.g. 3 megapixel) and is used by the practitioners to assess mammographic image quality. The reporting workstation,

however, is typically supplied with two specialist medical-grade 5 megapixel monitors (IAEA, 2011). A wide range of software options are available within the reporting workstation. These include: magnification; windowing in which both image contrast and brightness can be manipulated; image rotation and flip; image window inversion (black/white) to view both image negative and positive; measurements such as size, area and angle; spatial resolution filtering, which helps in image noise reduction and edge enhancement. All of these software tools have the advantage of post-acquisition image processing, allowing for mammographic image quality improvement without additional patient radiation dose. This is one of FFDM's main advantages over conventional FSM (James, 2004; Kotre & Reis, 2015).

3.5 Digital Breast Tomosynthesis (DBT)

Mammography is an essential imaging modality for breast cancer detection with about 85% sensitivity and 90% specificity (Destounis & Gruttadauria, 2015). It has been reported that mammography's ability to detect breast cancer reduces as breast tissue density increases. In fact, 41% of breast lesions in high density breasts images are obscured by breast tissue (ALMousa, Ryan, Mello-Thoms, & Brennan, 2014). Mammography can detect about 80-90% of breast cancers in low density breasts and 50-60% in dense breasts (Baptista et al., 2014; Thomassin-Naggara et al., 2015). Reduced cancer detectability in dense breast tissue is a result of the tissue overlapping with the tumours in two-dimensional mammographic images (Blue Crossand Blue Shield Association, Kaiser Foundation Health Plan, & Southern California Permanente Medical Group, 2014; Diekmann & Bick, 2011). To overcome this problem in 2D FFDM images, a three-dimensional imaging technique known as digital breast tomosynthesis (DBT) has been developed (Smith, 2012).

DBT is derived from the conventional tomography technique which depends on the relative motion of the X-ray source, image receptor and patient (Gilbert et al., 2015; Thomassin-Naggara et al., 2015). The theoretical background and the earliest practical tomographic systems were introduced in the 1930s (Mertelmeier, Speitel, & Frumento, 2012). However, the first DBT images were produced by Niklason et al. (1997) around 1-2 years before the widespread clinical use of FFDM (Palazuelos, Trujillo, & Romero, 2014; Sechopoulos, 2013a). Niklason et al. (1997) used the breast tomographic technique of moving X-ray tube

and fixed image receptor to scan the phantom of the American College of Radiology (ACR) and four mastectomy samples. Both types of image receptors, film-screen and digital flat panel detectors, were utilised in this study. They reported superior lesion visibility of tomographic three-dimensional images when compared to that of two-dimensional FFDM images for three samples, and comparable lesion visibility by both techniques for the last sample. The main purpose of using DBT is therefore to produce a series of low-dose mammographic images with high spatial resolution (per one mammographic projection), enabling visualisation of the breast tissue in slices. This results in the minimisation or elimination of breast tissue overlap. Consequently, the shape and size of tumours can be clearly delineated (Destounis & Gruttadauria, 2015). The total MGD of one DBT projection is more than that of one FFDM projection but less than that of two FFDM projections (Destounis & Gruttadauria, 2015). Overall, the DBT MGD of 4.5 cm PMMA phantom was 20% higher than the MGD of FFDM for the same phantom (Strudley, Looney, & Young, 2014).

3.5.1 DBT Physics and Instrumentation

DBT is a recently developed technique based on digital mammography (Palazuelos, Trujillo, & Romero, 2014). The image acquisition geometry of DBT is similar to that of FFDM with a moving X-ray tube at regular angular intervals, in a plane around the compressed breast which rests on static support. The X-ray tube movement range is different for each manufacturer. During exposure, the image receptor is either fixed or rotated to keep it perpendicular to the X-ray tube (Feng & Sechopoulos, 2012; Sechopoulos, 2013a). Several DBT prototype machines have been introduced by different manufacturers. Examples of these include GE Essential, Hologic Selenia Dimenssion, IMS GiottoTOMO, Philips MicroDose, Planmed Nuance Excel, and Siemens MAMMOMAT Inspiration. All of these machines have the same purpose but each has its specific characteristics. So far, the Hologic Selenia Dimensions machine is the only one that has been approved in America by the FDA, in 2011 (Destounis & Gruttadauria, 2015; Sechopoulos, 2013a).

3.5.1.1 Image Acquisition

The DBT machine has the same structure as FFDM units, consisting of an X-ray tube mounted within the arm, a breast compression paddle, a breast support and a digital image

receptor (Sechopoulos, 2013a). The only difference between FFDM machines is that the DBT X-ray tube, as well as the image receptor in some DBT brands, can rotate across an arc of 11^{o} to 50^{o} during exposure, depending on manufacturer design, see **Figure (3-4)**. This produces between 9 and 25 images (Lim & Maxwell, 2015). For instance, the Hologic Selenia Dimensions has a range of 15 degrees, between -7.5 and +7.5 degrees. It generates 15 images per view (Feng & Sechopoulos, 2012). The image acquisition process is achieved either by continuous exposure during X-ray tube movement, or pulsed exposure at each angle of tube movement. Shorter acquisition times are required for the continuous method, however lower image resolution can result due to motion blur. For both methods the acquisition time ranges from 3s to 25s per single view (Lim & Maxwell, 2015). The image acquisition time should be minimised to be as short as possible to avoid patient movement blur. For DBT imaging the required X-ray energy is slightly higher than that for FFDM. Therefore, the spectra of a tungsten target with Al, Rh, or Ag filters are typically used (Sechopoulos, 2013a; Yaffe & Maidment, 2014).

The Sectra MicroDose from Philips is a different DBT machine design which is based on the slit-scan photon counting technique. In this machine, a collimated fan shaped X-ray beam and multi-slit linear detector are used to scan the compressed breast across an arc (Sechopoulos, 2013a). The geometry of this machine is completely different to that of other DBT units. The focal-image receptor distance of this machine is 66 cm. Also, there is a 1.93 cm gap between the breast support and the image receptor. The rotation centre is located 104 cm below the focal spot level (Dance, Young, & van Engen, 2011). The main advantages of Sectra MicroDose unit over the traditional DBT units are that less electronic noise is produced, there's a lower patient radiation dose of about 1/20, and it can determine the energy of a transmitted X-ray photon which is useful for both breast absorption measurements and breast composition (Schmitzberger et al., 2011). However, the main disadvantage of this machine is that it cannot be used to acquire conventional two-dimensional images (Sechopoulos, 2013a).

Gilbert, Young, Astley, Whelehan, and Gillan (2010) documented in NHSBSP publication #69 that the breast compression in DBT is the same as in FFDM and they preferred to achieve them both in one compression. However, a Monte Carlo study by Saunders, Samei,

Lo, and Baker (2009) found that a 12.5% reduction in breast compression during DBT examinations results in approximately the same MGD and constant lesion conspicuity for both breast microcalcification and mass. Work by Förnvik et al. (2010) investigated the effect of half compression force on image quality during DBT examination for 45 women. They reported equivalent image quality for both compression values. A comparable effect of half breast compression on image quality for 130 Malaysian women has been obtained by Suhaimi, Mohamed, and Ahmad (2015). Overall, more studies are required to consider the effect of breast compression reduction in DBT on both image quality and patient radiation dose.

3.5.1.2 DBT Image Reconstruction

The tomographic images are reconstructed from the series of projections through filtered back projection or iterative reconstruction algorithms (Sechopoulos, 2013b). The image reconstruction process is achieved by shifting the projection images with respect to the frame of the image. Therefore, the structures at the specific plane are visualised in the same place, at the frame. Then the images are added together, reinforcing the contrast of the structures' image in the selected plane and blurring out the structures in other planes. **Figure (3-5)** illustrates the tomosynthesis image reconstruction process, (Kotre & Reis, 2015). Tomosynthesis produces the highest spatial resolution in the planes and poorer resolution between them. The limited range of acquisition angles in DBT makes the data of the tomosynthetic projection less complete than computed tomography (CT). Therefore, the tomosynthesis reconstructed images are pseudo three-dimensional images of breast tissues (Yaffe & Maidment, 2014).

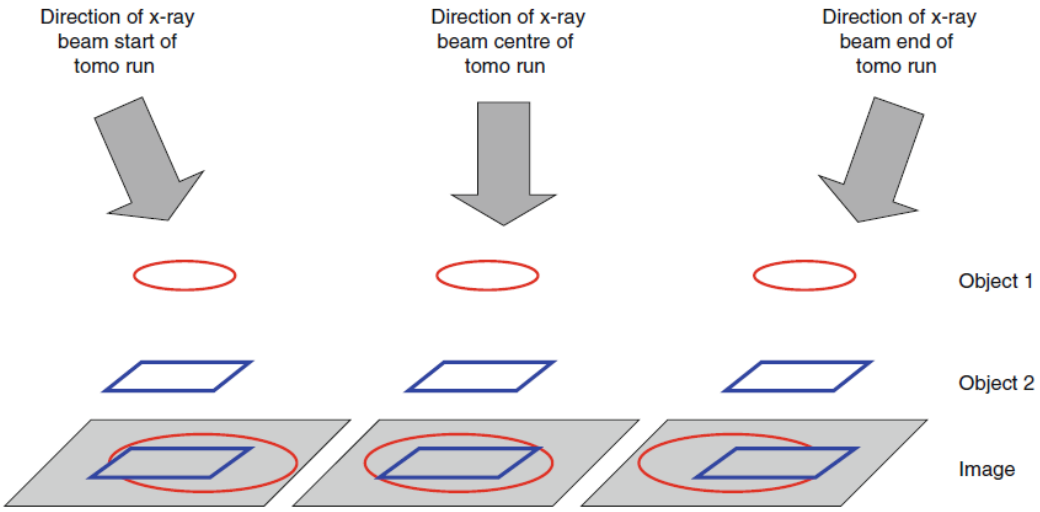

Figure (3-4) Demonstrates the image acquisition process in DBT (Kotre & Reis, 2015).

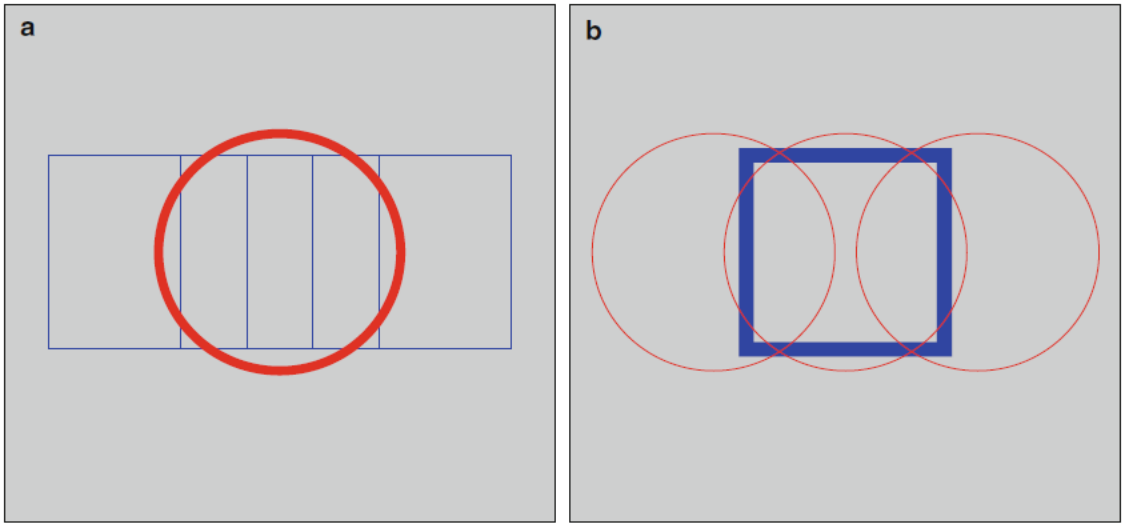

Figure (3-5) Demonstrates the image reconstruction process in DBT **(a)** In the level of circle plane and **(b)** In the level of square plane (Kotre & Reis, 2015).

3.5.2 Clinical Performance of DBT (for both diagnosis and screening)

DBT images are produced in the standard conventional 2D mammography projections (cranio-caudal and medio-lateral oblique) in the form of slices, similar to computed tomography (CT) (Skaane, 2012; Tagliafico, Tagliafico, & Houssami, 2013). The clinical improvement of DBT was first demonstrated using phantoms and mastectomy images (Gilbert et al., 2010). Many researchers have investigated the clinical benefit of DBT for

screening and diagnostic purposes (Skaane, 2012). **Table (3-2)** details the studies that investigated the effect of integrated DBT with 2D FFDM on breast cancer detectability, recall rate, and the time required for imaging. Overall, the majority of these studies concluded that the addition of DBT to 2D FFDM resulted in better cancer detectability, lower recall rates, more details about the lesion size and location, and longer acquisition and interpretation times when compared to just using 2D FFDM. However, the work by Lang et al. (2016) was the only one which examined the use of DBT alone for screening purposes. Lang et al. (2016) reported that one-view (MLO) DBT screening of 7500 women showed a statistically significant increase in both breast cancer detection and recall rates, while this recall rate is still acceptably low. Accordingly, they suggested that for breast cancer screening the use of one-view DBT alone might be suitable (Lang et al., 2016).

The diagnostic performance of DBT for breast mass characterisation compared to that of spot-view mammograms and supllemental diagnostic mammograms was considered by Noroozian et al. (2012) and Zuley et al. (2013). Noroozian et al. (2012) evaluated DBT images and spot-view mammographic images in 67 breast masses. In this study both DBT and spot-view mammography showed similar diagnostic efficacy in terms of mass visibility and BI-RADS assessment. The main limitation of this work was the small number of radiologists (four) who read the images. However, statistically significant higher diagnostic accuracy of DBT images was reported by Zuley et al. (2013) compared to supplemental dianostic mammograms. The conclusions of this work were based on the image evaluation of 182 women who underwent both diagnostic 2D FFDM and DBT (Zuley et al., 2013). Regardless of the purpose of DBT usage (screening or diagnostic), it demonstrates the breast tissue architecture more clearly than 2D FFDM, especially in dense breasts (Destounis & Gruttadauria, 2015).

Table (3-2) Lists the studies that investigated the clinical performance of DBT compared to digital mammography (DM).

Study Author	Study Population	Study Results
Gur et al. (2009)	125 examinations by both DM and DBT	DM+DBT resulted in 30% reduction in recall rate, DBT showed 10% (non-significant) reduction in recall rate. Comparable sensitivity for DM, DBT, DM+DBT.
Kopans, Gavenonis, Halpern and Moore (2011)	119 women with breast calcification	DBT can demonstrate the breast calcification with equal or better clarity compared to DM.
Michell et al. (2012)	738 symptomatic women	Addition of DBT increases the accuracy of screen-detected soft-tissue mammographic abnormalities.
Bernardi et al. (2012)	20 for acquisition time,100 cases for each DM, DM+DBT	DBT+DM increase both the acquisition and interpretation times.
Mun et al. (2013)	173 malignant breast lesions by both DM and DBT	DBT is significantly better than DM in the evaluation of small lesion size and this superiority increase with dense breasts.
Haas et al. (2013)	13158 women, 6100 of them receive DBT in addition to DM	Significant reduction in recall rate with DM+DBT especially for younger than 50 years and dense breast, 9.5% non-significant increment in cancer detectability.
Rafferty et al. (2013)	1192 women by both DM and DBT	DM+DBT resulted in significant increase in diagnostic accuracy and significant decrease in recall rate.
Rose et al. (2013)	13856 examination by DM, 9499 by DM+DBT	DBT result in significant decrease in recall rate and increase cancer detection rate especially in invasive cancer.
Ciatto et al. (2013) (STORM study)	7292 women by both DM and DBT	DBT significantly increase breast cancer detection and can reduce recall rate.
Skaane et al. (2013) (Oslo trial)	12621 women by both DM and DBT	DBT significantly increase cancer detectability and decrease the false-positive rate.
Dang, Freer, Humphrey, Halpern and Rafferty (2014)	1502 by DM+DBT and 2163 by DM	The use of DBT with DM in screening increase the interpretation time.
Friedewald et al. (2014)	281187 by DM, 173663 DM+DBT	DM+DBT results in decrease in recall rate and increase in cancer detection rate.
Thomassin-Naggara et al. (2015)	155 lesion diagnosed by DM, DBT, biopsy	The addition of DBT improves breast cancer detection by reducing the percent of undiagnosed cancer.
Gilbert et al. (2015) (TOMMY trial)	7060 women screened by both FFDM and DBT	Borderline significant increase in sensitivity (p = 0.07) from 87% for DM to 89% for FFDM+DBT, the difference increase for invasive cancers & dense breast
Lang et al. (2016) MBTST(Malmo trial)	7500 screened by MLO DBT & DM	One-view DBT has significant increase in cancer detection and recall rate.

3.6 Anatomical Characteristics of the Breast in Mammographic Images

In mammograms, the breast tissue pattern is primarily created by the shadow of fatty components as well as the functional element (glandular tissue) of the breast (Kopans, 2007). The differential radiographic contrast of these elements enables X-ray breast imaging to occur (Wentz & Parsons, 1997). Breast composition differs among women, through the relative proportions of fatty and glandular tissue, the higher the proportion of glandular tissue, the more dense the breast. Since the glandular tissue attenuates X-ray more than adipose tissue, the radiolucent fat arises as dark areas, whereas dense glandular tissue appears as light areas, see **Figure (3-6)** (Boyd et al., 2007; Boyd et al., 2010). However, these attenuation differences are small, therefore high contrast mammographic imaging systems are required to make breast anatomy visible (Wentz & Parsons, 1997).

As was noted in section 3.5.2 (page 46), mammography examinations may require supplementary views in addition to the two basic CC / MLO views (Yankaskas & Gill, 2005). The basic mammographic views were the CC and lateral, used until the late 1970s wherein the MLO view was first described by Lundgren (1977). The MLO view depended on the anatomical fact that when the arm is raised the breast will appear continuous with the pectoral muscle in caudo-medial direction (Lundgren, 1977). It has been found that the use of single-view mammography results in a higher recall rate and leads to reduction in mammographic breast cancer detectability, wherein 11% - 25% of breast cancers can be missed (Kopans, 2007). The radiation dose limit for standard mammographic views was determined by the European Commission, IPEM and NHSBSP to be less than 2.5 mGy per image (European Commission, 2006; IPEM, 2005; Strudley et al., 2014). Since the pectoral muscle is displayed in MLO view, the breast MGD is more than in CC view. This MGD difference between CC and MLO may be up to 30% (Gomes et al., 2011).

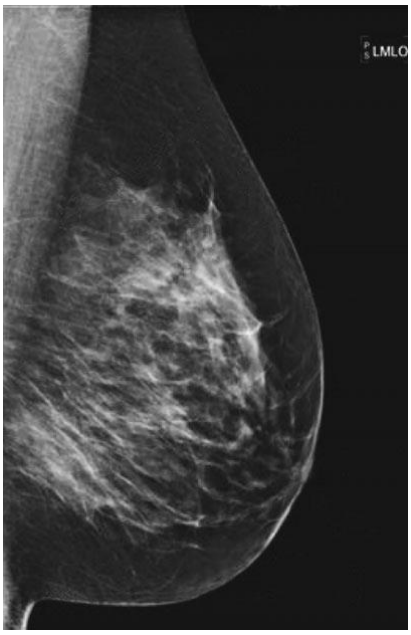

Figure (3-6) Breast MLO image illustrates the radiographic appearance of different breast tissues (Darlington, 2015).

Breast imaging is performed while the breast is compressed onto the image receptor. As mentioned in section 3.4.2 (page 37), breast compression helps to improve image quality and reduces the breast radiation dose (Kita, Highnam, & Brady, 1998). The compression should be sufficient to prevent the slip of breast tissue during exposure but not too much as to cause patient discomfort. Sometimes, pain may result from skin pinch during compression; in this case the compression should be stopped and released (Kopans, 2007).

3.6.1 Cranio-caudal (CC) Projection

CC projection is one of the routinely obtained projections when using conventional, two-dimensional breast X-ray imaging (Kopans, 2007). In CC projection, the X-ray beam is directed to enter the superior aspect of the breast and leave through the inferior aspect. The image receptor is positioned parallel in the horizontal orientation and perpendicular to the central ray (Magnus, 1995). The breast should be positioned on the AEC device. CC projection is used to visualise the beast tissue as a whole, except the most lateral and axillary portion (European Commission, 2006). The ideal CC projection should visualise several important anatomical structures including: the sharp shadow of the pectoral muscle on the border of the image; the shadow of retro-mammary fat tissue; the medial and lateral glandular tissue without folds; a symmetrical view of the right and left breasts; and the nipple

seen in profile, **Figure (3-7)** (Gomes et al., 2011; European Commission, 2006). Another positioning consideration when producing CC images is to set the height of the breast support correctly in relation to the infra-mammary angle (Smith, Szczepura, Mercer, Maxwell, & Hogg, 2015; European Commission, 2006). The typical compressed breast shape in CC projection is semi-circular with approximately 10 cm between the nipple and the chest wall and an approximate breast base length of 20 cm for an 'average' woman (Feng , Patel, & Sechopoulos, 2013). The average compressed breast area in the CC projection, which was assessed in 880 British women by Diffey (2012), was 157.6 cm^2. A similar result (157.3 cm^2) was reported by Boone, Lindfors, Cooper, and Seibert (2000).

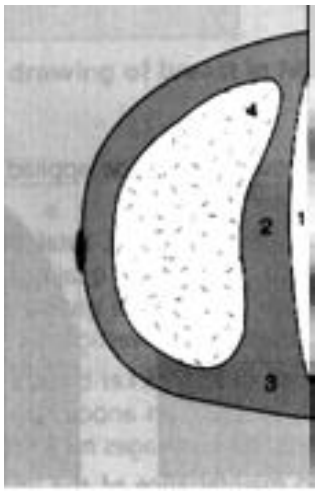

1. Represent the shadow of pectoral muscle.
2. The shadow of retro-mammary fat line.
3. Shadow of medial breast tissue.
4. Lateral glandular tissue shadow.
5. Nipple shadow in profile.

Figure (3-7) Shows a diagram of the breast anatomical criteria that should be seen in typical CC projection (IAEA, 2005).

3.6.2 Medio-lateral Oblique (MLO) Projection

The MLO projection visualises the whole breast tissue in one view; especially the supero-lateral part of the breast which is more commonly affected by cancer than other breast parts (Magnus, 1995). For this reason the MLO projection is chosen for DBT imaging. The typical MLO projection should image the breast from the axilla down to include the infra-mammary angle. Unlike other radiography areas, the word oblique in mammography refers to the breast compression plane (Kopans, 2007). Much more care is required to produce MLO images than CC images because an imperfect MLO projection affects the image quality criteria more than that in CC (IAEA, 2005). In MLO projection, the X-ray beam enters the breast through supero-medial aspect and leaves it through the infero-lateral aspect (Magnus, 1995). The

image receptor is set at an angle of approximately 45^{o} from horizontal, but can range from 40^{o} to 60^{o} depending on the woman's body habitus (Mercer, Hill, Kelly, & Smith, 2015).

According to the European Commission (2006), the breast anatomical criteria that should be seen in MLO images are: the infra-mammary angle, although the visualisation of this angle as a whole is affected by breast size , it is strongly related to breast positioning; supero-lateral glandular tissue, this criteria can be easily achieved; the shadow of nipple and retro-glandular adipose tissue; the symmetrical image of both breasts with no recognised skinfold; the reproduction of the pectoral muscle in the image angle, which is one of the most important anatomical criteria to indicate the correct positioning in MLO projection, see **Figure (3-8)** (Gomes et al., 2011; Bentley, Poulos, & Rickard, 2008; European Commission, 2006). In the upper posterior margin of the image, the pectoral muscle should be visualised as a triangular shadow with a mean value of its length and the width at approximately 140 mm and 46 mm (Spuur, Poulos, Currie, & Rickard, 2010). The shape and size of the pectoral muscle in the mammogram image generally depends on individual body variations, thorax length and muscle development, and positioning angulation (Bentley, Poulos, & Rickard, 2008). The breast area demonstrated in the MLO mammogram is greater than that in CC by approximately 17.7 cm^2 (Diffey, 2012). Kunosic (2012) stated that in MLO projection the mean compressed breast thickness is 20-23% higher than that in CC projection, but other researchers found that this increment to be around 5mm (Dellie, Rao, Admassie, & Meshesha, 2013; Helvie, Chan, Adler, & Boyd, 1994; IAEA, 2005).

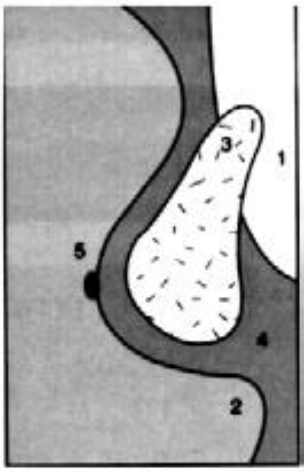

1. Shadow of pectoral muscle.
2. Infra-mammary angle.
3. Superio-lateral glandular tissue.
4. Shadow of retro-glandular fat tissue.
5. Shadow of the nipple in full profile.

Figure (3-8) Shows a diagram of the breast anatomical criteria that should be seen in typical MLO projection (IAEA, 2005).

3.6.3 Supplementary Mammographic Projections

Diagnostic mammography can include extra projections in addition to the standard projections (CC and MLO). These supplementary mammographic projections are usually performed for either symptomatic women with palpable breast abnormality, breast discharge, painful breasts, or abnormal skin changes, or for women with suspected or positive screening results (Yankaskas & Gill, 2005). Due to chest geometry, the extreme medial and extreme lateral tissues of the breast cannot be included in the CC/MLO standard mammographic projections, and supplementary projections are usually utilised to investigate the lesions in these aspects of the breast (Kelly, 2015; Kopans 2007). However, these increase patient radiation dose by 3.9 - 5.2 mGy depending on the number of projections (Destounis & Gruttadauria, 2015).

3.7 Screening Mammography

Early diagnosis and treatment of breast cancer is the key to reduce mortality. Mammography is considered to be a cost effective technique for the early detection of breast cancer and for many years it has remained to be the recommended modality for both diagnosis and screening (Nsiah-Akoto, Andam, Adisson, & Forson, 2011). Screening mammography involves the evaluation of asymptomatic women with the intention of detecting impalpable breast cancer early in its growth, when recovery is still possible (Kopans, 2007). The first attempt to use X-ray breast imaging as a tool for the early detection of breast cancer was in 1960 by Robert Egan. He used mammography and clinical breast examination to screen 2000 healthy asymptomatic women and identified occult carcinoma in 53 of them (Nass et al., 2001).

The suitable measure for screening mammography benefit is its contribution to the reduction in breast cancer mortality (Marmot et al., 2013). The first screening mammography trial to show a reduction in breast cancer mortality, by using mammography only, was the Swedish two-county trial which demonstrated a reduction of 30% in breast cancer mortality among women aged between 40 and 74 years (Tabár et al., 2011). The most reliable information about screening mammography is provided by the randomised controlled trials. In **Table (3-3)** all the randomised trials of mammographic breast cancer screening are summarised. Since a very long time is required for follow up in these trials, most of the randomised controlled

trials for screening mammography assessment are from the 1980s and earlier. However, many developments in breast cancer treatment and diagnosis (mammography) have occurred since this work (Marmot et al., 2012). Therefore, the effect of screening mammography has continuously been investigated by many researchers throughout the world as time has progressed.

Table (3-3) Summarises the common randomised trials of mammographic breast cancer screening.

Screening trial	Trial start date	Participant age range (year)	Breast cancer mortality reduction
New York Health Insurance Plan (HIP) (Shapiro, 1997)	1963	40-69	25% reduction in breast cancer mortality for women aged 40–49 and 50–59 at time of entry.
Malmö trial (Andersson et al., 1988)	1976	44-68	Mortality reduction is age dependent; no overall reduction but 20% reduction for women aged 55 year and older.
Swedish Two-County (Tabár et al., 2011)	1977	40-74	30% reduction in breast cancer mortality resulted from screening mammography.
Edinburgh trial (Alexander et al., 1994)	1978	45-64	20% reduction in breast cancer mortality resulted from screening mammography for women 50 years and older.
Canada trial (Miller et al., 2014)	1980	40-59	No resulted reduction in breast cancer mortality due to screening mammography.
Stockholm trial (Frisell, Lidbrink, Hellstrom, & Rutqvist, 1997)	1981	40-64	In women 40-49 year there was tendency for mortality reduction, 50-64 year women showed better survival with screening mammography.
Göteborg trial (Bjurstam et al., 2003)	1982	39-59	20-30% reduction in breast cancer mortality and this reduction may be achieved for younger than 50 year old women by short screening interval.
UK Age trial (Moss et al., 2015)	1990	39-41	Annual screening mammography for women 40-49 year results in mortality reduction.

The recurrent evaluations of the Swedish two-county trial outcome data demonstrated that the relative breast cancer mortality remained constant despite the continuous increase in breast screening invitations. However, the absolute number of lives saved due to screening has increased with time. This is because long screening time is required to reduce the breast cancer mortality. Accordingly, long-term follow up is necessary to prove the benefit effect

from screening on breast cancer deaths. Overall, a significant and substantial reduction in breast cancer mortality due to screening mammography has been reported by the latest update of Swedish two-county trial (Tabár et al., 2011). These results are consistent with outcome data of other screening trials (Shapiro, 1997; Andersson et al., 1988; Alexander et al., 1994; Frisell, Lidbrink, Hellstrom, & Rutqvist, 1997; Bjurstam et al., 2003; Moss et al., 2015). The Canadian screening trial was the only one which documented that screening mammography does not affect breast cancer mortality (Miller et al., 2014).

In the UK, Marmot et al. (2012) assessed the performance of the UK mammography screening programme by reviewing the results of 11 relevant randomised trials. Marmot and his colleagues concluded that the UK mammography screening programme should continue as it resulted in approximately 20% reduction in breast cancer mortality. In the US, the ACS (2013a) reviewed evidence too, along with the International Agency for Research on Cancer (IARC)(2015) and the US Preventive Services Task Force (Nelson et al., 2016). They illustrated that screening mammography significantly reduces breast cancer mortality for women aged 50-69 years. The Norwegian mammography screening programme invites women aged 50-69 years for biennial screening mammography. The effect of this on breast cancer mortality was studied on four groups of women by Kalager, Zelen, Langmark, and Adami (2010). They reported that only one third of the reduction in breast cancer mortality was due to screening mammography and the other two thirds were attributed to the improvement in breast cancer management and treatment. Consequently, the absolute reduction in breast cancer deaths resulting from the Norwegian mammography screening programme was attributed as 10%.

Gotzsche and Jorgensen (2013) reviewed and critically analysed data from the mammography screening trials and the meta-analysis studies; they documented that breast cancer mortality reduction is mainly due to the improvement in breast cancer awareness and treatment and a minor reduction was brought about by mammography. They also reported that breast cancer mortality reduction is not a reliable measure for screening mammography performance because of overdiagnosis and overtreatment which may result in unnecessary mastectomies and deaths. Accordingly, they recommended the reassessment of screening mammography because of the errors associated with published screening trials and

overdiagnosis. Similarly, work by Harding et al. (2015), who investigated the breast cancer incidence and mortality in the US counties over 10 years (2000 - 2010), reported that the prominent effect of screening mammography in US population was overdiagnosis and the breast cancer mortality reduction was not significant. Harding et al. (2015) built their conclusions on the fact that there was no reduction in the rate of large breast cancers detection. To this day breast cancer screening remains a controversial area (Gøtzsche & Jørgensen, 2013; Independent UK Panel on Breast Cancer Screening, 2013).

Since the introduction of screening mammography there have been ongoing debates about its harms versus its benefits. Djulbegovic and Lyman (2006) stated that screening mammography could not be recommended unless its benefits outweigh its harms. However, several disadvantages of screening mammography have been identified in literature. Firstly, its false negative rate, which is its inability to detect all breast cancers. Secondly, its false positive rate (wrong diagnosis), which results in time wasted in extra examinations and undesired anxiety. Finally, overdiagnosis, which results in the treatment of low risk breast cancers that may not always cause health problems (Gøtzsche, Hartling, Nielsen, & Brodersen, 2012; Jin, 2014; NHSBSP, 2003). The performance of any screening programme should be assessed by three important parameters. These parameters are sensitivity, specificity, and the positive predictive value. Programme sensitivity is the proportion of truly diagnosed cancer cases to the total number of actual cancer cases in the participants. Programme specificity is defined as the ratio of women truly identified without cancer. Positive predictive value is the ratio of the actual number of cancer cases against the number of abnormal cases detected by the programme. These parameters can be calculated using the following equations (Forrest, 1986; Nass et al., 2001):

$$Sensitivity = \frac{number\ of\ true\ positive\ cases}{true\ positive\ cases + false\ negative\ cases}$$

$$Specificity = \frac{true\ negative\ cases}{true\ negative\ casese + false\ positive\ cases}$$

$$Positive\ Predictive\ value = \frac{true\ positive\ cases}{true\ positive\ cases + false\ positive\ cases}$$

The performance of any screening programme depends on the participant's age (Jin, 2014). It has been found that annual screenings from 20-29 years of age may result in more radiation-induced cancer deaths than it prevents (Berrington de Gonzalez & Reeves, 2005). For women aged under 39, screening mammography is not recommended due to the low breast cancer incidence rate within this age group and the lack of evidence of cancer death reduction (Toward Optimized Practice [TOP] Working Group for Breast Cancer Screening, 2013). A reduction in breast cancer mortality of 4 deaths per 10000 screened women is achieved for women aged 40-49 years and 5-8 per 10000 women for the 50-59 years age group. The highest reduction, 12-21 cases per 10000 screened women, occurs in women aged 60-69 years (Nelson et al., 2016). The importance of screening mammography in breast cancer death reduction extends to women aged 70-74 years (IARC, 2015). The net benefit of screening mammography is also related to lifetime risk of radiation-induced cancer, which is an age dependent factor because younger tissues are more radiosensitive. According to NHSBSP (2003), the risk of radiation-induced breast cancer reduces from 16 per million per mGy to 4.2 per million per mGy as women's age increase from 40 to 75 years.

Some researchers consider that the reduction in breast cancer mortality of less than 10%, by screening mammography, has no net benefit because of the radiation risk. Consequently they do not recommend screening mammography before the age of 50 years (Berrington de Gonzalez & Reeves, 2005; Djulbegovic & Lyman, 2006). This has added another controversial point of screening mammography. In this context, the recommendations of the Swedish mammography screening programme were changed twice by the National Board of Health and Welfare in Sweden (Olsson et al., 2000). The first change was in 1987 to exclude women aged 40-49 years from screening mammography and the second, in 1998, re-included them in the screening programme (Lind, Svane, Kemetli, & Tornberg, 2010). Malmgren, Parikh, Atwood, and Kaplan (2014) studied the screening outcomes of 1162 women aged 75 years and older. They found that for this age group the obvious mammographic cancer detectability is comparable to that of younger women (younger than 75 years). Beyond the age of 50 years the risk of radiation induced cancer is considered acceptable due to the

reported benefits of screening mammography (Agt, Fracheboud, Steen, & Koning, 2012; Dellie et al., 2013). This relates directly to the central aim of this thesis; which has been considered in section 1.2 (page 1). Overall screening trials demonstrated a 20% - 30% reduction in breast cancer mortality due to screening mammography. Consequently, the risk of radiation-induced cancer from screening mammography is considered small and acceptable when compared to this mortality reduction.

The risk-benefit argument resulted in the introduction of organised mammography screening programmes in many countries. It must also be noted that the recommendations for screening mammography differ between countries. These differences are related to the age of screening commencement, cessation age of the screens, and the time interval between screens, **Table (3-4)**. The majority of mammography screening programmes (i.e. Belgium, Croatia, Cyprus, Denmark, Finland, Germany, Italy, Latvia, Lithuania, Luxembourg, Norway, Poland, Slovenia, Spain / Catalonia, Switzerland) include women aged 50-69 years. However, other countries (i.e. Australia, Canada, Iceland, India, Japan, Korea, Nigeria, Sweden, United States, and Uruguay) extend screening mammography to those at 40 years and may continue after 70 years. The New Zealand, Portuguese, and Spine (Navarra) mammography screening programmes cover women aged 45-69 years. Because of the early incident breast cancer in China, women aged 40-59 are invited for screening mammography. Biennial screening mammography is recommended by most of the mammography screening programmes except in the United States, United Kingdom, Malta and China. The US recommends annual screening and the others recommend triennial screening (Lerda et al., 2014; ICSN, 2015).

The effect of the screening frequency change from annual to biennial was studied by Coldman et al. (2008) in British Columbia. They used the data from the mammography screening programme of British Columbia (SMPBC) between 1988 and 2005. In the first decade of SMPBC (1988 -1997) annual screening was recommended. However, after July 1997 SMPBC had started to invite women for biennial screenings. Coldman et al. (2008) analysed the data of 658151 women to compare breast cancer detectability and mortality during these two periods. They found that this alteration in mammographic screening frequency affected neither the breast cancer detection rate nor the mortality rate.

Table (3-4) Illustrates the recommendations of mammography screening programmes in different countries across the world for women with an average risk of developing breast cancer (Lerda et al., 2014; ICSN, 2015).

Country(s)	Age of screening	Time interval between screens	Number of screens
Australia, Japan, Korea, United State (AAFP, NCI, and USPSTF)	40-75	2 years	18
Belgium, Croatia, Cyprus, Denmark, Finland, Germany, Italy, Latvia, Lithuania, Luxembourg, Norway, Poland, Slovenia, Spain (Catalonia), Switzerland	50-69	2 years	10
Canada , France, Israel, Netherlands	50-74	2 years	13
China	40-59	3 years	7
Czech	44-75	2 years	16
Estonia	50-62	2 years	7
Hungary	45-65	2 years	11
Iceland	40-69	2 years	15
India	40-74	1 year (40-49) 2 years (50-74)	23
Ireland	50-64	2 years	8
Malta	50-60	3 years	4
New Zealand, Portugal, Spain (Navarra)	45-69	2 years	13
Nigeria	40-70	2 years	16
Sweden	40-74	18 months (40-49) 2 years (50-74)	19
United Kingdom	47-73	3 years	9
United State (ACOG)	40-75	2 years (40-49) 1 year (50-75)	31
United State (ACS, ACR, and NCCN)	40-75	1 year	36
Uruguay	40-69	2 years (40-49) 1 year (50-69)	25

All the above explained screening categories in **Table (3-4)** are recommended for average breast cancer risk women. Some mammography screening programmes exclude high risk women, considering them as special cases (e.g. the Australian programme) (Cancer Australia, 2014), while other programmes have a specially designed screening category for them, (e.g. Canada, US and UK programmes), see **Table (3-5)** (ACS, 2013b; ICSN, 2015; Nelson et al., 2009; NHSBSP, 2013b). Some programmes also use other imaging modalities for screening, for instance ultrasound or magnetic resonance imaging *in addition* to screening mammography (NHSBSP, 2013).

Table (3-5) Illustrates the recommendations of mammography screening programmes in different countries across the world for women with a high risk of breast cancer (ACS, 2013b; ICSN, 2015; Nelson et al., 2009; NHSBSP, 2013b).

Country(s)	Age of screening	Time interval between screens	Number of screens
Canada	40-74	1 year (40-49) 2 years (50-74)	23
United Kingdom	40-73	1 year	34
United State (ACS)	30-75	1 year	46
United State (NCCN)	25-75	1 year	51

In the UK, the Forrest report (1986) recommended the introduction of single view (MLO) screening mammography for women aged 50-65 years with an interval of 3 years (Forrest, 1986). In 1988, the NHSBSP started to invite women aged 50-64 years for MLO, triennial screening mammography. In 2000, the NHS Cancer Plan proposed additional expansion in NHSBSP by using two views (MLO and CC) in screening mammography and extending the screening age to include women aged 64-70 years (NHSBSP, 2006). The latest age extension in NHSBSP commenced in 2012, to include women aged 47-73. This age extension was predicted to be completely implemented by 2016 (NHSBSP, 2014). These extensions approximately duplicated the number of screens within a woman's lifetime and hence the cumulative MGD is duplicated also. The consequent increase in risk of radiation-induced cancer is mainly attributed to earlier screening commencement because breast tissue radio-sensitivity decreases with age (NHSBSP, 2003). According to NHSBSP (2013b) publication #74, high risk women should be invited for annual screening mammography from 40 years old.

In 2009, the US Preventive Services Task Force changed their recommendation of screening mammography to be biennial for women aged 50-74 years (Nelson et al., 2009). However, the American Medical Association, American College of Radiology, American Cancer Society, and National Comprehensive Cancer Network have considered the annual screening mammography starting from 40 years old to be superior (Nelson et al., 2016). For high risk women, such as those with a family history of cancer, the American Cancer Society stated that annual screening mammography should start at 30 years old and continue as long as the women were in good health (ACS, 2013b). Nevertheless, the National Comprehensive

Cancer Network (NCCN) and the American Academy of Family Physicians (AAFP) recommended that the annual screening mammography for high risk women should commence either at 25 years old or from the earliest age of cancer onset in the client's family (5-10 years before the youngest breast cancer case in the family) (Tirona, 2013; Vetto, Luoh, & Naik, 2009). Screening frequency recommendation is critical as it directly relates to the mammographic radiation risk; the radiation risk of annual is twice that of biennial screening. Since breast tissues younger than 40 years are very radio-sensitive, mammographic radiation of early high risk women screening should be considered carefully. Early screening mammography radiation risk causes an additional breast cancer lifetime risk for women younger than 40 years.

3.8 Chapter Summary

Since the first use of X-rays for breast tissue imaging, a great development has been made in both mammographic equipment and techniques. In the early stages the main purpose of these developments was to produce better mammographic images (improve mammographic image quality). After that, the researchers started to consider both mammographic image quality and patient radiation dose. The most revolutionary development was the production of a dedicated mammography machine. This machine's use of Mo/Mo target/filter combinations reduced breast radiation dose and improved mammographic image quality. The introduction of other target/filter combinations (Mo/Rh, W/Rh) led to further reductions in radiation dose without affecting the mammographic image quality. Although the use of anti-scatter grids improved image quality, they increased the patient radiation dose. Both image quality and patient dose were improved with developments in breast compression devices. Finally, the development of image recording methods from conventional radiography films to xeroradiography and industrial films, then finally to film-screen decreased the radiation dose several times. After this the introduction of digital detectors resulted in more image quality and a lower radiation dose.

Although FFDM has better breast cancer detectability than film-screen mammography, FFDM still has the same limitations as film-screen. DBT has been developed to overcome the 2D image limitation by producing pseudo 3D images of the breast tissue. Many controversial points about screening mammography have been identified in the literature.

The most controversial point is the net benefit of screening mammography due to the high reported overdiagnosis rate. Another is the screening programme design (starting / cessation ages and frequency of screening). These controversies lead to major differences in screening mammography recommendations throughout the world. Surprisingly the radiation risk variation due to recommendations differences is not considered. Overall, mammography has been considered as a cost-effective technique for breast cancer screening, and the radiation risk, which generally related to MGD, is minimal and accepted.

Chapter Four
Mammography Dosimetry

4.1 Chapter Overview

This chapter will demonstrate the dosimetric considerations of mammography, including a general background about the risk of radiation-induced cancer and the minimal radiation dose for this risk occurrence. In this context, the two models, linear no-threshold and threshold, are discussed. Literature from different data sources (e.g. childhood cancers following early life irradiation, cancers following recurrent CT examinations, and cancer incidence in medical radiation workers and in high radiation background areas residence) are reviewed to investigate the reliability of these two models. Mammography dosimetry is then discussed in regard to three areas: MGD, its importance and limitations, with the corresponding calculation methods; the radiation dose for other organs from mammography; and the effective dose and effective risk from screening mammography.

The last three sections of this chapter contain detailed explanations about mammography dosimetric tools, including Monte Carlo simulation software, direct dose measurement instruments and breast tissue equivalent materials, respectively. Monte Carlo simulation software is of great importance in mammographic studies. In addition to its importance in dosimetric studies, to obtain MGD conversion factors, Monte Carlo simulation software is used to develop three-dimensional mammographic imaging modalities (e.g. digital breast tomosynthesis and dedicated breast computed tomography). Monte Carlo simulation softwares are available in different forms and several of them can be used in mammographic studies, especially those designed to simulate electron/photon transport (e.g. PENELOPE and MCNPX (Di Maria et al., 2011). Different dose measurement instruments are utilised in dosimetric studies (e.g. ionisation chambers, semiconductor detectors, thermo-luminescence detectors, and optically stimulated luminescence dosimeters), and each type of these dosimeters are suitable to be used in different circumstances. For instance, thermo-luminescence detectors are more likely to be used for *in vivo* dose measurement due to their small size and tissue equivalency. Since mammography examination uses ionising radiation (X-ray), dose measurement experiments cannot be directly performed on patients. Therefore,

breast tissue equivalent materials are used to make breast phantoms necessary for assessing MGD. Different breast tissue equivalent materials and their properties are discussed in the last section of this chapter.

4.2 Risk of Low Radiation Dose

According to epidemiologists, the term "risk" is utilised to describe the association of data (cancer incidence and radiation exposure) in two different styles: relative risk, which is the ratio of cancer incidence rate in an exposed population to that in an unexposed population; and absolute risk, which is the simple rate of cancer incidence in a specific population (NAS, 2006). Several methods can be used to express radiation lifetime risk:

1) ELR (Excess Lifetime Risk), which compares cancer incidence or mortality in two groups of the same population - one of them is [theoretically] exposed to radiation and the other is not;

2) REID (Risk of Exposure Induced-Death), which compares the death rate of specific causes in [theoretically] unexposed and exposed groups of a certain age and gender;

3) LLE (Loss of Life Expectancy), which gives an impression of the period of life lost due to radiation;

4) LAR (Lifetime Attributable Risk), which gives an account of excess mortality or incidence of cancer over a study period, with the backgrounds defined by a [theoretically] unexposed population (ICRP, 2007).

The radiation risk refers to the damage produced by ionising radiation due to energy deposition in tissues. This energy may result in ionisation within the tissues if the photons pass near an orbital electron and provide sufficient energy for the electron to be liberated from the atom (Statkiewicz-Sherer, Visconti, & Ritenour, 2010). The amount of damage is related to radiation dose, type of radiation, whether it is internal or external, time of exposure, radiation distribution (type of exposed tissue), and the individual's sensitivity which is influenced by gender and age (HPA, 2011). Females are at higher risk of radiation-induced cancer than males (Balonov & Shrimpton, 2012). Younger patients are at a higher risk because they have a longer remaining life span. For example, the risk of radiation

damage for a 20 year old patient is twice that of a 40 year old patient. The latter has double the risk when compared to a 60 year old patient. The radiosensitivity of young children is 3-4 times more than that of adults (Lin, 2010).

In general, the radiation interactions with tissue are either direct, wherein the radiation energy is directly transferred to the DNA causing structural changes in its molecules; or indirect interaction, where the radiation energy is absorbed by water molecules forming free radicals which in turn cause damage to DNA molecules. It has been found that for X-rays with 100 mGy, 30-40% of the DNA damage is due to direct interaction and the remaining 60-70% of the damage results from indirect interactions (Suzuki & Yamashita, 2012). The adverse health effects of radiation can be classified into two groups: deterministic effects, which follow high radiation doses and result in relatively immediate and predictable tissue reactions and damage (this damage can occur within minutes, hours, days and even weeks); and stochastic effects, which follow low radiation doses and may result in cancer development (ICRP, 2007). Development is based on probability. The lag period between irradiation and cancer development for stochastic effects is at least 5 years and may reach to 10 or 20 years (Lin, 2010).

Stochastic effects usually occur due to mutations in DNA which occur randomly. In general, the probability of stochastic effects' occurrence increases as the radiation dose increases. The dose-response curve determines the probability of stochastic effects' occurrence, with radiation dose being the root cause. Both linear and linear-quadratic dose-response curves are used to describe the relationship. However, the severity of the resultant disease is not related to radiation dose because the cancer produced by a 2 Sv radiation dose is not more severe than cancer produced by 0.2 Sv radiation dose. Stochastic effects are classified into radiation-induced cancer and reproductive cell damage, which affects sperm and ova and causes defects in offspring (Statkiewicz-Sherer et al., 2010). For radiological doses ranging from 5 to 100 mSv, data from life-span studies (LSS) of atomic bomb survivors revealed that the risk of radiation-induced cancer was strongly related to the radiation dose received. However, for lower doses and since more than 60% of the LSS cohort received radiation doses between 5 and 100 mSv, no strong evidence is available to describe the relationship between the risk of radiation-induced cancer and these low doses (Brenner, 2014).

Persistent controversy exists in literature regarding the risk of radiation-induced cancer from low dose ionising radiation. This creates a big challenge for epidemiological studies. In this context the controversy arises in questions about the dose threshold of cancer production, linearity and gradient of dose-response curves (Griffey & Sodickson, 2009). Overall, there are two opposing risk models to estimate the risk of low radiation doses. The first adopts the linear no-threshold principle. According to this model any dose, however small, can result in cancer incidence. However, the second model proposes that there is a specific threshold for radiation-induced cancer and below this threshold the radiation dose can be considered as safe (Prasad, Cole, & Hasse, 2004). Although, the ICRP (2007) and the National Academy of Sciences (NAS) (2006) have adopted the linear no-threshold (LNT) model, United Nations Scientific Committee on the Effects of Atomic Radiation UNSCEAR (2008) considered the LNT to be uncertain at radiation doses less than 100 mSv and it is no longer recommended for radiation-induced cancer assessment from such doses. This motivates many researchers to investigate the reliability of this model using different data sources.

Dobrzynski, Fornalski, and Feinendegen (2015) evaluated the risk of radiation-induced cancer and early childhood death for populations living in regions with different natural background radiation. They concluded that the risk of radiation-induced cancer due to such small doses and dose rates tends not to exist or is lower than expected by the LNT model. This can be explained by the adaptive physiological mechanism of tissues. In conclusion, Dobrzynski et al. (2015) found that for low doses and low dose rates, the LNT model is likely to be exaggerating the risk of radiation-induced cancer (Dobrzynski et al., 2015). The analysis of LSS cohort data for participants who received radiation doses ranging between 0-150 mSv illustrated that the risk of radiation-induced solid cancers is linear but at less than 100 mSv the cancer incidence increment is statistically insignificant (Suzuki & Yamashita, 2012).

The feasibility of the LNT model has also been investigated using cancer risk data in children after diagnostic and/or therapeutic radiation exposure (Kleinerman, 2006; Linet, Kim, & Rajaraman, 2009). Kleinerman (2006) reviewed several major studies that investigated childhood cancers following benign disease radiation treatment and diagnostic procedures. This study reported that the rates of brain, thyroid, breast, skin (non-melanoma) cancers, and

leukemia, were seen to be increased due to childhood irradiation. He also found that cancer risk increases with dose increment (Kleinerman, 2006). More recently Linet et al. (2009) highlighted studies that investigated the association of maternal prenatal and postnatal newborn irradiation with childhood cancers. They stated that the data about this relationship is limited and more research is required (Linet et al., 2009).

Some investigators evaluated the low dose risk of radiation-induced cancer in patients subjected to recurrent CT scan examinations. A retrospective cohort study for the assessment of CT examinations' subsequent risk of radiation-induced leukemia and brain tumours was carried out by Pearce et al. (2012). Pearce et al. (2012) analysed data for patients younger than 22 years who had attended CT scan examinations within the UK NHS between 1985 and 2002, with the follow-up process continuing until the end of 2008. They found that when patient radiation cumulative dose increased from 5 mSv to approximately 50 mSv the relative risk of radiation-induced leukemia became 3.18, and 2.82 for brain tumours when the cumulative dose increased from 5 mSv to approximately 60 mSv. Similarly, Mathews et al. (2013) evaluated the cancer incidence in 680,211 patients (0-9 years old) who had undergone CT scan examinations between 1985 and 2005 with follow-up until 2007. A 24% increase in different tissue cancers was noted when compared to the general Australian population within the same age range (Mathews et al., 2013).

Since radiologists and radiographers were the initial occupational groups exposed to low radiation doses, the risk of radiation-induced cancer from low radiation doses was also assessed by retrospective analysis of the epidemiological cancer data in eight cohorts of radiologists and radiographers. In total, the data from more than 270,000 radiologists and radiographers working in different countries was analysed. The study cohorts were three cohorts from the US (radiologists, radiographers, and radiographers working in the US army during War World II), one UK radiologists cohort, Danish radiation therapy cohort, Japanese radiographers cohort, Chinese medical radiation workers and Canadian radiation workers (medical and industrial) cohorts. It has been found that there was an increased risk of leukemia in early radiation workers who worked before 1950. Solid cancer data was inconsistent and showed an insignificant increase in risk of different cancer types. In general, the risk of radiation-induced cancer in radiation workers (e.g. radiologists and radiographers)

tends to be zero or negligible in recent years (Yoshinaga, Mabuchi, Sigurdson, Doody, & Ron, 2004). According to Vaiserman (2010), this gradual reduction in the risk of radiation-induced cancer among radiation workers is attributed to the noteworthy developments in radiation protection.

The risk of radiation-induced cancer within the mammographic dose range was experimentally estimated by Brenner et al. (2002). In this work, C3H10T½ cells were irradiated *in vitro* using a 15–25 keV mono-energetic X-ray beam. The analysis of oncogenic transformation indicated that mammography increases the risk of breast cancer development by approximately two fold. This effect is age dependent making screening mammography commencing at the age of 50 more beneficial than that which commences at 40 (Brenner et al., 2002).

Tubiana, Feinendegen, Yang, and Kaminski (2009) considered that radiation doses below 100 mSv are safe (the threshold for risk of radiation-induced cancer). They provided evidence for this from radiation biological data and the results of epidemiological studies. The biological data includes the protective mechanisms that cells exhibit after exposure to low dose radiation, which are considered sufficient to protect the cell from DNA damage and oncogenic changes. With regard to epidemiological studies, Tubiana et al. (2009) concluded that the linear no-threshold model is not consistent and unsuitable for describing the risk of low dose radiation-induced cancer. Nevertheless, LSS found the linear and linear-quadratic dose-response relationships are applicable for all cancer types, especially solid cancers (Ozasa et al., 2012).

In conclusion, the accurate determination of radiation-induced cancer from low radiation dose is not easy. The limited data available about the risk from low radiation dose (used in conventional radiography) has resulted in controversy and uncertainty (Brenner, 2014; de González & Darby, 2004). According to the available data, the risk of radiation-induced cancer from low dose radiation is very small but unlikely to be zero (Wall et al., 2006). Therefore, the linear no-threshold model may be the best reasonable risk model for describing the relationship between the exposure to low energy radiation and solid cancer incidence (ICRP, 2007; Little, Wakeford, Tawn, Bouffler, & Gonzalez, 2009; NAS, 2006). To overcome uncertainty about the LNT model (Dobrzynski et al., 2015), Wall et al. (2006)

recommended the classification of low dose radiation cancer risk into four categories, as illustrated in **Table (4-1)**.

Table (4-1) Lists the four categories of low dose radiation risk described by Wall et al. (2006).

Risk category	Risk of radiation-induced cancer (case/10^6)
Negligible risk	Less than 1
Minimal risk	1-10
Very low risk	More than 10-100
Low risk	More than 100-1000

4.3 Mammography Dosimetry

Medical radiation exposure includes the radiation resulting from therapy and imaging, whether it is diagnostic or screening procedures. Medical imaging represents the major source of man-made ionising radiation for people (Olarinoye & Sharifat, 2010; Zenone et al., 2012). In the UK, radiographic examinations constitute 90% of artificial radiation sources and have resulted in a 23% increase of the UK per caput dose between 1998 and 2008 (Hart, Wall, Hillier, & Shrimpton, 2010). In the US, however, a six fold increase in medical radiation exposure was reported between 1980 and 2012, making medical radiation to be the cause of 50% of the US per caput dose (Linet et al., 2012). Therefore, for all radiographic procedures image quality should be produced with the least possible radiation dose; doses should be kept as low as reasonably achievable (ALARA) (Uffmann & Schaefer-Prokop, 2009).

Mammography is the most common imaging modality of the breast used for both screening and diagnosis. Since the breast cancer incidence is growing in many countries, the number of women undergoing mammography is also increasing (Bluekens et al., 2015). Mammography is the fifth most common X-ray examination in the UK and the sixth largest source of ionising radiation to the UK population from diagnostic imaging (Hart et al., 2010). Accordingly, there is a growing need for health professionals to be more conscious of the radiation risk associated with mammography especially for screening practice where asymptomatic healthy women are invited (Bosmans & Marshall, 2013). Extra attention should be exercised when assigning a woman into a high risk cancer category in which early

onset and more frequent mammography screening is required (Yaffe & Mainprize, 2011). Overall, it is necessary for any medical screening procedure involving X-radiation to be justified in term of its benefits and risk from ionising radiation.

With more than 50 years of mammography development, massive changes have been made in mammographic dosimetry. It has been reported that breast radiation dose is reduced from about 150 mGy when using industrial film to less than 2 mGy for FFDM (Huda, Nickoloff, & Boone, 2008). Incident radiation exposure (R) at breast surface and the entrance surface dose (ESD), which is measured by TLD at the breast surface, were the early quantities used to determine the radiation risk of mammography (Dance, Skinner, & Carlsson, 1999). However, since mammography uses low energy X-ray photons, the dose inside the breast rapidly reduces as the depth increases (Di Maria et al., 2011). Accordingly, different quantities were suggested as measures for mammographic radiation risk, such as midline breast dose and total breast energy (Dance et al., 1999). Work by Karlsson, Nygren, Wickman, and Hettinger (1976) proposed the use of breast glandular tissue radiation dose as a measure for mammographic radiation risk. Karlsson et al. (1976) utilised a mixture of alcohol and water as a breast phantom to study dose distribution within the breast. They also compared the radiation dose of different image receptors which resulted in equivalent mammographic image qualities. Later, in 1987, a mean glandular dose (MGD) for breast dosimetry was recommended for use by the ICRP (Dance et al., 1999). Mammography is a common screening practice and it is considered to be one of the most highly optimised techniques (Huda et al., 2008).

4.3.1 Mean Glandular Dose (MGD)

The risk of radiation-induced cancer from breast X-ray examination is small and is generally related to mean glandular dose (MGD) (Myronakis, Zvelebil, & Darambara, 2013). MGD is the amount of energy imparted from ionising radiation per unit mass of breast glandular tissue; glandular tissue has the highest radiation sensitivity among breast tissues (IAEA, 2011). MGD is utilised as a standard quantity in breast dosimetry, which is an essential part in quality control protocols of mammography and is recommended by several international committees such as ICRP, NCRP, and IPEM. MGD is fundamentally related to target/filter combination (radiation spectrum), X-ray tube output (kV, mA, and time), breast density

(glandularity), and breast size (compressed breast thickness) (Dance, 1990; Di Maria et al., 2011; IPEM, 2005). The effect of client age on MGD was investigated by Beckett and Kotre (2000) and Suad, Suada, Samek, Amila, and Samir (2013). Both studies reported lower MGD in older women than in younger because both breast density and compressed breast thickness decrease with age. Beckett and Kotre (2000) analysed their data in more detail and found that there is a linear inverse relationship between client age and the reduction percentage of required mAs.

Direct estimation of MGD is difficult and it has to be calculated from multiplying the incident air kerma by conversion factors, obtained by Monte Carlo simulation, as published by Dance, Skinner, Young, Beckett, and Kotre (2000a). This method is recommended in IPEM report 89 (IPEM, 2005), IAEA (2011), and the European Commission (2006). However, conversion factors published by Wu, Gingold, Barnes, and Tucker (1994) have been recommended by the American College of Radiology (Tsai, Chong, Ho, & Tyan, 2010).

MGD is considered to be an important element of mammographic quality assurance programmes. This is because it can be used as a parameter to evaluate the mammographic system performance, patient risk assessment, and different mammographic imaging techniques with regards to dosimetry (Säbel & Aichinger, 1996). Accordingly, MGD has been of great interest to a large number of researchers (Assiamah, Nam, & Keddy, 2005; Benevides, 2005; Di Maria et al., 2011; Dong et al., 2011; Geeraert, Klausz, Muller, Bloch, & Bosmans, 2012; Nsiah-Akoto, Andam, Adisson, & Forson, 2011; Oliveira et al., 2007; Sookpeng & Ketted, 2006; Tsai et al., 2010; Tyler, Strudley, Hollaway, & Peet, 2009; Zeidan, 2009). For instance, Hauge, Pedersen, Sanderud, Hofvind, and Olerud (2012) compared the MGD of 24 film-screen mammography systems with that of 7 FFDM systems using population based data from a Norwegian screening programme. They used data from 50 women for each machine and found that the average MGD value from FFDM machines was lower than that of FSM by 0.3 mGy (Hauge et al., 2012). Work by McCullagh, Baldelli, and Phelan (2011) calculated the MGD from the BreastCheck, the screening programme of Ireland, to assess clinical dose performance of 28 FFDM systems for three different manufacturers (Hologic, GE Healthcare and Sectra). Similar MGD values were reported for

Hologic and GE Healthcare machines. However, the Sectra photon-counting FFDM machines gave the lowest MGD value (McCullagh et al., 2011).

MGD values for three AEC operation modes (DOSE [dose], STD [standard], CNT [contrast]) of the GE Senographe 2000DS FFDM system were analysed by Chen et al. (2012). Chen et al. (2012) concluded that the MGD differences in the three modes were mainly attributed to the mAs selected by the system. Also, the MGD, together with image quality, are usually used to evaluate the mammographic system performance. In this context, Ciraj-Bjelac et al. (2012) investigated the image quality and MGD in 17 Asian, African and Eastern European countries. They expressed concerns about the recorded MGD value in some countries (Ciraj-Bjelac et al., 2012). The outcome performance of two CR mammographic systems (Siemens Mammomat 3000 Nova with Kodak Direct View CR850 digitiser and Fuji CR system model Profect ONE with HR-BD image plate) in Brazil were assessed by Oliveira et al. (2011) and Jakubiak, Gamba, Neves, and Peixoto (2013), using both MGD and mammographic image quality. Both studies utilised a PMMA breast phantom for MGD calculation and CDMAM phantom for image quality assessment. Diagnostic mammography MGD was estimated in Ethiopia by Dellie, Rao, Admassie, and Meshesha (2013). Dellie et al. (2013) used Dance's conversion factors to calculate the MGD from incident air kerma. They concluded that the MGD of diagnostic mammography in Ethiopia was within the accepted ranges recommended by the Institute of Physics and Engineering in Medicine (IPEM) and the American College of Radiology (ACR) which are 2 mGy and 3 mGy, respectively (Dellie et al., 2013).

The main limitation of MGD calculations using conversion factors is that, during Monte Carlo simulation, a homogenous breast phantom of different breast densities was used. As concluded by Sechopoulos, Bliznakova, Qin, Fei, and Feng (2012), the use of this homogenous phantom results in significant MGD overestimation. The greatest value of MGD overestimation has been recorded at low photon energies and this overestimation decreases as the photon energy increases. The result of this work, agrees with that of previously published work by Dance et al. (2005) who reported that the use of conversion factors may result in up to a 43% difference in calculated MGD due to glandular tissue spatial distribution. Accordingly, Geeraert, Klausz, Muller, Bloch, and Bosmans (2015) calculated the MGD for six breast phantoms with different glandular tissue distributions. Different MGD values have

been recorded for different phantoms. Therefore, Geeraert et al. (2015) suggested the use of total energy imparted in glandular tissue (GIE) instead of MGD.

4.3.2 Mammography: Dose to Organs Other Than the Examined Breast

Surprisingly few investigators have considered the radiation dose received by organs and tissues, other than the examined breast, from mammography. Most of these investigators utilised mathematical models to simulate mammography. Sechopoulos, Suryanarayanan, Vedantham, D'Orsi, and Karellas (2008) utilised the Geant4 Monte Carlo toolkit to simulate four-view film-screen mammography. Sechopoulos and colleagues estimated the radiation dose to all body tissues other than breast. They concluded that the doses were extremely small and that the Rh/Rh target/filter combination resulted in higher organ doses than those from Mo/Mo and Mo/Rh target/filter combinations. They also found that the second and third highest radiation dose, after examined breast, was received by the pectoral muscle and contralateral breast, respectively (Sechopoulos et al., 2008). The same procedure has more recently been used by Sechopoulos and Hendrick (2012) to estimate the radiation dose received by the thyroid gland during mammography. They considered the thyroid dose to be negligible in regard to radiation-induced cancer because four-view mammography would result in 1 cancer case per 166 million women. Sechopoulos and Hendrick (2012) also argued that the use of a thyroid shield may result in discomfort to the women and interfere with positioning which may cause image artifacts. Leidens, Goes, and Nicolluci (2013) used the Monte Carlo PENELOPE toolkit to estimate lung, heart and red bone marrow radiation dose during standard CC mammography with film-screen systems. They reported that only the lung received a considerable radiation dose (0.14% of the examined breast dose), while doses to the heart (0.033%) and bone marrow (0.0013%) were negligible (Leidens et al., 2013).

A study by Whelan, McLean, and Poulos (1999) used TLDs for the direct measurement of radiation dose received by women's skin overlying the thyroid during standard screening mammography (CC and MLO views for each breast) and diagnostic mammography. For more accurate measurements, two sachets, each one comprising three TLDs, were fixed on both sides of the women's necks. This study concluded that the average measured thyroid dose, which was 0.04 mGy, was insignificant compared to the 4 mGy dose received by the breast. Hatziioannou et al. (2000) also utilised TLDs accommodated inside an upper body

anthropomorphic Lucite phantom, which was made of Perspex slices designed to simulate female body contour. This was done to investigate the *in vivo* measurement of dose to the breast, sternum red bone marrow (SRBM), thyroid, liver, lung, stomach, and oesophagus during screening mammography using a Giotto mammography machine with Mo/Mo target/filter combination. Three PMMA breast phantoms of different thickness (2 cm, 4.5 cm, and 6 cm) were used in this study to replicate 2.3 cm, 4.9 cm and 6.5cm breast thickness, respectively. They found that the breast dose contributes over 98% of the overall effective dose. SRBM and thyroid receive a radiation dose between 0.4-1.27 and 0.05-0.17 μGy/mAs, respectively, and the other organ doses were negligible (Hatziioannou et al., 2000). The main limitations of this study are that the simulated mammographic positions were CC and ML (90^o angle) for each breast, and the homogenous Lucite phantom is not a good simulator of the different body tissues.

Other organ radiation dose from digital breast tomosynthesis (DBT) and dedicated breast CT were investigated by Baptista et al. (2015) and Sechopoulos, Vedantham, Suryanarayanan, D'Orsi, and Karellas (2008). Baptista et al. (2015) utilised Monte Carlo MCNPX toolkit with mathematical "Laura" voxel phantom to estimate the organ dose from the CC position using W/Rh target/filter combination from both digital mammography and DBT. For both digital mammography and DBT the estimated organs dose data showed that the radiation dose received by the ipsilateral lung and thyroid ranked as second and third highest dose in relation to examined breast. However, their work did not extend to include all the body organs and only considered the dose received by breasts, thyroid, lungs, liver, kidneys, ovaries and uterus. Monte Carlo Geant4 toolkit software was used to simulate dedicated breast CT by Sechopoulos et al. (2008). The aim of Sechopoulos et al.'s (2008) work was to evaluate body organs' radiation doses from different kVp (40-80) breast CT. They found that the radiation dose received by all organs increases as the kVp increases. For instance, the surface radiation dose of the sternum, which was the highest among other organs' dose, increases from 3.52% to 7.18% of the examined breast dose when the kV is increased from 40-80 kV. Finally, they considered that any radiation dose less than 0.1% of the examined breast dose is negligible (Sechopoulos et al., 2008).

In summary, there is evidence to suggest that the radiation dose received by organs other than the breast requires further consideration as the radiation dose and the risk associated with it is not captured by MGD. For a more thorough and accurate estimation of the radiation risk from mammography, the dose to all organs should be taken into account.

4.3.3 Mammographic Effective Dose and Effective Risk

The internationally accepted method for estimating the risk from an X-ray procedure is to use effective dose. Effective dose has enabled doses to be summed from whole and partial body exposure from external radiation of various types to estimate the risk of cancer development (ICRP, 2007). As recommended by the ICRP, effective dose is not suitable for epidemiological evaluations or the assessment of individual exposure and risk, but can be used as a radiation protection quantity by comparing it with reference values. The calculation of the effective dose depends on tissue weighting factors which are regularly updated by the ICRP based on the available evidence from epidemiological data (Nuclear Energy Agency [NEA], 2011). Since the ICRP considered that it is more suitable for radiation protection calculations to utilise averaged gender and age tissue weighting factors, effective dose does not take into account an individual's age and gender. Accordingly, Brenner (2008) recommended the replacement of effective dose by effective risk.

Effective risk is a useful quantity which was originally proposed by Brenner (2008). It is a more suitable quantity for epidemiological assessment of radiation risk than effective dose (Brenner, 2012). Effective risk is a good indicator of the radiation dose that the patient received (Brenner & Huda, 2008). In contrast to effective dose, which averages cancer incidence, cancer mortality, life shortening, and heredity risks, the only focus of effective risk is cancer incidence arising from the exposure to ionising radiation. The effective risk of developing cancer is less for people who have 20 years to live compared to those who have 60 years, because it is related to tissue specific, age specific, and gender specific lifetime attributable risk (LAR). Therefore, the calculation of effective risk involves summing the products of age, and gender lifetime-attributable risk of cancer incidence, per unit equivalent dose for each type of tissue and the dose received by that tissue. The effective risk calculation is not more complicated or difficult than the calculation of the effective dose.

However, the data from the effective risk calculation are more understandable to the general public than that produced by effective dose calculation (Brenner, 2012).

Brenner's recommendation (Brenner, 2008) to replace effective dose by effective risk has been criticised by Dietze, Harrison, and Menzel (2009) for a number of reasons. Firstly, they consider that the continuous change in tissue weighting factor is not a reasonable criticism for the ICRP because the continuous update of tissue weighting factors increases their reliability. Secondly, with regard to age, they stated that the ICRP discussion in their recommendations (2007) suggests the need to find another alternative quantity to consider the individual's age, but not as a replacement for effective dose. Finally, Dietze et al. (2009) suggest that the effective risk is not suitable for all radiation protection applications such as the assessment of radiation dose received by astronauts. Also, Huda was not enthusiastic about the introduction of effective risk because he considered the main advantage of the effective risk calculation is to compare different types of non-uniform exposures qualitatively. However, this can be achieved by comparing the effective dose of a specific procedure with that of annual background radiation (Brenner & Huda, 2008). In fact, effective risk is a more suitable quantity for the evaluation of radiation-induced cancer from screening mammography than effective dose because this examination is continuously repeated at different ages during women's lifetime. Accordingly, effective risk is adopted into this thesis as the main tool for assessing radiation risk from screening mammography when comparing different mammography screening programmes.

Before the suggestion of effective risk by Brenner (2008), some investigators used radiation-induced cancer as a dosimetric measure for radiation risk assessment of each organ separately. For example, Sulieman et al. (2007) calculated the risk of radiation-induced cancer in thyroid, testes and ovaries from paediatric micturating cystography using the direct surface dose measurement by TLDs placed on the child's skin. The radiation-induced fatal cancer for each organ (thyroid, ovaries, and testis) was then calculated using ICRP 60 LAR factors. However, Perisinakis et al. (2001) calculated the risk of radiation-induced cancer in all body organs from radiofrequency catheter ablation procedures by multiplying the effective dose by the total LAR reported in BEIR V report by National Academy of Siences. In the work of Perisinakis et al. (2001), organ radiation doses were measured using a Rando

phantom loaded with dosimeters. Although many researchers used the effective risk concept, after Brenner's proposal for radiation risk assessment from different radiographic examination, they did not use the term "effective risk", see **Table (4-2)**. It can be seen that all the studies in **Table (4-2)** used the term lifetime attributable risk (LAR), and this may result in misunderstanding as to whether it refers to cancer incidence in specific tissue or in all body tissues. However, only Li et al. (2011) used the term risk index to indicate the effective risk.

The lifetime attributable risk of radiation-induced breast cancer from mammography has been calculated by Hendrick (2010) and more recently by Yaffe and Mainprize (2011). Hendrick (2010) calculated the incidence and mortality of radiation-induced cancer from mammographic imaging procedures. Yaffe and Mainprize (2011) assessed the LAR of radiation-induced breast cancer following mammography at different client ages. Beemsterboer, Warmerdam, Boer, and de Koning (1998) and Freitas-Junior, Correa, Peixoto, Ferreira, and Tanaka (2012) justified screening mammography with regard to breast cancer mortality reduction and risk of radiation-induced breast cancer from screening mammography in the Netherlands and Brazil, respectively. In general, both studies found that radiation risk from mammography was small and that the benefits outweigh the risks. The number of lives saved by early screening mammography in BRCA mutation carriers was compared to the number of radiation-induced breast cancer by Berrington de Gonzalez, Berg, Visvanathan, and Robson (2009) and Jansen-van der Weide et al. (2010). Berrington de Gonzalez et al. (2009) concluded that there was no net benefit of early screening before 35 years of age for BRCA mutation carriers. However, there was a 1.3 fold additional breast cancer risk due to the exposure of high breast cancer risk women to low radiation doses reported by Jansen-van der Weide et al. (2010).

Nevertheless, the above authors did not progress their work to include effective lifetime risk of radiation induced-cancer from screening mammography; they only considered the examined breast radiation risk. Therefore, in this thesis the effective risk of radiation-induced cancer from screening mammography will be assessed, for different female ages and country-based screening programmes, considering the radiation dose received by all body tissues in addition to the examined breast.

Table (4-2) Lists studies that utilised effective risk for radiation-induced cancer assessments from different radiographic examinations.

Study Author	Examination	Study Details
Huang, Law, and Khong (2009)	Whole-body PET/CT	Rando phantom and TLDs used for organ dose measurement. LAR calculated using BEIR VII method utilised for total LAR calculation.
Griffey and Sodickson (2009)	Emergency multiple or repeated CT	Cumulative effective dose and BEIR VII report total LAR were used.
Huang et al. (2010)	ECG-gated coronary CT angiography	ImPACT Monte Carlo software used for organ dose estimation then LAR calculated using BEIR VII method utilised for total LAR calculation.
Li et al. (2011)	Paediatric chest CT	Monte Carlo simulation for organ dose estimation. The risk index calculated using Brenner's equation.
Johnson et al. (2014)	Children with heart disease imaging	Child ATOM phantom used for effective dose calculation. Then total LAR of all cancers from BEIR VII multiplied by effective dose.
Seo et al. (2015)	Neck X-ray radiography	PCXMC and BEIR VII LAR factors were used to calculate total LAR.
Law et al. (2016)	Spine radiography for scoliosis patient	PCXMC and BEIR VII LAR were used to calculate total LAR during patient lifetime.

4.4 Dose Modeling

4.4.1 Monte Carlo (MC) Simulation

Advances in computer technologies have led to the introduction of Monte Carlo (MC) methods to simulate complex problems (Guimarães, Moralles, & Okuno, 2008). MC simulation was developed in the 1940s by scientists working on nuclear weapons. It is a class of numerical methods based on the utilisation of random numbers (Salvat, Fernández-Varea, & Sempau, 2011). The simulation accuracy of MC software is strongly related to the accuracy of the probability functions (Ye, Brezovich, Pareek, & Naqvi, 2004). The main purpose of using MC simulation is to solve complex mathematical and physical problems. MC can be used for the simulation of radiation transport and interactions such as random sequences (Salvat et al., 2011). Accordingly, it is of great interest to radiation physics scientists (Salvat & Fernández-Varea, 2009). The extensive work of several groups throughout the world resulted in the introduction of different MC codes that simulate the

process of radiation energy transfer to matter. This allows accurate calculations to be made for medical physics, radiation dosimetry and radiation protection (Guimarães et al., 2008).

In diagnostic radiology different codes of MC are used, depending on the situation being simulated. The irradiation simulation can achieve both image quality and dose characteristic of different techniques (Delis, Spyrou, Costaridou, Tzanakos, & Panayiotakis, 2007). Some of these codes used in diagnostic radiology are EGS, MCNP, PENELOPE and GEANT4. EGS (Electron Gamma Shower) is available in different versions (e.g EGSnrc and EGS4) and widely used in medical physics for the calculation of ionisation chamber response (Assiamah, 2004). EGS is a general purpose code used for the simulation of coupled electrons/photons (Ye et al., 2004). The MCNP (Monte Carlo N-Particle transport) code has also been distributed in different versions (e.g. MCNP4, MCNP5) (Assiamah, 2004). This code was primarily supplied to simulate neutron and photon transport in nuclear reactors, but has since been extended to be used for electron transport. It is now the general purpose code for neutron, photon, electron or coupled neutron/photon/electron simulations. It also allows the simulation of 3D systems composed of many homogeneous bodies (Ye et al., 2004).

The acronym PENELOPE is derived from (PENetration and Energy LOss of Positron and Electron) (Lin, Tung, & Tsai, 2011). PENELOPE is used to simulate coupled electron/photon transport within any material and for a wide range of energies. Like MCNP, PENELOPE has the flexibility of 3D system simulations (Ye et al., 2004). PENELOPE was designed to assess low energy X-ray beam absorbed dose. In this context, PENELOPE has been found to have excellent agreement with EGS4 and MCNP4 (Lin et al., 2011). Both MCNP and PENELOPE were evaluated in comparison to experimental data and good agreement was concluded by Assiamah (2004). GEANT4 is a freely available code based on C++, utilised to simulate particle transport within matters (Guimarães , Moralles, & Okuno, 2007).

X-ray tube quality control is essential in diagnostic X-ray. It is a measure of X-ray tube performance and usually determined by the first and second HVL, homogeneity and the mean energy of the X-ray spectrum. Also, the determination of inherent and total filtration is required to reduce patient radiation dose. MC simulation is a powerful technique used for these purposes (Pozuelo, Gallardo, Querol, Verdu, & Rodenas, 2012). Work by Pozuelo et al. (2012) used both PENELOPE and MCNP5 MC software to evaluate the QC of the diagnostic

imaging X-ray tube. X-ray spectrum is an essential factor for the evaluation of image quality and patient radiation dose in radiography. Experimental evaluation of X-ray spectrum requires special equipment which has limited availability. Therefore, MC simulation is widely used as an accurate method for X-ray spectrum studies, even ones with complex imaging geometries. Also, MC can track secondary radiation in addition to primary beam. For X-ray photon simulation, some researchers have written their own computer code, while others used MC general purpose codes such as EGS4 and MCNP (Taleei & Shahriari, 2009). EGS, PENELOPE, and GEANT4 are widely used to simulate the X-ray spectra of diagnostic X-ray machines. Compared to the available data from measurements, the X-ray spectra generated by MC codes are very accurate (Salehi, Ya Ali, & Yusoff, 2012).

Mathematical heterogeneous human body phantoms are usually used with MC for organ dose assessment during imaging procedures. Within these phantoms, body tissues and organs are mathematically described considering their shape, size and location. Radiation doses are calculated by the determination of the average radiation energy imparted in each organ. Different human body phantoms are available for use in radiation dosimetry (e.g. Medical Internal Radiation Dose [MIRD] phantom, Christy phantom, Female/Male Adult voXel [FAX/MAX] phantoms) (Kramer et al., 2004). To facilitate the use of MC with such mathematical phantoms, they are programmed together and distributed in an executable form. PCXMC is one of these executable programmes based on MC and the mathematical human body Christy phantom to assess the organ doses from different radiographic examinations (Servomaa & Tapiovaara, 1998). PCXMC is often described as an industry standard MC simulation for the estimation of dose to patients from different medical imaging procedures.

MC is also used to simulate the different types of dosimeters to assess their dose measurement performance. For instance, Guimarães et al. (2007) used a GEANT4 toolkit to simulate the angular dependence of TLD response. In this work the simulation was achieved in three steps. The first step was the X-ray generation; the second, X-ray beam filtration; the third, the X-ray detection process (Guimarães et al., 2007). Lin et al. (2011) also used the Monte Carlo PENELOPE to investigate the accuracy of mammographic beam HVL estimation by TLDs.

4.4.2 Mammography Simulation

MC simulation is an important tool in the development and optimisation of mammographic imaging techniques. It can be used to evaluate each part of the imaging system separately (image receptor, X-ray spectrum and system geometry) (Bliznakova, Sechopoulos, Buliev, & Pallikarakis, 2012). For instance, the promising performance of the Cadmium Zinc Telluride (CZT) detector for digital mammography was concluded by Alsager and Spyrou (2007) who used MC MCNPX to assess CZT detector performance (Alsager & Spyrou, 2007). Cunha, Tomal, and Poletti (2013) studied three mammographic spectra produced by different target/filter combinations (Mo/Mo, Rh/Rh and W/Rh) using PENELOPE 2008. They investigated the effect of a copper (Cu) filter on the X-ray spectra of different mammographic anodes in contrast enhancement digital mammography (Cunha et al., 2013). Delis, Spyrou, Panayiotakis, and Tzanakos (2005) used the DOsimetry SImulation Studies (DOSIS) programme based on MC to investigate the effect of different mammographic imaging parameters (e.g. tube voltage and added filter) on radiation energy and dose distribution within the breast. They found for 6 cm breast thickness and for Mo/Mo target/filter combination the use of 30 kV tube voltage resulted in lower ESD (by 42%) than 25 kV (Delis et al., 2005). Finally, the scatter radiation in DBT was estimated by Diaz et al. (2014) using GEANT4 toolkit.

Currently MC simulation is widely used in new diagnostic modality development. It is of great importance in designing, testing and performance prediction of new imaging modalities before their manufacture and prior to be approved for clinical use. Amongst those tested in this manner are breast imaging systems and their applications that produce 3D image (DBT and breast CT). For more accurate results, the simulation process is usually followed by experimental validation. Traditionally this is achieved by breast modelling and radiation simulation using MC software to obtain breast images (Bliznakova et al., 2010). For instance, Ma and Alghamdi (2011) used the MCNPX MC to produce a mammographic image for the realistic computational breast phantom that they developed (Ma & Alghamdi, 2011).

The breast is often simulated using the geometrical structure of standard breast described in work by Dance (1990). According to Dance (1990), the standard breast is semicircular with

4.5 cm thickness and 16 cm diameter. The central region of the breast consists of 50:50 mixture of glandular and adipose tissues. This mixture is surrounded by 0.5 cm adipose tissue to simulate the breast skin adipose tissue (Dance, 1990). The elemental composition of glandular and adipose tissues described by Hammerstein et al. (1979) is usually used. The resultant density of this composition is 1.02 g/cm^3 and 0.93 g/cm^3 for glandular and adipose tissue (Dance, 1990). This phantom has been widely used to establish the conversion factors which are utilised to calculate MGD from incident air kerma for different breast thicknesses, breast densities and target/filter combinations (Dance et al., 2000a; Dance, Young, & van Engen, 2009), or to investigate the effect of scatter radiation on mammographic image quality of conventional 2D and 3D DBT images (Baptista et al., 2014; Dance, Persliden, & Carlsson, 1992). On the other hand, complex mathematical breast phantoms are useful tools in studies on complicated breast imaging modalities (Bliznakova et al., 2010). The use of such realistic breast phantoms is becoming common in mammographic studies in several different ways. Firstly, they are used for breast dosimetry in order to investigate dose distribution within the breast (Dance et al., 2005) and other organs' radiation dose assessment from different mammographic modalities (Sechopoulos et al., 2008; Sechopoulos et al., 2008). Secondly, to investigate the effect of breast compression reduction on lesion conspicuity in DBT (Saunders, Samei, Lo, & Baker, 2009). Thirdly, to produce 3D mammographic images through newly introduced modalities to assess the mammographic image quality (Duarte, Caldeira, Soares, Silva, & Janela, 2010).

As previously discussed in section 4.3.1 (page 70) MGD cannot be directly measured and its calculation is dependent on conversion factors derived by MC simulation for each breast thickness, breast density and beam quality (HVL and target/filter combination). These factors are used to calculate the MGD either from incident air kerma as described by Dance et al. (2000a), or from radiation exposure at the breast surface as described by Wu et al. (1994). Since the conversion factors published by Wu et al. (1994) were for a maximum breast thickness of 8 cm, Boone (1999) extended these conversion factors to accommodate for thicker breasts of up to 12 cm thickness. Dance, Young, and van Engen (2011) and Dance and Young (2014) extended the conversion factors published by Dance et al. (2000a) to accommodate the MGD calculations for DBT and contrast enhancement digital mammography, respectively. However, some investigators utilised MC simulation for direct

estimation of the MGD (Cassola & Hoff, 2010; Myronakis et al., 2013). Di Maria et al. (2011) validated the mammographic dose values (MGD, ESD and BSF) estimated by two different Monte Carlo methods (PENELOPE and MCNPX) with those experimentally obtained by TLD. They found that the variations in MGD obtained by the three methods are negligible (Di Maria et al., 2011).

In mammography, MC simulation is not only used to investigate the optimisation of mammographic image quality and MGD (Delis et al., 2005), but it is also used for screening mammography protocol optimisation (Jansen & Zoetelief, 1995). Jansen and Zoetelief (1995) developed a computer MC based model called (MBS) to analyse the net benefit of different mammography screening categories in relation to the risk of radiation-induced breast cancer and breast cancer mortality reduction by screening mammography. This model is based on random selection depending on relevant parameters, including age of tumour start, rate of tumour growth and thresholds of tumour detection. This model is characterised by its ability to consider the risk of radiation-induced fatal breast cancers, the probability of 10 years survival (as a function of tumour size), distributions of tumour onset and the growth rate of the tumour. The output of this model includes the number and size (diameter) of the observed tumours without screening, number of tumours detected by screening, number of tumours detected between two successive screens, breast cancer mortality reduction as a result of screenings, and the risk of radiation-induced cancer from screenings. The validation of this model was based on the data of the Swedish two-county trial (Jansen & Zoetelief, 1995). This model has been extended by Jansen and Zoetelief (1997a) to calculate the net screening benefit in terms of lifetime gain due to screening. Work by Jansen and Zoetelief (1997b) used the same mathematical MC model to investigate the net benefit of different screening frequencies (half annual, annual, biennial and triennial) for different age intervals (0-39 year, 40-45 year, 46-51year, 52-57 year…etc). However, the main disadvantage of this model is that since it was based on the Swedish two-county trial, it was affected by the trial uncertainties as discussed by Gotzsche and Jorgensen (2013).

Since this thesis has a demonstrable interest in scattered radiation dose, both PENELOPE and Geant4 are the most suitable MC methods to simulate screening mammography (Leidens et al., 2013; Sechopoulos & Hendrick, 2012; Sechopoulos et al., 2008). A significant period of

time within the first year of this PhD study was spent attempting to simulate the clinical situation of screening mammography using PENELOPE. However, no acceptable results have been obtained due to the complexity of the computer coding required. Another trial has been undertaken using PCXMC, but the radiation beam cannot be made to run parallel to a patient's body as it has not been designed to simulate mammography examinations.

Overall, although the *in vivo* dose measurements using dosimeters accommodated inside a physical phantom are difficult and time consuming, they are more accurate than dose estimation by Mote Carlo modelling. The accuracy of MC calculations is affected by the mathematical phantom used to simulate a patient's body and by the radiation field characterisation (radiation quality and field geometry) utilised in radiological examination (Fulea, Cosma, & Pop, 2009). For CT dose calculations the use of MC simulation results in 18-40% underestimations. These underestimations are mainly attributed to the differences between physical and mathematical phantoms, wherein simplified geometrical shapes of the organs are used in mathematical phantoms (Tootell, Szczepura, & Hogg, 2014). Groves et al. (2004) compared the measured organs' radiation dose by TLDs with those estimated by an MC simulation from whole body CT examination. They found an 18% underestimation in organ radiation dose for MC simulation compared with those measured by TLDs (Groves et al., 2004).

4.5 Radiation Dose Measurement Instrumentation

In diagnostic radiology the measurement of air kerma or absorbed dose is required in many situations. In some countries, it is required by legislation. It is also required to optimise image quality and patient dose (Hourdakis, 2014). Since the radiation doses from diagnostic radiology are small, accurate and long-term stability dosimeters are required (IAEA, 2007). There are several types of radiation dosimeters used in diagnostic radiologic practice. Most of these dosimeters are either ionisation chambers or solid state detectors which include thermo-luminescence dosimeters (TLD), optically stimulated luminance dosimeters (OSL), and semiconductor detectors (Bushong, 2013). The choice of the most suitable dosimeter depends on the clinical situation in which the measurements are required (Lemoigne & Caner, 2011). For instance, the measuring instrument should have the same properties

(absorb the same amount of energy) as the medium in which the dose is measured (Hendee & Ritenour, 2002; Hobbie & Roth, 2007).

4.5.1 Ionisation Chambers

An ionisation detector consists of two electrodes contained within an air filled chamber. An electric field across the two electrodes is used to collect the charges produced in the air by the ionisation. Since the ionisation chambers used in diagnostic radiology are vented air, a correction factor should be applied to the reading from the dosimeter. The correction factor is calculated using the following equation:

$$k_{TP} = (P_0.T) / (P.T_0)$$

Where P, T are the pressure and temperature of the ambient and P_0, T_0 are the pressure and temperature of the reference condition - 101.3 kPa and 293.2 K. The ionisation detectors are available in different types (Hourdakis, 2014).

4.5.1.1 Free-Air Ionisation Chambers

This type of detector is used by standard laboratories as a reference to calibrate the simpler dosimeters. For the accurate measurement of ionisation in the chamber, the range of liberated electrons by incident radiation should be less than the distance between the two electrodes of the detector. The measurement accuracy of this type of detector is within ± 0.5%. Free-Air ionisation chambers are fragile and too large for routine use (Hendee & Ritenour, 2002).

4.5.1.2 Chambers for Dose or Air Kerma Measurement

This is the most common type of ionisation chamber. It is commercially available in two different designs, either as two parallel plates (disk shape) or as a cylindrical shape. The disk shaped detectors are widely used in radiography, fluoroscopy, and mammography. However, because of the uniform sensitivity of cylindrical detectors around their central axis, they are only used with the x-ray beams which have effective volumes of 3-6 cm^3 (Hourdakis, 2014).

4.5.1.3 Kerma Area Product (KAP) Chambers

A KAP chamber is a large surface area detector mounted on the X-ray tube housing encompassing the entire radiation field in order to include all extra-focal and focal radiation in its measurement. Accordingly, it is made of transparent material for both X-ray and light. KAP chambers are used to measure kerma-area product as a quantity for patient exposure

monitoring. If the X-ray attenuation by air is neglected, the kerma-area product is same along the central X-ray beam (IAEA, 2007). Depending on their use and calibration, the KAP chambers measure either incident radiation or transmitted radiation (Hourdakis, 2014).

4.5.2 Semiconductor Detectors

Because of the small size and instantaneous response of semiconductor detectors, they are widely used in diagnostic radiology (IAEA, 2007). There are two types of semiconductor detectors, namely, silicon diodes and metal oxide semiconductor field effect transistors (MOSFETs) (Hourdakis, 2014).

4.5.2.1 Silicon Diode Detectors

When a silicon p-n junction diode dosimeter is exposed to X-ray, electron-holes are formed in the diode body resulting in an electrical current in the reverse direction. The magnitude of generated electrical current is proportional to the radiation dose. The main advantages of diode dosimeters over ionisation chambers are their higher sensitivity and reproducibility. However, the diode dosimeter sensitivity is dependent on dose rate and diode temperature (Lemoigne & Caner, 2011).

4.5.2.2 MOSFET Detectors

The MOSFET detector consists of silicon transistor capacitors. One of the capacitor electrodes is replaced by semiconductor material. The incidence of X-ray on the gate region of the MOSFET will produce electron-holes pairs. The holes will move toward the silicon-gate interface producing a change in the current of the n-type channel. Consequently, a shift in the threshold voltage of the gate bias will occur. The value of this shift is directly proportional to the absorbed dose. Therefore, during irradiation MOSFET requires a connection to a bias voltage. This type of detector is mostly used for patient dosimetry (Hourdakis, 2014).

4.5.3 Thermo-luminescence Detectors (TLD)

4.5.3.1 Principle

Thermo-luminescence is a phenomenon of light emission from an insulator or a semiconductor, resulting from previous energy absorption from a source of ionising radiation. It was initially discovered in 1663. Since then, many theories have been proposed

to explain the thermo-luminesce of semiconductors or insulators. The explanation which depends on the electronic energy band theory is the most acceptable one (Rivera, 2012). In perfect semiconductor or insulator crystals most of electrons occupy the valence band which is detached from the conduction band, the highest energy level, by a forbidden gap (Bos, 2007).

According to a one trap-one centre model, there are two levels in the forbidden band gap: T level, which is located down to the conduction band above the Fermi level of equilibrium; and R level which is located above the valence band and below the equilibrium Fermi level. At equilibrium, both these levels are empty (Bos, 2007). The absorption of radiation energy by thermo-luminescent material may result in the liberation of valence electrons to conduction band creating positive holes in the valence band. Then, the negative charge carriers, the electrons, are trapped in T level and positive ones, the holes, are trapped in the R level. The increased temperature speeds the return to equilibrium by de-trapping the electrons which are released to conduction band and then recombine with holes at luminescent centres in the R level. Since this process involves electron movement from high energy level to ground state, light quanta are emitted (Bos, 2001a). The ratio of emitted visible light energy to the absorbed ionising radiation energy is called the luminescence intrinsic efficiency (Bos, 2007). In order to increase the luminescence intrinsic efficiency of a material, more energy levels are localised in the forbidden band gap by adding impurities to that material (Bos, 2001a).

In brief, the thermo-luminescence process occurs in several steps: a) the production of electron-hole pairs in thermo-luminescence material by the absorption of ionising radiation energy, b) the trapping of the charge carriers in R and T levels, c) the de-trapping of charge carriers by temperature rising, d) light production by recombination of charge carriers in luminescence centres at R level (Bos, 2001b).

4.5.3.2 Thermo-luminescence Dosimetry

Tissue equivalency of some thermo-luminescent materials led to the first utilisation of thermo-luminescence as a radiation dosimeter in the middle of twentieth century. The perfect dosimetric material should have an atomic number similar to that of human tissue which is 7.42 (Bos, 2001b; Kitis, Furetta, Prokic, & Prokic, 2000). In addition to tissue equivalency,

several characteristics are required for good thermo-luminescence dosimeters: a) linearity, a linear response over wide range of radiation dose; b) sensitivity, the amount of light produced per unit absorbed dose; c) independency of radiation energy; d) simple glow curve, resulting in a simple heating protocol; e) good mechanical strength and static chemical activity; f) low fading (Kortov, 2007; Rivera, 2012). The fading composes of two components: pre-fade, which is the decrease in thermo-luminescence dosimeter response to radiation; and post-fade, which is the reduction in the storage signal in thermo-luminescence dosimeter with time (Luo, 2008).

Owing to their suitable dosimetric characteristics, TLDs are extensively used in many medical and personal monitoring applications. TLDs are applied in different areas such as radiotherapy and diagnostic radiology (Moscovitch & Horowitz, 2007). In diagnostic radiology, the main application area of TLDs is personal dosimetry (Olko, 2010). TLDs are also widely used by many quality assurance programmes for radiation dose measurement because they can assess radiation doses with backscatter when they are placed on patients or phantoms (European Commission, 1996; Gaona, Nieto, Góngora, Arreola, & Enríquez, 2007). Since radiotherapy aims to maximise the radiation dose to tumour tissue and minimise it to normal tissue, it is necessary to use suitable dosimeters for assessing this purpose. The most suitable dosimeters are TL dosimeters because they have the ability for *in vivo* dose measurement (Venables, Miles, Aird, Hoskin, & Group, 2004).

There are currently several commercial groups of TLDs. According to the material from which dosimeters are manufactured, they are classified into LiF, CaF_2, and Al_2O_3 groups. The LiF group include TLD-100, TLD-100H, TLD-600, and TLD-600H. TLD-100 was the first used TL dosimeter. It is characterised by its good tissue equivalency (Z=8.04), its sensitivity to low doses, its wide range of linear response (10μGy-10Gy), and its slow fading rate of around 5-10% per year. TLD-100H dosimeters can be used in diagnostic radiology and are around 20 times more sensitive than TLD-100 detectors. They have a wider dose range (1 μGy – 20 Gy), and lower fading rate of around 3% per year. The TLD-600 H dosimeter is used for neutron dosimetry. The main drawback of the CaF_2 group is their fading rate - 16% per 2 weeks and 15% per three months for TLD-200 and TLD-400. TLD-500 which is made of Al_2O_3 has a useful dose range of 0.05 μGy – 10 Gy, with a 3% per year fading rate

(Kortov, 2007). The selection of dosimeter depends on the application in which the dosimeter is to be used. For diagnostic radiology the required dose range is 0.001-10 mSv, while that for radiotherapy is 0.1-100 mSv (Rivera, 2012).

The main advantages of TLDs are their accuracy and precision. Their small physical size, availability in different forms and tissue equivalency make TLDs suitable for *in vivo* measurements and they can be used within phantoms to measure the radiation dose at different depths and locations. Moreover, TLDs are easy to handle because they are not sensitive to light. Other important characteristics of TLDs are they are independent of radiation direction in their measurements, and consequently the backscatter is included in their readings. Despite the advantages listed above, TLDs have many drawbacks. Firstly, they cannot give instant measurements because the readout and calibration processes are time consuming. Secondly, TLDs allow only one time reading during heating because of the signal efface during the readout procedure. Finally, in some types of TLDs the storage signal may fade with time due to the effect of temperature or light (Olko, 2010; Rivera, 2012).

4.5.4 Optically Stimulated Luminescence Dosimeters (OSLD)

OSLDs were developed in the late 1990s. The operating principle of these dosimeters is similar to that of TLDs where the luminescence process is stimulated by laser lighting rather than heat (Canadian Nuclear Safety Commission [CNSC], 2012). These detectors are made of aluminium oxide (Al_2O_3) which emits visible light. The amount of emitted light is proportional to the absorbed dose. For occupational radiation monitoring purposes OSLD is preferred over TLDs (Bushong, 2013).

Within this thesis the organs dose measurement was performed using TLD 100-H dosimeters. The selection of TLDs 100-H was based on their human tissue equivalency making them more suitable for *in vivo* dosimetry where they are accommodated inside human body physical phantom. Since the focus of this study is the other organ radiation dose resulting from scattered radiation (small dose), the high sensitivity of TLDs and their linear response at low energies makes them suitable for dose measurements. The possibility of using a large number of TLDs for many organs dose measurement at the same time is of great importance in this work. This enables the dose measurement received by all body organs at single exposure. However, the main disadvantages of using TLDs are: it is a time

consuming process and has a small percent of error. More details about the using of TLDs and the errors associated with their readings are available in methodology chapter (section 5.2.1, page 100).

4.6 Breast Tissue Equivalent Materials

Anthropomorphic phantoms made of tissue substitutes have been used extensively to physically represent human anatomy and mimic its radiation attenuation characteristics in dosimetric studies (Winslow, Hyer, Fisher, Tien, & Hintenlang, 2009). The purpose of using phantoms in dosimetric studies is to simulate the patient's radiation exposure during specific radiological procedures in order to assess organ radiation dose or to mimic conditions for reference calibration of a dosimeter system or beam (e.g. radiotherapy beam calibrations by the use of water phantoms) (Green, Palethorpe, Peach, & Bradley, 1999). Materials that have similar X-ray scattering and absorption to tissue are useful phantom materials (Farquharson, Spyrou, al-Bahri, & Highgate, 1995). Additional requirements for phantom material are that they should remain stable/constant over time, especially those with complex designs which need to be used for a long time. Phantoms are also necessary for the evaluation of radiographic equipment by the interpretation of phantoms images (Byng, Mainprize, & Yaffe, 1998).

In mammography, breast tissue equivalent materials are widely used to produce phantoms which simulate female breast. Breast phantoms are essential devices for the evaluation of mammographic equipment performance including X-ray field uniformity, AEC consistency, primary to scatter radiation ratio, grid and image receptor performance (IAEA, 2011). Since mammography is associated with biological effects to human breast tissues (Ossati, 2015), phantoms are also utilised for the assessment of mammographic image quality (resolution test) and for the accurate measurement of radiation dose (Argo, Hintenlang, & Hintenlang, 2004; Poletti, Goncalves, & Mazzaro, 2002). Phantom materials are models for simulating the X-radiation interaction with breast tissues and therefore they should have similar elemental composition and density to real breast tissue. These materials should scatter and absorb X-ray similar to breast tissues. In other words, phantom materials should have mass attenuation coefficients similar to that of breast tissues (Farquharson et al., 1995; Poletti et al., 2002).

There are many kinds of phantoms used to simulate breast tissue for mammography-related experiments (Sobotka et al., 2012). Poly(methyl methacrylate) (PMMA) slabs of different thicknesses have been used by many international organisations as a model to simulate breast tissue (Dance et al., 2009). The European Commission (1996) stated that although PMMA is not an exact tissue substitute, it can be used to simulate an average breast to enable correct operation for the X-ray machine under automatic exposure control. Glandular tissue dose may also be calculated by converting the dosimeter reading. The PMMA phantom of standard breast has a thickness of 45 mm either rectangular ≥150 mm X 100 mm or semicircular with a radius of ≥100 mm (European Commission, 2006). NHSBSP (2009) use a 45 mm thickness PMMA phantom to measure the radiation dose to a standard breast which has a thickness of 53 mm. Other breast thicknesses and compositions are simulated by different thicknesses of PMMA slabs. Moreover, IAEA (2011) propose PMMA slabs of 20, 45, 70 mm thicknesses as a basic requirement for digital mammography system quality assurance. The thickness precision for slabs should be ±0.5 mm and the shape either rectangular ≥150 mm X 100 mm, or semicircular with radius ≥120 mm. Regarding the area of the breast phantom, it is not considered to be an important quantity since it causes only small variations in measured radiation dose (Dance, 1990), this difference may be as little as 3% (Benevides et al., 2011).

Since many recent automatic exposure control (AEC) systems depend on breast thickness, 8 mm thickness polystyrene spacers are utilised to make the PMMA thickness equal to the thickness of simulated breast (European Commission, 2013). However, the use of spacer may affect the radiation scattering profile of the phantom (Bouwman et al., 2013). To avoid spacer issues, Bouwman et al. (2013) recommended the use of PMMA slabs with polyethylene (PE) slabs to make the phantom thickness equal to that of simulated breast. The use of PMMA-PE slabs as breast simulators in dose estimation studies gives a maximum error of 10% or less (Bouwman et al., 2013).

The mammographic accreditation phantom is another type of mammographic phantom which simulates a 45 mm thick compressed breast of about 50% glandularity. It is designed to comply with the phantom specifications of the Mammography Quality Standard Act (MQSA) and the American College of Radiology (ACR) quality control programmes. The

mammography accreditation phantom is a 102 mm X 108 mm X 44 mm-thick phantom. It is made of a 7 mm wax block and contains many test objects. The wax block is placed on a 34 mm thick PMMA base and covered with 3 mm thick PMMA (Cardinal Health, 2003). These phantoms are produced by Nuclear Associates and Computerised Imaging Reference System (CIRS). The main disadvantage of this type of phantom is that there is a big radiological difference between these phantoms and real breast tissue at low X-ray energies (Argo et al., 2004).

CIRS photo-timer consistency testing slabs (BR-12) are resin type slabs used to simulate breast tissue. These slabs are designed to comply with ACR and MQSA recommendations for mammography quality assurance. CRIS slabs are available in different glandular equivalencies but those equivalent to 47% glandularity breast are widely used. They are better than PMMA slabs because their thickness is tightly controlled in the manufacturing process and they simulate breast tissue accurately (Computerized Imaging Reference Systems [CIRS], 2013). BR-12 fabricated inside a PMMA box has also been used as breast tissue substitute in the commercially available 'Rachel' breast phantom. The design of this phantom was firstly described by Yaffe , Byng, Caldwell, and Bennett (1993) and it was based on matching the optical densities distributed within the mammographic image with the BR-12 thickness required to produce the same optical density. In the early stage of this phantom's development the mammographic optical densities were calibrated against PMMA thicknesses which produce the same optical densities in the mammographic image (Caldwell & Yaffe, 1990), then Yaffe et al. (1993) improved the work to use BR-12 instead of PMMA. Poletti et al. (2002) studied the scattering properties of CIRS slabs, they stated that the adipose tissue equivalent material in CIRS slabs is a good simulator for breast adipose tissue, but for glandular tissue it is bad simulator.

Hydrophilic materials which are commercially known as bio-gels are polymers insoluble in water, but are swollen by it. When these materials are fully hydrated, they will be in equilibrium with their environment. The amount of uptake water to reach the equilibrium is dependent on the number of hydrophilic centres in the chains of the monomer (Farquharson et al., 1995). Two types of these materials, known as ED4C and ED1S, have been experimentally tested as breast tissue equivalent materials by Farquharson et al. (1995). They

used a finely collimated photon beam and high purity germanium detector to assess the linear attenuation coefficient of the gels under different hydration conditions. They found that both, in dry and completely hydrated states, are unsuitable to simulate adipose tissue because their linear attenuation coefficients are higher than that of adipose tissue and that of the overall breast tissue. However, the gels were found to be good simulators for human body soft tissue (Farquharson et al., 1995).

A template of an epoxy resin was used to build a series of breast phantoms called BRTES. Different chemicals were added to this template to get the required radiological features. These chemicals are polyethylene powder, magnesium oxide powder, phenolic microspheres, and a hardener (Jeffamine). The phantoms of this series can be made to simulate different breast thicknesses and densities depending on the compositions of the materials used. By changing the ratios of these compounds, the physical properties and mass attenuation coefficients can be varied thereby resulting in different breast densities. In order to facilitate the dosimetric comparison with the ACR phantom, BRTES phantoms have been designed to have approximately the same dimensions (108 mm X 108 mm). The correlation of compressed breast thickness with breast density was considered when these phantoms were created. Despite their advantages, the accuracy of BRTES phantoms may be affected by the mixing process of different compounds and air bubble formation within the mixture (Argo et al., 2004).

Polyvinyl alcohol (PVAL) dissolved in 50:50 mixture of water and ethanol has been used to simulate breast tissue (Price, Gibson, Tan, & Royle, 2010). The linear attenuation coefficient of the resultant PVAL gel was measured using a tungsten anode beam with 30 kV and 4 mAs, filtered by 30 μm molybdenum to obtain a mono-energetic characteristic beam of molybdenum (17.5kV photons). Price et al. (2010) found, at this energy, the linear attenuation coefficient of the PVAL was acceptable (0.76 – 0.86 cm^{-1} for 5% - 20% weight/volume) compared to that of breast with 50% glandularity (0.8 – 0.9 cm^{-1} in different publications). A 0.02 difference in effective atomic number between phantom material and 50% glandular breast tissue has been reported by Koukou et al. (2015). Although, the PVAL gel was unstable over time, its low cost and mechanical properties, being similar to breast tissue, encourage many researchers to use it as a breast tissue substitute. The same phantom

composition with simulated lesions made of PVAL mixed with radiographic contrast agent was used by Ossati (2015) to analyse the effects of breast compression magnitude on lesion visibility. Moreover, Koukou et al. (2015) utilised the same phantom design with simulated calcification lesions to assess the mammographic image quality and MGD of dual energy images.

There are many other kinds of anthropomorphic breast phantoms made of different breast tissue equivalent materials. One of these phantoms is made from a mixture of refined lard as an adipose tissue equivalent material and fresh egg white to simulate the glandular tissue (Freed et al., 2011). The mixing process should be achieved in controlled laboratory conditions. Depending on the mold shape in which the mixture is poured, this phantom can simulate both compressed and non-compressed breasts. For mammographic use the mixture can be put into a compressed breast mold with 4.5 cm thickness, while for MRI use the non-compressed breast mold can be used. Its instability over time, lack of simulated breast skin and the advanced chemical laboratory required to produce this phantom are its main drawbacks (Freed et al., 2011).

On the other hand, Saito (2007) used a homemade phantom to assess mammographic image quality and MGD of dual energy subtraction mammography. The compressed breast phantom used in Saito's (2007) work was a box of PMMA filled with olive oil to simulate the breast adipose tissue, and PMMA spheres of different diameter to simulate the glandular tissue distributed within breast fat. A blend of distilled water and olive oil in flexible plastic containers, to simulate different breast thicknesses and thereby different breast densities, was also used to simulate breast tissues in both the FFDM and DBT examinations to assess MGD. Distilled water was used as a glandular tissue equivalent material and olive oil analogs for breast adipose tissue (Feng & Sechopoulos, 2012). In brief, water is the best material to simulate glandular tissue in breast phantoms because it has a linear scattering coefficient similar to that of glandular tissue (Poletti et al., 2002).

Although PMMA does not accurately simulate breast tissue, it is the most common material used as a breast tissue substitute by many international dosimetry protocols and many researchers because it is cheap, available, and consistent over time. PMMA is manufactured as slabs in order to simulate compressed breasts of different thicknesses. However, the main

limitation of the PMMA phantom is that its thickness is less than the thickness of the simulated breast. For the simulation of average breast which is 53 mm, a 45 mm PMMA thickness is required. To overcome this issue, the European Commission (2006) and IAEA (2011) recommended the use of 8 mm thickness polystyrene spacers between PMMA slabs. The use of polystyrene spacer results in X-ray scattering different from that resulted from breast tissue due to air gaps within the phantom. Therefore, in this work additional slabs of polyethylene are utilised with PMMA slabs to make the phantom thickness equal to simulated compressed breast thickness as recommended by Bouwman et al. (2013). More information about the PMMA-polyethylene phantom design used in this thesis is presented in section 5.2.3 (page 111).

4.6 Chapter Summary

Cancer incidence is the prominent stochastic effect of radiation exposure. Controversy about the risk of radiation-induced cancer at low radiation dose levels (diagnostic radiology range) has been outlined in the reviewed literatures. Presently LNT is the most reasonable model to describe the association of cancer incidence with low radiation dose. LTN is recommended by the ICRP and the Academy of Sciences. According to the LNT model, no radiation dose, however small, is safe and risk free. For mammography, since the glandular tissue is the radiosensitive portion of the breast, MGD is widely used to quantify the radiation risk. However, the radiation risk to other organs from mammography is not captured by MGD, suggesting that whilst MGD is a simple approach to quantifying risk, it does have limitations. Effective dose is the internationally accepted method used for considering the radiation risk to all body tissues from an X-ray examination. Effective dose calculations are dependent on the tissue weighting factors published by the ICRP. These factors are averaged for both sex and age. Since women at different ages are the target of screening mammography, a more reliable quantity is required to quantify the radiation risk from screening mammography; such an approach would take into account gender and age. On reviewing the literature it can be proposed that the use of effective risk as an alternative method to describe the risk of radiation-induced cancer from screening mammography would be reasonable, as it takes into account gender and age. Effective risk calculations are not more complicated than effective dose calculations and they are heavily dependent on age/tissue specific lifetime attributable

risk (LAR), as published in the BEIR VII report by the National Academy of Sciences. Moreover, the generated data from effective risk calculations may be more understandable by general public than effective dose calculations.

Dosimetric studies cannot be directly undertaken on patients because hazardous ionising radiation is involved. Therefore, two alternative methods can be used. The first method includes the use of computer programmes based upon Monte Carlo simulations. These were initially used to develop nuclear weapons and then their use was extended to medical physics simulations. In the second method, human body tissue equivalent materials can be used to construct phantoms which use with different types of dosimeters to evaluate the radiation dose received by body tissue and organs during specific radiological procedures. In mammography, PMMA is the most commonly used material to simulate compressed breast tissue. The main disadvantage of the PMMA phantom is that the equivalent thickness of PMMA is less than the thickness of simulated breast. To overcome this problem the European Commission recommend the use of polystyrene spacers between the PMMA slabs, but this may affect the X-ray scattering by the phantom and the use of PMMA-PE phantom is more reasonable method.

Chapter Five
Material and Methods

5.1 Chapter Overview

The aim of this thesis is to develop a new method for estimating radiation risk from screening mammography. According to this method, the effective risk is used as a quantity to assess the radiation risk. An experimental approach is used for the calculation of the effective lifetime risk of radiation-induced cancer from screening mammography for different client ages and different country-based mammography screening programmes. To achieve this, an accurate measurement of radiation dose received by the examined breast and other body tissues was required. An ATOM dosimetry phantom, a bespoke breast phantom designed from best available evidence, TLD dosimeters and a range of mammography machines were used. A flowchart in **Figure (5-1)** demonstrates the main six stages of the methods used in this PhD thesis.

This chapter includes a comprehensive explanation of the materials and methods used in this thesis. The initial section comprises of the materials and methods utilised for organs dose measurement during screening mammography. Firstly, the errors associated with organs dose measurement due to the uncertainty of the dosimeters are considered. These errors include homogeneity and reproducibility errors associated with TLDs. Next, the calibration method for TLDs against a solid state dosimeter, used to convert TLD charge to a radiation dose value, is explained. The TLDs were accommodated inside a human tissue equivalent ATOM dosimetry phantom in order to directly measure the radiation dose received by 20 types of radio-sensitive tissues including brain, salivary glands, thyroid, oesophagus, thymus, heart, lung, stomach, liver, gall bladder, spleen, pancreas, adrenals, kidneys, intestine, urinary bladder, ovaries, uterus, bone marrow (in different locations), and the contralateral breast tissues. Two breast phantoms were used; one to simulate the examined breast in a CC projection and the other to simulate the breast in an MLO projection. Both the ATOM phantom (loaded with TLDs) and the breast phantom were positioned on sixteen FFDM systems in order to replicate typical screening mammography scenario. For each machine

four exposures were performed; CC and MLO for each breast. Three exposures were made for each projection in order to further minimise random error.

The latter sections concentrate on the calculation of examined breast MGD, effective dose and the risk of radiation-induced cancer from screening mammography. Internationally recommended procedures have been used to calculate MGD, effective dose, and effective risk for 25-75 year old clients using organ doses data measured from sixteen FFDM systems. As described by IPEM (2005), the examined breast MGD was calculated using incident air kerma and conversion factors. Tissue weighting factors listed by the ICRP (2007) were utilised to calculate the effective dose for one screening visit for each of the sixteen FFDM systems. The effective risk was calculated using BEIR VII report lifetime attributable risk factors. The effective risk values are finally used to calculate the total effective risk during a female's lifetime. The total effective risk data were subsequently utilised to establish three risk models that can be easily used by practitioners to assess the total effective risk value for different screening categories generating more understandable data for general public than MGD or effective dose. One of these models was based on mathematical regression and the other two models were based on data extrapolation from a series of graphs. The main purpose of these risk models is to provide an accurate and easy method for the determination of radiation-induced cancer from screening mammography.

The last section comprises of the method for using a contralateral breast shield in order to minimise unnecessary radiation dose to breast tissue. In this section details about the design and equivalent lead thickness estimation for the contralateral breast shield have been included.

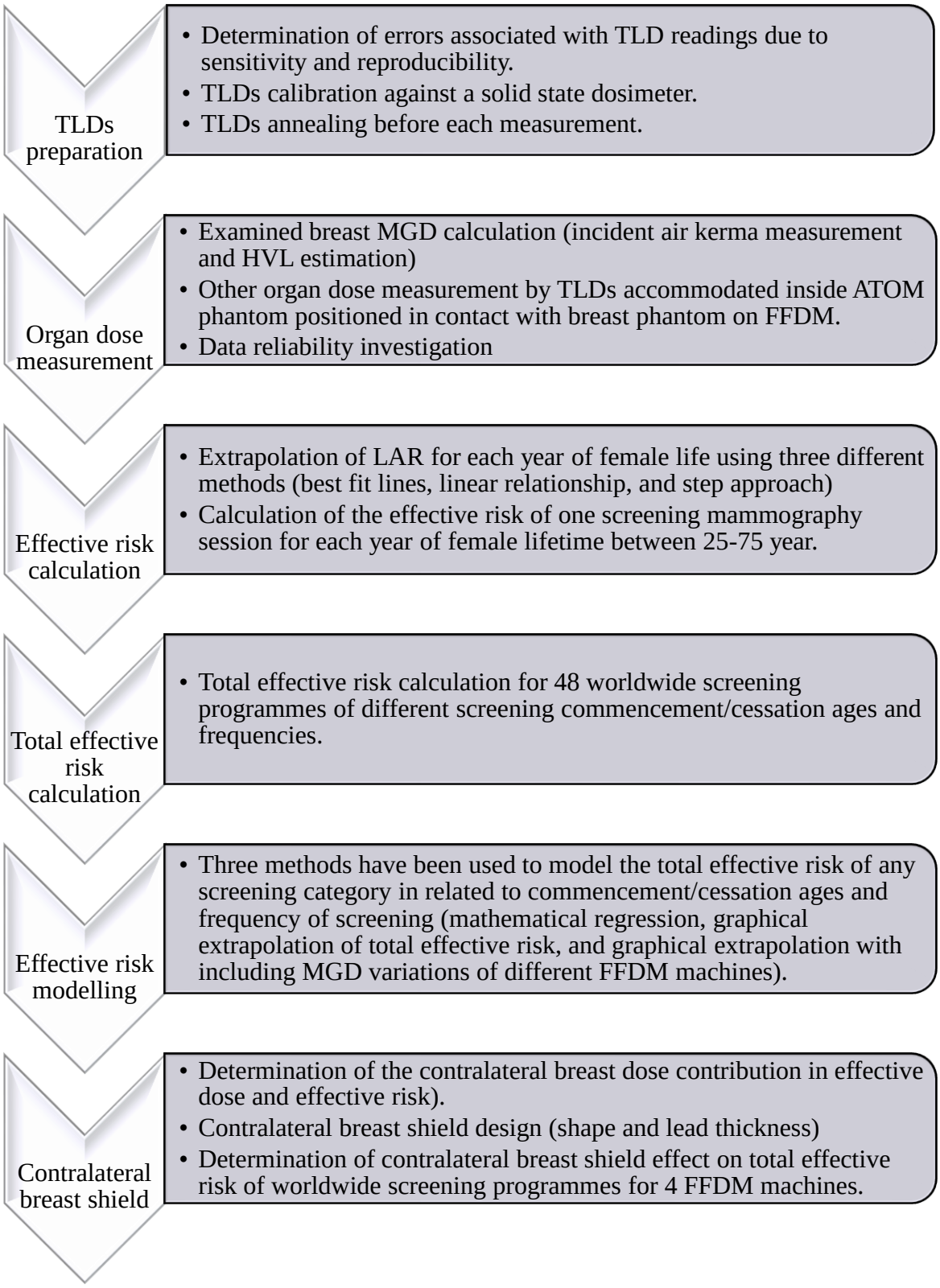

Figure (5-1) A flowchart illustrating the methods used in this PhD thesis.

5.2 Organ Dose Measurement

280 Harshaw TLD-100H dosimeters (Thermo Scientific, USA) (section 4.5.3.2, page 87) were placed inside a CIRS adult ATOM dosimetry phantom (CIRS Inc, Norfolk, Virginia, USA) in order to measure the absorbed radiation dose to body tissues and organs during screening mammography and for a complete screening visit (cranio-caudal [CC] and medio-lateral oblique [MLO] for each breast, sections 3.6.1 on page 50 and 3.6.2 on page 51). The selection of radiosensitive organs to which radiation absorbed doses were measured depended on the ICRP (103) recommendations (ICRP, 2007).

5.2.1 TLDs

TLD-100H (LiF:Mg,Cu,P) dosimeters (Thermo Scientific, USA) were used to measure organ radiation dose during screening mammography. This type of dosimeter was chosen because of their sensitivity, size and tissue equivalency making them suitable for *in vivo* dose measurements. TLD-100H dosimeters are 20-50 times more sensitive than TLD-100. This high sensitivity is essential because of the relatively small radiation doses measured within this thesis. The small size (0.125 X 0.125 X 0.035 inches) of TLD-100H dosimeters minimises any resultant X-ray field distortion. Another important characteristic of TLD-100H dosimeters is their tissue equivalency ($Z_{eff\ TLD}$ = 8.04 compared to $Z_{eff\ tissue}$ = 7.42) which makes them have similar response to radiation as would human tissue (Kitis, Furetta, Prokic, & Prokic, 2000; Triolo, Brai, Bartolotta, & Marrale, 2006). TLD-100H dosimeters used in this thesis can measure radiation doses over a wide range, 1 pGy - 10 Gy, with a linear response across this energy range. The fading rate of these dosimeters is negligible, approximately 3% per year (Thermo Scientific, 2015), making them more suitable for this thesis because TLDs were irradiated in hospitals and read out in the university laboratory at different points. Consequently, systematic errors such as those resulting from dosimeter energy response, dosimeter size, and radiation field perturbation by dosimeters are minimised with the use of TLD-100H (Camargo-Mendoza, Poletti, Costa, & Caldas, 2011). Since the TLDs are sensitive to small scratches and surface contamination, which may affect the light emission process, they were carefully handled by the use of Dymax 5 vacuum tweezers (Charles Austen Pumps, Surry, UK), see **Figure (5-2)**. Mechanical tweezers and fingers are not recommended to be used for TLD handling (Thermo Scientific, 2015).

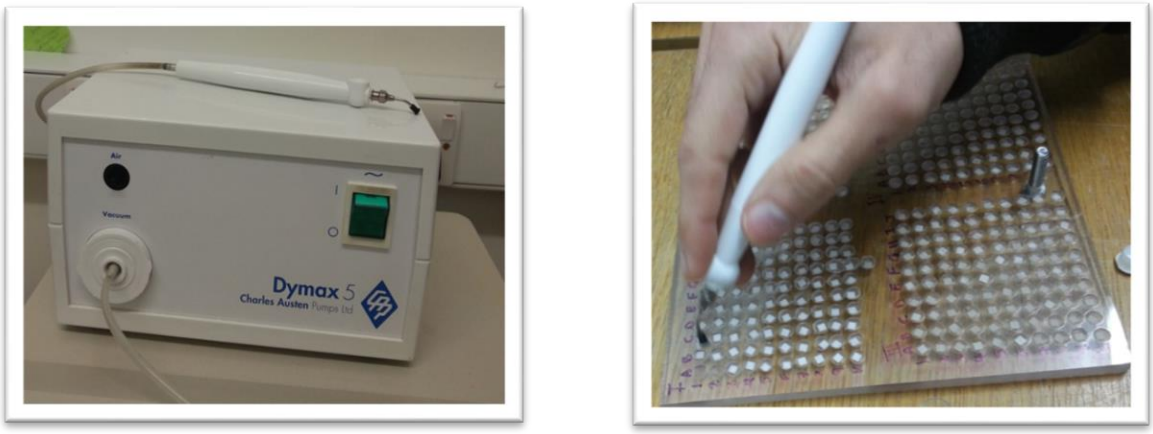

(a) **(b)**

Figure (5-2) Illustrates TLD handling **(a)** Vacuum pump **(b)** TLDs handling by vacuum tweezers.

5.2.1.1 TLDs Reading

The TLD reading system comprised of a Harshaw 3500 TLD reader (Thermo Scientific, USA) with WinREMS software installed on a personal computer (PC), **Figure (5-3)**. The reader consists of a drawer containing a metallic tray suitable for a single TLD, wherein the irradiated TLD is heated, then a photomultiplier tube (PMT) receives the thermo-luminescent light emitted by the TLD and converts it to an electronic signal and an electrometer records the output signal of the PMT. The intensity of emitted thermo-luminescent light is related to the reader heating rate of irradiated TLD. The graphical plot of light intensity versus temperature is the TLD glow curve, see **Figure (5-4)**. The use of a constant heating rate is essential for accurate dose measurements by TLDs (Izewska & Rajan, 2005); the Harshaw 3500 TLD reader is automatically controlled for rate.

The TLD-100H reading process in the Harshaw 3500 TLD reader has four phases. The first phase, known as preheat phase, persists for approximately 12 seconds in which the TLD is heated to 134^{o}C. After 134^{o}C has been achieved the TLD light signal is detected. The acquisition phase ends at 239^{o}C after 30 seconds. After this the annealing phase continues for 10 seconds. The purpose of the anneal phase is to clear the TLDs of all residual exposure (signal). Finally the cooling phase cools the annealed TLD from 239^{o}C to 60^{o}C. In order to provide a consistent temperature during reading and to avoid any background light signals being produced by the TLD reader metallic tray and by the impurities in the air, the TLDs are

read in a constant pressure nitrogen atmosphere provided by a regulated compressor tank (Collins, 2005; Savva, 2010).

Figure (5-3) Shows the TLD reading system.

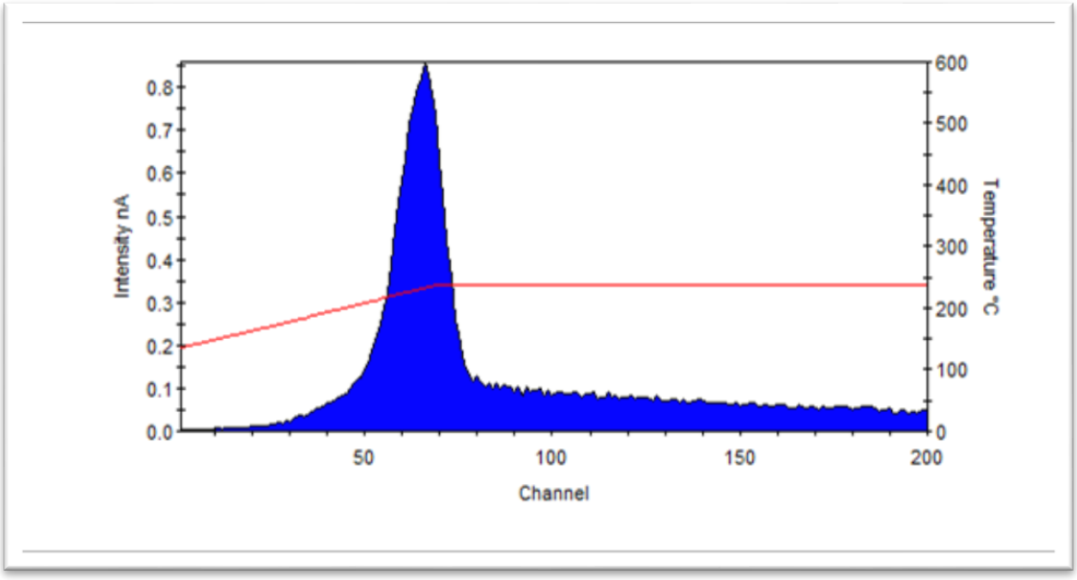

Figure (5-4) Shows a TLD 100H glow curve.

5.2.1.2 TLDs Preparation

Prior to use, TLDs underwent a process of preparation which included annealing and determining errors associated with their readings. These errors are mainly attributed to differences in sensitivity between TLDs and the consistency of TLDs. As recommended by the manufacturer (Thermo Scientific, 2015), TLDs were annealed at 240^{o}C for 10 minutes in a special rapid cooling high temperature (TLD/3) model oven (Carbolite, England, UK) using an annealing tray, **see Figure (5-5)**. This oven is equipped with a Eurotherm 3508 temperature programmable controller which allows accurate annealing temperature regulation. The main purpose of the annealing process is to ensure that TLDs are free from any residual charge. TLD overheating should be avoided as this can affect TLD sensitivity (Thermo Scientific, 2015). After annealing, an aluminium block is used to ensure a rapid cooling rate because the TLD cooling rate may affect its energy response (Lisa, Claire, Helen, Mamoon, & Tomas, 2004). According to Furetta and Weng (1998) the TLDs sensitivity is dramatically changed as the cooling rate changes. However the selection of best cooling rate depends on the TLDs material.

According to the European Commission (1996) the total uncertainty in TLD dosimetric measurements should be less than 10%. Therefore, the TLDs sensitivity and consistency were established. As discussed in section 3.4.1 (page 34), the mammographic X-ray beam is designed to be non-uniform to accommodate breast thickness uniformity differences. Therefore, a Wolverson Arcoma Arco Ceil general radiography X-ray machine (Arcoma, Annavägen, Sweden) was used to expose the TLDs to investigate their sensitivity and consistency. For more accuracy, the X-ray beam uniformity of this machine is tested using an Unfors Multi-O-Meter solid state dosimeter (Billdal, Sweden). The dosimeter reading is recorded at the four sides of the X-ray field for the same exposure factors, see **Figure (5-6)**. There is a difference in dosimeter readings across the anode and cathode axis due to the anode heel effect but this was negligible across the other perpendicular axis. Therefore, during the exposure to calculate sensitivity and consistency, the TLDs were arranged to be as close as possible to the midline between anode and cathode sides to minimise anode-heel effect, see **Figure (5-7)**.

(a) **(b)**

Figure (5-5) Shows the TLD annealing equipment **(a)** Annealing oven **(b)** Annealing tray on an aluminium cooling block.

Figure (5-6) Illustrates dose measurements using Unfors Multi-O-Meter solid state dosimeter for X-ray beam uniformity investigation.

Figure (5-7) Illustrates the TLD positioning during exposure. The TLDs are positioned as close as possible to the central ray to minimise the impact of the anode-heel effect.

For improved TLD reading accuracy the sensitivity factor for each TLD should be estimated (Costa et al., 2010) using the following equation:

$$Ecc = \frac{Ri}{R}$$

Where *Ecc* is the correction coefficient for a given TLD, *R* is the individual TLD reading, and *Ri* is the average reading of all TLDs in the batch (Shirazi, Mahdavi, Khodadadee, Ghaffory, & Mesbahi, 2008). However, since a large number of TLDs were used, all TLDs were exposed three times and according to their average response they were divided into five groups of homogeneous sensitivity. The sensitivity difference (coefficient of variance, standard deviation of TLD readings divided by the average of these readings) for each group was less than 3%; see **Table (5-1)** which contains the TLDs readings summary for sensitivity investigation.

Table (5-1) Demonstrates the TLD readings for sensitivity investigation.					
TLDs group	TLDs readings (nC)*				Coefficient of variance (%)
	Minimum	Maximum	Average	SD	
Group 1	33.20	35.95	35.00	0.79	2.26
Group 2	36.24	38.71	37.73	0.64	1.70
Group 3	38.77	40.96	39.84	0.65	1.63
Group 4	41.01	43.57	42.18	0.75	1.78
Group 5	43.64	47.14	44.74	0.89	1.98
*(nC) means nano-Coulomb					

For TLD consistency estimation, all TLDs were exposed and read three times with time intervals of around five days between each exposure, see **Table (5-2)** which includes the readings for 100 randomly selected TLDs after exposing them to an X-ray beam at the same exposure factors on the three different occasions. TLD responses were analysed using SPSS 22.0 (IBM, Armonk, New York, USA) to determine TLD consistency (Intraclass Correlation). The calculated consistency was 99%. The total uncertainty of the dose results, which was due to both sensitivity and consistency, was 4%. To improve accuracy further, the average background signal of three unexposed TLDs was subtracted from the readings of exposed TLDs (Sulieman et al., 2007). As described by Tootell, Szczepura, and Hogg (2013), the TLDs were calibrated against an Unfors Multi-O-Meter solid state detector (Billdal, Sweden) as a reference dosimeter; this was placed on three slabs (1 cm thick each) of Perspex scatterer (Tootell et al., 2013), see **Figure (5-8)**. To minimise possible errors due to TLD response energy dependence, a calibration was accomplished for each mammographic machine to be used in organs dose measurement using the same beam qualities as that utilised for phantom exposure (Olgar, Bor, Berkmen, & Yazar, 2009).The aim of the calibration process is to convert the output charge reading of TLDs to their equivalent radiation dose.

Figure (5-8) Demonstrates the TLD calibration process against the Unfors solid state dosimeter on three Perspex slabs.

Table (5-2) Shows the consistency of TLD readings on three different occasions.

TLD number	TLD readings (nC)			TLD number	TLD readings (nC)			TLD number	TLD readings (nC)		
	R1	R2	R3		R1	R2	R3		R1	R2	R3
1	5.61	5.87	5.43	34	5.22	5.30	4.99	67	4.83	4.93	4.59
2	4.37	4.48	4.19	35	5.53	5.56	5.40	68	5.44	5.28	4.98
3	5.70	5.68	5.44	36	5.42	5.48	5.17	69	4.75	4.75	4.59
4	5.76	5.96	5.56	37	5.10	5.06	4.81	70	5.00	5.06	4.79
5	5.71	5.86	5.52	38	5.21	5.22	5.01	71	5.95	6.05	5.74
6	5.71	5.81	5.55	39	5.14	5.20	5.00	72	6.00	5.87	5.65
7	6.11	6.18	5.84	40	4.98	5.08	4.82	73	4.88	4.92	4.58
8	5.63	5.65	5.46	41	5.15	5.22	4.97	74	5.50	5.59	5.29
9	5.70	5.56	5.20	42	5.20	5.07	4.69	75	4.82	4.93	4.70
10	6.22	6.17	5.95	43	5.61	5.63	5.33	76	5.46	5.47	5.15
11	5.79	5.83	5.26	44	4.89	4.98	4.63	77	5.25	5.25	4.95
12	5.96	5.89	5.66	45	4.83	5.02	4.70	78	4.92	4.97	4.67
13	5.60	5.65	5.34	46	5.14	5.16	4.87	79	5.69	5.71	5.33
14	6.00	6.04	5.69	47	4.91	4.97	4.73	80	5.02	5.15	4.88
15	5.29	5.28	5.05	48	4.93	4.97	4.74	81	4.76	4.82	4.89
16	5.50	5.56	5.26	49	5.04	5.07	4.82	82	5.12	5.09	4.79
17	6.10	6.20	6.00	50	5.59	5.59	5.43	83	5.07	5.17	4.95
18	5.38	5.33	5.06	51	5.56	5.59	5.33	84	4.52	4.57	4.28
19	5.77	5.80	5.61	52	5.21	5.27	5.09	85	4.50	4.55	4.36
20	6.01	6.07	5.88	53	4.97	5.02	4.75	86	4.75	4.86	4.59
21	5.92	5.95	5.64	54	5.38	5.51	4.90	87	4.73	4.91	4.53
22	5.57	5.65	5.36	55	5.23	5.29	5.20	88	5.03	4.90	4.68
23	5.22	5.11	4.68	56	5.38	5.39	5.16	89	4.61	4.67	4.45
24	6.08	6.05	5.77	57	5.03	5.06	4.79	90	4.67	4.75	4.56
25	5.08	5.15	4.90	58	5.24	5.22	5.06	91	5.14	5.38	5.15
26	5.13	5.14	4.84	59	5.51	5.64	5.26	92	4.98	4.95	4.74
27	5.55	5.56	5.30	60	5.47	5.54	5.29	93	4.94	4.99	4.83
28	5.44	5.51	5.18	61	5.04	4.93	4.71	94	5.35	5.33	5.04
29	5.46	5.59	5.37	62	5.70	5.67	5.44	95	5.01	4.92	4.74
30	5.67	5.72	5.44	63	5.62	5.75	5.41	96	4.84	4.80	4.61
31	5.77	5.86	5.58	64	4.98	4.94	4.75	97	4.60	4.68	4.41
32	5.53	5.56	5.33	65	5.18	5.26	4.95	98	4.65	4.69	4.47
33	5.28	5.31	5.05	66	5.36	5.42	5.13	99	4.99	4.93	4.75
Intraclass Correlation-Consistency = 99%								100	5.20	5.07	4.69

Usually the calibration process is accomplished for a complete batch of TLDs because the calibration of individual TLDs is too time consuming and the individual approach shows only a minimal improvement in accuracy compared with the batch approach (the sensitivity difference of TLDs within any batch was less than 3%). For greater precision, the dose-TLD

response curve was utilised to obtain the TLD calibration factor (Shirazi et al., 2008), see **Figure (5-9)**. In this figure the solid state dose readings are presented on Y-axis against charge TLD readings on X-axis (R^2 = 99.75%). The R^2 value gives an indication that TLDs response is linear at this dose range. The establishment of the dose-TLD response curve requires TLD responses for at least five different radiation doses (e.g. at 10, 30, 50, 70, and 90 mAs) using the same beam quality (kV and filtration). In each case, the average of three TLD responses was used to minimise random error. Consequently, for TLD calibration a total of 15 TLDs are required in addition to another three for background measurement and correction. The whole process of TLD calibration was repeated for each TLD group and for each mammographic machine used in the organ dose measurement.

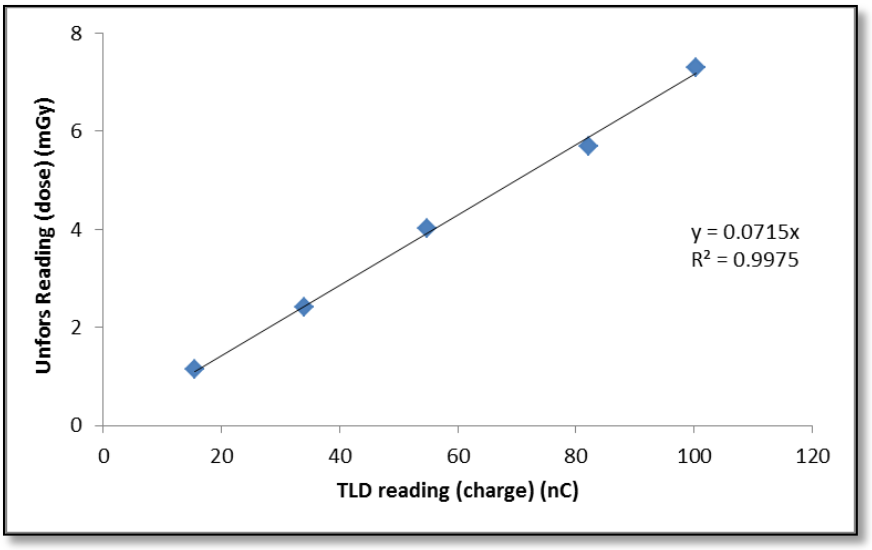

Figure (5-9) Represents a sample of calibration curve of TLDs against Unfors solid state dosimeter.

5.2.2 Anthropomorphic ATOM Dosimetry Phantom

To simulate a women's body, an adult ATOM dosimetry phantom, model 701, (CIRS Inc, Norfolk, Virginia, USA) was used, see **Figure (5-10)**. The ATOM phantom is 173 cm high and weighs 75 kg with chest dimension of 23 cm (AP) by 32 cm (left to right / side to side). It is made from resins and polymers by CIRS computer models which consider the tissue to be simulated, x-ray imaging modality energy level, and raw material to be utilised. The phantom comprises of 39 cross-sectional contiguous slices which are 25 mm thick. Within the slices there are pre-drilled holes which are placed at specific positions in 20

radiosensitive organs. Using the manufacturer's TLD location map (CIRS Tissue Simulation and Phantom Technology, 2012), the absorbed radiation dose for each organ was calculated by averaging the radiation dose values inside the organ. The number of TLDs used for each organ are listed in **Table (5-3**). These numbers have been determined by the manufacturer, for this phantom model, and are consistent with other researchers (Tootell et al., 2013).

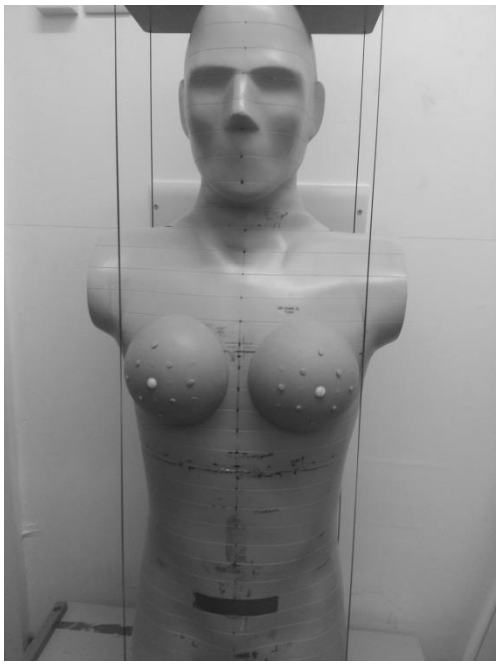

Figure (5-10) Shows the ATOM dosimetry phantom used to simulate women's body during screening mammography.

Table (5-3) Demonstrates the number of TLDs utilised for dose measurements inside each organ (280 TLDs in total).

Organ	No. of TLDs	Organ	No. of TLDs
Adrenal	2	Pancreas	5
Brain	11	Pelvis BM*	17
Clavicle BM*	4	Ribs BM*	18
Cranium BM*	4	Salivary glands	6
Cervical spine BM*	2	Scapulae BM*	16
Gall bladder	5	Spleen	12
Heart	2	Sternum BM*	4
Intestine	16	Stomach	14
Kidneys	16	Thoraco-lumber spine BM*	8
Liver	29	Thymus	4
Lungs	36	Thyroid	6
Mandible BM*	6	Urinary Bladder (UB)	13
Oesophagus	3	Uterus	3
Ovaries	2	Contralateral breast (8 for each side)	16

**BM means bone marrow*.

A breast attachment, from the manufacturer, was used to measure the radiation absorbed dose received by contralateral breast. The breast attachment is designed to simulate a standard breast in standing position with 50% glandularity and 350 cm^3 breast volume. The breast attachments have a grid of 20 holes in each breast to accommodate the detectors (CIRS Tissue Simulation and Phantom Technology, 2012). As described by Parker et al. (2008) eight TLDs were used to measure the radiation dose received by each breast attachment. These TLDs were distributed depending on the anatomical quarters of the breast wherein four TLDs positioned in upper, lower, medial, and lateral aspects of the breast attachment and the other four TLDs positioned in midpoint of each breast's anatomical quarter, see **Figure (5-11)**. Whatever their location all the TLDs were arranged to be in the midpoint antero-posteriorly within the breast attachment. The contralateral breast dose was obtained by averaging the TLD readings within the breast attachment.

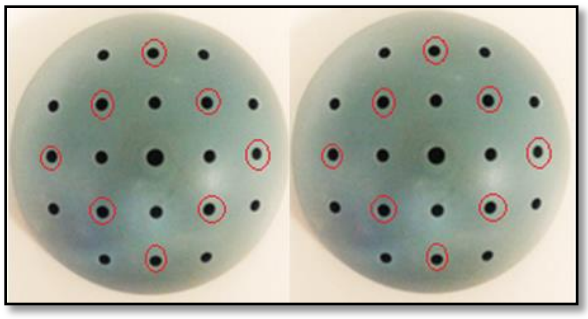

Figure (5-11) Shows dosimeters holes in left and right breast attachments. The circled holes were used for TLD accommodation.

5.2.3 Breast Phantom

Since this thesis focuses on organ radiation dose measurement from scattered radiation during screening mammography, it is necessary to use a breast phantom which has X-ray scattering similar to that of standard breast, which is 53 mm thick and 50% glandularity. Breast phantom thickness, composition, shape, and area are essential factors which determine the phantom's X-ray scattering (Boone, Lindfors, Cooper, & Seibert, 2000). To simulate a standard breast 45 mm PMMA slabs have been used. However, this phantom thickness is less than that of a simulated breast. Therefore, the European Commission (2006) and the IAEA (2011) recommended the use of U-shaped 8 mm radiolucent polystyrene spacer between PMMA slabs and compression paddle to replicate standard breast thickness. However, the use of spacers resulted in air gaps within the phantom which affect X-ray scattering by the phantom (Boone et al., 2000; Bouwman et al., 2013). Therefore, a breast phantom described by Bouwman et al. (2013) was used as a standard breast for the purpose of this thesis.

Bouwman's design consists of a 53.0 mm thick phantom containing 32.5 mm thick Poly(Methyl Methacrylate) (PMMA) and 20.5 mm thick polyethylene (PE) slabs. The PE slabs were placed above and the PMMA slabs beneath. The shape and area of the PMMA-PE phantom depends on the mammographic breast projection. For the average breast in CC projection, the shape of the compressed breast is approximately semicircular with a 95 mm radius. However, because the pectoral muscle is included in the MLO projection a rectangular phantom with 100 mm X 150 mm was used with a required thickness of PMMA (32.5 mm) and polyethylene (25.5 mm) (Diffey, 2012; Wang et al., 2013). Consequently, as recommended by the IAEA (2011) breast thickness in MLO position is 5 mm thicker than in CC position.

5.2.4 Positioning of the ATOM and Breast Phantoms

The ATOM and breast phantoms were positioned using a full field digital mammography system to simulate a woman's position during screening mammography. In order to minimise errors due to differences in ATOM phantom positioning in relation to the range of experiments to be carried out at the same or different hospital sites, several lines were drawn on the ATOM phantom chest wall, see **Figure (5-12)**. The lines (1) and (2) were useful for CC projection to determine the vertical and horizontal position of the CC breast phantom, respectively. The other three lines were for MLO projection. Line (3) was for the upper boarder of the MLO phantom while line (4) was for the lower boarder. Finally line (5) represented the transverse midline in the MLO phantom.

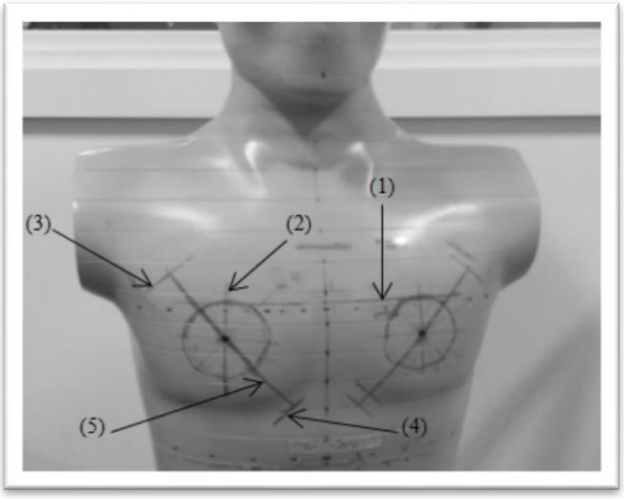

Figure (5-12) Shows the breast phantoms position lines on ATOM phantom chest wall. Lines (1) and (2) are for CC positioning, and lines (3), (4), and (5) are for the MLO positioning.

5.2.4.1 Positioning phantoms for MLO

For MLO projection simulation **(Figure 5-13)**, the gantry was tilted to 47^{o}. This value of angulation is determined depending on ATOM phantom body contour (Mercer , Hill, Kelly, & Smith, 2015). The MLO phantom was centred on the detector on the chest wall side and the compression paddle with standard compression (100 N) was used to fix it in position. The ATOM phantom was arranged in contact with the breast phantom where the midpoint in the side of the breast phantom coincides with the centre point in the breast site on the ATOM phantom. The detector was placed against the ribs with its corner in the axilla (Lee, Stickland, Wilson, & Evans, 2003; Mercer et al., 2015).

5.2.4.2 Positioning phantoms for CC

The CC projection **(Figure 5-14)** was achieved with a vertical X-ray beam / perpendicular to the floor. Initially, the CC breast phantom was centred on the detector on the chest wall side and fixed in position by the compression paddle using standard compression (100 N). The midpoint in the side of the breast phantom was arranged to coincide with the centre point in the breast site on the ATOM phantom, which faced the mammography system (Kopans 2007; Mercer et al., 2015).

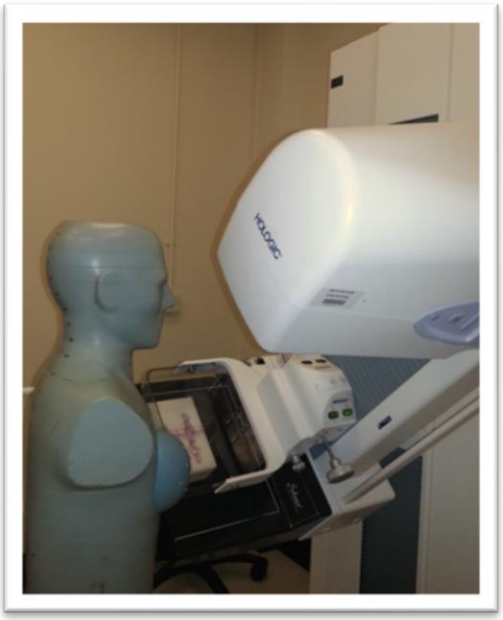

Figure (5-13) ATOM and MLO breast phantoms on FFDM system in MLO position.

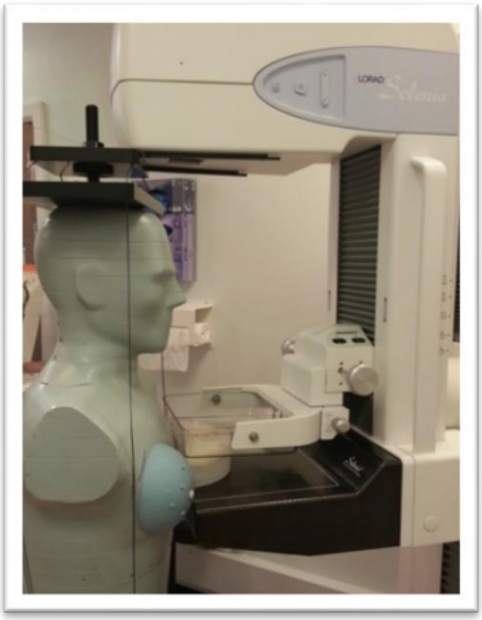

Figure (5-14) ATOM and CC breast phantoms on FFDM system in CC position.

The MLO and CC projections explained above were carried out for both breasts to imitate a clinical screening mammography event. Since automatic exposure control (AEC) is the most commonly used technique in screening mammography, it was also adopted to expose the breast phantom for the experimental work in this thesis. For each projection (CC and MLO for each breast) the phantom was exposed three times and then the results were averaged to minimise random error. TLDs were then collected and read to obtain the organ radiation dose for a 'complete screening event'.

5.3 Estimation of Examined Breast Dose

Examined breast MGD was calculated as recommended by IPEM (2005) (Report 89) using the equation defined by Dance, Skinner, Young, Beckett, and Kotre (2000):

$$MGD=K.g_{53}.c_{53}.s$$

Where K is the incident air kerma for the phantom, g_{53} is a factor to convert the incident air kerma to MGD for a 53 mm thick standard breast, c_{53} is a conversion factor which allows for the density of a 53 mm thick standard breast, s is the spectral correction factor. The values for the above factors are listed in same IPEM (2005) report (89), except s factor for W/Ag target/filter combination which was taken from IAEA quality assurance programme for digital mammography, for different half-value layers (HVL) between 0.30 and 0.60 mm Al. For harder x-ray beams (HVL more than 0.60 mm Al) the factors presented in European Commission (2013) mammographic quality assurance guidelines were used. **Tables (5-4)** and **(5-5)** list g_{53} and s factors used in this thesis, respectively.

In this thesis the c_{53} correction factor was not used (considered equal to 1) in the calculation of MGD as this factor is used for the correction of MGD from the equivalent glandularity of the phantom which is 29% to 50% glandularity breast. The use of this factor would mean that the MGD would be calculated for a 50% glandularity breast. This would introduce uncertainties since the other organ doses are measured for a 29% glandularity breast (the representing glandularity of used breast phantom).

Table (5-4) Lists g_{53} factor for different HVL (European Commission, 2013; IPEM, 2005)

HVL	g_{53} factor
0.30	0.155
0.35	0.177
0.40	0.198
0.45	0.220
0.50	0.245
0.55	0.272
0.60	0.295
0.65	0.317

Table (5-5) Lists *s* factor for different target/filter combinations (IPEM, 2005)	
Target/filter combination	*s* factor
Mo/Mo	1.000
Mo/Rh	1.017
Rh/Rh	1.061
W/Rh	1.042
W/Ag*	1.042
* *this value is taken from IAEA (2011)*	

5.3.1 Incident Air kerma Measurement

The incident air kerma was measured using the Unfors Multi-O-Meter solid state dosimeter (Billdal, Sweden). This solid state dosimeter was used because it is more accurate than TLDs for two reasons, namely, it is a direct dose measurement tool which can avoid small errors associated with the TLD calibration process and backscatter is not included in the Unfors Multi-O-Meter solid state dosimeter reading. The use of TLDs for incident air kerma measurement requires division of the measured kerma value by a backscatter factor to eliminate the effect of backscatter (Nelson & Hill, 2011). The measurement process was performed using the method described by IAEA (2011). According to this method the Unfors Multi-O-Meter solid state dosimeter was attached to the lower surface of the compression paddle at the midpoint, approximately 4 cm from the chest wall. The height of compression paddle was arranged to replicate the breast thickness. Incident air kerma was measured using the same exposure factors which were used for all exposures of the breast phantom for each mammography machine used within this thesis (IAEA, 2011).

5.3.2 Half-Value Layer (HVL) Estimation

The thickness of a specific material required to attenuate the air kerma of a narrow X-ray beam to half of its value is known as the half-value layer (Ma et al., 2001). Mammographic X-ray beam half value layer is a parameter of great importance in MGD calculation (IPEM, 2005). In this thesis the HVL of the mammographic X-ray beam was experimentally derived according to the procedure described by IPEM (2005) in report 89. An Unfors solid state dosimeter and high purity aluminium foils of thickness ranging from 0.1 mm to 0.6 mm with 0.1 mm steps were used. The foils were placed in front of the X-ray beam window with the compression paddle midway between the foils and detector. During HVL assessment the

presence of the compression paddle is essential for accurate results. Hourdakis, Boziari, and Koumbouli (2009), who investigated the effect of the compression paddle on mammography dosimetric measurements, found that compression paddle results in beam hardening and hence higher HVL. Tung et al. (2010) found the use of TLDs for HVL determination is associated with ±7% difference compared to HVL estimated by other dosimeters type. Therefore, TLDs are not recommended to be used for HVL assessment (Tung et al., 2010). Finally, as recommended by the European Commission (1996), the HVL was graphically derived by an interpolation method. This was done by plotting the detector readings algorithms against the relevant foil thickness. For this purpose and to increase the accuracy of the extrapolated HVL, at least five points were used to draw the graph; see **Figure (5-15)**. The HVL was estimated for each of the sixteen FFDM machines studied within this thesis. For same FFDM machine, the HVL of each CC and MLO projections has been assessed separately, if beam of different quality had been selected by AEC, see **Table (5-4)**.

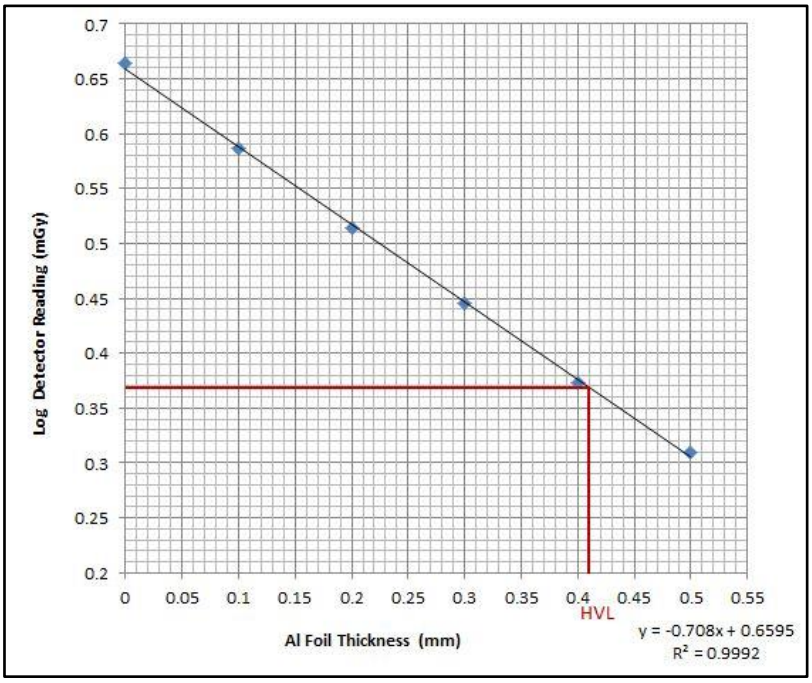

Figure (5-15) Shows the graphical extrapolation method of HVL.

Table (5-6) Illustrates the HVL (mm Al) for CC and MLO beams for each studied machine.					
Mammographic machine number	CC beam HVL	MLO beam HVL	Mammographic machine number	CC beam HVL	MLO beam HVL
(1)	0.40	0.50	(9)	0.45	0.45
(2)	0.60	0.65	(10)	0.55	0.55
(3)	0.40	0.45	(11)	0.45	0.45
(4)	0.40	0.45	(12)	0.55	0.55
(5)	0.45	0.45	(13)	0.45	0.45
(6)	0.45	0.50	(14)	0.45	0.45
(7)	0.60	0.60	(15)	0.60	0.60
(8)	0.65	0.65	(16)	0.60	0.60

5.4 Effective Dose Estimation

As described by the ICRP (2007), the calculation of female effective dose includes the radiation dose received by 14 radiosensitive tissues (red bone marrow, colon, lung, stomach, breast, ovaries, urinary bladder, oesophagus, liver, thyroid, bone surface, brain, salivary glands and skin) within the body in addition to the dose received by the 13 less radiosensitive tissues. The latter are referred to as remainder tissues (adrenals, extra thoracic region, gall bladder, heart, kidneys, lymphatic nodes, muscle, oral mucosa, pancreas, small intestine, spleen, thymus, and uterus). The following equation, with ICRP (2007) publication 103 tissue weighting factors **(Table 5-7),** was used for the calculation of screening mammography effective dose:

$$E = \sum w_T H_T$$

Where E is the effective dose, w_T and H_T are the tissue weighting factor and radiation absorbed dose by tissue T, respectively. Breast tissue radiation dose includes the overall dose of both examined and contralateral breasts. As reported by Linet et al. (2012) MGD was used to represent examined breast radiation dose. Bone marrow radiation absorbed dose was calculated using Cristy (1981) red bone marrow distribution as recommended by the ICRP (1995). This was achieved by summation of the radiation dose received by bone marrow in each site multiplied by its percentage in that site. Since the bone surface and skin have low radio-sensitivity, w_T of each is 0.01, and small part of them is exposed to radiation during mammography, their radiation dose is negligible and not considered in the calculations. With

regard to remainder tissues, the radiation dose to the extra thoracic region, lymphatic nodes, muscle and oral mucosa were excluded because the ATOM phantom did not have dosimeter locations for these structures. The effect of this is likely to be negligible and to compensate the available 9 remainder tissue doses were averaged. This approach has been reported by Tootell et al. (2013).

Table (5-7) Lists ICRP (2007) publication 103 tissue weighting factors.

Tissue	w_T
Red bone marrow	0.12
Colon	0.12
Lung	0.12
Stomach	0.12
Breast	0.12
Gonads	0.08
Urinary bladder	0.04
Oesophagus	0.04
Liver	0.04
Thyroid	0.04
Bone surface	0.01
Brain	0.01
Salivary glands	0.01
Skin	0.01
Remainder tissues (Adrenals, Extrathoracic region, Gall bladder, Heart, Kidneys, Lymphatic nodes, Muscle, Oral mucosa, Pancreas, Small intestine, Spleen, Thymus, Uterus or Prostate	0.12
Total	**1.00**

5.5 Effective Risk Calculation and Screening Programme Total Effective Risk Assessment

The effective risk was calculated using the equation described by Brenner (2012) as follows:

$$R = \sum r_T H_T$$

Where R is the effective risk, r_T is the lifetime attributable risk (LAR) of radiation-induced cancer for tissue T per unit equivalent dose to that tissue, and H_T is the equivalent dose received by tissue T.

The lifetime attributable cancer risk of different tissues (r_T) were taken from BEIR VII – Phase 2 report of National Academy of Sciences (NAS) (2006). Since these values are only presented for each decade of female age **(Table 5-8)**, they were plotted graphically against age in order to extrapolate an approximate value for each year of female life. For this purpose three approaches have been used.

Table (5-8) Lifetime attributable risk of radiation-induced cancer for tissues which received radiation dose during screening mammography for each decade of female age as listed in Table 12D-1 of the BEIR-VII report (NAS, 2006).

Tissue*	Lifetime Attributable Risk (cases /10,000 persons /Gy) at different ages						
	20	30	40	50	60	70	80
Breast	429	253	141	70	31	12	4
Stomach	52	36	35	32	27	19	11
Liver	14	10	10	9	7	5	2
Lung	346	242	240	230	201	147	77
Thyroid	113	41	14	4	1	0.3	0
Other	323	207	181	148	109	68	30

**The LAR values for colon, ovaries, uterus and urinary bladder are not presented because they don't receive radiation dose during screening mammography.*

In the first approach curve fitting was used. For all tissue types the change (reduction) in tissue radio-sensitivity (LAR) between the ages of 20 and 30 is completely different from that after the age of 30, see **Figure (5-16)** for lung tissue. Accordingly, in order to minimise the error in the fitting process two lines of best fit were created for each type of tissue. The first one obtains the LAR for years 21-29 inclusive and the second determines the LAR for years 31-39, 41-49, 51-59, 61-69, and 71-79 inclusive. Since the best fit line of linear relationship between two points (risk for ages 20 and 30 years) has been used in the first fit line, the coefficient of determination (R^2) has to be 1 as there are only two points available to plot the graph, see **Figures (5-17) and (5-18)**. However, in the second best fit line a second order polynomial relationship has been used for all tissue types ($R^2 > 0.99$) except for thyroid tissues where an exponential relationship has been used ($R^2 = 0.9984$), see **Figures (5-19) and (5-20)**. This was done because the R^2 of second order polynomial relationship of thyroid tissue was (0.95).

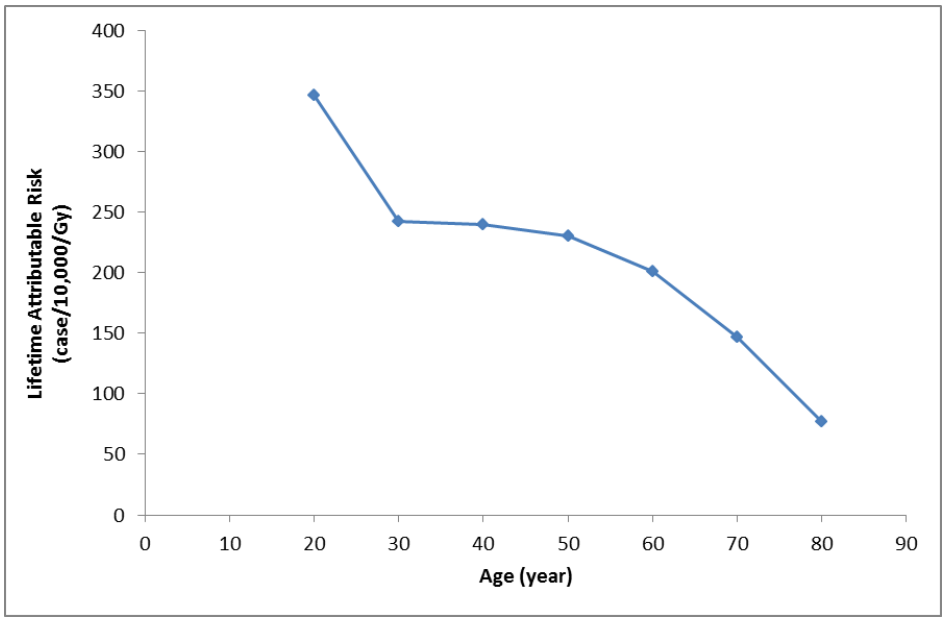

Figure (5-16) Demonstrates the lung tissue radio-sensitivity change (LAR change) against age. This provides an illustration of the complete difference in tissue LAR change for those aged 20-30 compared to older ages.

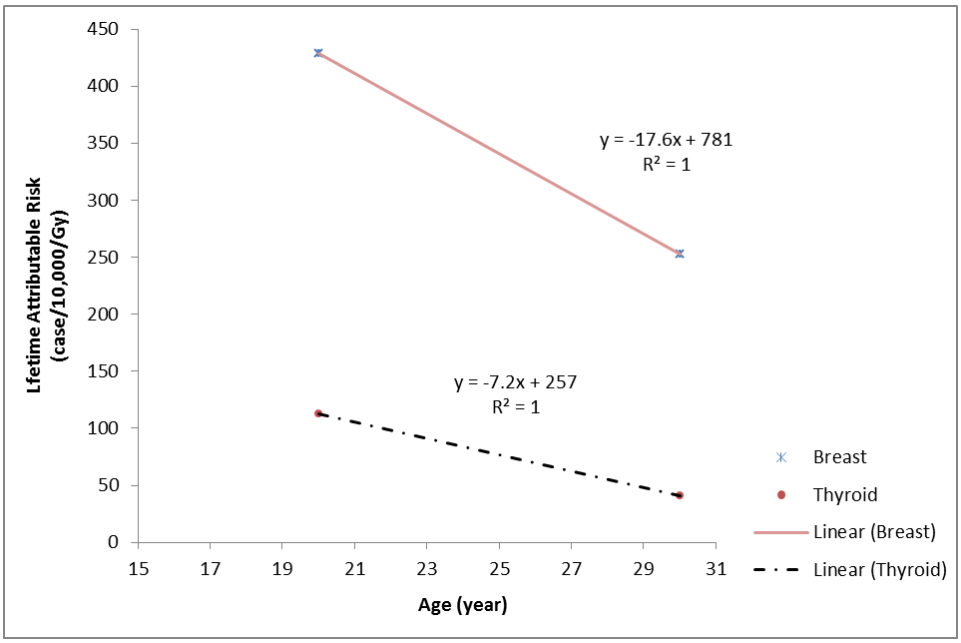

Figure (5-17) Shows the lifetime attributable risk of radiation-induced cancer in breast and thyroid tissues for women age 20-30 years using a linear relationship.

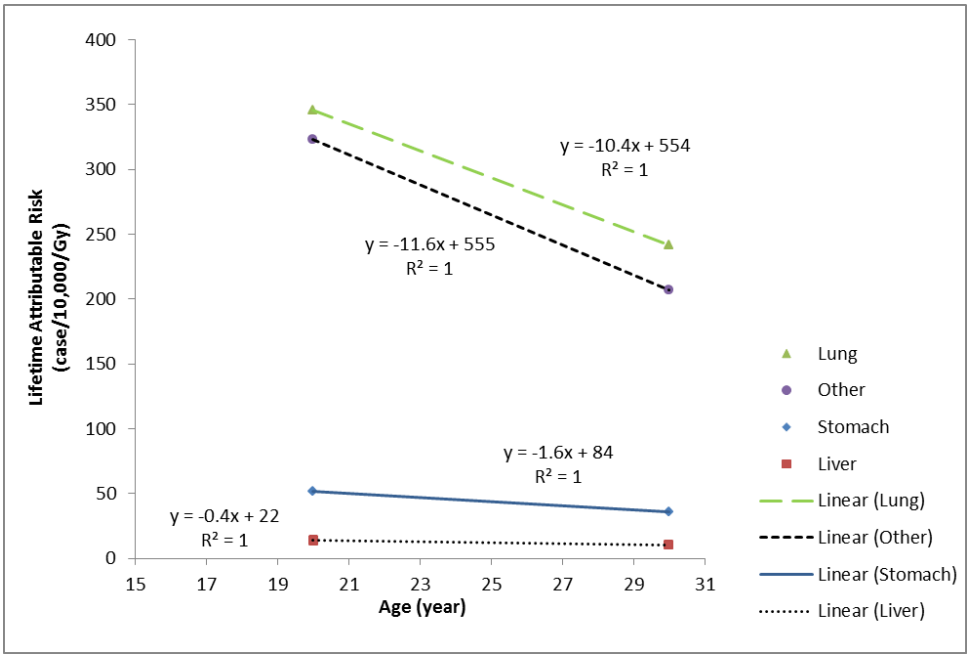

Figure (5-18) Shows the lifetime attributable risk of radiation-induced cancer in lung, stomach, liver, and other tissues for women age 20-30 years using a linear relationship.

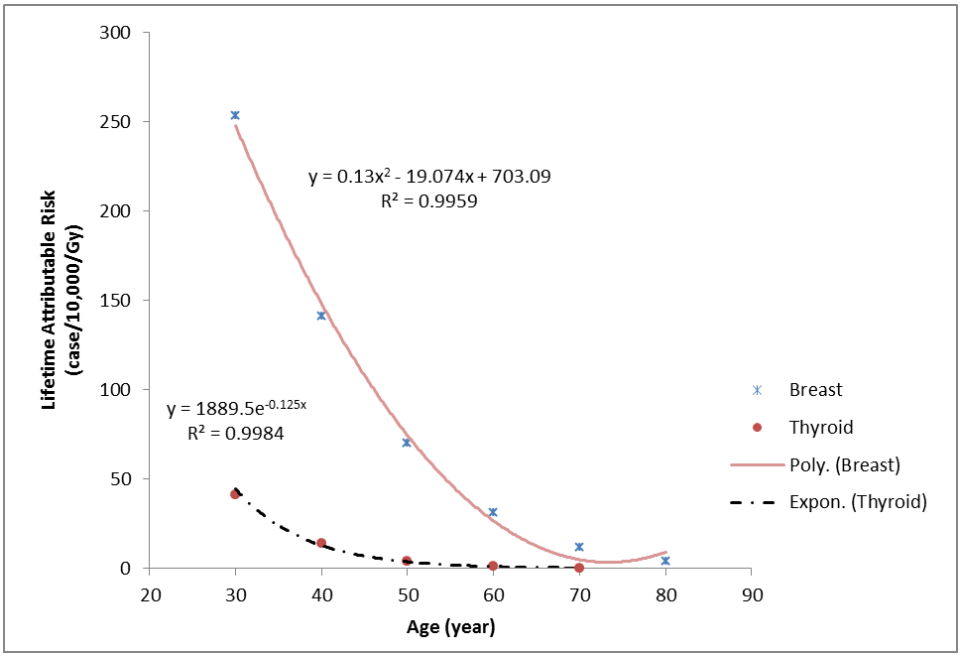

Figure (5-19) Shows the extrapolation of the lifetime attributable risk of radiation-induced cancer in breast and thyroid tissues for women age 30-80 years using a polynomial relationship for breast tissue and an exponential relationship for thyroid tissue. Breast tissue LAR increment between 70 and 80 year is due to curve fitting error.

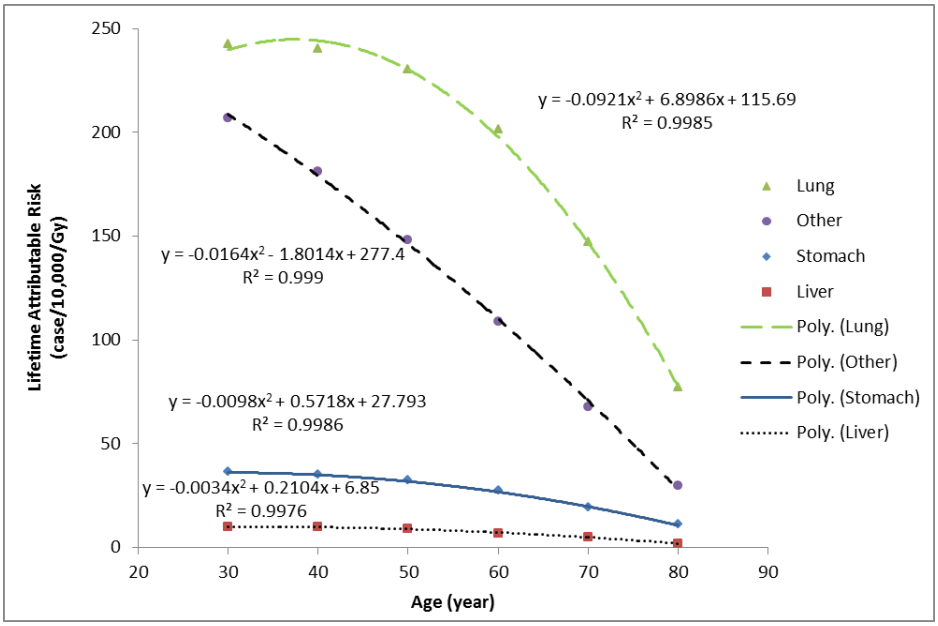

Figure (5-20) Shows the extrapolation of the lifetime attributable risk of radiation-induced cancer in lung, stomach, liver, and other tissues for women age 30-80 years using a polynomial relationship.

The second approach depends on the use of linear relationships between the risk values for successive decades to extrapolate the LAR value for each year of female lifetime as recommended by Li et al. (2011), see **Figures (5-21)** and **(5-22)**.

For the third approach, a stepping method was used in which the same risk value has been used for whole decade (i.e. the same risk value has been used for age 20-29, 30-39…etc.), see **Figures (5-23)** and **(5-24)**.

Using the three approaches, the experimental dose data of each FFDM machine **(Appendix A)** were used to calculate the radiation effective risk for females aged 25-75 years, the earliest and the latest possible ages of screening mammography **(Appendix B)**. For the effective risk calculation other tissues were not indicated in the BEIR VII. Therefore, the other tissue dose was determined from the radiosensitive tissues as indicated in the ICRP to include: the radiation dose to brain, bone marrow, adrenals, heart, kidneys, gall bladder, pancreas, spleen, thymus, oesophagus and salivary glands. Finally, the total radiation effective risk, during a woman's life, from screening mammography was calculated for different country-based mammography screening programmes listed in **Table (3-4)** (page 59) and **Table (3-5)** (page 60).

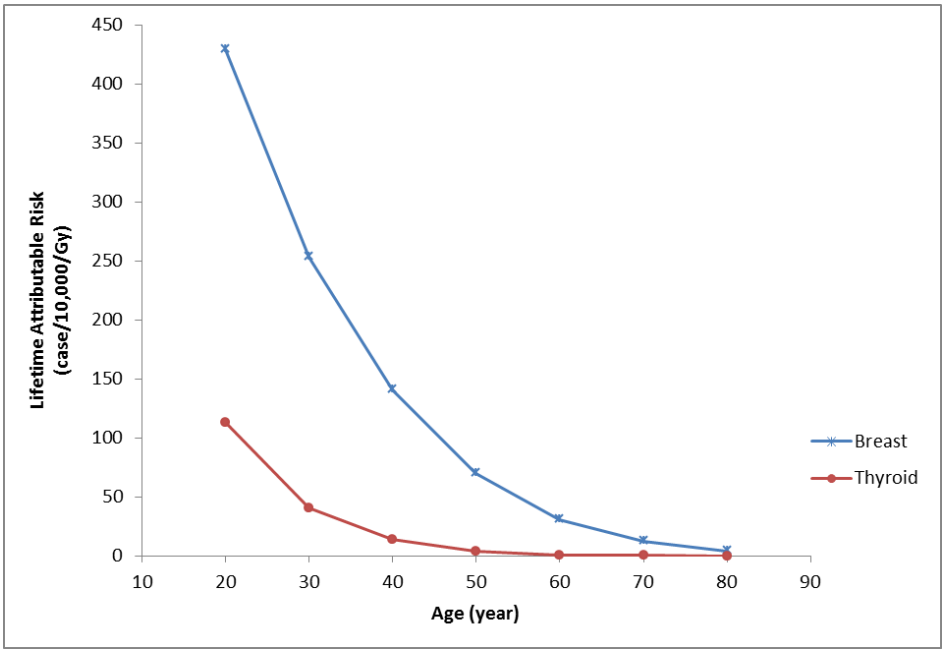

Figure (5-21) Demonstrates the extrapolation of the lifetime attributable risk of radiation-induced cancer in breast and thyroid tissues using a linear relationship between two successive decade values.

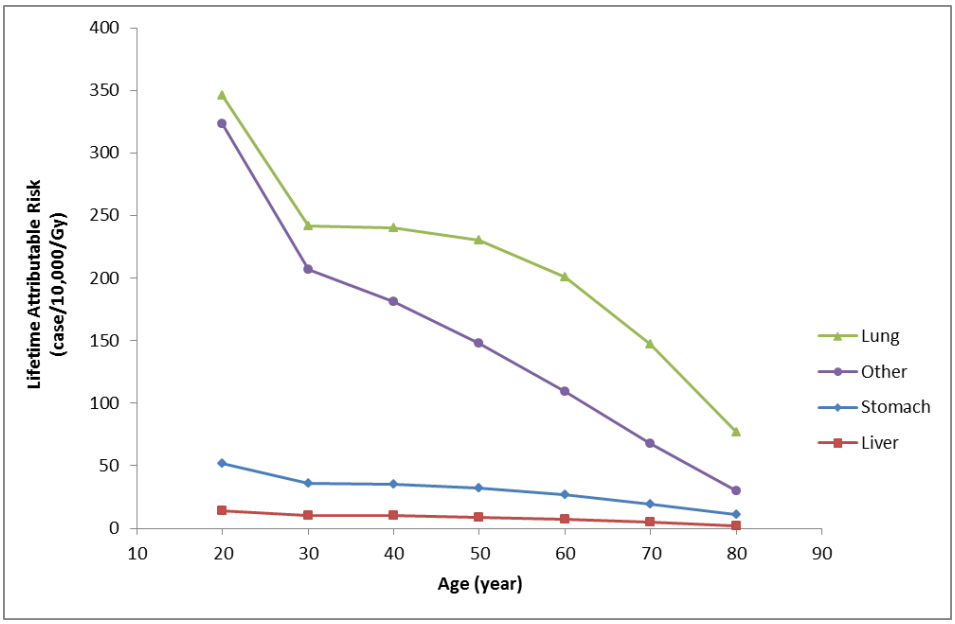

Figure (5-22) Demonstrates the extrapolation of the lifetime attributable risk of radiation-induced cancer in lung, stomach, liver and other tissues using a linear relationship between two successive decade values.

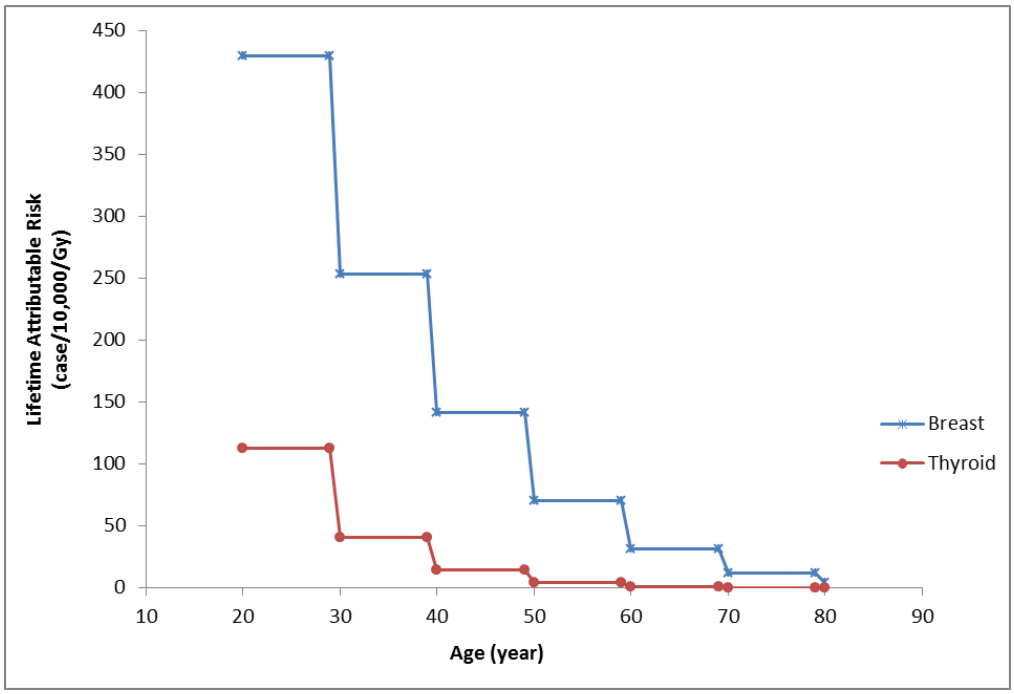

Figure (5-23) Demonstrates the extrapolation of the lifetime attributable risk of radiation-induced cancer in breast and thyroid tissues using a stepping approach.

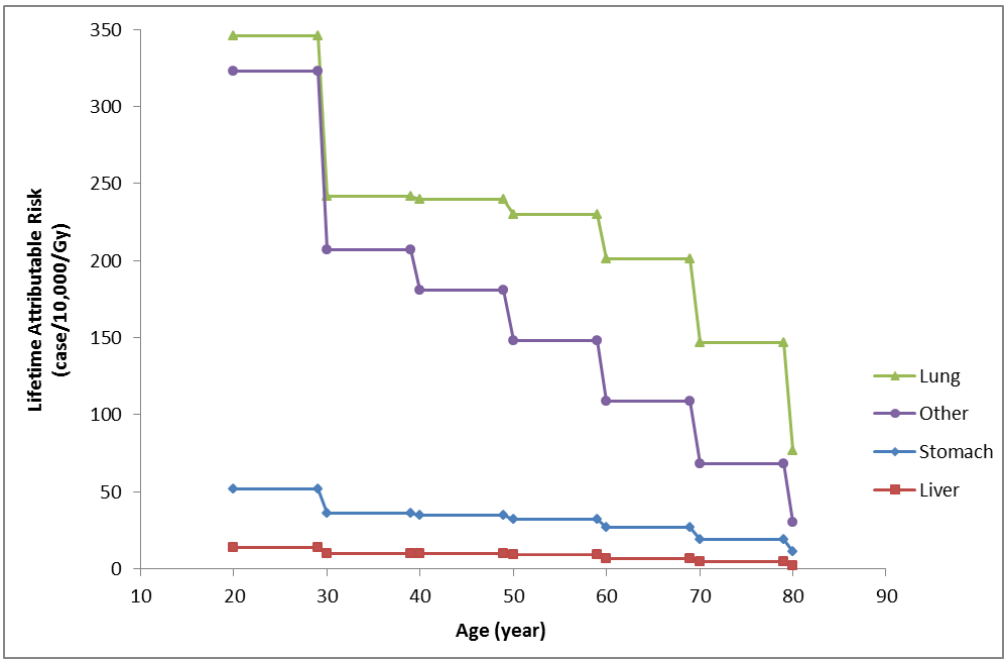

Figure (5-24) Demonstrates the extrapolation of lifetime attributable risk of radiation-induced cancer in lung, stomach, liver and other tissues using a stepping approach.

5.6 Mammographic Machines

In order to validate the method, organ radiation dose measurement and radiation effective dose/risk estimation were repeated for sixteen full field digital mammography (FFDM) machines. These are from the actual machines used in the NHSBSP. All of the machines fell within the quality control programme of NHSBSP which includes: evaluation of beam alignment, detector performance, AEC, image display monitors, image display printers, image quality, and radiation dose (NHSBSP, 2009). The mammography machines were from four different manufacturers. Eight were Seno Essential from GE Healthcare with a Rh/Rh target/filter combination. Five machines were Hologic: three Selenia and two Selenia Dimensions. Two of the Selenia machines had a Rh/Rh and the other had a Mo/Mo anode/filter. The Selenia Dimensions machines had a W/Rh target/filter combination. The two Siemens Mammomat Inspiration machines had a W/Rh anode/filter combination. Finally, One Giotto machine from IMS had a W/Ag target/filter combination. In order to differentiate each machine from the others, each one was given a unique number. For this purpose the numbers from 1 to 16 have been used **(Table 5-9)**. For the first two machines the whole process was repeated three times in order to investigate experimental repeatability.

Table (5-9) The sixteen FFDM machines used in this study.		
Machine Number	Machine Brand	Target/filter combination
1*	Hologic Selenia	Mo/Mo
2*	Hologic Selenia	Rh/Rh
3	Hologic Selenia Dimensions	W/Rh
4	Hologic Selenia	Rh/Rh
5	GE Seno Essential	Rh/Rh
6	GE Seno Essential	Rh/Rh
7	Hologic Selenia Dimensions	W/Rh
8	Giotto	W/Ag
9	GE Seno Essential	Rh/Rh
10	GE Seno Essential	Rh/Rh
11	GE Seno Essential	Rh/Rh
12	GE Seno Essential	Rh/Rh
13	GE Seno Essential	Rh/Rh
14	GE Seno Essential	Rh/Rh
15	Siemens Mammomat Inspiration	W/Rh
16	Siemens Mammomat Inspiration	W/Rh
*Mammography machines exposure to a further two retests in order to evaluate the reliability of the experimental data acquired from the FFDM machines.		

5.7 Pilot Experiment

A pilot experiment was conducted. The main purpose of the pilot experiment was to assess the feasibility of the proposed method. In this experiment the data was collected from one FFDM machine (machine number 1 / Hologic Selenia / **Table (5-9)**) which had a Mo/Mo target/filter combination. This pilot experiment required two visits to the FFDM machine. The first visit included organ dose measurement as previously described in section 5.3 and examined breast entrance air kerma measurement for MGD calculation. The purpose of the second visit was to calibrate the TLDs and HVL assessment. TLDs were calibrated against the Unfors solid state dosimeter. As recommended by Olgar et al. (2009), TLDs were calibrated by the same mammographic machine because the TLDs sensitivity is dose dependent. Since different kV values have been selected for CC and MLO breast phantoms (by AEC), the HVL was assessed for each to derive a more accurate MGD calculation.

During each visit three TLDs from each TLD group were used to assess background radiation; this was subtracted from the other TLDs, which were used for organ dose measurement readings.

During the first visit the exposure factors selected by the AEC were recorded so they could be replicated for kerma measurement, HVL assessment and TLD calibration. Three exposures were made for each projection to minimise the random error. Then all TLDs were collected and read to obtain organ doses as previously described in section 5.2.2. The organ dose calculations together with calculated MGD (section 5.3) were used to obtain an effective dose. The total effective risk during female lifetime was then calculated for the NHSBSP screening programme for the UK average and high breast cancer risk categories; this was based upon screening age commencement, cessation age and also the screening interval (the time between screening events). This required the calculation of effective risk for women aged 40-73 because in the UK the average risk women are invited for triennial screening mammography between the ages of 47 and 73, while the high risk women aged 40-73 are invited for annual screening mammography.

The main outcome of this pilot experiment was that firstly, the required angle for MLO position was determined by an expert practitioner and fixed for the whole next work. Secondly, the errors due to ATOM phantom positioning in relation to breast phantom were identified and for more consistent positioning additional lines were drawn on the ATOM to improve reproducibility of position. Finally, since the contralateral breast received the highest radiation dose when compared to other organs, the potential importance of using a contralateral breast shield was raised; this resulted in an additional component to the thesis – an evaluation of a secondary radiation breast shield to minimise dose to the contralateral breast. The result of this pilot experiment was presented as a scientific poster in the UKRC 2015 (M.Ali, England, & Hogg, 2015). The method for this thesis together with pilot experiment results was also published (M.Ali, England, McEntee, & Hogg, 2015).

5.8 Effective Risk Modeling

In some countries an individual has the right to know the risk of radiation associated with any radiological examination. One could argue this is especially important in screening mammography as healthy (asymptomatic) women are involved. This is part of the European Commission legislation (European Commission, 2014). To comply with this requirement and in order to make data suitable for daily use in screening mammography centres, three methods have been used in this thesis to model the risk of radiation-induced cancer from screening mammography. All these methods are based on total effective risk calculation. The main purpose of all of the modelling methods was to produce an estimate of screening mammography effective risk without the need for complex and time consuming calculations, this is important because time is critical in clinical work. However, when undertaking this work the accuracy of these models was found to be different. In general, the first and second models (sections 5.8.1 and 5.8.2, respectively) can be considered as preliminary steps that led to the development of the final more accurate model (third model / section 5.8.3). The first and second models involve the effective risk prediction depending on the average risk value for the sixteen studied machines, age of commencement/cessation of screens, number of screens, and time interval between successive screens (screening frequency). The additional factor that is likely to help improve the accuracy of the resultant data from the third model was the inclusion of MGD variations of the different sixteen studied FFDM machines.

5.8.1 Multiple Regression for Total Effective Risk Modelling (First Effective Risk Model)

Regression is a statistical concept used to assess the effect of one or more independent variables on an outcome (dependent) variable (Zou, Tuncali, & Silverman, 2003). The importance of regression models in medical studies is seen in two different areas. The first area is to investigate the effect of an explanatory factor or factors on an outcome variable after adjusting other explanatory variables. The second area represents the most common one and includes the building of predictive models for the dependent variable in relation to independent variables (Gareen & Gatsonis, 2003; Zou, Tuncali, & Silverman, 2003). According to the number of independent variables the regression models are either simple regression when the effect of one independent variable is evaluated against an outcome

dependent variable; or multiple regression when the effect of more than one variable is investigated on an outcome variable (Gareen & Gatsonis, 2003).

In diagnostic imaging research regression is increasingly used (Gareen & Gatsonis, 2003). The regression model construction is, generally, based on research question and data nature. Sometimes the regression model may be invalid when the assumption on which the model is built is incorrect and hence the data generated by the regression model is also incorrect (Gareen & Gatsonis, 2003). In this thesis an effective risk model was built based on multiple linear regression using the average effective risk values for the sixteen mammography machines to predict the total effective risk of any screening programme throughout the world (as dependent variable) from commencement/cessation ages of screening and screening frequency.

The reliability of a regression model is dependent on sample size of collected data. Although the pervasive rule determined required sample size for regression by the number of predictors (10-15 cases of data per each predictor), but Field (2013) stated that the required sample size for regression is determined by the strength of relationship being measured and the required statistical power. Generally he reported that the bigger the sample size, the better the regression model is generated. Therefore, in order to improve the statistical power, two hundred and seventy four different screening scenarios were proposed which comprised of different commencement / cessation ages (25-75 years) and time intervals between screens. For each proposed lifetime interval, such as 25-75 years, 30-75 years, and 30-70 years, three different screening categories with regard to screening frequency (annual, biennial, or triennial) were used **(Appendix C)**. These three screening frequencies were chosen because these are the only ones recommended by worldwide screening programmes. Lifetime risk data, arising from the 274 scenarios was analysed using SPSS 22.0 software (IBM, Armonk, New York, USA) to generate a mathematical regression model and to assess the relationship between total effective risk and different time intervals and commencement/cessation ages.

5.8.2 Graphical Extrapolation of Total Effective Risk (Second Effective Risk Model)

In addition to regression modelling a further approach was used to estimate total effective risk – graphical extrapolation. Since tissue radio-sensitivity decreases with age, especially

after 70, and most of the screening programmes end at 70 or slightly higher, the end age of screening in this total effective risk model is set to 75 years.

To establish this model the average total effective risk data of the sixteen machines was used to present the relationship between screening commencement age and total effective risk graphically. In this model, 50 different screening commencement ages (25-74 years) were selected and the total effective risk for three different screening frequencies (annual, biennial, and triennial) was calculated. Consequently, the total effective risk extrapolation graph contains three relationship lines; one for each screening frequency. The same method has been used to generate a model for each set of extrapolated LAR factors.

5.8.3 Graphical Extrapolation of Total Effective Risk with Including MGD Variation (Third Effective Risk Model)

This model is the final and a more comprehensive model in which the effect of MGD variations of different mammographic machine on the total effective risk was considered. The same scenarios used to generate the previous model (section 5.8.2) were also used to generate this model. However, before generating the risk model, the relationship between the MGD and total effective risk for each scenario was established using the data from the 16 FFDM machines to accommodate the effect of MGD variations of different FFDM machines on women's total effective risk **(Appendix D)**. The resultant graphs of this risk model present the relationship between screening commencement age and MGD conversations factor to total effective risk. Therefore, the total effective risk can be determined for any screening category (commencement age and screening frequency) at recorded MGD.

5.9 Contralateral Breast Shield Intervention Study

One important characteristic of good radiographic practice is that the radiation dose to the patient is kept as low as possible with adequate and consistent image quality. Many steps can be taken to reduce the radiation dose (Iball & Brettle, 2011). Protective radiation shielding is widely used to protect radiosensitive body tissues and organs from potential damage resulting from ionising radiation. Radiosensitive areas have been determined by the ICRP (2007) and they include those tissues with higher tissue weighting factors **(Table 5-7)**. These organs and tissues may be selectively protected by the use of specific area shielding. Specific area shields are available in two different types, namely, contact shields such as gonads shield and

shadow shields which are fixed in the X-ray tube within primary beam field such as both breast and gonad shield which used for scoliosis patients during full spine imaging (Statkiewicz-Sherer, Visconti, & Ritenour, 2010).

The main purpose of using specific area shielding is to protect the radiosensitive tissues from the primary X-ray beam. However, in this thesis a breast shield has been used to protect the contralateral breast tissue, which is one of the radiosensitive tissues with a 0.12 tissue weighting factor (ICRP, 2007), from scattered radiation during screening mammography because in the pilot study the contralateral breast received the highest radiation dose after examined breast. Previous studies found that the use of specific area shielding against scattered radiation during radiography may significantly reduce organ dose and effective dose (Iball & Brettle, 2011). The theoretical effect of a contralateral breast shield (by considering the contralateral breast radiation dose equal to zero) showed that it can reduce both the effective dose and effective risk by approximately 1.5%, see **Table (5-10)** and **Table (5-11)** for effective dose and effective risk, respectively.

Accordingly, the effect of the contralateral breast shield was experimentally investigated on a women's organ doses, effective dose (for one screening visit), and total effective risk (during a women's lifetime) for different worldwide screening programmes. In this thesis the contralateral breast shield was made from a redundant lead rubber protective apron.

Table (5-10) Demonstrates the effect of contralateral breast dose on the effective dose of one screening session.

Machine number	Effective dose (µGy)		Reduction (%)
	Including all organ dose	Excluding contralateral breast dose	
1	325.85	322.66	0.98
2	315.72	312.16	1.13
3	248.50	242.79	2.30
4	232.94	228.64	1.85
5	244.87	241.92	1.21
6	216.36	213.57	1.29
7	343.73	338.40	1.55
8	270.33	265.71	1.71
9	223.16	220.62	1.14
10	259.70	256.57	1.21
11	204.45	202.20	1.10
12	241.28	238.09	1.32
13	226.97	224.00	1.31
14	230.89	227.88	1.31
15	214.93	211.57	1.56
16	210.65	208.37	1.08
Mean (SD)	250.65 (42.70)	247.20 (42.18)	1.38 (0.34)

Table (5-11) Shows the effect of contralateral breast dose on effective risk of one screening session at different female ages (25-75 years) - average value for the sixteen machines with standard deviation (SD).

Age (year)	Reduction (%)*, Mean (SD)	Age (year)	Reduction (%)*, Mean (SD)
25	1.39 (0.33)	51	1.39 (0.33)
26	1.39 (0.33)	52	1.39 (0.33)
27	1.39 (0.33)	53	1.39 (0.33)
28	1.39 (0.33)	54	1.39 (0.33)
29	1.39 (0.33)	55	1.39 (0.33)
30	1.39 (0.33)	56	1.39 (0.33)
31	1.39 (0.33)	57	1.39 (0.33)
32	1.39 (0.33)	58	1.39 (0.33)
33	1.39 (0.33)	59	1.38 (0.32)
34	1.39 (0.33)	60	1.38 (0.32)
35	1.39 (0.33)	61	1.38 (0.32)
36	1.39 (0.33)	62	1.38 (0.32)
37	1.39 (0.33)	63	1.38 (0.32)
38	1.39 (0.33)	64	1.37 (0.32)
39	1.39 (0.33)	65	1.37 (0.31)
40	1.39 (0.33)	66	1.37 (0.31)
41	1.39 (0.33)	67	1.36 (0.31)
42	1.39 (0.33)	68	1.36 (0.30)
43	1.39 (0.33)	69	1.35 (0.30)
44	1.39 (0.33)	70	1.34 (0.30)
45	1.39 (0.33)	71	1.33 (0.29)
46	1.39 (0.33)	72	1.33 (0.29)
47	1.39 (0.33)	73	1.33 (0.29)
48	1.39 (0.33)	74	1.33 (0.29)
49	1.39 (0.33)	75	1.37 (0.38)
50	1.39 (0.33)		

*Reduction (%) represents the reduction percentages in effective risk when contralateral breast dose is equal to zero. These were calculated using LAR extrapolated by a best fit line method. Approximately the same reduction values were found for the other two sets of extrapolated LAR data.

5.9.1 Testing of the Lead Protective Apron

Before using the protective lead apron in the experiment, it was tested as described by Oyar and Kislalioglu (2012) using a Wolverson Arcoma Arco Ceil general radiography X-ray machine (Arcoma, Annavägen, Sweden) with 100 kV and 20 mAs. During exposure, the apron's images were recorded using a 35 X 43 cm AeroDR 1417 digital radiography cassette (KONICA MINOLTA, Tokyo, Japan) to investigate the presence of any defects (fractures, cracks, or holes in the lead apron). The X-ray beam was collimated according to the detector size. The focal-film distance was arranged as in conventional radiography to be 110 cm. The intact area (defect free area) of the apron was determined and used for manufacturing the contralateral breast shield.

5.9.2 Determination of Apron Equivalent Lead Thickness

Different materials have been used to manufacture X-ray protective aprons. These materials are mainly composed of heavy metals (e.g. copper, yttrium, tin, antimony, barium, tungsten, and lead). However, the protective efficiency of all protective aprons, regardless the material from which they are made, is expressed as lead-equivalent thickness (Mori, Koshida, Ishigamori, & Matsubara, 2014). Since the contralateral breast shield aims to protect the breast from low energy X-ray radiation (scatter radiation), a low equivalent lead thickness is required. According to KIRAN (2010), a 0.25 mm equivalent lead thickness is sufficient to absorb approximately 96% of a 80 kV primary beam, while for 50 kV BC Centre for Disease Control (2016) reported that 0.25 mm lead equivalency can provide up to 99.5% protection. Prior to designing the contralateral breast shield, the equivalent lead thickness of used apron material was experimentally measured. Lead equivalent thickness measurement method described by Mori et al. (2014) was used. This method was based on the computational method using the equation of apron attenuation.

$$I = I_o\, e^{-\mu x}$$

I and I_o represent the radiation doses with and without lead equivalent material, respectively. The μ is the linear attenuation coefficient of the lead and x is the equivalent lead thickness. The utilisation of this equation requires the use of a mono-energetic beam because μ values are available for each photon energy. Therefore, before using the equation for the lead material, it was applied to aluminium foils of known thicknesses to find the μ value of the

aluminium material and therefore the effective energy of the beam could be determined using Hubbell and Seltzer (1996) tables of X-ray attenuation coefficients. Then the same beam was used to obtain the equivalent lead thickness. This procedure has been repeated for same mAs with three different X-ray beams with different energies of 40, 80 and 120 kV to minimise any errors. The average calculated equivalent lead thickness of apron material at the three energies was 0.225 mm (0.234, 0.193 and 0.249 mm, respectively). This value is slightly lower than the nominal equivalent lead thickness of the apron which is 0.25 mm. Similarly, Mori et al. (2014) found that the calculated equivalent lead thickness of aprons is usually less than the nominal thickness.

5.9.3 Contralateral Breast Shield Design

The contralateral breast shield designed for this thesis was suitable for use with the ATOM phantom; it is not suitable for clinical use due to a lack of a fixation mechanism. It was designed to comply with two basic requirements as follows:

- It can accommodate the ATOM phantom's breast attachment well to provide maximal protection against radiation.
- It should not interfere with breast support and compression paddle of the mammographic machine.

Accordingly pieces of paper were first used to develop a series of different shield shapes. These prototypes were tested to see whether they could comply with the basic requirements or not. A suitable design was determined to be a diverging cone, see **Figure (5-25)**. Diverging rather than a symmetric cone was chosen because the symmetric cone may interfere with breast support and compression paddle of the mammography system. Then the chosen design was used to make the lead contralateral breast shield.

Figure (5-25) Illustrates the designed contralateral breast shield.

5.9.4 Data Collection with the Use of Contralateral Breast Shield

In order to investigate the effect of the contralateral breast shield on breast dose, effective dose, and effective risk, the whole procedure of organ dose measurement was repeated for four FFDM machines. These machines were selected after grouping the original sixteen machines into four categories according to their calculated effective risk values. One machine was chosen from each category. In order to find the effect of the contralateral breast shield, organ dose measurements without and with contralateral breast shield were repeated within the same week. The same procedure previously explained in section 5.2 was used to measure organ dose, see **Figure (5-26)**. After organ dose measurement the effective dose and effective risk along with total effective risk of worldwide screening programmes calculations were repeated.

(a) **(b)**

Figure (5-26) Shows contralateral breast shield intervention **(a)** In CC projection, **(b)** In MLO projection.

Chapter Six
Results

6.1 Chapter Overview

This chapter presents the results of this PhD thesis. In general screening mammography dosimetric data from sixteen FFDM machines are included. This data is represented in two different ways, namely absorbed dose (μGy) and effective risk (case/10^6), which is the number of radiation-induced cancers. Following this, based on the data acquired, a novel method has been established to assess the risk of radiation-induced cancer from screening mammography.

Within this chapter the results are organised into four main sections. Results of organ dose measurements and the examined breast MGD are the focus of the first section. Dose measurement reliability data have also been considered in this section. The results of LAR factors extrapolated by three different methods and total effective risk of worldwide screening programmes are illustrated in the second section. The third section includes graphs and data from the mathematical modelling of total effective risk. In this context, resultant data of three different risk models are demonstrated. Correlation coefficients of the relationship between total effective risk during a woman's lifetime and different screening commencement/ending ages, number of screens and time interval between screens along with risk regression model (the first risk model) are presented for the three LAR extrapolation methods.

Following this, for the three extrapolation methods, the graphs of the second and third risk models are introduced. Since the majority of screening programmes end between the ages of 70 and 75 and during this time the tissues become more radio-resistant, the cessation age of screening has a small effect on the total effective risk of the screening programme. Accordingly in these two risk models the cessation of screening mammography is considered to be constant at the age of 75 years. The purpose of the second risk model is to provide an easy method to obtain the total effective risk of various screening recommendations of different screening commencement ages and frequencies. However, the MGD variability of

the different FFDM machines has not been considered in this model because the average risk value across the sixteen machines has been used. Therefore, the third risk model is introduced to overcome this limitation by generating a set of conversion factors that can be used to assess total effective risk of any screening programme depending on screening parameters (i.e. commencement age and frequency of screening) and the women's MGD established during the initial mammogram. Finally, the effect of a contralateral breast shield data on both contralateral breast dose and effective risk is shown in the last section.

6.2 Organ Dose Data

As mentioned in methodology chapter (section 5.2.2, page 108), the radiation dose of 20 radiosensitive tissue were measured using TLDs accommodated inside the ATOM dosimetry phantom. The phantom was exposed, under normal breast screening conditions, across sixteen different FFDM machines. In the first step and in order to investigate organ dose measurement reliability, the organs' radiation doses were measured on three occasions for two FFDM machines (machines number 1 and 2). This demonstrated a minor level of variation across the three visits. These variations are greater for the first FFDM machine than those obtained by the second FFDM machine; see **Figure (6-1)** and **Figure (6-2)** for the first and second machine, respectively. In these Figures error bars were used to present the mean organ doses (μGy) ± 1SD for the three visits, for machine 1 and machine 2. The effect of such measured dose variations on the total effective risk of worldwide screening programmes is subsequently presented in **Table (6-1)** for machine 1; and **Table (6-2)** for machine 2 (for all three LAR extrapolation methods). For both tables, the first column lists worldwide screening programmes sorted in ascending order according to their total effective risk. Opposite each screening programme in the second, third, and fourth columns of the tables, the average total effective values with standard deviation (SD), of the sixteen machines, calculated using each of LAR sets are presented.

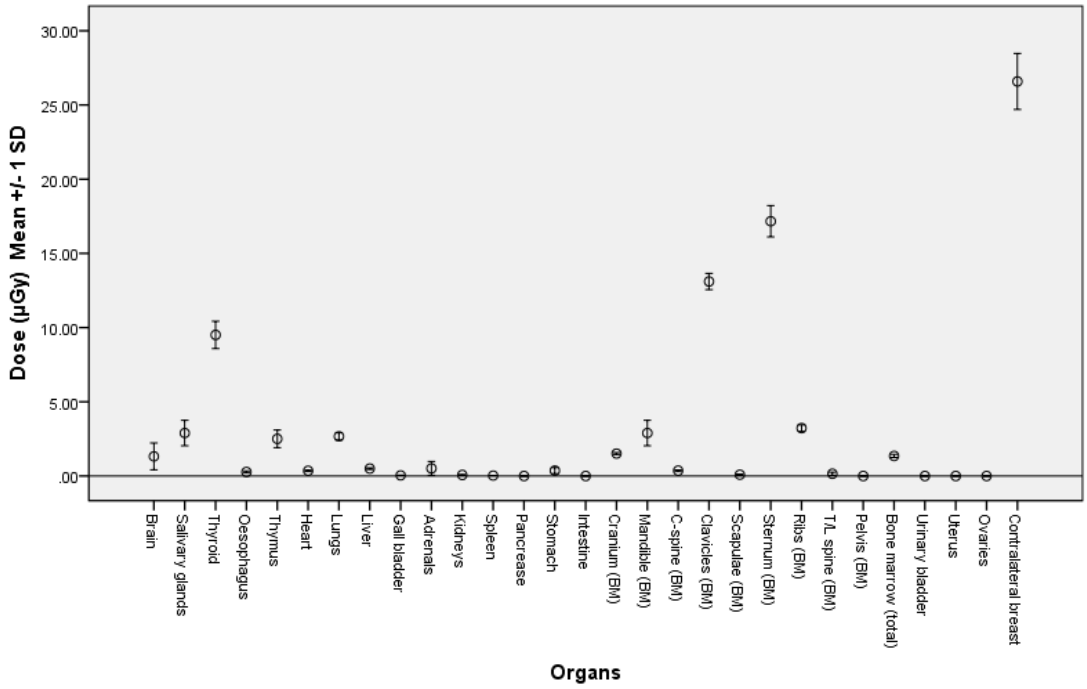

Figure (6-1) Demonstrates the organ dose variations (mean ± 1SD) measured across three different visits for machine number 1.

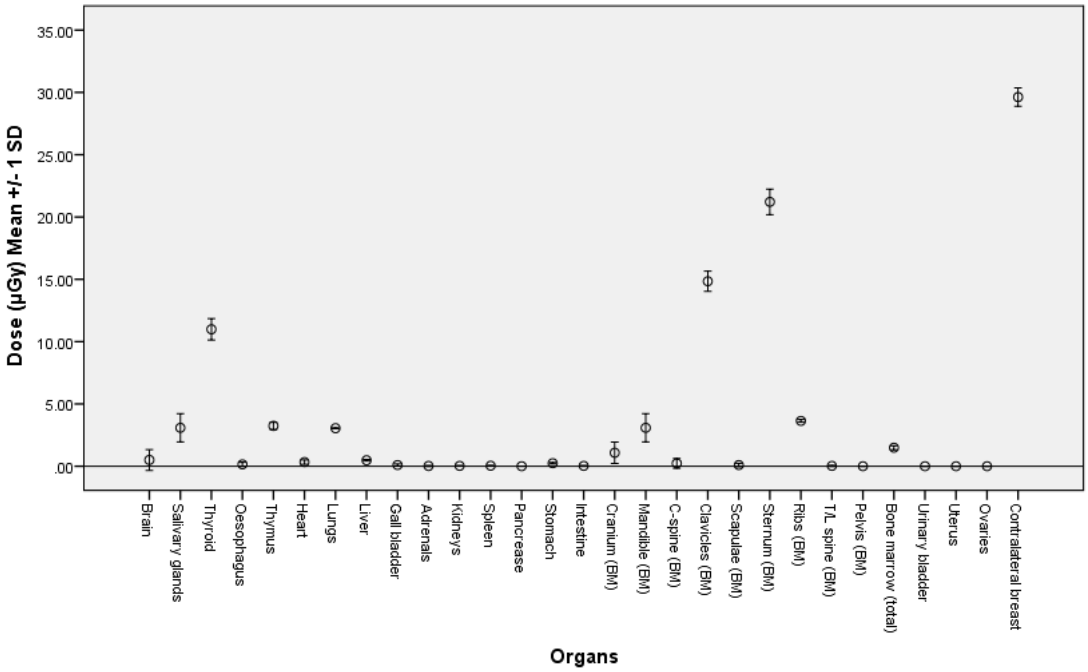

Figure (6-2) Demonstrates the organ dose variations (mean ± 1SD) measured across three different visits for machine number 2.

Table (6-1) Lists the variations in total effective risk, calculated using LAR factors extrapolated by the three methods, of worldwide screening programmes which resulted from the variations in organ doses as measured on three visits for machine 1.

Programme*	Total effective risk (case/10^6), Mean (SD) of the three visits		
	Method 1	Method 2	Method 3
Malta	50.57 (0.05)	51.85 (0.05)	69.13 (0.07)
Estonia	77.40 (0.08)	81.64 (0.09)	101.78 (0.10)
Ireland	81.10 (0.09)	87.45 (0.09)	109.46 (0.11)
United Kingdom	84.75 (0.09)	93.19 (0.10)	129.92 (0.13)
Belgium, Croatia, Cyprus, Denmark, Finland, Germany, Italy, Latvia, Lithuania, Luxembourg, Norway, Poland, Slovenia, Spain (Catalonia), Switzerland	85.55 (0.10)	96.25 (0.11)	124.83 (0.13)
Canada , France, Israel, Netherlands	88.64 (0.11)	104.05 (0.12)	133.81 (0.14)
Hungary	142.63 (0.14)	148.81 (0.15)	213.70 (0.20)
New Zealand, Portugal, Spain (Navarra)	146.32 (0.15)	156.67 (0.16)	229.06 (0.21)
China	147.26 (0.13)	145.00 (0.13)	190.83 (0.17)
Czech	163.44 (0.17)	176.85 (0.18)	238.05 (0.23)
Iceland	229.20 (0.22)	235.05 (0.22)	298.55 (0.27)
Nigeria	230.46 (0.22)	238.05 (0.23)	301.55 (0.28)
Australia, Japan, Korea, United States (AAFP, NCI, and USPSTF)	232.29 (0.23)	242.85 (0.24)	307.54 (0.29)
Sweden	270.71 (0.26)	279.89 (0.27)	374.04 (0.34)
Uruguay	305.88 (0.31)	324.16 (0.32)	423.38 (0.40)
United States (ACOG)	311.81 (0.33)	339.15 (0.35)	441.35 (0.43)
India	366.72 (0.35)	372.91 (0.35)	481.27 (0.43)
United States (ACS, ACR, and NCCN)	446.24 (0.45)	469.22 (0.46)	615.08 (0.57)
Canada	366.72 (0.35)	372.91 (0.35)	481.27 (0.43)
United Kingdom	444.46 (0.44)	465.02 (0.45)	609.09 (0.56)
United States (ACS)	942.16 (0.84)	968.21 (0.86)	1238.06 (1.07)
United States (NCCN)	1318.68 (1.15)	1344.74 (0.17)	1766.34 (1.51)

Screening programmes designed for high breast cancer risk women are highlighted in grey.
**The programmes are ordered according to total effective risk calculated using LAR extrapolated by best fit lines method.*

Table (6-2) Lists the variations in total effective risk, calculated using LAR factors extrapolated by the three methods, of worldwide screening programmes which resulted from the variations in organ doses as measured on three visits for machine 2.

Programme	Total effective risk (case/10^6), Mean (SD)		
	Method 1	Method 2	Method 3
Malta	48.48 (0.04)	49.67 (0.03)	66.21 (0.04)
Estonia	74.20 (0.07)	78.21 (0.05)	97.49 (0.06)
Ireland	77.76 (0.07)	83.78 (0.06)	104.85 (0.07)
United Kingdom	81.27 (0.08)	89.28 (0.06)	124.44 (0.08)
Belgium, Croatia, Cyprus, Denmark, Finland, Germany, Italy, Latvia, Lithuania, Luxembourg, Norway, Poland, Slovenia, Spain (Catalonia), Switzerland	82.05 (0.08)	92.22 (0.06)	119.58 (0.08)
Canada , France, Israel, Netherlands	85.04 (0.10)	99.70 (0.07)	128.20 (0.09)
Hungary	136.70 (0.11)	142.54 (0.09)	204.66 (0.11)
New Zealand, Portugal, Spain (Navarra)	140.27 (0.12)	150.08 (0.10)	219.39 (0.13)
China	141.07 (0.09)	138.86 (0.08)	182.73 (0.09)
Czech	156.69 (0.14)	169.42 (0.11)	228.01 (0.13)
Iceland	219.63 (0.16)	225.13 (0.13)	285.92 (0.16)
Nigeria	220.84 (0.17)	228.01 (0.13)	288.80 (0.16)
Australia, Japan, Korea, United States (AAFP, NCI, and USPSTF)	222.63 (0.17)	232.61 (0.14)	294.54 (0.17)
Sweden	259.42 (0.19)	268.08 (0.16)	358.21 (0.20)
Uruguay	293.18 (0.24)	310.52 (0.19)	405.50 (0.23)
United States (ACOG)	298.93 (0.26)	324.90 (0.21)	422.74 (0.25)
India	351.38 (0.25)	357.16 (0.20)	460.89 (0.25)
United States (ACS, ACR, and NCCN)	427.69 (0.34)	449.45 (0.27)	589.09 (0.33)
Canada	351.38 (0.25)	357.16 (0.20)	460.89 (0.25)
United Kingdom	425.97 (0.33)	445.42 (0.27)	583.34 (0.33)
United States (ACS)	902.53 (0.57)	927.20 (0.49)	1185.53 (0.60)
United States (NCCN)	1263.04 (0.74)	1287.70 (0.66)	1691.33 (0.84)

Screening programmes designed for high breast cancer risk women are highlighted in grey.

For the sixteen FFDM machines, the examined breast received the highest radiation dose during 'screening mammography exposures' where total MGD from one screening visit (for both CC and MLO projections) ranged between 1.678 mGy and 2.431 mGy with a mean (95% CI) of 2.019 (1.871-2.166) mGy. All of the machines showed that MGD for the MLO projection was higher than that of the CC projection. However, the variation percentage of MGD between MLO and CC projections is different amongst the 16 machines. It ranged from slightly more than 1% to just under 29%, approximately 14% on average; see **Table (6-3)** which demonstrates the CC and MLO projections MGD (mGy) along with percentages of MGD difference between them for each of the 16 machines. These MGD variations between CC and MLO will be more discussed in section 7.3.1 on page 182.

Table (6-3) Shows examined breast MGD for the sixteen FFDM machines.

Machine number	MGD (mGy)		Percentage Difference (%)	Total MGD (mGy)
	CC view	MLO view		
1	1.160	1.271	8.733	2.431
2	1.050	1.273	17.517	2.323
3	0.843	1.164	27.577	2.007
4	0.811	1.082	25.046	1.893
5	0.927	1.082	14.325	2.009
6	0.825	0.949	13.066	1.774
7	1.169	1.637	28.589	2.806
8	0.983	1.219	19.360	2.202
9	0.854	0.977	12.590	1.831
10	1.060	1.071	1.027	2.131
11	0.825	0.853	3.283	1.678
12	0.921	1.055	12.701	1.976
13	0.918	0.941	2.444	1.859
14	0.930	0.961	3.226	1.891
15	0.787	0.969	18.782	1.756
16	0.771	0.959	19.604	1.730
Mean (95% CI)	0.927 (0.865-0.989)	1.091 (0.998-1.185)	14.242 (9.898-18.586)	2.019 (1.871-2.166)

For organs other than the examined breast, it was found that for some the radiation dose was zero and this means that either these organs do not receive radiation dose during screening mammography exposure or the dose received by these organs is below the sensitivity threshold of the TLDs. However, some organs received radiation dose ranging from less than 1μGy to more than 25 μGy; see **Figure (6-3)** which shows the average organs' dose for the

sixteen machines with 95% CI. The organ dose values for each machine are presented in **Appendix A**. In general the three highest organ doses after the irradiated/examined breast are received by the contralateral breast, sternum red bone marrow and thyroid, in descending order respectively. The organs which received an average radiation dose of ≥0.1 μGy are presented in **Table (6-4)** as a percentage of the MGD. The first column of this table lists the organs which received a radiation dose of ≥0.1 μGy, the second column contains the average organ's doses together with their standard deviation (SD) of the studied machines and the final column presents the average organ's doses as percentages of average MGD with (SD).

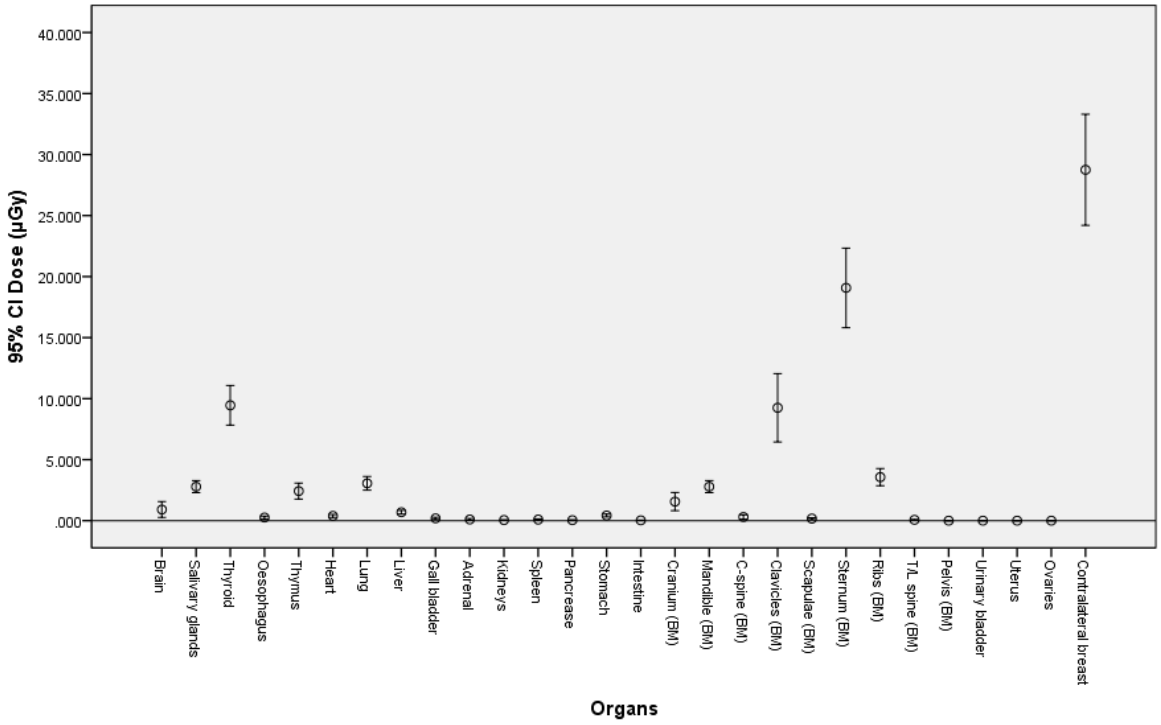

Figure (6-3) Demonstrates the mean organ doses across the sixteen machines (circles) with 95% CI (error bars) for one screening visit (CC and MLO projections for each breast).

Table (6-4) The mean organ doses for the sixteen FFDM machines from one screening visit along with their percentages in relation to the average examined breast MGD.

Organ	Radiation dose, mean (SD), µGy	Organ's dose percentages, mean (SD) , % MGD
Brain	0.912 (1.214)	0.048 (0.071)
Salivary	2.789 (0.934)	0.139 (0.048)
Thyroid	9.453 (3.050)	0.467 (0.133)
Oesophagus	0.256 (0.214)	0.013 (0.012)
Thymus	2.426 (1.232)	0.119 (0.058)
Heart	0.393 (0.226)	0.020 (0.012)
Lung	3.061 (1.056)	0.151 (0.046)
Liver	0.689 (0.289)	0.034 (0.013)
Gall bladder	0.188 (0.161)	0.009 (0.008)
Adrenals	0.102 (0.140)	0.005 (0.006)
Stomach	0.422 (0.210)	0.021 (0.009)
Cranium (BM)	1.563 (1.394)	0.081 (0.082)
Mandible (BM)	2.789 (0.934)	0.139 (0.048)
Cervical spine (BM)	0.300 (0.341)	0.016 (0.020)
Clavicles (BM)	9.250 (5.253)	0.451 (0.241)
Scapulae (BM)	0.169 (0.142)	0.009 (0.008)
Sternum (BM)	19.074 (6.121)	0.942 (0.251)
Ribs (BM)	3.569 (1.313)	0.175 (0.053)
Contralateral breast	28.749 (8.541)	1.419 (0.346)
Examined breast (MGD)	2018.498 (300.327)	100.000

Many factors may affect the organ's radiation dose during screening mammography. Target/filter combination is one of these factors. As earlier mentioned in **Table (5-9)** (page 126) four different target/filter combinations have been considered in this thesis (Rh/Rh, W/Rh, W/Ag and Mo/Mo). However, the number of machines of different target/filter combinations may cause some concern about drawing definitive conclusions from the results because only one W/Ag and one Mo/Mo target/filer combinations were included. In general, it can be noted that for the majority of organs the Rh/Rh target/filter combination resulted in the lowest radiation dose. It produces the lowest breast tissue radiation dose for both examined and contralateral breasts. **Figure (6-4)** shows the average examined breast MGD ± 1SD of each target/filter combination presented as error bars. Also the same graph type (error bars ± 1SD) has been used to demonstrate the average contralateral breast dose of different target/filter combinations, see **Figure (6-5)**. For most other tissue types, other than breast

tissue, Rh/Rh resulted in lowest dose; see **Figure (6-6)** where error bars (mean ± 1SD) have been used to present average organ radiation dose, of one screening event exposures, for different target/filter combinations.

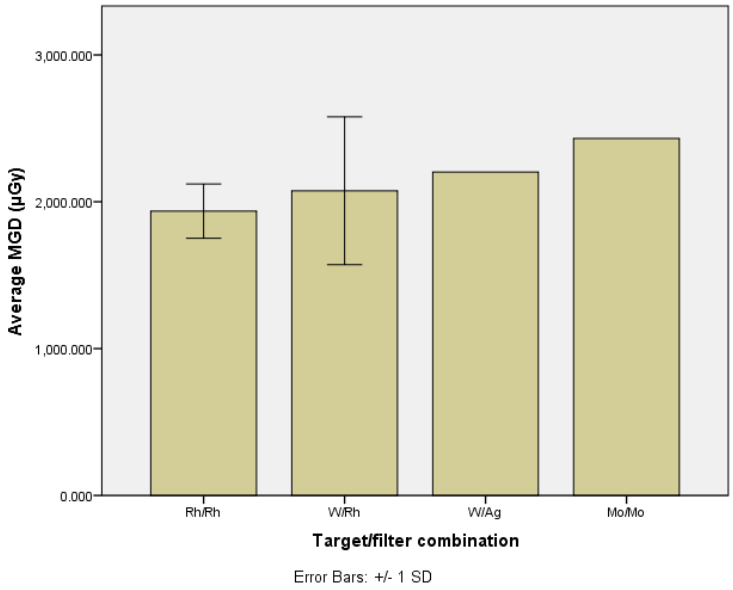

Figure (6-4) Shows mean MGD ± 1SD for the different target/filter combinations.

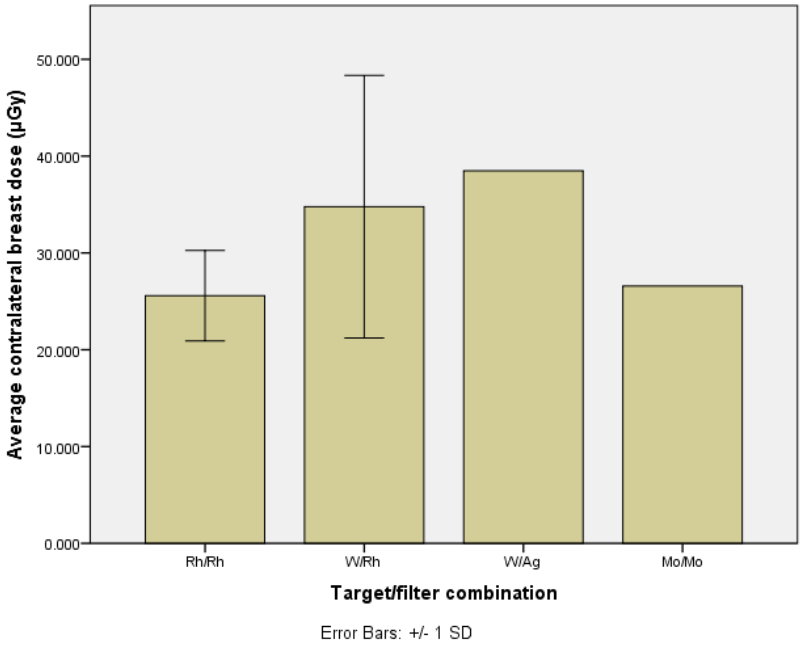

Figure (6-5) Shows mean contralateral breast dose ± 1SD for different target/filter combinations.

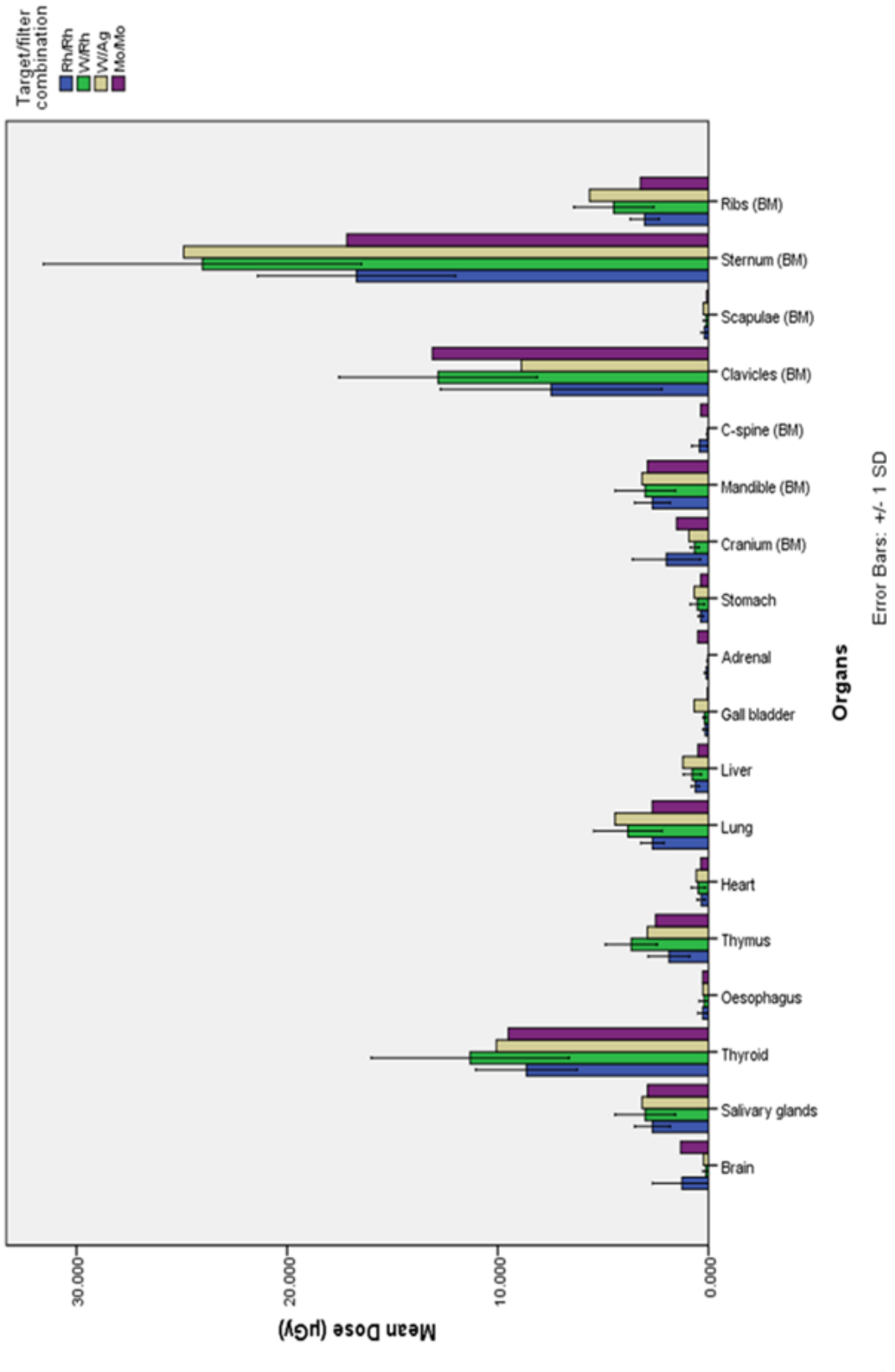

Figure (6-6) Demonstrates the effect of target/filter combination on organ's radiation dose (for organ that received more than 0.1 µGy radiation doses from screening mammography).

The product of X-ray tube current and exposure time (mAs), beam half-value layer (HVL), and MGD are other factors which may affect the organs radiation dose during screening mammography. Spearman's rho correlation coefficients, for non-parametric data, demonstrate that most organ doses are weakly (not statistically significant) correlated to beam HVL. On the contrary, a moderate to strong correlation has been found between the radiation dose for most organs and mAs, see **Table (6-5)** which comprises both Spearman's rho correlation coefficient and correlation P-value for organs which received more than 0.1 μGy radiation dose.

Backward multiple linear regression models have been established for further assessment of the relationship between radiation dose of each organ and 'mAs, HVL and MGD' in order to investigate the possibility of predicting individual organ radiation dose. Regression modelling was not significantly better than expressing mean values when predicting some organs doses. Regression modelling can, however, predict up to 87% of dose variability for other organs, see **Table (6-6)**. For each organ dose, the regression model data are presented in one row within **Table (6-6)**. For **Table (6-6)**, the first column includes the dependent variable (the organ dose to be predicted), while the regression model predictors' coefficients with 95% CI are presented in the second column. The R^2 and adjusted R^2 of the regression models are seen in the third and fourth columns of the table, respectively. The fifth column contains the regression equations that can be used to predict the organ doses. The standard errors associated with each regression equation output are listed in the last column of the table.

Table (6-5) Lists Spearman's rho correlation of different organs doses with MGD, mAs, and beam HVL using organs dose data from the sixteen FFDM machines.

Spearman's rho correlation		MGD	mAs	HVL
Brain	Correlation Coefficient	-0.088	-0.355	-0.335
	P-value	0.745	0.178	0.204
Salivary glands	Correlation Coefficient	0.394	0.429	-0.252
	P-value	0.131	0.097	0.346
Thyroid	Correlation Coefficient	0.688	0.771	0.085
	P-value	0.003	0.000	0.756
Oesophagus	Correlation Coefficient	0.015	0.024	-0.553
	P-value	0.957	0.931	0.026
Thymus	Correlation Coefficient	0.394	0.818	0.076
	P-value	0.131	0.000	0.781
Heart	Correlation Coefficient	0.371	0.415	-0.130
	P-value	0.158	0.110	0.630
Lung	Correlation Coefficient	0.668	0.650	0.022
	P-value	0.005	0.006	0.935
Liver	Correlation Coefficient	0.465	0.247	-0.162
	P-value	0.070	0.356	0.550
Gall bladder	Correlation Coefficient	0.106	0.250	-0.008
	P-value	0.696	0.350	0.976
Adrenals	Correlation Coefficient	0.051	-0.083	-0.714
	P-value	0.850	0.760	0.002
Stomach	Correlation Coefficient	0.532	0.288	-0.107
	P-value	0.034	0.279	0.694
Cranium (BM)	Correlation Coefficient	0.059	-0.232	-0.356
	P-value	0.829	0.387	0.176
Mandible (BM)	Correlation Coefficient	0.394	0.429	-0.252
	P-value	0.131	0.097	0.346
Cervical spine(BM)	Correlation Coefficient	-0.124	-0.198	-0.575
	P-value	0.648	0.463	0.020
Clavicles (BM)	Correlation Coefficient	0.506	0.876	0.077
	P-value	0.046	0.000	0.777
Scapulae (BM)	Correlation Coefficient	-0.088	-0.176	-0.519
	P-value	0.745	0.513	0.039
Sternum (BM)	Correlation Coefficient	0.382	0.709	0.176
	P-value	0.144	0.002	0.513
Ribs (BM)	Correlation Coefficient	0.644	0.624	0.073
	P-value	0.007	0.010	0.789
Contralateral breast	Correlation Coefficient	0.671	0.732	0.234
	P-value	0.004	0.001	0.383
MGD	Correlation Coefficient	1.000	0.426	0.289
	P-value	-	0.072	0.277

Highlighted cells represent the significant P-values (P<0.05)

Table (6-6) Demonstrates the multiple linear regression data for each organ dose.

Dependent variable	Predictor(s) Coefficient (95% CI)	Equation	R^2	Adj. R^2	Std. error of estimate
Salivary glands dose (SGD)	mAs = 0.014 (0.002 - 0.026)	SGD = 1.624 + 0.014 mAs	30%	25%	0.807
Thyroid dose (TD)	MGD = 0.004 (0.001-0.007) mAs = 0.063 (0.040-0.086) HVL = –10.569 (–20.947 - –0.191)	TD = 1.909 + 0.004 MGD + 0.063 mAs – 10.569 HVL	83%	79%	1.415
Oesophagus dose (OD)	HVL = –1.314 (–2.583 - –0.045)	OD = 0.925 – 1.314 HVL	26%	21%	0.190
Thymus dose (THD)	mAs = 0.030 (0.023 - 0.038)	THD = –0.115 + 0.030 mAs	83%	82%	0.522
Lung dose (LD)	mAs = 0.020 (0.008 - 0.032)	LD = 1.397 + 0.020 mAs	49%	45%	0.783
Adrenals (AD)	HVL = –1.192 (–2.003- –0.381)	AD = 0.333 – 1.192 HVL	45%	36%	0.112
Mandible dose (MD)	mAs = 0.014 (0.002 - 0.026)	MD = 1.624 + 0.014 mAs	30%	25%	0.807
Clavicles (CLD)	MGD = 0.004 (0.000 - 0.008) mAs = 0.119 (0.086 - 0.152)	CLD = –8.064 + 0.004 MGD + 0.119 mAs	87%	84%	2.073
Scapulae (SCD)	HVL = –0.864 (–1.710 - –0.017)	SCD = 0.609 – 0.864 HVL	26%	20%	0.127
Sternum dose (SD)	MGD = 0.006 (0.000 - 0.013) mAs = 0.114 (0.059 - 0.169)	SD = –3.528 + 0.006 MGD + 0.114 mAs	73%	68%	3.444
Ribs dose (RD)	MGD = 0.002 (0.000 - 0.004) mAs = 0.019 (0.004 - 0.034)	RD = –1.466 + 0.002 MGD + 0.019 mAs	58%	52%	0.911
Contralateral breast dose (CD)	MGD = 0.011 (0.000 - 0.022) mAs = 0.133 (0.044 - 0.222)	CD = – 4.589 + 0.011 MGD + 0.133mAs	63%	58%	5.551

Regression model is not significant for brain, heart, liver, gall bladder, stomach, cranium (BM), cervical spine (BM) radiation doses, and MGD.

6.3 Effective Risk Data

Effective lifetime risk refers to an individual's chance of acquiring a radiation-induced cancer. Since effective risk calculations include organ radiation doses and LAR factors which decrease with age as tissue becomes more radio-resistant, its value also decreases with age. If organ radiation doses resulting from screening mammography are considered to be constant during a female's lifetime, the changes in effective risk during a female's lifetime are only dependent on LAR reduction with age, see **Table (6-7)**, **Table (6-8)** and **Table (6-9)** for the three LAR extrapolation methods. The effective risk values listed in these tables represent the average effective risk (case/10^6) for the sixteen FFDM machines, with 95% confidence interval (CI) for each year of female life. The effective risk values for each machine are presented in **Appendix B**.

Table (6-7) Presents mean calculated effective risk values using LAR extrapolated by best fit lines method (**method 1**) for each year of female life with 95% CI.

Age (year)	Effective lifetime risk (case/10^6)		Age (year)	Effective lifetime risk (case/10^6)	
	Mean	95% CI		Mean	95% CI
25	70.00	[64.88 - 75.12]	51	14.10	[13.07 - 15.13]
26	66.38	[61.53 - 71.24]	52	12.93	[11.99 - 13.88]
27	62.77	[58.18 - 67.36]	53	11.82	[10.96 - 12.69]
28	59.16	[54.83 - 63.48]	54	10.76	[9.98 - 11.55]
29	55.54	[51.48 - 59.60]	55	9.76	[9.04 - 10.47]
30	51.93	[48.13 - 55.72]	56	8.81	[8.16 - 9.45]
31	48.59	[45.04 - 52.15]	57	7.91	[7.33 - 8.49]
32	46.36	[42.97 - 49.75]	58	7.06	[6.54 - 7.58]
33	44.18	[40.95 - 47.41]	59	6.27	[5.81 - 6.73]
34	42.06	[38.98 - 45.13]	60	5.53	[5.12 - 5.93]
35	39.99	[37.06 - 42.91]	61	4.84	[4.49 - 5.20]
36	37.97	[35.19 - 40.74]	62	4.21	[3.90 - 4.52]
37	36.00	[33.37 - 38.63]	63	3.63	[3.36 - 3.89]
38	34.09	[31.60 - 36.58]	64	3.10	[2.87 - 3.33]
39	32.23	[29.88 - 34.59]	65	2.63	[2.44 - 2.82]
40	30.43	[28.20 - 32.65]	66	2.21	[2.05 - 2.37]
41	28.68	[26.58 - 30.78]	67	1.84	[1.71 - 1.98]
42	26.98	[25.01 - 28.95]	68	1.53	[1.41 - 1.64]
43	25.34	[23.48 - 27.19]	69	1.27	[1.17 - 1.36]
44	23.75	[22.01 - 25.48]	70	1.06	[0.98 - 1.14]
45	22.21	[20.58 - 23.83]	71	0.90	[0.84 - 0.97]
46	20.72	[19.21 - 22.24]	72	0.80	[0.74 - 0.86]
47	19.29	[17.88 - 20.70]	73	0.75	[0.70 - 0.81]
48	17.91	[16.60 - 19.22]	74	0.75	[0.70 - 0.81]
49	16.59	[15.38 - 17.80]	75	0.75	[0.69 - 0.80]
50	15.32	[14.20 - 16.44]			

Table (6-8) Presents mean calculated effective risk values using LAR extrapolated by linear relationship method (**method 2**) for each year of female life with 95% CI.

Age (year)	Effective lifetime risk (case/10^6)		Age (year)	Effective lifetime risk (case/10^6)	
	Mean	95% CI		Mean	95% CI
25	70.00	[64.88 - 75.12]	51	13.62	[12.62 - 14.61]
26	66.38	[61.53 - 71.24]	52	12.82	[11.88 - 13.76]
27	62.77	[58.18 - 67.36]	53	12.02	[11.14 - 12.90]
28	59.15	[54.83 - 63.48]	54	11.22	[10.40 - 12.04]
29	55.54	[51.48 - 59.60]	55	10.42	[9.66 - 11.18]
30	51.93	[48.13 - 55.72]	56	9.62	[8.92 - 10.32]
31	49.63	[46.00 - 53.26]	57	8.82	[8.17 - 9.46]
32	47.34	[43.87 - 50.80]	58	8.02	[7.43 - 8.61]
33	45.04	[41.75 - 48.33]	59	7.22	[6.69 - 7.75]
34	42.74	[39.62 - 45.87]	60	6.42	[5.95 - 6.89]
35	40.45	[37.49 - 43.41]	61	6.03	[5.59 - 6.47]
36	38.15	[35.36 - 40.94]	62	5.64	[5.22 - 6.05]
37	35.86	[33.23 - 38.48]	63	5.25	[4.86 - 5.63]
38	33.56	[31.11 - 36.01]	64	4.85	[4.50 - 5.21]
39	31.27	[28.98 - 33.55]	65	4.46	[4.14 - 4.79]
40	28.97	[26.85 - 31.09]	66	4.07	[3.77 - 4.37]
41	27.51	[25.50 - 29.53]	67	3.68	[3.41 - 3.95]
42	26.06	[24.15 - 27.96]	68	3.29	[3.05 - 3.53]
43	24.60	[22.81 - 26.40]	69	2.90	[2.69 - 3.11]
44	23.15	[21.46 - 24.84]	70	2.51	[2.32 - 2.69]
45	21.69	[20.11 - 23.28]	71	2.34	[2.17 - 2.51]
46	20.24	[18.76 - 21.72]	72	2.18	[2.02 - 2.34]
47	18.78	[17.41 - 20.16]	73	2.01	[1.86 - 2.16]
48	17.33	[16.06 - 18.60]	74	1.84	[1.71 - 1.98]
49	15.87	[14.71 - 17.03]	75	1.68	[1.55 - 1.80]
50	14.42	[13.36 - 15.47]			

Table (6-9) Presents mean calculated effective risk values using LAR extrapolated by step method (**method 3**) for each year of female life with 95% CI.

Age (year)	Effective lifetime risk (case/10^6)		Age (year)	Effective lifetime risk (case/10^6)	
	Mean	95% CI		Mean	95% CI
25	88.07	[81.63 - 94.51]	51	14.42	[13.36 - 15.47]
26	88.07	[81.63 - 94.51]	52	14.42	[13.36 - 15.47]
27	88.07	[81.63 - 94.51]	53	14.42	[13.36 - 15.47]
28	88.07	[81.63 - 94.51]	54	14.42	[13.36 - 15.47]
29	88.07	[81.63 - 94.51]	55	14.42	[13.36 - 15.47]
30	51.93	[48.13 - 55.72]	56	14.42	[13.36 - 15.47]
31	51.93	[48.13 - 55.72]	57	14.42	[13.36 - 15.47]
32	51.93	[48.13 - 55.72]	58	14.42	[13.36 - 15.47]
33	51.93	[48.13 - 55.72]	59	14.42	[13.36 - 15.47]
34	51.93	[48.13 - 55.72]	60	6.42	[5.95 - 6.89]
35	51.93	[48.13 - 55.72]	61	6.42	[5.95 - 6.89]
36	51.93	[48.13 - 55.72]	62	6.42	[5.95 - 6.89]
37	51.93	[48.13 - 55.72]	63	6.42	[5.95 - 6.89]
38	51.93	[48.13 - 55.72]	64	6.42	[5.95 - 6.89]
39	51.93	[48.13 - 55.72]	65	6.42	[5.95 - 6.89]
40	28.97	[26.85 - 31.09]	66	6.42	[5.95 - 6.89]
41	28.97	[26.85 - 31.09]	67	6.42	[5.95 - 6.89]
42	28.97	[26.85 - 31.09]	68	6.42	[5.95 - 6.89]
43	28.97	[26.85 - 31.09]	69	6.42	[5.95 - 6.89]
44	28.97	[26.85 - 31.09]	70	2.51	[2.32 - 2.69]
45	28.97	[26.85 - 31.09]	71	2.51	[2.32 - 2.69]
46	28.97	[26.85 - 31.09]	72	2.51	[2.32 - 2.69]
47	28.97	[26.85 - 31.09]	73	2.51	[2.32 - 2.69]
48	28.97	[26.85 - 31.09]	74	2.51	[2.32 - 2.69]
49	28.97	[26.85 - 31.09]	75	2.51	[2.32 - 2.69]
50	14.42	[13.36 - 15.47]			

As discussed in section 3.7 (page 53) worldwide screening mammography programmes recommendations are different, variations are possible relating to screening commencement age, number of screens, time interval between screens, and cessation age of screening. These differences result in large variations in total effective risk of worldwide screening programmes. **Tables (6-10)**, **(6-11)**, and **(6-12)** demonstrate the average, for the sixteen FFDM machines, total effective risk (case/10^6) with 95% CI of worldwide screening programmes in ascending order for the three extrapolated LAR methods. Total effective risks

of worldwide screening programmes for each FFDM machine are presented in **Appendix E**. In general, the lowest total effective risk results from the Maltese screening programme for average risk women (42.21 [39.12 - 45.30], 43.28 [40.11 - 46.44], and 57.67 [53.46 - 61.89] case/10^6 for the three LAR methods), while the highest total effective risk results from the American screening programme for high risk women recommended by National Comprehensive Cancer Network (NCCN) (1099.67 [1019.25 - 1180.09], 1121.36 [1039.36 - 1203.36], and 1472.73 [1365.04 - 1580.42] case/10^6 for the three LAR methods). The variations in total effective risk of worldwide screening programmes resulted from LAR extrapolation method are shown in **Figure (6-7)**. In this figure the average total effective risk of worldwide screening programmes along with ±1 SD errors bar are presented for all the three LAR extrapolation methods. In general the third extrapolation method ('step' method) resulted in the highest total effective risk for all worldwide screening programmes.

Table (6-10) Illustrates total effective risk (mean [95% CI] for the sixteen FFDM machines) of worldwide screening programmes using LAR factors extrapolated by **method 1**.

Programme	Total effective risk (case/10^6)	
	Mean	95% CI
Malta	42.21	[39.12 - 45.30]
Estonia	64.62	[59.89 - 69.35]
Ireland	67.72	[62.76 - 72.68]
United Kingdom	70.77	[65.59 - 75.95]
Belgium, Croatia, Cyprus, Denmark, Finland, Germany, Italy, Latvia, Lithuania, Luxembourg, Norway, Poland, Slovenia, Spain (Catalonia), Switzerland	71.45	[66.22 - 76.68]
Canada , France, Israel, Netherlands	74.06	[68.64 - 79.49]
Hungary	119.04	[110.33 - 127.75]
New Zealand, Portugal, Spain (Navarra)	122.15	[113.21 - 131.08]
China	122.83	[113.85 - 131.81]
Czech	136.45	[126.46 - 146.43]
Iceland	191.25	[177.26 - 205.24]
Nigeria	192.30	[178.24 - 206.37]
Australia, Japan, Korea, United States (AAFP, NCI, and USPSTF)	193.86	[179.67 - 208.04]
Sweden	225.89	[209.37 - 242.42]
Uruguay	255.30	[236.62 - 273.98]
United States (ACOG)	260.32	[241.27 - 279.37]
India	305.96	[283.58 - 328.34]
United States (ACS, ACR, and NCCN)	372.42	[345.18 - 399.67]
Canada	305.96	[283.58 - 328.34]
United Kingdom	370.92	[343.79 - 398.06]
United States (ACS)	785.82	[728.35 - 843.30]
United States (NCCN)	1099.67	[1019.25 - 1180.09]

Screening programmes designed for high breast cancer risk women are highlighted in grey.

Table (6-11) Illustrates total effective risk (mean [95% CI] for the sixteen FFDM machines) of worldwide screening programmes using LAR factors extrapolated by **method 2**.

Programme	Total effective risk (case/10^6)	
	Mean	95% CI
Malta	43.28	[40.11 - 46.44]
Estonia	68.15	[63.16 - 73.14]
Ireland	73.01	[67.66 - 78.35]
United Kingdom	77.79	[72.10 - 83.48]
Belgium, Croatia, Cyprus, Denmark, Finland, Germany, Italy, Latvia, Lithuania, Luxembourg, Norway, Poland, Slovenia, Spain (Catalonia), Switzerland	80.37	[74.49 - 86.25]
Canada , France, Israel, Netherlands	86.90	[80.54 - 93.25]
China	120.94	[112.10 - 129.79]
Hungary	124.18	[115.10 - 133.27]
New Zealand, Portugal, Spain (Navarra)	130.76	[121.20 - 140.33]
Czech	147.61	[136.81 - 158.41]
Iceland	196.11	[181.77 - 210.46]
Nigeria	198.86	[184.37 - 213.35]
Australia, Japan, Korea, United States (AAFP, NCI, and USPSTF)	202.64	[187.82 - 217.46]
Sweden	233.53	[216.45 - 250.61]
Uruguay	270.53	[250.74 - 290.31]
United States (ACOG)	283.08	[262.38 - 303.79]
India	311.11	[288.36 - 333.86]
United States (ACS, ACR, and NCCN)	391.55	[362.91 - 420.19]
Canada	311.11	[288.36 - 333.86]
United Kingdom	388.03	[359.65 - 416.41]
United States (ACS)	807.51	[748.46 - 866.56]
United States (NCCN)	1121.36	[1039.36 - 1203.36]

Screening programmes designed for high breast cancer risk women are highlighted in grey.

Table (6-12) Illustrates total effective risk (mean [95% CI] for the sixteen FFDM machines) of worldwide screening programmes using LAR factors extrapolated by **method 3**.

Programme	Total effective risk (case/10^6)	
	Mean	95% CI
Malta	57.67	[53.46 - 61.89]
Estonia	84.93	[78.72 - 91.14]
Ireland	91.35	[84.67 - 98.03]
United Kingdom	108.41	[100.48 - 116.34]
Belgium, Croatia, Cyprus, Denmark, Finland, Germany, Italy, Latvia, Lithuania, Luxembourg, Norway, Poland, Slovenia, Spain (Catalonia), Switzerland	104.19	[96.57 - 111.81]
Canada , France, Israel, Netherlands	111.71	[103.54 - 119.89]
China	159.13	[147.50 - 170.77]
Hungary	178.26	[165.22 - 191.29]
New Zealand, Portugal, Spain (Navarra)	191.10	[177.12 - 205.07]
Czech	198.62	[184.09 - 213.15]
Iceland	249.04	[230.82 - 267.25]
Nigeria	251.54	[233.15 - 269.94]
Australia, Japan, Korea, United States (AAFP, NCI, and USPSTF)	256.56	[237.80 - 275.32]
Sweden	311.99	[289.17 - 334.81]
Uruguay	353.22	[327.39 - 379.06]
United States (ACOG)	368.27	[341.34 - 395.21]
India	401.41	[372.05 - 430.76]
United States (ACS, ACR, and NCCN)	513.12	[475.59 - 550.65]
Canada	401.41	[372.05 - 430.76]
United Kingdom	508.10	[470.95 - 545.26]
United States (ACS)	1032.39	[956.90 - 1107.88]
United States (NCCN)	1472.73	[1365.04 - 1580.42]

Screening programmes designed for high breast cancer risk women are highlighted in grey.

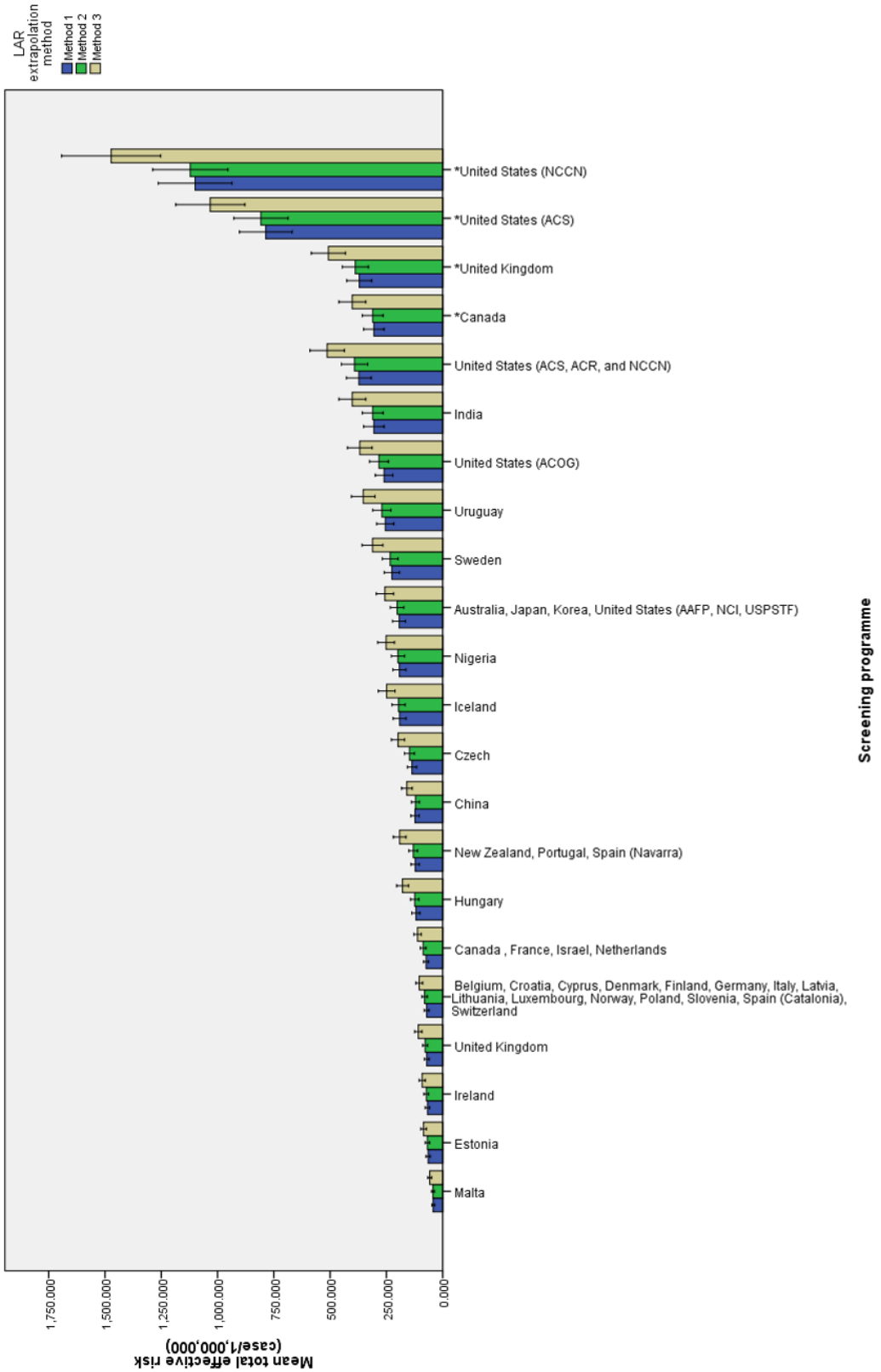

Figure (6-7) Shows the effect of LAR extrapolation method on total effective risk of worldwide screening programmes.
*Programmes for high risk women

A Spearman's rho correlation coefficient demonstrated that there was a strong correlation between the total effective risk of worldwide screening programmes and screening commencement age, cessation age of screening, time interval between screens, and number of screens during female life time; see **Table (6-13).** In spite of the small number of worldwide screening recommendations (n = 22 cases, number of worldwide screening recommendations) used in the regression, a further investigation of the relationship between total effective risk and associated factors using a backward regression model shows that the commencement age does not significantly affect the total effective risk and because of this it has been excluded from regression model by the SPSS. This was the same for the total effective risk calculated using the LAR factors extrapolated by each of the three methods; **see Table (6-14)**. This table shows the predictors' coefficients, regression equation, R^2, and standard error of estimate for each extrapolation method.

Table (6-13) Shows Spearman's rho correlations between total effective risk of worldwide screening programmes (N=22) and each of commencement/cessation ages and frequency of screening for the three LAR calculation methods.

LAR Extrapolation Method	Screening Age		Screening Frequency	
	Commencement	Cessation	Number of screens	Time interval
(Method 1)	-0.915	0.709	0.960	-0.877
(Method 2)	-0.897	0.721	0.971	-0.892
(Method 3)	-0.901	0.726	0.970	-0.884
All values presented in this table were statistically significant (P<0.001)				

Table (6-14) Demonstrates the backward regression models which estimate the effect of different factors on total effective risk calculated using LAR factors extrapolated by the three methods

Method	Predictors coefficient (95% CI)*	Regression Equation	R^{2**}	Std. error of estimate
M1	E = –8.885 (–18.271 - 0.501) T = 155.257 (41.639 - 268.874) N = 26.893 (21.093 - 32.694)	R = 57.993 – 8.885 E + 155.257 T + 26.893 N	91%	79.867
M2	E = –8.624 (–17.837 - 0.589) T = 152.656 (41.135 - 264.176) N = 27.179 (21.485 - 32.872)	R = 48.606 – 8.624 E + 152.656 T + 27.179 N	92%	78.393
M3	E = –11.212 (–23.342 - 0.918) T = 200.635 (53.808 - 347.461) N = 35.378 (27.882 - 42.873)	R = 60.027 – 11.212 E + 200.635 T + 35.378 N	92%	103.211

**R, total effective risk; N, number of screens; E, ending age of screening; T, time interval between screens.*

***R^2 approximately equal to adjust R^2 for the three models.*

6.4 Effective Risk Modelling Data

6.4.1 Mathematical Regression Model

To obtain a good regression model capable of predicting the total effective risk of different screening programmes with more precision than the one established with the small sample size (n=22 cases) (**Table (6-14)**, section 6.3), additional data were generated to create 274 screening scenarios; these were subsequently analysed. Spearman's rho correlations of these data revealed that the commencement age of screening and the number of screens were the most important factors affecting the total effective risk of any screening programme (both are correlated strongly with total effective risk); see **Table (6-15)** which contains both correlation coefficient and P-value for the three LAR extrapolation methods. Since the time interval between screens does not significantly affect the output total effective risk of the backward regression model, it is excluded by SPSS; see **Table (6-16)**. In the first column of

Table (6-16) the LAR extrapolation methods are listed. Then the regression model data including predictors' coefficients, regression equation, R^2, and standard error of estimates are contained in the next columns, respectively.

Table (6-15) Shows Spearman's rho correlations between the total effective risk of 274 proposed screening programmes and each of the commencement/cessation ages and frequency of screening for the three LAR methods.

LAR Extrapolation Method	Screening Age		Screening Frequency	
	Commencement	Cessation	Number of screens	Time interval
(Method 1)	-0.876	-0.368	0.692	-0.399
(Method 2)	-0.865	-0.346	0.714	-0.420
(Method 3)	-0.856	-0.332	0.727	-0.433
All values presented in this table were statistically significant (P<0.001)				

Table (6-16) Demonstrates the backward regression models which are established to predict the total effective risk of any screening programme using LAR factors extrapolated by the three methods.

Method	Predictors coefficient (95% CI)*	Regression Equation	R^{2**}	Std. error of estimate
M1	C = –8.049 (–9.508 - –6.590) E = –6.379 (–7.928 - –4.829) N= 17.248 (15.828 - 18.668)	R = 734.676 – 8.049 C – 6.379 E + 17.248 N	86%	93.249
M2	C=–7.763 (–9.189 - –6.338) E= -6.085 (–7.599 - –4.571) N = 17.569 (16.181 - 18.957)	R= 705.170 –7.763 C – 6.085 E + 17.569 N	87%	91.127
M3	C = –9.980 (–11.817 - –8.144) E = -7.730 (–9.681 - –5.779) N = 23.248 (21.459 - 25.036)	R= 900.962 – 9.980 C –7.730 E + 23.248 N	87%	117.411

*R, total effective risk; N, number of screens; C, commencement age of screening; E, ending age of screening.
**R^2 = adjusted R^2 for the three models.

6.4.2 Graphical Extrapolation of Total Effective Risk

If screening mammography cessation age is set at a constant level (75 years old) for all screening programmes, the factors that affect the total effective risk will be reduced down to only two (commencement age and screening frequency). The resultant graphical relationship between screening commencement age (year) on the X-axis and average total effective risk (case/10^6) for the sixteen FFDM machines on the Y-axis is demonstrated in **Figure (6-8)**, **Figure (6-9)** and **Figure (6-10)** for the three LAR extrapolation methods. Each of these figures contains three relationship lines; one for each screening frequency (annual, biennial, and triennial). Consequently, these graphs can be used to predict the total effective risk during a female's life for any screening commencement age and frequency by interpolation method.

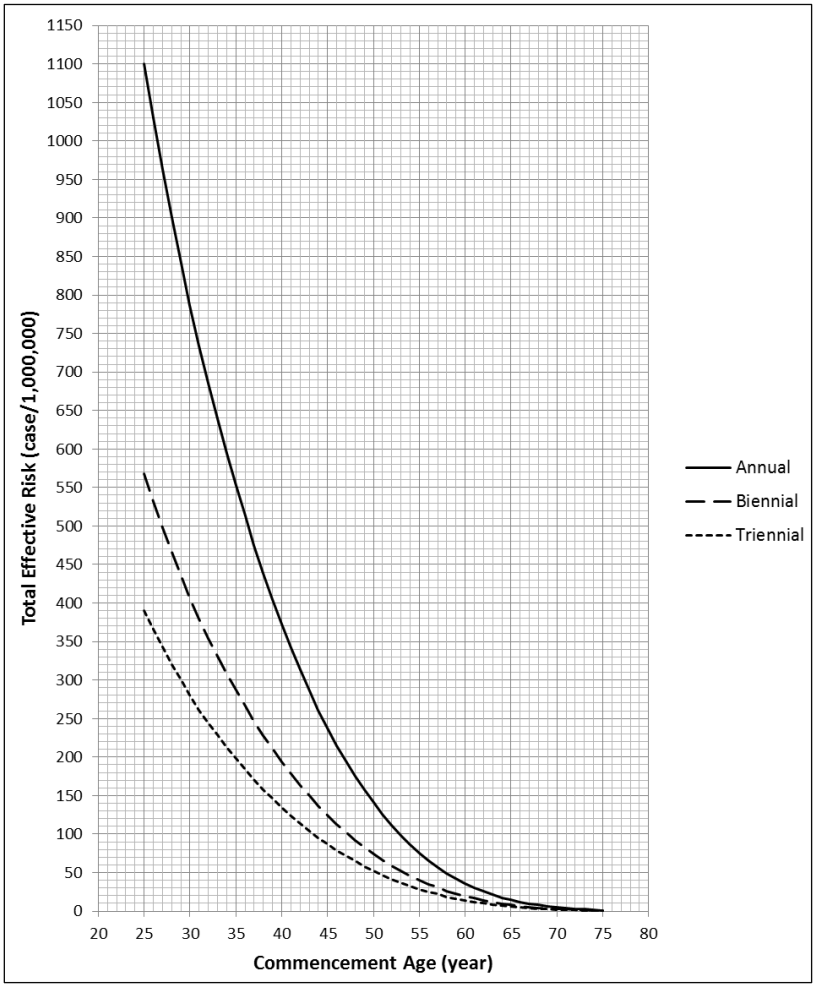

Figure (6-8) Represents the relationship between the total effective risk and the screening commencement age of different screening frequencies. Total effective risk calculated using LAR factors extrapolated by the best fit lines method (method 1).

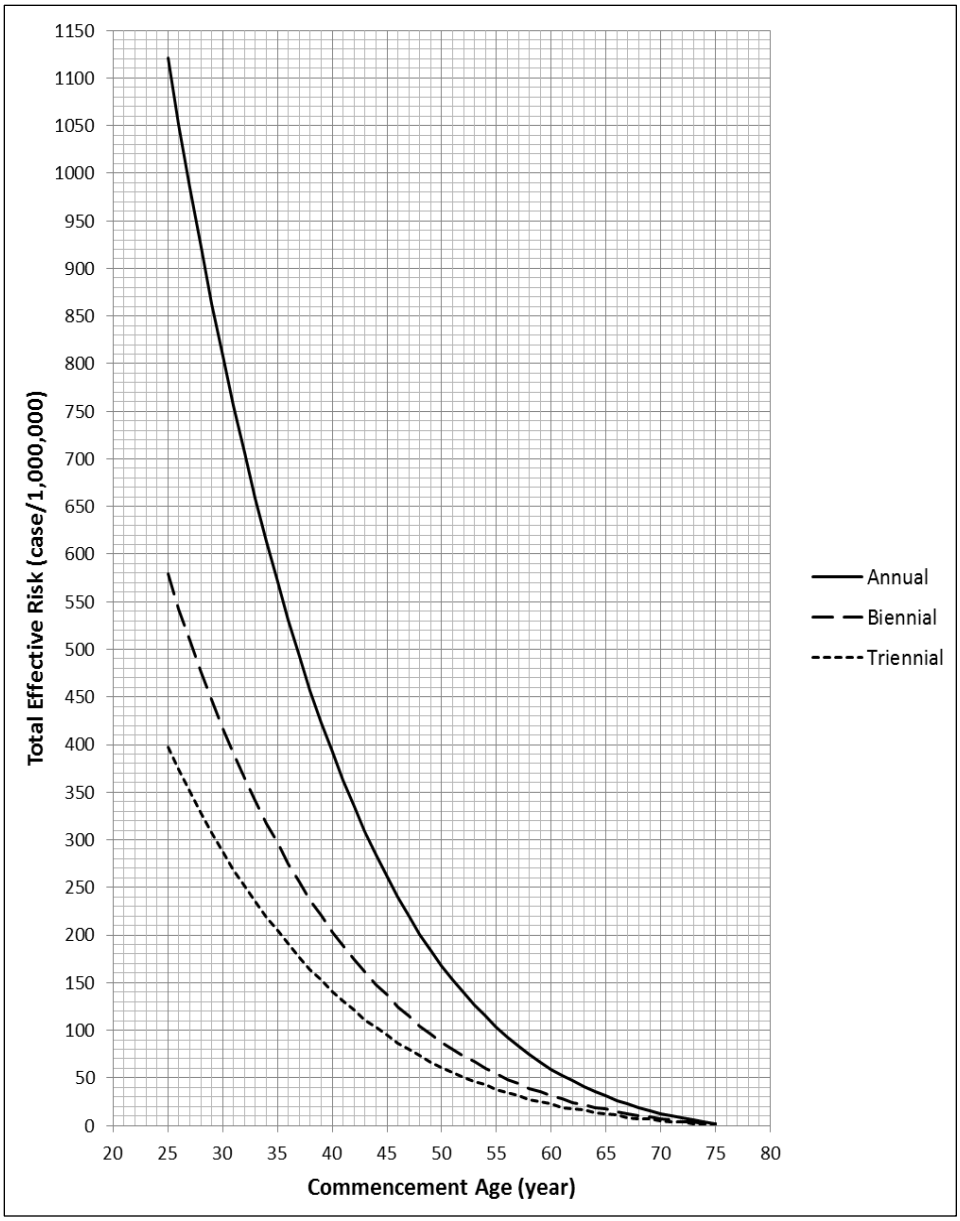

Figure (6-9) Represents the relationship between the total effective risk and the screening commencement age of different screening frequencies. Total effective risk calculated using LAR factors extrapolated by the linear relationship method (method 2).

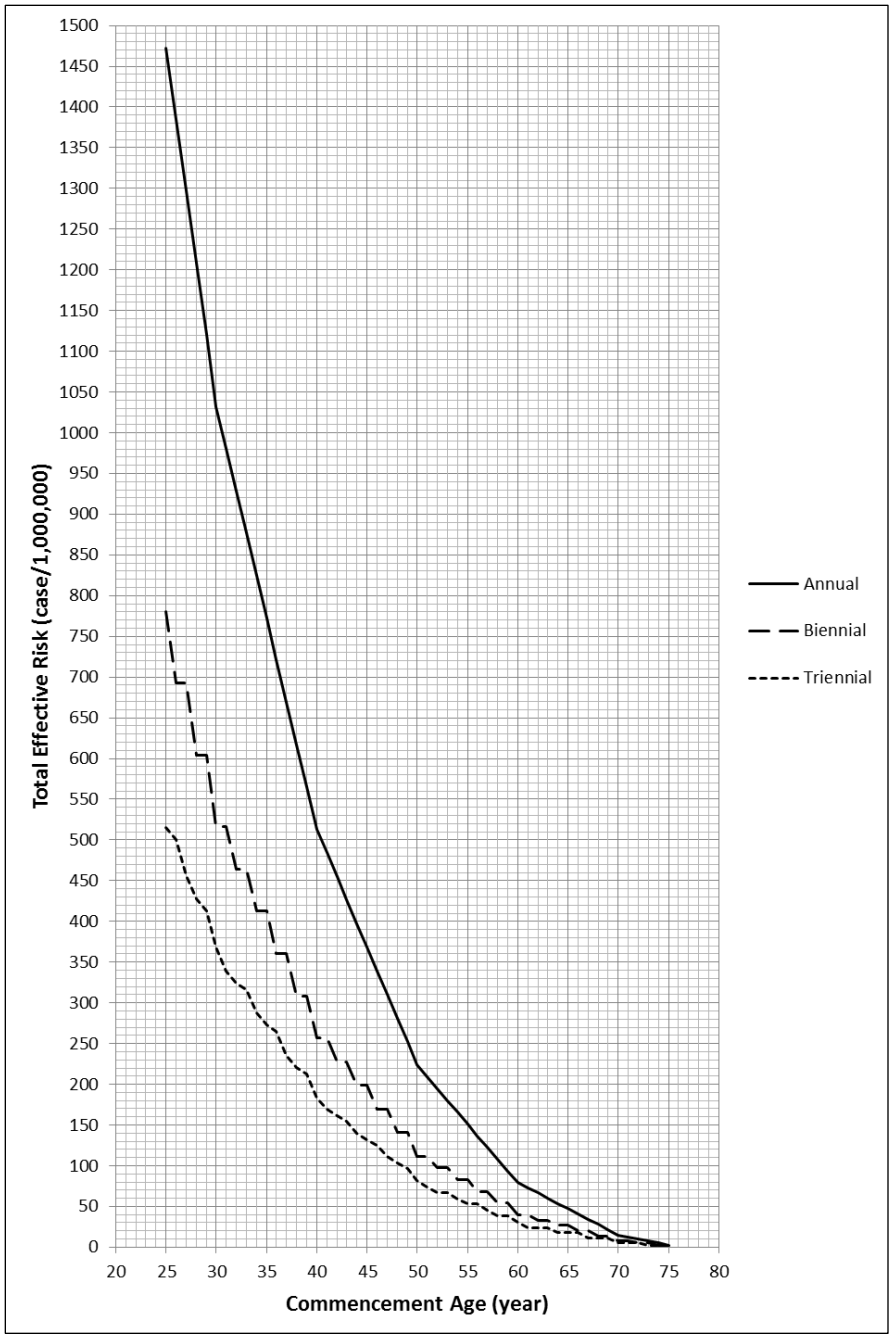

Figure (6-10) Represents the relationship between the total effective risk and the screening commencement age of different screening frequencies. Total effective risk calculated using LAR factors extrapolated by the step method (method 3).

6.4.3 Extrapolation of Total Effective Risk Using Baseline MGD Values

Using the data of sixteen FFDM machines, the relationship between MGD (μGy) and the total effective risk (case/10^6) of each screening scenario, of specific screening commencement age and frequency **(Appendix D)** resulted in set of conversions factors (case/10^6/μGy); see **Tables (6-17)**, **(6-18)**, and **(6-19)**. In these tables, opposite each screening commencement age between ages 25 and 75 (first and third columns of the tables), three conversion factors (second and fourth columns in the tables) are presented; one conversion factor for each screening frequency (annual, biennial, and triennial). These factors enable total effective risk to be obtained for any screening programme, of specific screening commencement age and frequency, whilst considering individual MGD which would be derived from an initial mammogram for each FFDM machine. Consequently, the graphs in **Figures (6-8)**, **(6-9)**, and **(6-10)** have been developed to generate the graphs as illustrated in **Figures (6-11)**, **(6-12)**, and **(6-13)**, respectively. The only difference in these graphs (**Figures (6-11)**, **(6-12)**, and **(6-13)**) compared with the former graphs (**Figures (6-8)**, **(6-9)**, and **(6-10))** is that the total effective risk is presented as a percent of MGD. In other words, the X-axis of the graphs still indicates the screening commencement age (year), while on the Y-axis the total effective risk represented as a percent of MGD.

Table (6-17) Lists the relationship factors between the total effective risk of the screening programme and the MGD based on the data collected from the 16 FFDM machines. These factors are for **method 1** of LAR extrapolation.

Commencement age (year)	Conversion factor % MGD (case/10^6/μGy)			Commencement age (year)	Conversion factor % MGD (case/10^6/μGy)		
	Annual	Biennial	Triennial		Annual	Biennial	Triennial
25	54.48	28.13	19.33	51	6.20	3.29	2.33
26	51.01	26.35	18.15	52	5.51	2.91	2.05
27	47.73	24.67	17.00	53	4.86	2.59	1.83
28	44.62	23.06	15.87	54	4.28	2.27	1.63
27	41.68	21.56	14.86	55	3.75	2.01	1.41
30	38.93	20.13	13.89	56	3.26	1.74	1.24
31	36.36	18.81	12.93	57	2.83	1.53	1.09
32	33.95	17.56	12.11	58	2.43	1.30	0.92
33	31.66	16.40	11.32	59	2.08	1.13	0.81
34	29.47	15.26	10.53	60	1.77	0.95	0.70
35	27.38	14.21	9.81	61	1.50	0.82	0.57
36	25.40	13.17	9.13	62	1.26	0.68	0.5
37	23.52	12.23	8.44	63	1.05	0.58	0.43
38	21.74	11.29	7.83	64	0.87	0.47	0.33
39	20.05	10.44	7.25	65	0.72	0.40	0.29
40	18.45	9.60	6.66	66	0.59	0.31	0.25
41	16.94	8.85	6.14	67	0.48	0.27	0.18
42	15.52	8.10	5.65	68	0.39	0.20	0.16
43	14.19	7.43	5.15	69	0.31	0.18	0.14
44	12.93	6.76	4.72	70	0.25	0.13	0.09
45	11.75	6.17	4.31	71	0.20	0.12	0.08
46	10.65	5.58	3.90	72	0.15	0.08	0.08
47	9.63	5.07	3.54	73	0.11	0.07	0.04
48	8.67	4.56	3.21	74	0.07	0.04	0.04
49	7.78	4.11	2.87	75	0.04	0.04	0.04
50	6.96	3.67	2.59				

When using this table to calculate total effective risk the commencement age and frequency of screening examinations must be selected and the relevant conversion factor can then be multiplied by the MGD.

Table (6-18) Lists the relationship factors between the total effective risk of the screening programme and the MGD based on the data collected from the 16 FFDM machines. These factors are for **method 2** of LAR extrapolation.

Commencement age (year)	Conversion factor % MGD (case/10^6/μGy)			Commencement age (year)	Conversion factor % MGD (case/10^6/μGy)		
	Annual	Biennial	Triennial		Annual	Biennial	Triennial
25	55.56	28.71	19.69	51	7.58	3.99	2.78
26	52.09	26.85	18.51	52	6.90	3.59	2.49
27	48.80	25.24	17.36	53	6.27	3.31	2.30
28	45.69	23.56	16.22	54	5.67	2.96	2.11
27	42.76	22.13	15.22	55	5.12	2.72	1.86
30	40.01	20.63	14.25	56	4.60	2.40	1.71
31	37.43	19.38	13.29	57	4.12	2.20	1.55
32	34.98	18.06	12.47	58	3.69	1.92	1.34
33	32.63	16.92	11.68	59	3.29	1.76	1.23
34	30.40	15.71	10.83	60	2.93	1.53	1.11
35	28.28	14.69	10.12	61	2.61	1.40	0.95
36	26.28	13.59	9.45	62	2.31	1.21	0.87
37	24.39	12.69	8.71	63	2.03	1.11	0.80
38	22.61	11.70	8.12	64	1.77	0.93	0.65
39	20.95	10.91	7.56	65	1.53	0.85	0.59
40	19.40	10.04	6.94	66	1.31	0.69	0.54
41	17.96	9.36	6.46	67	1.11	0.62	0.41
42	16.60	8.60	6.01	68	0.93	0.49	0.37
43	15.31	8.00	5.50	69	0.77	0.44	0.33
44	14.09	7.31	5.09	70	0.62	0.32	0.22
45	12.94	6.78	4.72	71	0.50	0.30	0.21
46	11.87	6.17	4.28	72	0.38	0.20	0.19
47	10.87	5.70	3.95	73	0.27	0.18	0.10
48	9.94	5.16	3.64	74	0.17	0.09	0.09
49	9.08	4.77	3.28	75	0.08	0.08	0.08
50	8.29	4.31	3.01				

When using this table to calculate total effective risk the commencement age and frequency of screening examinations must be selected and the relevant conversion factor can then be multiplied by the MGD.

Table (6-19) Lists the relationship factors between the total effective risk of the screening programme and the MGD based on the data collected from the 16 FFDM machines. These factors are for **method 3** of LAR extrapolation.

Commencement age (year)	Conversion factor % MGD (case/10^6/μGy)			Commencement age (year)	Conversion factor % MGD (case/10^6/μGy)		
	Annual	Biennial	Triennial		Annual	Biennial	Triennial
25	72.97	38.66	25.53	51	10.36	5.53	3.66
26	68.60	34.30	24.81	52	9.64	4.82	3.35
27	64.24	34.30	22.62	53	8.93	4.82	3.35
28	59.88	29.94	21.17	54	8.21	4.11	2.95
27	55.51	29.94	20.45	55	7.50	4.11	2.63
30	51.15	25.57	18.26	56	6.78	3.39	2.63
31	48.58	25.57	16.80	57	6.07	3.39	2.24
32	46.00	23.00	16.08	58	5.35	2.68	1.92
33	43.43	23.00	15.69	59	4.64	2.68	1.92
34	40.86	20.43	14.23	60	3.93	1.96	1.52
35	38.29	20.43	13.51	61	3.61	1.96	1.20
36	35.71	17.86	13.11	62	3.29	1.64	1.20
37	33.14	17.86	11.66	63	2.97	1.64	1.20
38	30.57	15.28	10.94	64	2.65	1.33	0.88
39	27.99	15.28	10.54	65	2.34	1.33	0.88
40	25.42	12.71	9.09	66	2.02	1.01	0.88
41	23.99	12.71	8.37	67	1.70	1.01	0.57
42	22.55	11.28	7.97	68	1.38	0.69	0.57
43	21.12	11.28	7.65	69	1.06	0.69	0.57
44	19.68	9.84	6.93	70	0.75	0.37	0.25
45	18.25	9.84	6.53	71	0.62	0.37	0.25
46	16.81	8.41	6.22	72	0.50	0.25	0.25
47	15.38	8.41	5.50	73	0.37	0.25	0.12
48	13.94	6.97	5.10	74	0.25	0.12	0.12
49	12.50	6.97	4.78	75	0.12	0.12	0.12
50	11.07	5.53	4.06				

When using this table to calculate total effective risk the commencement age and frequency of screening examinations must be selected and the relevant conversion factor can then be multiplied by the MGD.

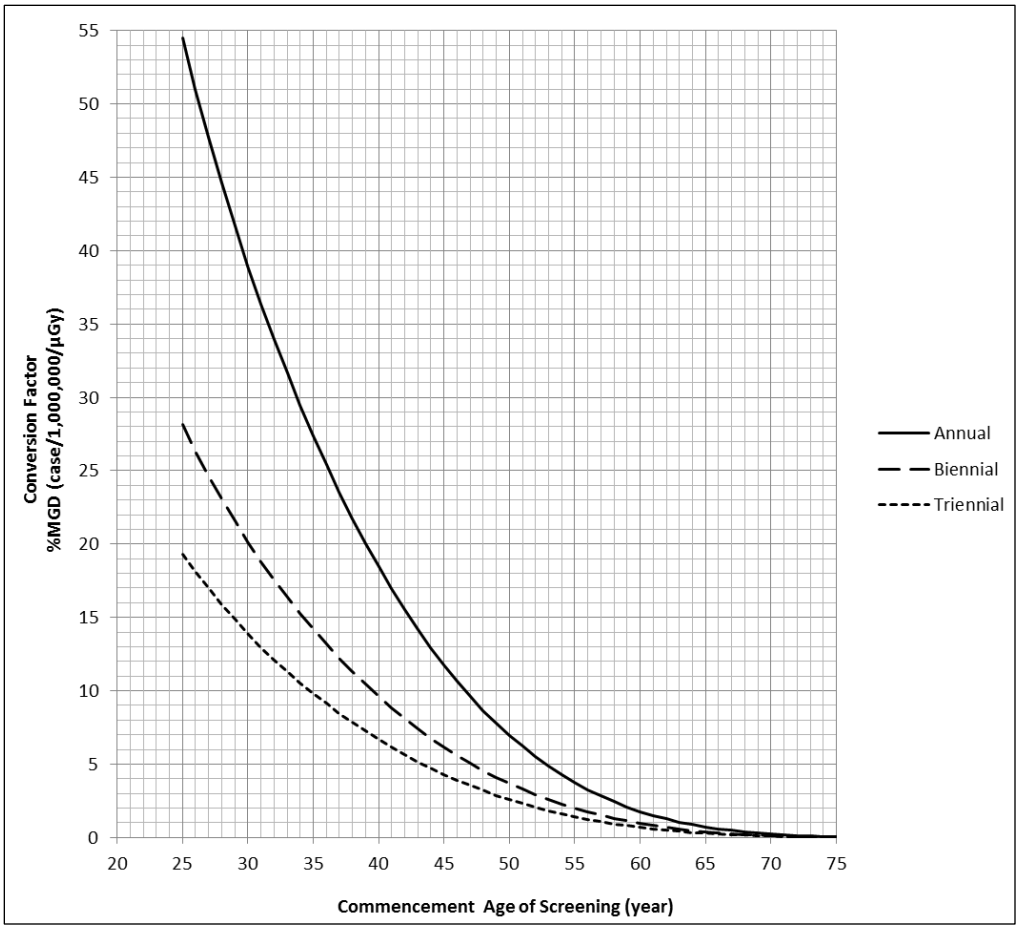

Figure (6-11) Represents the relationship between the total effective risk as a percent of MGD and the screening commencement age of different screening frequencies. Total effective risk calculated using LAR factors extrapolated by best fit lines method (method 1).

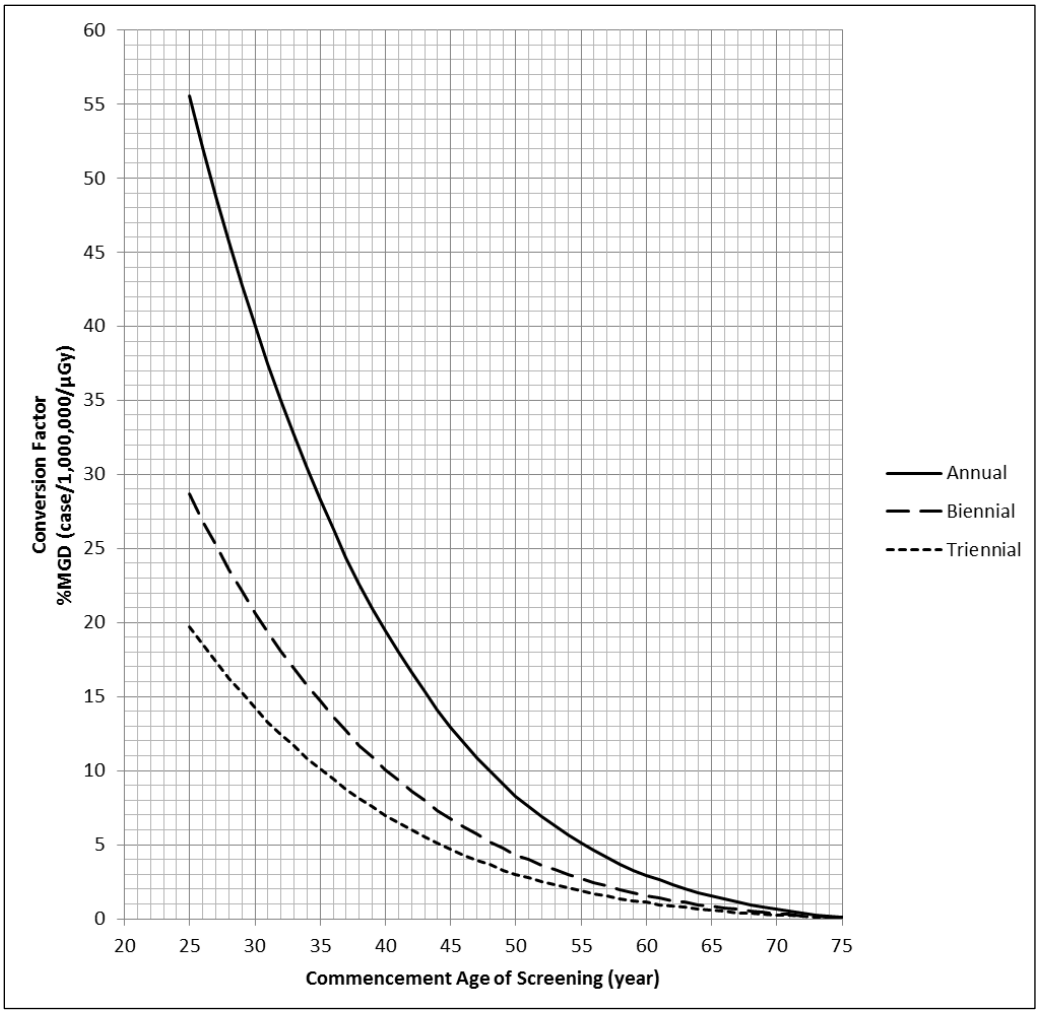

Figure (6-12) Represents the relationship between the total effective risk as a percent of MGD and the screening commencement age of different screening frequencies. Total effective risk calculated using LAR factors extrapolated by linear relationship method (method 2).

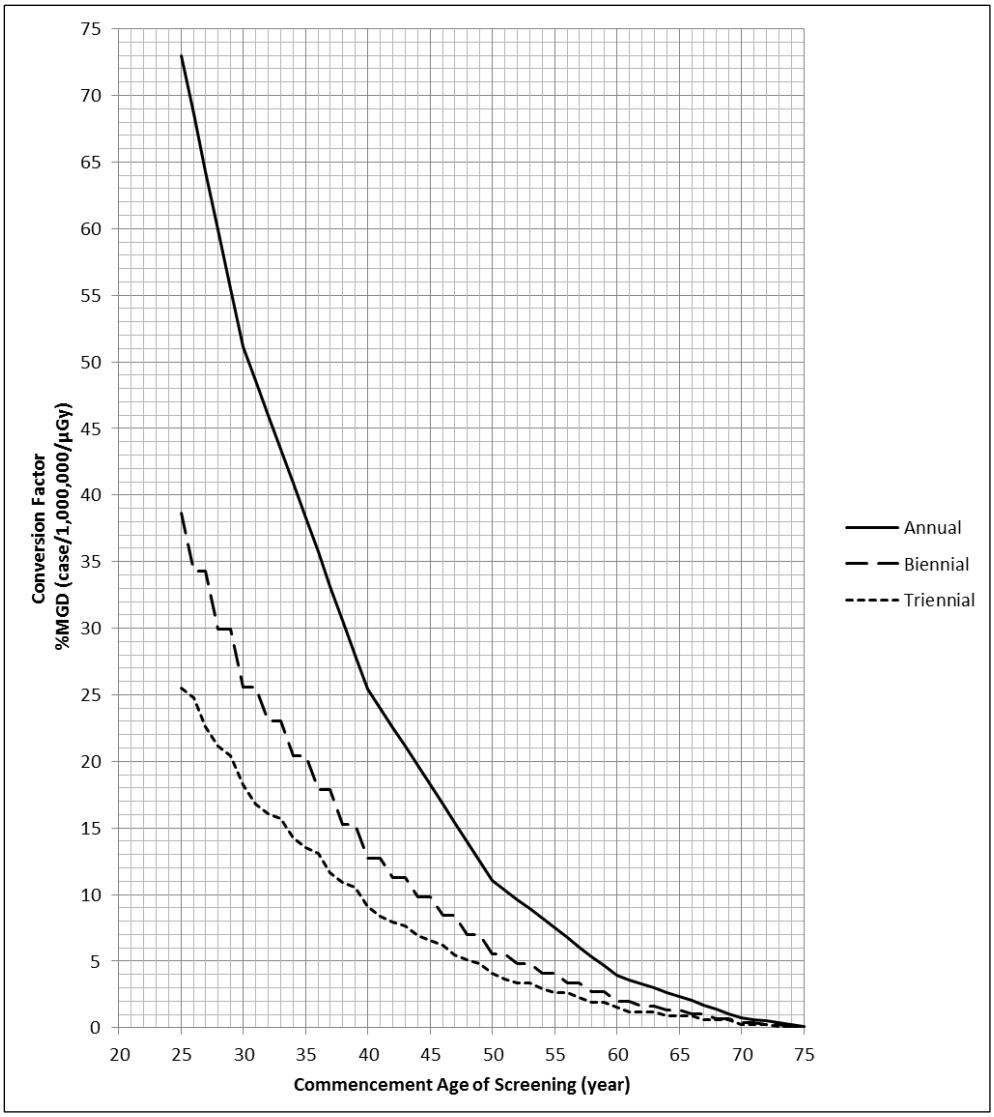

Figure (6-13) Represents the relationship between the total effective risk as a percent of MGD and the screening commencement age of different screening frequencies. Total effective risk calculated using LAR factors extrapolated by step method (method 3).

6.5 Shield Intervention Data

Analysis of effective dose for the sixteen FFDM machines demonstrates that the contralateral breast dose is the second highest contributor, after examined breast MGD, to the effective dose for one screening session; see **Table (6-20)**. For the sixteen machines, the effective dose of one screening session (second column of the table) along with the contribution of the examined breast MGD (third column), contralateral breast dose (fourth column), and other organ doses (fifth column) to the overall effective dose are seen in **Table (6-20).** Since organ dose measurements were repeated for FFDM machines 1 and 2 (three times on different

occasions to investigate reliability), each of these machines has three sets of data ('visit 1', 'visit 2', and 'visit 3'). An average value for the three visits has been calculated to represent the overall value for these machines. The average ± 1SD contralateral breast dose contribution was (1.346% ± 0.31) of the effective dose. Accordingly, the effect of contralateral breast shield was investigated on organ dose for four FFDM machines; justification for the four machines is indicated within the methods chapter (section 5.9.4, page 136). It was found that the contralateral breast shield greatly reduces the contralateral breast dose; see **Table (6-21)** which demonstrates the organ doses data for the four FFDM machines measured without and with the use of the contralateral breast shield.

Table (6-20) Radiation effective dose of one screening visit along with examined breast MGD, contralateral breast, and other tissue contribution in ED for the 16 FFDM machines.

Machine Number		Effective dose (µSv)	Contribution percent in effective dose (%)		
			Examined breast	Contralateral breast	Other tissue*
1	visit 1	295.958	98.565	1.052	0.383
	visit 2	296.151	98.501	1.163	0.336
	visit 3	295.672	98.660	1.019	0.321
2	visit 1	283.565	98.281	1.288	0.431
	visit 2	283.311	98.369	1.246	0.385
	visit 3	283.236	98.395	1.230	0.375
3		248.504	96.930	2.301	0.769
4		232.944	97.496	1.846	0.658
5		244.873	98.430	1.206	0.364
6		216.363	98.383	1.291	0.326
7		343.731	97.977	1.550	0.473
8		270.333	97.777	1.709	0.514
9		223.155	98.458	1.138	0.404
10		259.702	98.438	1.206	0.356
11		204.445	98.467	1.098	0.435
12		241.280	98.304	1.324	0.372
13		226.972	98.295	1.309	0.396
14		230.892	98.276	1.306	0.418
15		214.934	98.012	1.563	0.425
16		210.655	98.549	1.084	0.367
Mean(SD)		255.334(37.27)	98.228(0.42)	1.346 (0.31)	0.425(0.11)

* *Other tissue includes all body tissue other than breast (examined and contralateral breasts) which received radiation dose from screening mammography exposures.*

Table (6-21) Shows the effect of a contralateral breast shield on organs doses (μGy) for the selected four FFDM machines.

Organ		Machine 2**		Machine 8**		Machine 10**		Machine 11**	
		without	with	without	with	without	with	without	with
Brain		0.82	0.54	0.00	0.00	0.68	1.92	0.17	1.46
Salivary glands		4.36	3.71	2.78	2.80	1.84	2.40	1.22	1.84
Thyroid		14.41	15.21	8.71	9.38	6.40	7.25	5.40	5.50
Oesophagus		0.04	0.08	0.00	0.00	0.03	0.35	0.14	0.07
Thymus		3.55	4.38	1.87	2.91	1.22	1.55	0.71	0.96
Heart		0.77	0.06	0.00	0.03	0.00	0.54	0.00	0.15
Lung		3.01	3.10	3.07	3.77	2.33	2.74	1.99	1.93
Liver		1.61	0.46	0.63	0.76	0.44	0.78	0.46	0.43
Gall bladder		0.42	0.10	0.00	0.00	0.00	0.29	0.05	0.10
Adrenal		0.46	0.00	0.00	0.00	0.00	0.13	0.00	0.00
Kidney		0.33	0.04	0.00	0.00	0.00	0.15	0.03	0.16
Spleen		0.31	0.00	0.06	0.00	0.00	0.27	0.01	0.00
Pancreas		0.09	0.01	0.00	0.00	0.00	0.14	0.00	0.00
Stomach		1.64	0.25	0.23	0.43	0.32	0.41	0.24	0.21
Intestine		0.00	0.00	0.00	0.00	0.00	0.02	0.00	0.00
Bone Marrow (BM)	Cranium (7.6%)*	3.33	2.05	0.06	0.32	1.66	2.82	0.91	2.84
	Mandibles (0.8%)*	4.36	3.71	2.78	2.80	1.84	2.40	1.22	1.84
	C-spine (3.9%)*	0.00	0.21	0.00	0.00	0.06	0.75	0.00	0.47
	Clavicles (0.8%)*	17.14	19.46	12.62	9.21	3.78	3.67	3.17	3.39
	Scapulae (2.8%)*	0.00	0.02	0.00	0.00	0.02	0.33	0.04	0.18
	Sternum (3.1%)*	27.98	24.07	29.65	24.54	16.74	12.78	12.32	11.12
	Ribs (16.1%)*	3.74	3.72	4.31	4.81	2.84	2.97	2.54	2.29
	T/L spine (28.4%)*	0.20	0.00	0.00	0.00	0.01	0.07	0.00	0.00
	Pelvis (27.4%)*	0.00	0.00	0.00	0.00	0.00	0.00	0.00	0.00
	Total BM dose	1.95	1.70	1.74	1.66	1.15	1.12	0.90	0.99
Urinary bladder		0.00	0.00	0.00	0.00	0.00	0.00	0.00	0.00
Uterus		0.00	0.00	0.00	0.00	0.00	0.00	0.00	0.00
Ovaries		0.00	0.00	0.00	0.00	0.00	0.00	0.00	0.00
Contralateral breast		35.20	1.93	41.40	0.01	22.85	1.24	22.76	1.66

* *These percentages represent the portion of bone marrow (BM) in different locations. They were adapted from ICRP report 70 (1995).*

** *Machine 2 is Hologic Selenia, machine 8 is Giotto, and both machines 10 and 11 are GE Seno Essential.*

The resultant reduction in total effective risk of worldwide screening programmes by the use of the contralateral breast shield, described in section 5.9.3 (page 135), for the four FFDM machines ranges from 0.75% to 1.68%, see **Tables (6-22)**, **(6-23)**, and **(6-24)** for the three LAR extrapolation methods. The first column of these tables includes the worldwide screening programmes. Opposite to each programme the reduction percentages in total effective risk due to the contralateral breast shield described in this thesis are listed in second, third, fourth, and fifth columns for machines 2, 8, 10, and 11, respectively.

Tables (6-22) Demonstrates the effect of a contralateral breast shield on the total effective risk of worldwide screening programmes calculated using LAR factors extrapolated by **method 1**.

Programme	Total effective risk reduction percent (%)			
	Machine 2	Machine 8	Machine 10	Machine 11
Australia, Japan, Korea, United States (AAFP, NCI, and USPSTF)	1.44	1.62	0.95	1.07
Belgium, Croatia, Cyprus, Denmark, Finland, Germany, Italy, Latvia, Lithuania, Luxembourg, Norway, Poland, Slovenia, Spain (Catalonia), Switzerland	1.45	1.55	0.89	1.06
Canada , France, Israel, Netherlands	1.46	1.52	0.86	1.06
China	1.43	1.66	0.98	1.08
Czech	1.44	1.59	0.92	1.07
Estonia	1.44	1.59	0.92	1.07
Hungary	1.44	1.61	0.94	1.07
Iceland	1.43	1.64	0.96	1.07
India	1.43	1.64	0.97	1.07
Ireland	1.45	1.58	0.91	1.07
Malta	1.44	1.61	0.93	1.07
New Zealand, Portugal, Spain (Navarra)	1.44	1.60	0.93	1.07
Nigeria	1.43	1.63	0.96	1.07
Sweden	1.43	1.63	0.96	1.07
United Kingdom	1.45	1.57	0.91	1.07
United States (ACOG)	1.44	1.59	0.65	1.07
United States (ACS, ACR, and NCCN)	1.44	1.62	0.75	1.07
Uruguay	1.44	1.61	0.94	1.07
Canada	1.43	1.64	0.97	1.07
United Kingdom	1.44	1.62	0.95	1.07
United States (ACS)	1.42	1.67	0.90	1.08
United States (NCCN)	1.42	1.68	0.94	1.08

Screening programmes designed for high breast cancer risk women are highlighted in grey.

Tables (6-23) Demonstrates the effect of a contralateral breast shield on the total effective risk of worldwide screening programmes calculated using LAR factors extrapolated by **method 2**.

Programme	Total effective risk (case/10^6)			
	Machine 2	Machine 8	Machine 10	Machine 11
Australia, Japan, Korea, United States (AAFP, NCI, and USPSTF)	1.43	1.63	0.95	1.07
Belgium, Croatia, Cyprus, Denmark, Finland, Germany, Italy, Latvia, Lithuania, Luxembourg, Norway, Poland, Slovenia, Spain (Catalonia), Switzerland	1.45	1.58	0.91	1.07
Canada , France, Israel, Netherlands	1.45	1.56	0.89	1.07
China	1.43	1.66	0.98	1.08
Czech	1.44	1.60	0.93	1.07
Estonia	1.44	1.60	0.93	1.07
Hungary	1.44	1.62	0.95	1.07
Iceland	1.43	1.64	0.96	1.07
India	1.43	1.65	0.97	1.07
Ireland	1.44	1.59	0.92	1.07
Malta	1.44	1.61	0.94	1.07
New Zealand, Portugal, Spain (Navarra)	1.44	1.61	0.94	1.07
Nigeria	1.43	1.63	0.96	1.07
Sweden	1.43	1.64	0.96	1.07
United Kingdom	1.44	1.59	0.92	1.07
United States (ACOG)	1.44	1.61	0.93	1.07
United States (ACS, ACR, and NCCN)	1.43	1.63	0.95	1.07
Uruguay	1.44	1.62	0.95	1.07
Canada	1.43	1.65	0.97	1.07
United Kingdom	1.43	1.63	0.95	1.07
United States (ACS)	1.42	1.67	0.99	1.08
United States (NCCN)	1.42	1.68	1.00	1.08

Screening programmes designed for high breast cancer risk women are highlighted in grey.

Tables (6-24) Demonstrates the effect of a contralateral breast shield on the total effective risk of worldwide screening programmes calculated using LAR factors extrapolated by **method 3**.

Programme	Total effective risk (case/10^6)			
	Machine 2	Machine 8	Machine10	Machine11
Australia, Japan, Korea, United States (AAFP, NCI, and USPSTF)	1.43	1.65	0.97	1.07
Belgium, Croatia, Cyprus, Denmark, Finland, Germany, Italy, Latvia, Lithuania, Luxembourg, Norway, Poland, Slovenia, Spain (Catalonia), Switzerland	1.44	1.61	0.93	1.07
Canada , France, Israel, Netherlands	1.44	1.59	0.92	1.07
China	1.42	1.68	1.00	1.08
Czech	1.43	1.63	0.96	1.07
Estonia	1.44	1.62	0.95	1.07
Hungary	1.43	1.66	0.98	1.08
Iceland	1.43	1.66	0.98	1.08
India	1.43	1.67	0.99	1.08
Ireland	1.44	1.62	0.94	1.07
Malta	1.43	1.64	0.96	1.07
New Zealand, Portugal, Spain (Navarra)	1.43	1.65	0.97	1.07
Nigeria	1.43	1.65	0.98	1.08
Sweden	1.43	1.66	0.98	1.08
United Kingdom	1.43	1.63	0.95	1.07
United States (ACOG)	1.43	1.63	0.96	1.07
United States (ACS, ACR, and NCCN)	1.43	1.65	0.97	1.07
Uruguay	1.43	1.64	0.97	1.07
Canada	1.44	1.62	0.94	1.07
United Kingdom	1.43	1.65	0.97	1.07
United States (ACS)	1.42	1.68	1.00	1.08
United States (NCCN)	1.41	1.70	1.01	1.08

Screening programmes designed for high breast cancer risk women are highlighted in grey.

Chapter Seven
Discussion

7.1 Chapter Overview

The objective of screening mammography is to detect breast cancer early when treatment and recovery are more likely to be successful. However, since the introduction of screening mammography there has been a great debate about the risks versus benefits; see section 3.7 on page 53. To understand the radiation risk associated with mammography many researchers have focused on screening mammography. The majority of researchers have used MGD as a parameter to quantify the radiation risk. In contrast others have used the years of a woman's life lost due to radiation-induced cancer from screening mammography. In this PhD thesis a novel method is proposed to quantify radiation risk from screening mammography. This method includes the calculation of effective risk of radiation-induced cancer as a parameter to assess mammography radiation risk. The effective risk calculation is no more difficult than the effective dose calculation. It takes the individuals' age and gender into account, and generates data that is likely to be more understandable to the general public when compared to MGD. In other words, for general public, it is probably easier to understand the risk of screening mammography in terms of radiation-induced cancer cases per million screened women rather than in mGy, in the case of MGD, or in mSv, in the case of effective dose.

Within this chapter the results demonstrated in chapter 6 will be discussed. This chapter will be divided into six major sections. The measured organ dose reliability study is the focus of the *first section* (Dose Measurement Reliability). The discussion of reliability data includes the measured organ doses from two FFDM machines. For each of the machines, the organ doses were measured on three separate occasions and analysed to obtain the coefficients of variance for each of the organ doses and the overall intra-class correlation using statistical software. The radiation dose to each organ along with factors affecting this dose will be discussed separately in a subsection within the *second section* (Organ Radiation Doses) of this chapter. Compared to previous published studies, which estimated the organ doses by Monte Carlo simulation, the measured organ doses in this thesis are larger. This can be

attributed to some limitations of Monte Carlo software in the exact simulation of the mammographic machine and mathematical phantom positioning.

The *third section* (Effective Risk) concentrates on total effective risk, during a female's lifetime and it explores the data of worldwide screening programmes to demonstrate the differences amongst these programmes. This includes the discussion of effective risk from 48 screening programmes (44 for average risk women and 4 for high risk women) of 22 different screening recommendations with different screening commencement/cessation ages and frequencies. The total effective risk modelling, during female lifetime, will be discussed in the *fourth section* (Effective Risk Modelling). In this context three different risk models are discussed. The first model, which is based on mathematical regression, is characterised by a large percentage error (approximately 30%) for the three LAR extrapolation methods. The second model is based on the use of a graphical representation of total effective risk against screening commencement age for each screening frequency separately. In this model (second model) interpolated total effective risk values are based on average organ dose for the 16 FFDM machines. To include the organ dose variations of different FFDM mammography machines, the third risk model was established based on the linear relationships between total effective risk and MGD from different FFDM machines. This was conducted because the MGD contributes to up to 98% of the effective risk and all other organs approximately 2%.

The effect of a contralateral breast shield on measured organs dose and calculated effective risk is the focus of the *fifth section* (Contralateral Breast Shield Effect). Organ dose data from four FFDM machines without and with the use of a contralateral breast shield are discussed in this section. The contralateral breast shield can reduce contralateral breast tissue radiation dose by 95%. Consequently the total effective risk reduces by approximately 1.5% with the use of a contralateral breast shield. Finally, the limitations of this thesis, proposed future work to address these limitations and recommendations are the focus of the *sixth section* (Limitations, Future Work and Recommendations).

7.2 Dose Measurement Reliability

Reliability is a measure of random error associated with measurement processes and gives an indication of the method's precision (Field, 2013). In this thesis the main purpose of

reliability estimation is to investigate the possibility of obtaining consistent organ doses measured by the same FFDM machine under the same experimental conditions on three different occasions. As mentioned earlier in section 6.2 (page139) the reliability study involves data from three separate visits (organ doses measurement) for two FFDM machines.

The reliability study for FFDM machine 1 (**Figure (6-1),** page 140) illustrates that there are some differences among measured organ doses across the three visits. These differences affect the measured radiation doses to the brain, salivary glands, thyroid, thymus, adrenals, stomach, mandible, clavicles, sternum and contralateral breast. Variations for mandible, clavicles, and sternum bone marrow radiation doses do not result in a large difference in the total bone marrow radiation dose (mean ± 1SD) 1.35 ± 0.10 µGy (coefficient of variation (CV) = 7.41%). With regard to the differences in measured organ dose to brain, salivary glands, thymus, and contralateral breast dose, although large standard deviations (SD) have been recorded for each, these SD values can be considered acceptable when compared with their mean values. For instance, for contralateral breast dose a SD of 1.89 µGy is acceptable when compared to 26.58 µGy mean dose (CV = 7.11%). The only organs that showed large differences in their measured organ doses are adrenal glands and stomach, where the mean ± 1SD for these was 0.51 ± 0.46 µGy (CV= 90.00%) and 0.36 ± 0.21 µGy (CV= 35.00%, respectively.

On the other hand, slightly smaller differences in measured organs doses, between the three visits, are seen for FFDM machine 2 (**Figure (6-2),** page 140), when compared to those of machine 1. For the three visits, the largest noticeable differences are recorded for radiation doses to brain, cervical spine bone marrow, cranium bone marrow, and the heart; the values (mean ± 1SD) were 0.50 ± 0.84 µGy (CV > 100%), 0.23 ± 0.40 µGy (CV > 100%), 1.08 ± 0.86 µGy (CV = 79.63%), and 0.33 ± 0.18 µGy (CV = 54.55%), respectively. In spite of the large variations in cranium and cervical spine bone marrow radiation doses in addition to small variations in mandible, clavicles and sternum bone marrow doses, the total bone marrow radiation dose does not show large differences between the three visits (1.49 ± 0.16 µGy, CV = 10.74%). As for FFDM machine 1 data, the variations in radiation dose to salivary glands, thymus, and contralateral breast are considered acceptable because their SD values are considered small when compared to their mean values.

A large part of the dose differences can be attributed to the inconsistency of the AECs because different exposure factors were recorded for the three visits; see **Table (7-1)**. For FFDM machine 1 the variation in exposure factors amongst the three visits was higher than the level recommended by the European Commission (2006) which suggests a maximum mAs variation of 5%. However, this FFDM machine met the routine QA standards performed by physics support within the NHSBSP and it was in constant use for routine breast screening. The exposure factors variations for machine 2 were within the acceptable range of the European Commission (2006). The mAs variations for machine 2 were 3.1% and 0.7% for CC and MLO projections, respectively. The effect of exposure factors (kV and mAs) on organ radiation doses has been reported by Hatziioannou et al. (2000) who found that some Lucite phantom organ radiation doses (e.g. sternum bone marrow and thyroid doses) are related to both kV and mAs. Also, the random nature of the X-ray beam and some experimental errors, such as those arising from phantom positioning, may contribute to these organ dose differences. However, as mentioned earlier in section 5.2.4 (page 112), the positioning error was minimised by the use of additional lines drawn on the ATOM phantom chest wall.

Although both machines 1 and 2 are of same brand (Hologic Selenia), their AEC systems used different exposure factors to expose same breast phantom. This may be attributed to the different target/filter combinations of these machines wherein the machine 1 had a Mo/Mo target/filter combination while machine 2 had a Rh/Rh combination. Also, the X-ray tube age may be considered another cause for exposure factors difference which are used by the machines. It can be seen in **Table (7-1)** the use of lower kV by machine 2 resulted in higher required mAs to produce equivalent image quality.

Overall, in spite of the organ dose differences, the consistency statistical analysis demonstrates an excellent agreement between the organ radiation doses measured on the three visits for each of the two FFDM machines (ICC > 99% for both machines). Moreover, these dose differences during the repeated measures on the three occasions do not produce important changes, which are not detectable statistically (ICC =1), in calculated total effective risk of worldwide screening programmes; see **Table (6-1)** (page 141) for FFDM machine 1 and **Table (6-2)** (page 142) for FFDM machine 2.

Table (7-1) Demonstrates the exposure factor variations amongst the three visits for FFDM machine 1 and FFDM machine 2.

FFDM Machine	Projection	Visit 1		Visit 2		Visit 3		Coefficient of Variation (%)	
		kV	mAs	kV	mAs	kV	mAs	kV	mAs
1	CC	29.0	65.5	29.0	65.5	28.0	76.8	2.0	9.4
	MLO	30.0	67.6	29.0	73.3	29.0	77.0	2.0	6.5
2	CC	28.0	124.5	29.0	118.2	28.0	125.2	2.0	3.1
	MLO	29.0	129.5	29.0	131.2	29.0	130.0	0.0	0.7

7.3 Organ Radiation Doses

7.3.1 Examined Beast Radiation Dose

As recommended internationally, radiation dose to glandular tissue (MGD) is used to indicate the breast radiation dose during screening mammography (IAEA, 2011; IPEM, 2005). As mentioned earlier in section 5.3 (page 114) the method described by Dance, Skinner, Young, Beckett, and Kotre (2000a), has been recommended in the UK and all European countries and is used to calculate the examined breast MGD. Compared to the other available method of MGD calculation, described by Wu, Gingold, Barnes, and Tucker (1994), the MGD calculated by Dance, Skinner, et al. (2000a) method gives a higher result by approximately 9-21% depending on target/filter combination (Tsai, Chong, Ho, and Tyan, 2010)

For the sixteen FFDM machines the total MGD (for both CC and MLO projections) ranged between 1.678 mGy (for FFDM machine 11) and 2.806 mGy (for FFDM machine 7) with a mean (95% CI) value of 2.019 (1.871 - 2.166) mGy; see **Table (6-3)** on page 143. These MGD values are lower than expected for a standard breast (with 53 mm thickness and 50% glandularity) because they were calculated for breasts with 29% glandularity (without the use of breast composition correction factor, c_{53} factor); see section 5.3 on page 114. This was undertaken in order to make both the calculated MGD and measured organs dose consistent for 29% breast glandularity, which was simulated by a PMMA-PE phantom. The standard breast composition recommended by mammographic international protocols has 50% glandularity (IAEA, 2011; IPEM, 2005), however as reported by Yaffe et al. (2009), breast glandularity used in this thesis (29%) represents the most common breast density. Yaffe et

al. (2009) studied breast composition in 2831 Canadian women and found 95% of their study participants had a breast density of less than 45%.

Since two breast phantoms were used to simulate the examined breast for CC and MLO projections, the MGD was calculated for each projection separately and the sum of these doses was used to represent the total breast MGD. For all FFDM machines the MGD of the MLO projection is higher than that of the CC projection; see **Table (6-3)** on page 143. The maximum difference (28.59%) was for FFDM machine 7 (Hologic Selenia Dimensions), while the minimum value (1.03%) was for machine 10 (GE Seno Essential). The mean (95% CI) difference, for the sixteen FFDM machines, between MLO MGD and CC MGD is 14.24 (9.90 - 18.59) %. This difference is lower than that of film-screen mammography reported by Gomes et al. (2011). For 63 women Gomes et al. (2011) found that MGD for CC film-screen mammography was 30% lower than that of the MLO projection. The variations amongst the sixteen FFDM machines in this thesis could be attributed to the AEC system of the different FFDM machines, image receptor, and/or target/filter combination (wide range of FFDM machines has been included). In general, MGD variation between CC and MLO is more related to the FFDM machine brand than to machine's target/filter combination.

FFDM machines of the same model from the same manufacturer show similar MDG percentage differences. For instance, FFDM machines 3 and 7 are both Hologic Selenia Dimensions and have a 27.58% and 28.59% difference between CC and MLO MGDs, respectively. Also, there is an 18.78% and 19.60% CC and MLO MGD differences recorded for FFDM machines 15 and 16 - which are both Siemens Mammomat Inspiration. However, FFDM machines of same target/filter combination of two different brands showed different MGD variations between CC and MLO; machine 4 (Hologic Selenia, Rh/Rh) has 25.046 % and machine 5 (GE Seno Essential, Rh/Rh) has 14.325 % MGD difference between CC and MLO. Overall, the wide difference in MGD between CC and MLO is because some AEC systems are likely to be more sensitive to small changes in breast thickness than others.

Target/filter combination is one of the factors which can affect examined breast MGD (Dance, Thilander, et al., 2000b). **Figure (6-4)** (page 146) demonstrates the MGD data for the four different target/filter combinations included within this thesis. In **Figure (6-4)** (page 146), average MGD ± 1SD error bars are presented for both Rh/Rh and W/Rh target/filter

combinations. However, for Mo/Mo and W/Ag combinations, the MGD value of one FFDM machine is presented for each because only a single FFDM machine of these combinations was included in this study. It can be seen, in **Figure (6-4)** (page 146), that the SD for W/Rh (503.57 µGy) is larger than that of Rh/Rh (184.97 µGy). This large SD for W/Rh combination is because W/Rh machines were from two different manufacturers (2 Hologic Selenia Dimensions and 2 Siemens Mammomat Inspiration). The two Hologic Selenia Dimensions machines (FFDM machines 3 and 7) gave higher MGD than the two Siemens Mammomat Inspiration FFDM machines (FFDM machines 15 and 16); see **Table (6-3)** on page 144. Overall, for the four combinations of targets and filters, the Rh/Rh combination resulted in the lowest MGD (1936.31 ± 184.97 µGy) while the highest value of MGD was with the Mo/Mo combination (2430.92 µGy). This is consistent with previous work (Dance, Thilander, et al., 2000b; Gingold, Wu, & Barnes, 1995). Both Gingold et al. (1995) and Dance, Thilander, et al. (2000b) found that the estimated MGD, by Monte Carlo simulation, using the Rh/Rh target/filter combination was less than that produced by the Mo/Mo and Mo/Rh combinations.

According to Rezaei, Feghhi, Aghamiri, Rezaei, and Ebrahimi (2011) the Monte Carlo simulation of a Mo/Mo target/filter combination demonstrated that MGD is related in a linear fashion to both X-ray tube kV and mAs - MGD increases with an increase in kV and/or mAs. Since MGD data are non-parametric (not normally distributed), Spearman's rho correlation coefficient (r) was used to assess the relationship between MGD and mAs / HVL; see **Table (6-5)** on page 149**.** It was found that MGD correlates positively with mAs (MGD increases as mAs increases), however, this relationship was not statistically significant (r = 0.426, p = 0.072). Also, a non-statistically significant (p = 0.277) relationship exists, with a weaker positive correlation (r = 0.289), between MGD and HVL. Similarly, the backward regression model demonstrates that both mAs and HVL do not significantly affect the MGD; see **Table (6-6)** on page 150.

In summary, for the same breast phantom, a wide MGD range has been recorded for the included 16 FFDM machines. However, all of these MGD values were within the acceptable range determined by the respected international mammographic quality assurance programmes (EC, IAEA, NHSBSP). This indicates a growing need for the revision of the

maximum acceptable MGD reported by international mammographic protocols. The examined breast MGD is related to the target/filter combination, mAs, and HVL. It has been found that the Rh/Rh combination results in the lowest MGD. This is because the Rh/Rh combination produces a harder beam which results in less X-ray absorption by the breast tissue. Also, with a harder beam lower exposure factors can be used to produce the required image quality. MGD is more dependent on mAs than on beam HVL because the higher mAs means more X-ray photons are produced.

7.3.2 Organ Radiation Dose (organs and tissues other than the examined breast)

Several researchers have assessed the radiation dose to *other* body tissues and organs from mammography; here *other* refers to all organs with the exclusion of the examined breast. In all instances, their approaches were different to the methods used in this thesis. For instance, Sechopoulos , Suryanarayanan , Vedantham , D'Orsi, and Karellas (2008) used Monte Carlo dose simulation, while Hatziioannou et al. (2000) used TLDs accommodated inside Lucite phantom to measure radiation dose received by several organs during craniocaudal and medio-lateral breast exposures.

As indicated in section 5.2 (page 100), organ radiation doses were measured by TLDs from radiation exposures of CC and MLO projections for each breast. These data have been presented in two different ways - as absorbed doses **(Figure 6-3)** on page 144 and as MGD percentages **(Table 6-4)** on page 145. The tissues ('other than the examined breast') include brain, salivary glands, thyroid, oesophagus, thymus, heart, lung, liver, gall bladder, adrenals, kidneys, spleen, pancreas, stomach, intestine, bone marrow (cranium, mandible, cervical spine, clavicles, scapulae, sternum, ribs, thoracic and lumbar spine, and pelvis), urinary bladder, uterus, ovaries, and contralateral breast.

For the sixteen FFDM machines, urinary bladder, uterus, ovaries and pelvis bone marrow do not receive radiation dose during screening mammography. This is because either they really don't receive a radiation dose or their radiation dose is lower than the TLDs sensitivity threshold. However, kidneys, pancreas, intestine, spleen, and T/L spine bone marrow receive negligible radiation doses (< 0.1 µGy), while the radiation dose received by the other tissues range between 0.10 µGy with 95% CI of (0.03 - 0.18) (for adrenals) and 28.75 (24.20 - 33.3) µGy (for contralateral breast); see **Figure (6-3)** on page 144. For the majority of these

organs which receive a radiation dose of more than 0.1 µGy, the Rh/Rh target/filter combination resulted in the lowest radiation dose. Organs receiving a radiation dose more than 0.1 µGy will be more discussed in the following sections.

7.3.2.1 Contralateral Breast Radiation Dose

During screening mammography, the radiation dose to the contralateral breast was the second highest radiation dose to any organ after the examined breast for all sixteen FFDM machines. The contralateral breast dose ranged from 18.70 to 47.66 µGy with a mean (95% CI) of 28.75 (24.20 - 33.3) µGy; see **Figure (6-3)** on page 144. This radiation dose is (mean ± 1SD) 1.419 ± 0.346 % of examined breast MGD; see **Table (6-4)** on page 145. A lower contralateral breast dose to MGD percent has been reported by Sechopoulos et al. (2008) using Monte Carlo simulation. They found that the contralateral breast dose is approximately 0.46 % of CC projection MGD and 0.59 % of MLO projection MGD at 30 kV from Rh/Rh target/filter combination X-ray tube. The differences between Sechopoulos and those reported in this thesis may be attributed to many factors. The wide range of FFDM machines used in this work was one likely cause. The geometrical limitation of human body mathematical phantoms using Monte Carlo simulation is another cause. The resultant organ dose underestimation by Monte Carlo compared to the measured dose, due to the geometrical limitation of the mathematical phantom, has previously been reported by Tootell, Szczepura, and Hogg (2014). Also, different simulated examined breast glandularity can affect the contralateral breast dose by changing the X-ray scattering profile from the examined breast. In this context Sechopoulos et al. (2008) simulated the examined breast with 50%, while in this thesis the examined breast PMMA-PE phantom simulates 29% breast glandularity.

Target/filter combination can be considered one of the factors which will affect the contralateral breast dose because the use of different combinations results in different doses to the contralateral breast; see **Figure (6-5)** on page 146. For instance, the Rh/Rh combination resulted in the lowest contralateral breast radiation dose 25.58 ± 4.68 µGy (mean ± 1SD), while the highest dose to the contralateral breast tissue resulted from the use of W/Ag combination 38.49 µGy.

The statistical analysis of the relationship between contralateral breast dose and MGD, mAs and HVL demonstrate that contralateral breast dose correlates positively with all of these

factors; see **Table (6-5)** on page 149. The correlation coefficients were 0.671, 0.732, and 0.234, respectively. This relationship was significant for both MGD and mAs ($p < 0.05$) but it was non-significant for HVL ($p = 0.383$). Further analysis of these relationships using backward regression (**Table (6-6),** page 150) shows that 63% (regression R^2) of contralateral breast dose variability can be predicted by MGD and mAs with 5.551 µGy standard error (coefficient of variance = 19.31 %). According to this regression model, a 1 µGy increment in contralateral breast dose results either from mean (95%CI) of 1.1% (0.0% - 2.2%) increment in MGD (µGy) or from 13.3% (4.4% - 22.2%) mAs increment.

In summary, target/filter combination, beam HVL, and mAs affect contralateral breast radiation dose. The Rh/Rh target filter/combination results in the lowest contralateral breast radiation dose. HVL has a very small effect on contralateral breast radiation dose. The mAs, however, is the most important factor affecting the contralateral breast radiation dose. All in all, the contralateral breast dose can be predicted by examined breast MGD - the higher the examined breast MGD, the higher the contralateral breast radiation dose.

7.3.2.2 Bone Marrow Radiation Dose

Bone marrow radiation dose includes the radiation dose received by bone marrow in nine different locations, namely, cranium, mandible, cervical spine, clavicles, scapulae, sternum, ribs, T/L spine, and pelvis. The bone marrow radiation dose received by each location was separately measured and analysed, as indicated in section 5.2.2 (page 108). In general, the most important factor affecting radiation dose distribution within bone marrow is related to the proximity to the examined breast (primary beam), being consistent with the inverse square law - the closer bone marrow to examined breast, the higher its radiation dose will be.

For the sixteen FFDM machines, the value of cranium bone marrow radiation dose fluctuated widely. It ranged from 0.16 µGy (for FFDM machine 6) to 5.82 µGy (for FFDM machine 11) with mean (95% CI) of 1.56 (0.82 - 2.31) µGy, see **Figure (6-3)** on page 144. Cranium bone marrow dose represents 0.0815 ± 0.082 % (mean ±1 SD) of examined breast MGD; see **Table (6-4)** on page 145. The highest cranium bone marrow dose was recorded for Rh/Rh target/filter combination 2.00 ± 1.61 µGy (mean ± 1SD). However, the lowest cranium bone marrow dose was for W/Rh combination (0.65 ± 0.20 µGy); see **Figure (6-6)** on page 147. Statistical analysis shows that there was a non-significant relationship between cranium bone

marrow dose and MGD, mAs and HVL using both correlation (**Table (6-5)**, page 149) and regression (**Table (6-6)**, page 150). Therefore, the different measured radiation dose to cranium bone marrow can be attributed to other factors such as FFDM machine design (e.g. differences in X-ray tube angulation within the tube assembly), random nature of the X-ray beam, the leakage radiation, and/or some other experimental errors. This is the same as noted previously in section 7.2.

Mandible bone marrow which constitutes 0.8% of total body bone marrow (ICRP, 1995) received 0.139 ± 0.048 % (mean ± 1SD) of MGD during screening exposures (**Table (6-4)**, page 145) which is 2.79 (2.29 - 3.29) µGy (mean with 95% CI); see **Figure (6-3)** on page 144. It has been found that Rh/Rh target/filter combination causes the lowest mandible bone marrow dose (2.66 ± 0.85 µGy), while all other combinations (Mo/Mo, W/Rh, and W/Ag) result in approximately the same mandible bone marrow dose; the values were 2.89, 3.00 ± 1.43, and 3.15 µGy, respectively, see **Figure (6-6)** on page 147. Although the Spearman's rho correlation (**Table (6-5)**, page 149) demonstrates that the relationship between mandible bone marrow dose and all of MGD, mAs and HVL values was not significant, the backward regression model (**Table (6-6)**, page 150) can predict 30% (regression R^2) of mandible bone marrow dose variability by mAs (1 µGy per 1.4% mAs).

Cervical spine bone marrow is one of the organs which received a very small radiation dose. It had 0.30 (0.12 - 0.48) µGy (mean (95% CI)); see **Figure (6-3)** on page 144. This wide range of 95% CI was due to wide range of cervical spine bone marrow doses for the 16 FFDM machines. Cervical spine bone marrow dose was approximately zero for some FFDM machines, while other machines resulted in up to 1.39 µGy. The average cervical spine bone marrow dose constitutes 0.016 ± 0.020 % (mean ± 1SD) of the average MGD; see **Table (6-4)** on page 146. FFDM machine 8 with a W/Ag target/filter combination was one of the FFDM machines which showed zero cervical spine bone marrow radiation dose. However, the Rh/Rh combination resulted in the highest cervical spine bone marrow dose 0.43 ± 0.37 µGy (mean ± 1SD); see **Figure (6-6)** on page 147. The statistical analysis of cervical spine bone marrow doses demonstrates that it is negatively correlated to MGD, mAs, and HVL; see **Table (6-5)** on page 149. Spearman's rho correlation was only significant with beam HVL ($p = 0.02$). Further analysis of this relationship by backward regression demonstrates that it was

non-significant (i.e cervical spine bone marrow dose variability cannot be predicted by HVL); see **Table (6-6)** on page 150. As for cranium bone marrow radiation dose, the variations of cervical spine bone marrow radiation dose cannot be explained by any of the factors which have been investigated in this thesis (e.g. target/filter combination, MGD, mAs, and HVL). Accordingly it could be attributed to other factors (e.g. FFDM machine design, unaware experimental error and the random nature of the X-ray beam) as earlier discussed in this section on page 187.

As seen in **Figure (6-3)** on page 144, clavicular bone marrow received the second highest bone marrow dose after sternum bone marrow. It was 9.25 (6.45 – 12.05) µGy (mean with 95% CI). This dose represents 0.451 ± 0.241% (mean ± 1 SD) of the examined breast MGD; see **Table (6-4)** on page 145. Lower clavicular bone marrow radiation dose has been reported by Sechopoulos et al. (2008) using a Monte Carlo methodology; radiation dose to bone marrow of the ipsilateral clavicle constituted 0.09 % and 0.04% of MGD for CC and MLO projections, respectively. This underestimation could have two explanations. Firstly, this radiation dose represents the dose to the ipsilateral clavicle bone marrow, while the dose to the contralateral clavicle bone marrow was not included. Secondly, as described by Tootell et al. (2014), the geometric shapes of organs within the mathematical phantoms were simplified resulting in underestimated organ doses.

Both Mo/Mo and W/Rh target/filter combinations resulted in high and approximately equal radiation dose levels to clavicular bone marrow. The dose values were 13.11 µGy and 12.83 ± 4.71 µGy (mean ± 1SD), respectively. However, lower clavicular bone marrow radiation dose values were recorded W/Ag and Rh/Rh combinations (8.88 µGy and 7.47 ± 5.26 µGy, respectively); see **Figure (6-6)** on page 147. These clavicular bone marrow radiation dose variations amongst different target/filter combinations can be explained by the fact that the use of harder beam (of W/Ag and Rh/Rh combinations) reduces the required exposure factors especially the mAs.

Clavicular bone marrow dose strongly and significantly correlates with MGD ($r = 0.506$, $p < 0.05$) and mAs ($r = 0.876$, $p < 0.05$), while it did not correlate with beam HVL ($r = 0.077$); see **Table (6-5)** on page 149. Accordingly, for the 16 FFDM machines 87% (regression R^2) of clavicular bone marrow dose variability can be explained by MGD and mAs variations;

see **Table (6-6)** (page 150) which contains full details of the backward regression model for the relationship between clavicular bone marrow dose and MGD and mAs. In summary, the target/filter combination and mAs are the most important factors affecting clavicular bone marrow radiation dose and this radiation dose can be predicted by examined breast MGD. High examined breast MGD is associated with high clavicular bone marrow radiation dose.

Scapulae bone marrow dose tends to be negligible 0.17 (0.09 - 0.24) µGy (mean with 95% CI) and constitutes approximately 0.009 ± 0.008 % (mean ± 1SD) of MGD. Since it is a very small radiation dose no large differences can be recognised in **Figure (6-6)** (page 147) amongst the different target/filter combinations. In general, the lowest scapulae bone marrow dose was recorded for Mo/Mo combination (0.09 µGy), while the highest value was for W/Ag combination (0.24 µGy). Spearman's rho correlation shows that scapulae bone marrow dose only correlated with beam HVL and this had a correlation coefficient (r) of -0.519, see **Table (6-5)** on page 149. This means that a harder beam results in lower scapulae bone marrow dose. The effect of beam HVL on scapulae bone marrow dose was further estimated by backward regression and was found to be 1 µGy scapulae bone marrow dose per 86.4% HVL (mm Al); see **Table (6-6)** on page 150. In summary, the scapulae bone marrow radiation dose was very small and constitutes only 2.8% of total bone marrow radiation dose (ICRP, 1995). Accordingly, the effect of this radiation dose can be considered negligible.

Sternum bone marrow radiation dose was the highest bone marrow dose and the third highest organ dose after the examined and contralateral breasts; see **Figure (6-3)** on page 144. The high radiation dose to sternum bone marrow can be explained by its close proximity to the primary beam. For the 16 FFDM machines, the sternum bone marrow radiation dose ranged between 12.86 µGy (FFDM machine 11) and 32.50 µGy (FFDM machine 7) with a mean (95% CI) of 19.07 (15.81 - 22.34) µGy. Compared to MGD, the sternum dose was 0.942 ± 0.251% (mean ± 1SD) of breast MGD; see **Table (6-4)** on page 145. Sternum bone marrow dose has been estimated using Monte Carlo modelling by Sechopoulos et al. (2008). The simulated sternum bone marrow radiation dose was less than the measured dose in this thesis. Sechopoulos et al. (2008) found that sternum bone marrow dose constitutes 0.49% and 0.23% of MGD for CC and MLO projections, respectively. The difference between estimated (Sechopoulos et al. (2008)), by Monte Carlo, and measured radiation doses (this thesis)

could be attributed to the geometrical limitation of mathematical phantoms as earlier discussed in this section.

Using sternum bone marrow radiation dose, the 16 FFDM machines can be classified into two groups; see **Figure (6-6)** on page 147. The first group includes the FFDM machines with W/Ag and W/Rh which result in high sternum bone marrow dose (24.91 and 24.02 ± 7.56 μGy, respectively). The second group of FFDM machines comprises those which gave low sternum bone marrow doses (Mo/Mo and Rh/Rh target filter combinations). The sternum bone marrow dose for this group was 17.16 μGy for Mo/Mo combination and 16.70 ± 4.70 μGy for Rh/Rh combination. For the Rh/Rh target/filter combination, the sternum bone marrow radiation dose was consistent with radiation dose to bone marrow in other organs, being the lowest compared to other combinations. However, for Mo/Mo, sternum bone marrow dose was inconsistent when compared to the bone marrow radiation dose in other organs, discussed earlier in this section. This because of only one Mo/Mo FFDM machine was included in this thesis. Accordingly, more research is required to understand the impact of FFDM machines with Mo/Mo target/filter combination.

The relationship between sternum bone marrow dose and MGD, mAs and HVL using Spearman's rho correlation (**Table (6-5)** on page 149) demonstrates that there is a weak and non-statistically significant positive correlation between sternum bone marrow dose and both MGD and HVL ($r < 0.5$, $p > 0.05$). However, there is a strong and significant positive correction with mAs ($r = 0.709$, $p = 0.002$). The sternum bone marrow radiation dose-mAs relationship was also investigated by Hatziioannou et al. (2000) who reported that the measured sternum bone marrow dose inside a Lucite phantom is directly related to mAs. A further analysis of this relationship by backward regression modelling (**Table (6-6)** on page 150) demonstrates that 73% (regression R^2) of sternum bone marrow variability can be predicted by both MGD and mAs where 1 μGy reduction in sternum bone marrow dose can be achieved either by 0.6% reduction in MGD (μGy) or by 11.4% reduction in mAs. The standard error of estimate for this regression model was 3.444 μGy (18.06 %). In summary, the sternum bone marrow receives the highest radiation dose of all bone marrow locations due to its close proximity to the examined breast. Also, similar to the examined breast, the sternum bone marrow is related to target/filter combination and mAs.

The bone marrow of the ribs received the third highest bone marrow dose after sternum and clavicles bone marrow; see **Figure (6-3)** on page 144. It was 3.57 (2.87 – 4.27) µGy (mean with 95% CI) and this was 0.175 ± 0.053% (mean ± 1SD) of the examined breast MGD. This measured dose was comparable with previously estimated values by Sechopoulos et al. (2008) using Monte Carlo simulation. Sechopoulos et al. (2008) found that the radiation dose within the bone marrow of the ribs for Rh/Rh target/filter combination with 30 kV tube voltage is 0.14% of examined breast dose for CC projection and 0.17% for MLO projection. With regard to the effect of target/filter combination on rib bone marrow dose, both Rh/Rh and Mo/Mo combinations resulted in approximately the same rib bone marrow dose (3.03 ± 0.69 and 3.23 µGy, respectively) which was the lowest dose. However, the W/Ag combination caused the highest rib bone marrow dose (5.64 µGy); see **Figure (6-6)** on page 147.

Statistical evaluation of the relationship between the ribs bone marrow radiation dose and MGD, mAs and HVL (**Table (6-5)** on page 149) demonstrates that there is a statistically significant and strong positive correlation ($r > 0.5$, $p < 0.05$) between ribs bone marrow dose and MGD and mAs; a very weak / negligible correlation exists between ribs bone marrow dose and HVL ($r = 0.073$). The additional evaluation of these relationships by regression modelling shows that the relationship coefficients for MGD and mAs were 0.002 and 0.019, respectively, per 1 µGy ribs bone marrow dose where 58% (regression R^2) of ribs bone marrow dose variations attributed to MGD and mAs variations; see **Table (6-6)** page 150. In summary, the rib bone marrow radiation dose was high, compared to other organ doses, because of its proximity to the primary beam. For the ribs, the bone marrow dose is dependent on target/filter combination (Rh/Rh results in the lowest ribs bone marrow dose) and mAs; it can be predicted by MGD values.

7.3.2.3 Thyroid Radiation Dose

Exposing the phantom to a complete screening exposures shows that the thyroid is one of the organs which receives a relatively high radiation dose - 9.45 (7.83 – 11.08) µGy (mean with 95% CI). On average for the 16 FFDM machines, thyroid dose was the third highest radiation dose after 'breast tissues' (including examined and contralateral breast) and sternum bone marrow (**Figure (6-3)** on page 144) and constitutes 0.467 ± 0.133 % (mean ± 1SD) of

examined breast MGD; see **Table (6-4)** on page 145. However, for seven FFDM machines (FFDM machines 1 to 4, 7, 15, and 16) the clavicular bone marrow dose was higher than that of thyroid dose; see **(Appendix A)**. The thyroid dose measured in this thesis was approximately 10 times that estimated by Sechopoulos and Hendrick (2012) who used Monte Carlo simulations (0.467% compared to 0.045% of MGD). Again, it is possible that the simplified organ geometry used in Monte Carlo simulation could be the cause of this underestimation (Tootell et al., 2014). However, the estimated thyroid dose from measured skin radiation dose overlying women's thyroid during screening mammography by Whelan, McLean, and Poulos (1999) was approximately 40 µGy which is 4 times the thyroid dose measured in this thesis (9.45 µGy). In their calculations Whelan et al. (1999) considered the thyroid dose to be 10 % of skin dose. This percent could be the source of error in their calculations (estimated thyroid radiation dose), as 10% was a mathematical assumption.

The statistical analysis investigating the factors affecting the thyroid radiation dose shows that thyroid dose is related to target/filter combination, MGD, mAs and HVL. The highest thyroid dose was recorded for FFDM machines which used W/Rh 11.31 ± 4.70 µGy (mean ± 1SD), while the lowest recorded thyroid dose was for Rh/Rh combination 8.64 ± 2.42 µGy (mean ± 1SD); see **Figure (6-6)** on page 147. The lower Rh/Rh thyroid radiation dose compared with other target/filter combinations could be due to the low exposure factors required with the hard beam of Rh/Rh target/filter combination. A statistically significant strong positive correlation has been shown between thyroid dose and each of MGD ($r = 0.688$, $p = 0.003$) and mAs ($r = 0.771$, $p = 0.000$); see **Table (6-5)** on page 149. Although the thyroid dose was approximately not correlated with HVL ($r = 0.085$), the backward regression model was significant and with higher regression R^2 (83%) when all the predictors (MGD, mAs, and HVL) were included; see **Table (6-6)** on page 150. Using this regression model, a 1 µGy reduction in thyroid radiation dose can be achieved by decreasing either MGD (0.4%) or mAs (6.3%). However, 10.569 times increment in HVL is required to reduce the thyroid dose by 1 µGy. This thyroid dose-mAs relationship is approximately consistent with that previously published work by Hatziioannou et al. (2000) who reported that 1 µGy thyroid radiation dose increment results from 0.10 ± 0.02 mAs. Also, Whelan et al. (1999) found that the thyroid radiation dose during mammography correlates significantly to mAs.

In summary, the thyroid radiation dose from screening mammography exposures tends to be high compared to the body tissues and organs. Thyroid dose is related to target/filter combination and mAs. Since a harder beam is produced by Rh/Rh target/filter combination, lower exposure factors will be required resulting in a lower thyroid dose. Overall the thyroid dose can be predicted by MGD; higher MGD is associated with higher thyroid radiation dose.

7.3.2.4 Lung Radiation Dose

Lung tissue is radiosensitive with a 0.12 tissue weighting factor (ICRP, 2007). For the 16 FFDM machines the mean (95% CI) radiation dose of lung tissue from exposures of a single screening event (**Figure (6-3)** on page 144) was 3.06 (2.50 – 3.62) µGy with a minimum of 2.04 µGy (FFDM machine 6) and a maximum of 5.66 µGy (FFDM machine 3). This lung radiation dose (0.151 ± 0.046 % of MGD) is comparable with that estimated for film-screen mammography by Leidens, Goes, and Nicolluci (2013) (0.14% of MGD) who used PENELOPE Monte Carlo simulation. However, a lower estimated lung radiation dose (approximately 0.07% of MGD) has been reported by Sechopoulos et al. (2008). The underestimated lung tissue dose by Sechopoulos et al. (2008) could be due to two reasons, namely, it represents the dose to the ipsilateral lung only and the mathematical phantom limitations as mentioned earlier in section 7.3.2.2.

Different lung tissue radiation doses have been recorded for different target/filter combinations (**Figure (6-6)** on page 147); the highest dose resulted from the use of W/Ag (4.43 µGy) and both Rh/Rh and Mo/Mo caused approximately equal lung tissue dose (2.66 ± 0.56 µGy and 2.67 µGy, respectively) which was the lowest lung tissue radiation dose. In general since the Mo/Mo target/filter combination produces the least hardening beam, the use of Mo/Mo requires higher exposure factors and will result in higher organ doses. However, the use of only one Mo/Mo FFDM machine in this thesis adds a limitation to the generalisability of the Mo/Mo target/filter combination results. The effect of MGD, mAs and HVL on lung radiation dose was investigated by using Spearman's rho correlation (**Table (6-5)** on page 149) for non-parametric data. Both MGD and mAs significantly ($p < 0.05$) affect the lung dose, while the HVL was not significant ($p > 0.05$). The effect magnitude evaluation by backward regression modelling (**Table (6-6)** on page 150) demonstrates that 49%

(regression R^2) of lung dose variation is attributed to mAs variation where lung dose is directly related to mAs with a factor of 1 µGy per 2% mAs.

In summary, lung tissue is radio-sensitive and receives several micro Grays of radiation from screening mammography exposures. This radiation dose is related to X-ray tube target/filter combination, where Rh/Rh resulted in the lowest lung tissue dose, mAs and examined breast MGD. MGD can considered a good indicator for the prediction of lung tissue radiation dose.

7.3.2.5 Salivary Glands Radiation Dose

Salivary glands are a relatively low radio-sensitive tissue with 0.01 tissue weighting factor (ICRP, 2007). They received 0.139 ± 0.048 % (mean ± 1SD) of MGD during screening exposures (**Table (6-4)** on page 145) which is 2.79 (2.29 - 3.29) µGy (mean with 95% CI); see **Figure (6-3)** on page 144. The hardest beam (produced by Rh/Rh target/filter combination) caused the lowest salivary glands radiation dose (2.66 ± 0.85 µGy), while all other combinations (Mo/Mo, W/Rh, and W/Ag) resulted in similar salivary glands doses; the values were 2.89, 3.00 ± 1.43, and 3.15, respectively; see **Figure (6-6)** on page 147. The low salivary glands radiation dose of Rh/Rh target/filter combinations is because lower exposure factors are sufficient for use with harder x-ray beam associated with Rh/Rh.

Although the Spearman's rho correlation (**Table (6-5)** on page 149) demonstrates that the relationship between salivary glands dose and MGD, mAs and HVL was not statistically significant, backward regression modelling (**Table (6-6)** on page 150) can significantly predict 30% (regression R^2) of salivary gland dose variability by mAs. Overall, as with radiation dose to other body tissues, the radiation dose to salivary glands is dependent on both target/filter combination and mAs. Rh/Rh resulted in the lowest salivary gland dose due to its harder x-ray beam.

7.3.2.6 Thymus Radiation Dose

Screening mammography exposures resulted in 2.43 (1.77 – 3.08) µGy (mean with 95% CI) radiation dose to thymus; see **Figure (6-3)** on page 144. This dose is equivalent to 0.119 ± 0.058 % (mean ± 1SD) of MGD; see **Table (6-4)** on page 145. The estimation of thymus radiation dose by Sechopoulos et al. (2008) using Monte Carlo simulation showed that it was 0.07% and 0.04% of MGD for CC and MLO projections, respectively. This estimated dose is

comparable with the measured dose in this thesis because within this thesis the measured thymus dose was for complete screening exposures (CC and MLO projections for each breast), while in Sechopoulos et al. (2008) the estimated dose was from one breast exposures. According to Sechopoulos et al. (2008), the estimated thymus radiation dose from Rh/Rh target/filter combination was higher than that from Mo/Mo combination. However, the findings of this thesis shows that the Rh/Rh combination results in lowest thymus radiation dose (1.88 ± 0.99 µGy) and the highest one resulted from W/Rh (3.66 ± 1.23 µGy); see **Figure (6-6)** on page 147. This difference in thymus radiation dose in related to different target/filter combinations could be attributed to Sechopoulos et al. (2008) using the same number of monoenergitc X-ray photons (mAs) for all target/filter combinations. However, in this thesis the exposure factors were automatically selected by the AEC as would be the case in routine clinical practice. In general, a lower mAs was selected for harder beam making the thymus dose the lowest for the Rh/Rh target/filter combination.

Thymus radiation dose showed a statistically significant strong positive correlation ($r = 0.818$, $p = 0.000$) to mAs but it correlated weakly ($r < 0.5$, $p > 0.05$) to MGD or HVL; see **Table (6-5)** on page 149. Further analysis of this relationship by backward regression modelling (**Table (6-6),** page 150) shows that 83% (regression R^2) of thymus radiation dose variation can be predicted by mAs with a factor of 1 µGy thymus dose per 3% mAs. In summary, the radiation dose to thymus is mainly related to target/filter combination and mAs.

7.3.2.7 Brain Radiation Dose

Brain radiation dose from screening exposures varies widely between the FFDM machines. It ranged between zero and 4.82 µGy with a mean (95% CI) of 0.91 (0.26 – 1.56) µGy; see **Figure (6-3)** on page 144. X-ray tube target/filter combination tends to be of negligible effect on brain radiation dose. This is evidenced by the large SDs of brain radiation dose for each of the target/filter combinations; see **Figure (6-6)** on page 147. The brain dose for different combinations were 0.12 ± 0.15 µGy for W/Rh, 0.23 µGy for W/Ag, 1.26 ± 1.41 µGy for Rh/Rh, and 1.32 µGy for Mo/Mo. There was no significant correlation ($p > 0.05$) between brain radiation dose and MGD, mAs and HVL; see **Table (6-5)** on page 149. Consequently, the backward regression modelling (**Table (6-6)**, page 150) was not significantly better than

expressing mean value when predicting the brain radiation dose. In conclusion, the radiation dose to brain cannot be attributed to any of the factors explored in this thesis; it might be attributed to the FFDM machine design and/or the leakage radiation from the X-ray tube.

7.3.2.8 Liver Radiation Dose

Liver radiation dose constitutes 0.034 ± 0.013 % (mean ± 1SD) of the examined breast MGD; see **Table (6-4)** on page 145. The mean liver dose (95% CI) for the 16 FFDM machines was 0.69 (0.54 – 0.84) µGy; see **Figure (6-3)** on page 144. The analysis of liver radiation dose of different target/filter combinations (**Figure (6-6),** page 147) shows that W/Ag causes the highest liver radiation dose (1.21 µGy), while the lowest liver dose results from Mo/Mo (0.50 µGy). The liver radiation dose from the other two combinations were 0.77 ± 0.43 µGy and 0.62 ± 0.19 µGy for W/Rh and Rh/Rh combinations, respectively. Although the effect of target/filter combination on liver radiation dose is not consistent with that of other body organs, the liver dose difference for different target/filter combinations was small. This variation can be attributed (imputed) to the number of FFDM machines of different target/filter combinations. MGD, mAs and HVL are not good predictors for liver radiation dose. This was indicated by both correlation analysis (**Table (6-5),** page 149), which was weak ($r < 0.5$) and not statistically significant ($p > 0.05$) for all predictors, and backward regression modelling (**Table (6-6),** page 150), which was also not significant. In summary, the liver radiation dose cannot be explained by the factors evaluated in this thesis. Accordingly, more research is required to investigate the factors which effect liver radiation dose during screening mammography.

7.3.2.9 Stomach Radiation Dose

Organ dose data demonstrate that the stomach radiation dose was 0.42 (0.31 – 0.53) µGy (mean with 95% CI); see **Figure (6-3)** on page 144. This radiation dose represents 0.021 ± 0.009 % (mean ± 1SD) of MGD; see **Table (6-4)** on page 145. Both Rh/Rh and Mo/Mo target/filter combinations recorded equal stomach radiation dose (0.36 µGy), which was lower than that of the other two combinations, with a SD for Rh/Rh of 0.13 µGy. On the other hand, the highest stomach dose resulted when using W/Ag (0.68 µGy); see **Figure (6-6)** on page 147. This is consistent with radiation dose to other body tissues where the Rh/Rh resulted in the lowest dose because lower exposure factors are required when a harder beam

is used. With regard to the stomach dose from Mo/Mo target/filter combination, it cannot be generalised easily because it is based on measurements from a single FFDM machine. Spearman's rho correlation (**Table (6-5),** page 149) and backward regression modelling (**Table (6-6),** page 150) shows that the stomach radiation dose is independent on MGD, mAs and HVL.

7.3.2.10 Heart Radiation Dose

Heart radiation dose from mammography was previously estimated by Leidens et al. (2013) and Sechopoulos et al. (2008) using Monte Carlo simulation. Leidens et al. (2013) reported that the heart receives 0.033% of the MGD. However, Sechopoulos et al. (2008) documented the heart radiation dose for each mammographic projection separately. For CC projection the estimated dose was 0.05% of MGD, while for MLO it was 0.035% of MGD (Sechopoulos et al., 2008). These estimated heart radiation doses are slightly more than the measured heart radiation dose in this thesis which was 0.020 ± 0.012% (mean ± 1SD) of MGD (0.39 [0.27 – 0.51] µGy, mean [95% CI]); see **Table (6-4)** on page 145. In the previous studies, by Leidens et al. (2013) and Sechopoulos et al. (2008), only one type of FFDM machine was simulated. However, in this thesis a wide range of FFDM machines were included. The lower heart radiation dose could be a consequence of including a wide range of FFDM machines.

Unlike Sechopoulos et al. (2008), who reported that the Rh/Rh resulted in a heart radiation dose higher than Mo/Mo target/filter combination, this thesis demonstrates that the Rh/Rh combination results in the lowest heart radiation dose 0.34 ± 0.19 µGy (mean ± 1SD). The highest radiation dose resulted from W/Ag (0.58 µGy); see **Figure (6-6)** on page 147. This difference, between the previously published work and this thesis, was because Sechopoulos et al. (2008) calculated the organs dose of different target/filter combinations using same mAs. However, in this thesis the mAs was automatically selected by the AEC which compromises the mAs and beam hardening. Similar to stomach radiation dose (section 7.3.2.9), heart radiation dose was not related to MGD, mAs or HVL. This is proved by both correlation statistical analysis and regression modelling (**Table (6-5)** on page 149 and **Table (6-6)** on page 150, respectively). In summary, the main factor affecting the heart radiation dose during screening mammography exposures was the target/filter combination. The variability of heart radiation dose from different mammographic machines cannot be

predicted by any of factors studied in this thesis (i.e. MGD, mAs and HVL). Therefore, further research is required investigating the factors affecting heart radiation dose from screening mammography.

7.3.2.11 Oesophagus Radiation Dose

FFDM machine 6 demonstrated that the radiation dose to the oesophagus from screening mammography exposures is equal to zero. This means that either the oesophagus does not receive radiation dose or its radiation dose is below the sensitivity of the TLDs. On the other hand, FFDM machine 11 results in the highest oesophagus radiation dose (0.67 µGy). The mean (95% CI) oesophagus radiation dose for the 16 FFDM machines is 0.26 (0.14 - 0.37) µGy (**Figure (6-3),** page 144) and this constitutes 0.013 ± 0.012 % (mean ± 1SD) of MGD; see **Table (6-4)** on page 145. Target/filter combinations show comparable oesophagus radiation dose (approximately 0.27 µGy), except for the W/Rh target/filter combination which is 0.21 µGy; see **Figure (6-6)** on page 147. The correlation analysis between oesophagus radiation dose and MGD, mAs and HVL demonstrate that HVL has a relationship. The oesophagus radiation dose had a moderate negative ($r = -0.553$, $p = 0.026$) correlation with HVL; see **Table (6-5)** on page 149. However, this relationship was not significant by backward regression modelling; see **Table (6-6)** on page 150. In summary, the radiation dose to oesophagus was small and consequently its variation cannot be easily predicted by target/filter combination, MGD or mAs. However, there was an inverse relationship between oesophagus radiation dose and HVL - a harder beam (higher HVL) results in a lower oesophageal radiation dose.

7.3.2.12 Gall Bladder Radiation Dose

The mean (95% CI) gall bladder radiation dose for the 16 FFDM machines is 0.19 (0.10 – 0.27); see **Figure (6-3)** on page 144. Compared to MGD, this dose represents 0.009 ± 0.008% (mean ± 1SD); see **Table (6-4)** on page 145. In Sechopoulos' et al. (2008) work they considered any organ radiation dose less than 0.01 % MGD to be negligible. However, in this thesis any radiation dose less than 0.1 µGy is considered to be negligible. With regard to the effect of target/filter combination on gall bladder radiation dose (**Figure (6-6),** page 147), Mo/Mo resulted in the lowest radiation dose to gall bladder (0.04 µGy), while W/Ag resulted in the highest gall bladder radiation dose (0.68 µGy). The relationship between gall bladder

radiation dose and MGD, mAs and HVL by correlation statistics (**Table (6-5),** page 149) and regression modelling (**Table (6-6),** page 150) demonstrates that gall bladder radiation dose is not related to any of these factors. In summary, the radiation dose to gall bladder from screening mammography is very small and likely to be negligible. Since the gall bladder radiation dose is very small, its variability cannot be explained by any of the studied factors and should be the subject of future work.

7.3.2.13 Adrenals Radiation Dose

Radiation dose to the adrenals glands from screening mammography exposures is tend to be negligible. It is equal to the threshold of a negligible dose (0.10 [0.03 – 0.18] µGy, mean [95% CI]); see **Figure (6-3)** on page 144. By comparison with gall bladder radiation dose (section 7.3.2.12), W/Ag resulted in zero adrenal radiation dose and Mo/Mo resulted in the highest dose (0.51 µGy); see **Figure (6-6)** on page 147. Since one W/Ag and one Mo/Mo FFDM machines were included, these findings cannot be generalised. Spearman's rho correlation (**Table (6-5),** page 149) shows that adrenal radiation dose only correlates with HVL ($r = -0.714$, $p = 0.002$). This means that a harder beam (higher HVL) results in lower adrenal radiation dose. Similarly, further analysis of this relationship (between adrenals radiation dose and HVL) by backward regression modelling shows that 45% (regression R^2) of adrenals dose variability can be predicted by beam HVL and the relationship coefficient was 1 µGy adrenals dose per 1.192 HVL (mm Al); see **Table (6-6)** on page 150. In summary, the adrenals radiation dose is very small and inversely related to beam HVL.

7.3.3 Organs Radiation Dose Summary

During screening mammography, the contralateral breast tissue receives the second highest radiation dose after the examined breast. For all organs and tissues, including examined breast, the target/filter combination of the X-ray tube was major contributing factor affecting the radiation dose from screening mammography. Rh/Rh target/filter combination resulted in the lowest absorbed radiation dose for most body tissues as well as for the examined breast. The second important factor controlling organ radiation dose was X-ray tube current; higher mAs values unsurprisingly resulted in higher organ doses.

7.4 Effective Risk

As discussed earlier in section 4.3.3 (page 75) the effective risk refers to the number of radiation-induced cancers in all body tissues from exposure to ionising radiation. In this thesis it has been used to assess the radiation risk from screening mammography. Many advantages have been identified with the use of effective risk. Unlike MGD, which indicates the radiation risk to breast tissue only, effective risk includes the radiation risk to all body tissues and organs. Although the effective dose can comply with this requirement, its calculation is mainly dependent on tissue weighting factors which are averaged for gender and age. On the other hand, the effective risk calculation is dependent on lifetime attributable risks (LARs) which are available for each gender and from 0 to 80 years of age, stepping through five years intervals for ages under 20 and 10 years steps after 20 years old (BEIR VII report) (NAS, 2006). Screening mammography is a recurrent examination conducted at different ages (depending on screening programme recommendations). Tissue radio-sensitivity changes with age and this can be accounted for with effective risk calculations. This makes effective risk more suitable for radiation risk assessment of screening mammography. Another important point is that the data generated from effective risk calculations is likely to be more understandable by clients/patients (cancer incidence case per million) than the information as illustrated by MGD or effective dose (mGy or mSv). It is worth mentioning also that the calculation of effective risk is no more complicated than the effective dose calculation.

If the organ radiation dose is considered to be constant at different screening ages the effective risk would only relate to tissue radio-sensitivity change with age (LAR). For instance, although the radiation dose to thyroid is considered high (section 7.3.2.3), its contribution to effective risk of screening mammography would be small. This is true because the thyroid tissue radio-sensitivity decreases after the age of 40 years; see **Table (5-8)** on page 119.

Table (6-7) on page 152, **Table (6-8)** on page 153, and **Table (6-9)** on page 154 demonstrate the effective risk for clients aged 25-75 years (the possible age of screening mammography for high and normal risk clients). For the 16 FFDM machines, as the client age increases from 25 to 75 the mean (95% CI) effective risk decreases from 70.00 (64.88 - 75.12) to 0.75

(0.69 - 0.80) case/10^6, from 70.00 (64.88 - 75.12) to 1.68 (1.55 - 1.80) case/10^6, and from 88.07 (81.63 - 94.51) to 2.51 (2.32 - 2.69) case/10^6 for the three LAR extrapolation methods, respectively. The highest effective risk values were recorded for FFDM machine 7 which were 97.492 - 1.047 case/10^6, 97.492 - 2.340 case/10^6, and 122.662 - 3.499 case/10^6 (for the three LAR sets, respectively) for ages 25-75 years. However, the lowest effective risk values for the three LAR methods were for FFDM machine 11 which were 57.995 - 0.621 case/10^6, 57.995 - 1.390 case/10^6, and 72.964 - 2.080 case/10^6, respectively, for ages 25-75. These effective risk differences between the considered FFDM machines are mainly attributed to MGD variations of the FFDM machines which ranged from 1.730 mGy to 2.431 mGy. Therefore, more consideration should be given to target/filter combination to reduce MGD. In spite of these differences amongst the different FFDM machines, the statistical analysis shows that for the first and second LAR extrapolation methods there was non-significant difference between these machines (Kruskal-Wallis test, $p > 0.05$), while the same test (Kruskal-Wallis test) shows that effective risk values of the 16 FFDM machines was significantly different ($p = 0.044$) for the third extrapolation method.

Total effective risk of screening mammography refers to the total risk of radiation-induced cancer during the clients' lifetime due to *the complete screening journey*. The total effective risk of any screening programme is related to commencement/cessation ages and frequency of screening. The worldwide screening mammography recommendations can be classified into two categories, the first category includes the recommendations for average breast cancer risk women (**Table (3-4),** page 59), and the second category includes those recommended for high breast cancer risk clients (**Table (3-5),** page 60); highlighted programmes in **Table (6-10)** on page 156. Usually the high risk women are invited for earlier and more frequent screening mammography resulting in additional risk of radiation-induced cancer; see **Tables (6-10)** on page 156, **(6-11)** on page 157, and **(6-12)** on page 158 for the three LAR methods, respectively.

The statistical analysis of the total effective risk of worldwide screening programmes shows significant differences amongst these programmes with regard to their total effective risk (1-Way ANOVA test, $p < 0.05$ for the three LAR methods). For the 16 FFDM machines, the lowest mean (95% CI) total effective risk resulted from Maltese screening mammography

programme. It was 42.21 (39.12 - 45.30) case/10^6 for the best lines of fit extrapolation method, 43.28 (40.11 - 46.44) case/10^6 for linear relationship approach, and 57.67 (53.46 - 61.89) case/10^6 for step approach. In contrast, the highest total effective risk for average risk women resulted from United States screening programmes recommended by ACS, ACR, and NCCN. These figures were 372.42 (345.18 - 399.67) case/10^6, 391.55 (362.91 - 420.19) case/10^6, and 513.12 (475.59 - 550.65) case/10^6 for the three LAR methods. These differences in total effective risk, of considered screening programmes, are attributed to their different recommendations wherein Maltese programme invite the women 50-60 years old for triennial screening, while the ACS, ACR, and NCCN invite the women aged 40-75 years for annual screening. According to risk classification by Wall et al. (2006) (**Table (4-1)**, page 69), the radiation risk of screening mammography is ranged from being very low risk (≤ 100 cases/10^6) to low risk (≤ 1000 cases/10^6). However, the radiation risk from some screening programmes designed for high risk women may exceed the threshold of low radiation risk (> 1000 cases/10^6), see the highlighted section in **Tables (6-10)** on page 156, **(6-11)** on page 157, and **(6-12)** on page 158 for the three LAR methods, respectively.

Not all worldwide screening programmes have published recommendations for high risk women because some programmes consider the high risk women as special cases that should not be included in a screening programme (CancerAustralia, 2014). Some programmes recommend breast screening by other imaging modalities (i.e MRI and/or ultrasonography) along with mammography (NHSBSP, 2013b). The National Cancer Comprehensive Network (NCCN) recommendations, in the United States, resulted in the highest total effective risk (1099.67 [1019.25 - 1180.09] case/10^6, 1121.36 [1039.36 - 1203.36] case/10^6, 1472.73 [1365.04 - 1580.42] case/10^6, for the three LAR extrapolation methods) because they have recommended annual screening mammography commences at the age of 25 years old. However, the high risk women recommendations of the British and Canadian programmes resulted in lower total effective risk than that of average risk women in the United States (ACS, ACR, and NCCN); see **Tables (6-10)** on page 156, **(6-11)** on page 157, and **(6-12)** on page 158 for the three LAR methods.

Compared to previous studies, which considered the total LAR of cancer incidence in breast tissue only, the calculated total effective risk in this thesis, which includes the risk of

radiation-induced cancer in all body tissues, tends to be comparable because the MGD contribution in total effective risk is up to 98%. For instance, in work by Yaffe and Mainprize (2011) the total risk of radiation-induced breast cancer from annual screening mammography between 40 and 49 years was found to be 590 case/10^6 for 3.7 mGy MGD. In this thesis for 2.019 (1.871-2.166) mGy MGD the total effective risk of the same screening regimen found there to be 231.89 (214.94 - 248.85), 224.21 (207.82 - 240.61), 289.69 (268.51 - 310.87) case/10^6 (mean with 95% CI) for the three LAR method.

Similarly for 3.7 mGy MGD, Hendrick (2010) found that the total incident of breast cancer due to annual screening mammography between 25 - 80 years was 2040 case/10^6. In this thesis for 2.019 (1.871-2.166) mGy MGD, the calculated total effective risk for annual screening mammography between 25 -75 years was 1099.67 (1019.25 - 1180.09), 1121.36 (1039.36 - 1203.36), and 1472.73 (1365.04 - 1580.42) case/10^6 for the three LAR extrapolation methods.

Recently, Warren, Dance, and Young (2016) evaluated the total risk, during a female's lifetime, of radiation-induced breast cancer from the UK screening recommendations and found that it ranges between 30.7 and 61.2 case/10^6/mGy of MGD. This is consistent with the figures in this thesis which were 70.77 (65.59 - 75.95), 77.79 (72.10 - 83.48), and 108.41 (100.48 - 116.34) case/10^6 for the three LAR methods and MGD of 2.019 (1.871-2.166) mGy (mean with 95% CI).

With regard to factors affecting the total effective risk, statistical analysis from the 22 different worldwide screening recommendations identified in this thesis (**Table (3-4)** on page 59 and **Table (3-5)** on page 60) shows that there is a strong correlation ($r > 0.5$, $p < 0.05$) between total effective risk and screening commencement age, cessation age of screening, time interval between screens and number of screens; see **Table (6-13)** on page 160. These correlations are positive with cessation age of screening and number of screens, and negative with commencement age of screening and time interval between screens. This means that the total effective risk increases as cessation age of screening and number of screening increase, while it reduces as commencement age of screening and time interval between screens increase. A further analysis of these relationships by backward regression modelling demonstrates that the cessation age of screening, time interval between screens and number

of screens are sufficient to significantly predict 91% (regression R^2), for best fit lines method, and 92%, for the other two LAR methods, of total effective risk variability; see **Table (6-14)** on page 161.

The use of the third LAR extrapolation method (step approach) resulted in the highest calculated total effective risk. The figures calculated using the two alternative methods are similar but the first LAR method resulted in the lowest total effective risk; see **Figure (6-7)** on page 159. A minor difference in the ranking of worldwide screening programmes, in related to their resultant total effective risk, can be seen amongst the three LAR methods (e.g. the UK and Chinese programmes for average risk women); see **Tables (6-10)** on page 156, **(6-11)** on page 157, and **(6-12)** on page 158 for the three methods. In general, the linear relationship method between the decades gives the best relationship with previous published work (Li et al., 2011).

7.5 Effective Risk Modelling

The main purpose of the effective risk modelling is to establish a method that can be easily used in daily practice in order to obtain the total effective risk of any screening regimen from screening commencement/cessation ages and screening frequency. This is particularly useful in the discussion of screening justification (benefits versus harms) with clients, especially those clients invited for early and more frequent screening due to their high breast cancer risk. Usually statistical regression is used to investigate the effect of one or more predictors on outcome variable and/or to predict outcome variable value for each set of predictors.

According to Field (2013), the minimum sample size required to establish a good regression model suitable for prediction is 10-15 data cases per each predictors; but Field (2013) reported that as a general rule of thumb a larger sample size would result in a better regression model. This means that the number of worldwide screening recommendations (22 cases) is not sufficient to generate a good regression model. Accordingly, 274 screening regimens have been proposed from the experimental data in this thesis to generate a suitably powered regression model. The statistical analysis of the new regression model (with sample size of 274 cases) shows different results from the regression model generated with small sample size (22 cases); see **Table (6-15)** on page 162. Strong correlations ($r > 0.5$) exist between total effective risk and commencement age of screening and number of screens,

while the correlation was weak between total effective risk and cessation age of screening and time interval between screens. This is consistent with Field's (2013) opinion about the effect of sample size on regression modelling. For the 274 screening scenarios, backward regression modelling (**Table (6-16),** page 162) can predict more than 85% of total effective risk variability by commencement/cessation ages of screening and number of screens. However, the large standard errors (93.249, 91.127, and 117.411 case/10^6 for the three LAR methods, respectively) for these regression models make them adequate for the prediction of total effective risk, although not exact.

Since the majority of worldwide screening programmes recommend a screening cessation age of between 70 and 75 years (**Table (3-4)** on page 59 and **Table (3-5)** on page 60) and at these ages (after 70 years) most tissue types become highly radio-resistant, the cessation age has a very small effect on total effective risk. Accordingly, if we consider the cessation age to be constant at 75, there would be only two factors affecting the total effective risk, namely commencement age of screening and screening frequency. In this case it becomes possible to graphically represent the total effective risk against screening commencement age for each screening frequency; see **Figures (6-8)** on page 163, **(6-9)** on page 164 **and (6-10)** on page 165 for the three LAR methods. Each of these figures contains three relationship lines - one for each screening frequency (annual, biennial, and triennial). These graphs might be easily used by practitioners and clients to obtain the total effective risk for any screening commencement age (25 - 74 years) and for each of the screening frequency. However, the main limitation of these graphs is that they are based on an average effective risk value for the sixteen FFDM machines. In other words, the interpolated data from these graphs are for the average MGD of the 16 FFDM machines which was 2.019 (1.871-2.166) mGy, mean (95% CI).

To overcome the above limitation a relationship has been established between MGD and total effective risk, for the 16 FFDM machines, for each screening scenario of specific screening commencement age and frequency (**Appendix D**) generating a set of conversion factors (case/10^6/μGy of MGD) which can be used to convert the initial MGD value from a client/woman to her total predicted effective risk from her lifetime FFDM screening; see **Table (6-17)** on page 167, **Table (6-18)** on page 168 and **Table (6-19)** on page 169 for the

three LAR extrapolation methods. These conversion factors, which are MGD percentages, have been plotted against the screening commencement age for each screening frequency to generate relationship graphs that can be used to obtain the total effective risk for a specific screening scenario (commencement age and frequency) in relation to the client's MGD; see **Figures (6-11)** on page 170, **(6-12)** on page 171, **and (6-13)** on page 172 for each of the LAR exploration methods, respectively. This effective risk model is the final model and should be easily used by practitioners and clients to obtain the total effective risk taking into account MGD variations of different FFDM machines for same breast thickness (53 mm) and composition (29% glandularity).

7.6 Contralateral Breast Shield Effect

As mentioned earlier in section 7.3.2.1, the contralateral breast received the second highest radiation dose after the examined breast; see **Figure (6-3)** on page 144. For the 16 FFDM machines, the mean ± 1SD contribution of contralateral breast dose expressed as effective dose percent is 1.391 ± 0.332 %, while 0.439 ± 0.119 % was from the contribution of all other body tissues except the examined breast; see **Table (6-20)** on page 173. Accordingly, the theoretical investigation of contralateral breast shield, by considering the contralateral breast dose being set to zero, leads to a 1.38 ± 0.34% (mean ± 1SD) reduction in the effective dose; **see Table (5-10)** on page 132. Effective risk reduction is age dependent, it decreases by 1.39 ± 0.33 % for women aged 25 - 58 and this percent reduces to 1.33 ± 0.29 % at 74. Then at 75 years of age it increases to 1.37 ± 0.38 %. These figures were for the first LAR extrapolation method (best fit line method). Similar values have been recorded for the other two LAR extrapolation methods; see **Table (5-11**) on page 133. These age-dependent differences are due to the different patterns of tissue radio-sensitivity (LAR) as they change with age.

The effect of a contralateral breast shield was experimentally investigated for 4 FFDM machines, which were selected according to their calculated effective risk as previously discussed in section 5.9.4 (page 136). For the 4 FFDM machines (FFDM machines 2, 8, 10, and 11) included in the shield intervention study, it was found that the contralateral breast shield can reduce the contralateral breast dose by more than 95%. The figures in µGy were (35.20 reduced to 1.93), (41.40 reduced to 0.01), (22.85 reduced to 1.24), and (22.76 reduced

to 1.66), respectively; see **Table (6-21)** on page 174. Also, a small reduction has been identified in sternum bone marrow dose due to the use of contralateral breast shield. Overall, the use of a contralateral breast shield during mammography is in itself novel work within this thesis. At the time of writing no previous work has been published investigating the effect of contralateral breast shield on breast radiation dose.

The effect of a contralateral breast shield on total effective risk of worldwide screening programme demonstrates that the shield can significantly (Wilcoxon test, $p < 0.05$) reduce the total effective risk of worldwide screening programmes and the reduction percent is independent of LAR extrapolation method (i.e. same reduction percentages have been recorded for the three LAR methods of same FFDM machine). However, the reduction percent in total effective risk is different for the 4 FFDM machines. It ranged between approximately 0.95 % (for machine 10) to approximately 1.44 % (for machine 2) with minor differences amongst different worldwide screening programmes; see **Tables (6-22)** on page 175, **(6-23)** on page 176, and **(6-24)** on page 177 for the three LAR extrapolation methods. Therefore, the contralateral breast shield is recommended to reduce the radiation dose to contralateral breast. However, more research is required to evaluate the effect of contralateral breast shield on examined breast MGD.

7.7 Limitations, Future Work, and Recommendations

The main point that could be considered as a limitation that the use of single human body dosimetry phantom together with two standard sized breast phantoms. This means that the data used in this thesis is applicable to an 'average women with average sized breasts'. Future work could use human body phantoms representing different sizes along with different breast phantoms for a range of different thicknesses and densities; see (**Appendix F**). In doing this data can be generated to predict the risk of radiation-induced cancer from screening mammography for a broader range of clients which have different breast sizes and glandularities and different body sizes.

The other limitation is that according to Alonzo-Proulx, Jong, and Yaffe (2012), due to the aging process, the breast density decreases by approximately 2% per year between 35 and 75, which will result in a continuous reduction in the required mAs and hence the MGD will decrease with age (Beckett & Kotre, 2000). However, more research is required to confirm

and further evaluate this breast density reduction magnitude. This breast tissue change was not included in generated total effective risk data in this thesis because the same MGD has been used for entire screening age range (25 - 75). Again this can be addressed by using a series of breast phantoms with different densities to simulate the breasts of different client's ages.

Recently, glandular tissue distribution within the breast was reported by Geeraert, Klausz, Muller, Bloch, and Bosmans (2015) as one of the factors affecting the MGD. Geeraert et al. (2015) found that MGD was different for breast phantoms, simulated within Monte Carlo software, with identical glandularity and thickness but with different glandular tissue distribution. However, the effect of glandular tissue distribution on MGD is not considered in this thesis because more investigations are required to improve this effect and determine its magnitude.

With regard to errors associated with data derived in this thesis, two main sources can be identified, namely, dosimeter reading errors and the LAR extrapolation process. The use of more accurate dosimeters will help to improve data accuracy. Although the linear relation between decade LAR values is recommended in previous works (Li et al., 2011; Warren et al., 2016), the use of the three methods (best-fit lines, linear relationship, and step approach) gives an idea of the effect of LAR extrapolation process.

Since only one FFDM machine has been included from each Mo/Mo and W/Ag target/filter combinations, there was a concern about the data generalisations of these two target/filter combinations. Accordingly, more measurements are required for FFDM machines using these two combinations.

With regard to the effect of contralateral breast shield, further work is required to investigate the effect of the shield on examined breast MGD because the back scatter from the shield could increase the MGD.

All in all, effective risk is likely to be a useful radiation protection quantity which may have value for radiation risk assessment and conveying this information to screening clients. Research should be conducted with clinicians and clients to determine what value it might have in practice. The method proposed in this thesis, which takes into account all body

tissues/organs, should be adopted in practice; it could be used alongside other quantities such as effective dose or MGD. MGD and effective dose are not useful quantities to use when assessing risk for a population or an individual who is examined over a long time period, as is the case for screening mammography. When referring to client risk these quantities should be used with greater caution. Graphical presentation of total effective risk in relation to screening commencement age and MGD is an easy way to obtain the total effective risk of any screening regimen instantly without the need for complex and time consuming calculations. These graphs can be used either by practitioner or screening clients after having the first screening session when they can know their MGD to predict the radiation risk of whole screening journey. This is particularly useful to consider the radiation risk of early and more frequent screening which recommended for women with high breast cancer risk. The use of contralateral breast shield could be a useful procedure to minimise the unnecessary radiation dose to breast tissue during screening mammography.

Chapter Eight
Conclusions

8.1 Conclusions

In this thesis, a novel method has been established to assess the radiation risk from FFDM screening. Total effective risk during a woman's lifetime has been used to determine the risk of radiation-induced cancer. The effective risk calculation is based on an experimental approach of organ dose measurement, for average adult female's body size and average breast with 53 mm thickness and 29 % glandularity, with TLDs accommodated inside an ATOM dosimetry phantom. The main characteristic of this method is that it can include the radiation dose to all body tissues in addition to examined breast MGD. Another important feature of the novel method is that gender and age are considered, making the method suitable for the investigation of radiation-induced cancer from any screening practice which uses ionising radiation or from any recurrent X-ray examination at different ages. The use of graphical representation of total effective risk data enables the extrapolation of the total effective risk using screening commencement age, screening frequency and MGD which greatly related to target/filter combination (Rh/Rh results in lowest MGD). This is an easy and convenient way to determine the risk of radiation-induced cancer in daily practice rather than the use of complicated and time consuming calculations. The use of graphs has the added value of being more accurate than regression modelling because mathematical regression is based on data fitting and this has associated error, while the use of graphs is based on calculated data of different screening regimens.

The data generated from this method is not complicated and should be easily understood by clients, however, further work is needed to assess this and also its clinical utility. Compared to MGD and effective dose, which are expressed in the unit of mGy and mSv, the effective risk is expressed as the number of cancer cases per million and this is likely to be a very useful and less abstract concept which can be used to discuss screening mammography justification with clients, especially those classified as high risk breast cancer clients. Since tissue radio-sensitivity changes with age, the risk of radiation-induced cancer from screening mammography depends on LAR and organ dose. Sometimes, even though the organ dose

looks high, the risk of radiation-induced cancer is small because the tissues are more radio-resistant due to their age. This is especially true for screening mammography above 70 years old, making the screening cessation age of less effect on total effective risk compared with commencement age of screening.

For both effective dose and total effective risk, the MGD contribution is more than 98%, while all body tissues other than the examined breast contribute up to 2%. Therefore, for any screening programme the most important factors affecting the total effective risk are screening commencement age, screening frequency and MGD. Screening commencement age is the most important factor, for example effective risk of the four screening exposures (LCC, RCC, LMLO and RMLO) at 25 is more than double that at 40. Accordingly, significant differences have been found amongst worldwide screening programmes in relation to their total effective risk. The Maltese screening programme for average risk women results in the lowest total effective risk (42.21 [39.12 - 45.30], 43.28 [40.11 - 46.44], and 57.67 [53.46 - 61.89] case/10^6 for the three LAR methods), while the American screening programme for high risk women recommended by National Comprehensive Cancer Network (NCCN) results in the highest total effective risk (1099.67 [1019.25 - 1180.09], 1121.36 [1039.36 - 1203.36], and 1472.73 [1365.04 - 1580.42] case/10^6 for the three LAR methods). Although the effective risk differences amongst the 16 FFDM machines are not significant statistically, the MGD variation of different FFDM machines should be considered.

Contralateral breast radiation dose is the highest radiation dose after the examined breast and it constitutes approximately 1.5 % of the total effective risk. Data from this thesis demonstrates that the use of a contralateral breast shield can help to reduce the radiation dose received by the contralateral breast by over 95%. Further work should be undertaken to determine whether or not a contralateral breast shield has value within the clinical routine.

In addition to radiation dose, client's age is another critical factor affecting the risk of radiation-induced cancer from screening mammography. For instance, although the radiation dose received by thyroid is large, the decline of thyroid tissue radio-sensitivity at screening age, after the age of 40 means this dose is of minor effect on the total effective risk. Therefore, screening commencement age should be carefully chosen because younger tissues

are more radio-sensitive. The use of contralateral breast shield could be more important in this case, when younger clients are invited for screening.

Appendices

Appendix A: Measured organ doses for the sixteen FFDM machines.

Table (A-1) Lists organs radiation dose, other than breast, from one screening visit for FFDM machine 1.

Organ		Absorbed dose, µGy			
		Visit 1	Visit 2	Visit 3	Mean (sd)
Brain		2.31	1.11	0.54	1.32 (0.91)
Salivary glands		3.83	2.71	2.14	2.89 (0.86)
Thyroid		10.42	9.53	8.57	9.51 (0.92)
Oesophagus		0.34	0.22	0.25	0.27 (0.06)
Thymus		3.18	2.28	2.06	2.51 (0.59)
Heart		0.39	0.37	0.30	0.35 (0.05)
Lung		2.94	2.61	2.46	2.67 (0.25)
Liver		0.48	0.56	0.46	0.50 (0.06)
Gall bladder		0.05	0.05	0.03	0.04 (0.02)
Adrenal		0.48	0.99	0.07	0.51 (0.46)
Kidney		0.09	0.05	0.07	0.07 (0.02)
Spleen		0.03	0.03	0.02	0.03 (0.01)
Pancreas		0.00	0.00	0.00	0.00 (0.00)
Stomach		0.32	0.18	0.59	0.36 (0.21)
Intestine		0.00	0.00	0.00	0.00 (0.00)
Bone Marrow (BM)	Cranium (7.6%)*	1.55	1.54	1.44	1.51 (0.06)
	Mandibles (0.8%)*	3.83	2.71	2.14	2.89 (0.86)
	C-spine (3.9%)*	0.42	0.32	0.34	0.36 (0.05)
	Clavicles (0.8%)*	13.71	12.65	12.96	13.11 (0.54)
	Scapulae (2.8%)*	0.10	0.08	0.08	0.09 (0.01)
	Sternum (3.1%)*	18.09	17.38	16.02	17.16 (1.05)
	Ribs (16.1%)*	3.47	3.17	3.04	3.23 (0.22)
	T/L spine (28.4%)*	0.26	0.06	0.14	0.15 (0.10)
	Pelvis (27.4%)*	0.00	0.00	0.00	0.00 (0.00)
	Total BM dose	1.47	1.32	1.27	1.35 (0.10)
Urinary bladder		0.00	0.00	0.00	0.00 (0.00)
Uterus		0.00	0.00	0.00	0.00 (0.00)
Ovaries		0.00	0.00	0.00	0.00 (0.00)
Contralateral breast		25.94	28.71	25.10	26.58 (1.89)

*These percentages represent the portion of bone marrow (BM) in different locations. They were adapted from ICRP report 70 (1995).

Table (A-2) Lists organs radiation dose, other than breast, from one screening visit for FFDM machine 2.

Organ		Absorbed dose, µGy			
		Visit 1	Visit 2	Visit 3	Mean (sd)
Brain		1.47	0.04	0.00	0.50 (0.84)
Salivary glands		4.39	2.52	2.34	3.08 (1.14)
Thyroid		11.63	11.33	10.01	10.991(0.86)
Oesophagus		0.33	0.00	0.13	0.15 (0.16)
Thymus		3.58	3.01	3.13	3.24 (0.30)
Heart		0.43	0.13	0.44	0.33 (0.17)
Lung		3.08	3.01	3.07	3.05 (0.04)
Liver		0.54	0.42	0.48	0.48 (0.06)
Gall bladder		0.18	0.01	0.10	0.10 (0.09)
Adrenal		0.07	0.00	0.00	0.02 (0.04)
Kidney		0.05	0.00	0.04	0.03 (0.03)
Spleen		0.07	0.00	0.05	0.038 (0.03)
Pancreas		0.01	0.00	0.00	0.00 (0.00)
Stomach		0.28	0.18	0.27	0.24 (0.05)
Intestine		0.07	0.00	0.02	0.03 (0.04)
Bone Marrow (BM)	Cranium (7.6%)*	2.06	0.71	0.47	1.080 (0.86)
	Mandibles (0.8%)*	4.39	2.52	2.34	3.08 (1.14)
	C-spine (3.9%)*	0.69	0.01	0.00	0.24 (0.40)
	Clavicles (0.8%)*	15.61	14.92	14.00	14.84 (0.80)
	Scapulae (2.8%)*	0.26	0.02	0.00	0.09 (0.15)
	Sternum (3.1%)*	22.40	20.59	20.65	21.21 (1.03)
	Ribs (16.1%)*	3.73	3.66	3.52	3.64 (0.11)
	T/L spine (28.4%)*	0.08	0.00	0.00	0.03 (0.05)
	Pelvis (27.4%)*	0.00	0.00	0.00	0.00 (0.00)
	Total BM dose	1.67	1.42	1.37	1.49 (0.16)
Urinary bladder		0.00	0.00	0.00	0.00 (0.00)
Uterus		0.00	0.00	0.00	0.00 (0.00)
Ovaries		0.00	0.00	0.00	0.00 (0.00)
Contralateral breast		30.44	29.41	29.02	29.62 (0.73)

*These percentages represent the portion of bone marrow (BM) in different locations. They were adapted from ICRP report 70 (1995).

Table (A-3) Lists organs radiation dose, other than breast, from one screening visit for FFDM machine 3.

Organ		Absorbed dose (µGy)
Brain		0.03
Salivary glands		4.86
Thyroid		16.27
Oesophagus		0.56
Thymus		5.28
Heart		0.97
Lung		5.66
Liver		1.20
Gall bladder		0.30
Adrenal		0.10
Kidney		0.04
Spleen		0.10
Pancreas		0.02
Stomach		0.88
Intestine		0.17
Bone Marrow (BM)	Cranium (7.6%)*	0.92
	Mandibles (0.8%)*	4.86
	C-spine (3.9%)*	0.10
	Clavicles (0.8%)*	17.74
	Scapulae (2.8%)*	0.31
	Sternum (3.1%)*	28.27
	Ribs (16.1%)*	6.11
	T/L spine (28.4%)*	0.11
	Pelvis (27.4%)*	0.00
	Total BM dose	2.16
Urinary bladder		0.00
Uterus		0.00
Ovaries		0.00
Contralateral breast		47.66

*These percentages represent the portion of bone marrow (BM) in different locations. They were adapted from ICRP report 70 (1995).

Table (A-4) Lists organs radiation dose, other than breast, from one screening visit for FFDM machine 4.

Organ		Absorbed dose (µGy)
Brain		0.78
Salivary glands		4.01
Thyroid		14.46
Oesophagus		0.41
Thymus		4.04
Heart		0.55
Lung		4.06
Liver		0.94
Gall bladder		0.25
Adrenal		0.23
Kidney		0.04
Spleen		0.08
Pancreas		0.01
Stomach		0.47
Intestine		0.02
Bone Marrow (BM)	Cranium (7.6%)*	2.01
	Mandibles (0.8%)*	4.01
	C-spine (3.9%)*	0.51
	Clavicles (0.8%)*	19.52
	Scapulae (2.8%)*	0.22
	Sternum (3.1%)*	28.00
	Ribs (16.1%)*	4.70
	T/L spine (28.4%)*	0.06
	Pelvis (27.4%)*	0.00
	Total BM dose	2.01
Urinary bladder		0.00
Uterus		0.00
Ovaries		0.00
Contralateral breast		35.83

*These percentages represent the portion of bone marrow (BM) in different locations. They were adapted from ICRP report 70 (1995).

Table (A-5) Lists organs radiation dose, other than breast, from one screening visit for FFDM machine 5.

Organ		Absorbed dose (µGy)
Brain		0.63
Salivary glands		2.08
Thyroid		7.67
Oesophagus		0.65
Thymus		1.93
Heart		0.34
Lung		2.60
Liver		0.53
Gall bladder		0.16
Adrenal		0.07
Kidney		0.03
Spleen		0.06
Pancreas		0.00
Stomach		0.35
Intestine		0.00
Bone Marrow (BM)	Cranium (7.6%)*	1.03
	Mandibles (0.8%)*	2.08
	C-spine (3.9%)*	0.24
	Clavicles (0.8%)*	5.01
	Scapulae (2.8%)*	0.33
	Sternum (3.1%)*	13.09
	Ribs (16.1%)*	2.66
	T/L spine (28.4%)*	0.11
	Pelvis (27.4%)*	0.00
	Total BM dose	1.02
Urinary bladder		0.00
Uterus		0.00
Ovaries		0.00
Contralateral breast		24.60

*These percentages represent the portion of bone marrow (BM) in different locations. They were adapted from ICRP report 70 (1995).

Table (A-6) Lists organs radiation dose, other than breast, from one screening visit for FFDM machine 6.

Organ		Absorbed dose (µGy)
Brain		0.00
Salivary glands		1.44
Thyroid		6.93
Oesophagus		0.00
Thymus		0.84
Heart		0.01
Lung		2.04
Liver		0.44
Gall bladder		0.05
Adrenal		0.00
Kidney		0.00
Spleen		0.02
Pancreas		0.00
Stomach		0.23
Intestine		0.00
Bone Marrow (BM)	Cranium (7.6%)*	0.16
	Mandibles (0.8%)*	1.44
	C-spine (3.9%)*	0.00
	Clavicles (0.8%)*	4.42
	Scapulae (2.8%)*	0.00
	Sternum (3.1%)*	15.38
	Ribs (16.1%)*	2.42
	T/L spine (28.4%)*	0.00
	Pelvis (27.4%)*	0.00
	Total BM dose	0.93
Urinary bladder		0.00
Uterus		0.00
Ovaries		0.00
Contralateral breast		23.28

*These percentages represent the portion of bone marrow (BM) in different locations. They were adapted from ICRP report 70 (1995).

Table (A-7) Lists organs radiation dose, other than breast, from one screening visit for FFDM machine 7.

Organ		Absorbed dose (µGy)
Brain		0.00
Salivary glands		3.33
Thyroid		14.18
Oesophagus		0.04
Thymus		3.94
Heart		0.41
Lung		4.73
Liver		1.06
Gall bladder		0.15
Adrenal		0.00
Kidney		0.00
Spleen		0.01
Pancreas		0.00
Stomach		0.76
Intestine		0.00
Bone Marrow (BM)	Cranium (7.6%)*	0.54
	Mandibles (0.8%)*	3.33
	C-spine (3.9%)*	0.00
	Clavicles (0.8%)*	15.81
	Scapulae (2.8%)*	0.01
	Sternum (3.1%)*	32.50
	Ribs (16.1%)*	6.15
	T/L spine (28.4%)*	0.00
	Pelvis (27.4%)*	0.00
	Total BM dose	2.19
Urinary bladder		0.00
Uterus		0.00
Ovaries		0.00
Contralateral breast		44.41

*These percentages represent the portion of bone marrow (BM) in different locations. They were adapted from ICRP report 70 (1995).

Table (A-8) Lists organs radiation dose, other than breast, from one screening visit for FFDM machine 8.

Organ		Absorbed dose (µGy)
Brain		0.23
Salivary glands		3.15
Thyroid		10.07
Oesophagus		0.26
Thymus		2.90
Heart		0.58
Lung		4.43
Liver		1.21
Gall bladder		0.68
Adrenal		0.00
Kidney		0.11
Spleen		0.02
Pancreas		0.03
Stomach		0.68
Intestine		0.02
Bone Marrow (BM)	Cranium (7.6%)*	0.93
	Mandibles (0.8%)*	3.15
	C-spine (3.9%)*	0.00
	Clavicles (0.8%)*	8.88
	Scapulae (2.8%)*	0.24
	Sternum (3.1%)*	24.91
	Ribs (16.1%)*	5.64
	T/L spine (28.4%)*	0.00
	Pelvis (27.4%)*	0.00
	Total BM dose	1.85
Urinary bladder		0.00
Uterus		0.00
Ovaries		0.00
Contralateral breast		38.49

*These percentages represent the portion of bone marrow (BM) in different locations. They were adapted from ICRP report 70 (1995).

Table (A-9) Lists organs radiation dose, other than breast, from one screening visit for FFDM machine 9.

Organ		Absorbed dose (µGy)
Brain		1.71
Salivary glands		2.63
Thyroid		8.02
Oesophagus		0.22
Thymus		1.51
Heart		0.24
Lung		2.41
Liver		0.55
Gall bladder		0.24
Adrenal		0.12
Kidney		0.02
Spleen		0.08
Pancreas		0.08
Stomach		0.32
Intestine		0.02
Bone Marrow (BM)	Cranium (7.6%)*	2.57
	Mandibles (0.8%)*	2.63
	C-spine (3.9%)*	0.36
	Clavicles (0.8%)*	5.52
	Scapulae (2.8%)*	0.18
	Sternum (3.1%)*	15.58
	Ribs (16.1%)*	2.76
	T/L spine (28.4%)*	0.10
	Pelvis (27.4%)*	0.00
	Total BM dose	1.23
Urinary bladder		0.00
Uterus		0.00
Ovaries		0.00
Contralateral breast		21.16

*These percentages represent the portion of bone marrow (BM) in different locations. They were adapted from ICRP report 70 (1995).

Table (A-10) Lists organs radiation dose, other than breast, from one screening visit for FFDM machine 10.

Organ		Absorbed dose (µGy)
Brain		1.98
Salivary glands		3.20
Thyroid		8.53
Oesophagus		0.21
Thymus		1.55
Heart		0.38
Lung		2.47
Liver		0.45
Gall bladder		0.08
Adrenal		0.00
Kidney		0.00
Spleen		0.01
Pancreas		0.00
Stomach		0.28
Intestine		0.00
Bone Marrow (BM)	Cranium (7.6%)*	2.99
	Mandibles (0.8%)*	3.20
	C-spine (3.9%)*	0.46
	Clavicles (0.8%)*	5.93
	Scapulae (2.8%)*	0.15
	Sternum (3.1%)*	14.73
	Ribs (16.1%)*	2.73
	T/L spine (28.4%)*	0.04
	Pelvis (27.4%)*	0.00
	Total BM dose	1.23
Urinary bladder		0.00
Uterus		0.00
Ovaries		0.00
Contralateral breast		26.10

*These percentages represent the portion of bone marrow (BM) in different locations. They were adapted from ICRP report 70 (1995).

Table (A-11) Lists organs radiation dose, other than breast, from one screening visit for FFDM machine 11.

Organ		Absorbed dose (µGy)
Brain		4.82
Salivary glands		3.79
Thyroid		6.19
Oesophagus		0.67
Thymus		1.73
Heart		0.34
Lung		2.42
Liver		0.45
Gall bladder		0.07
Adrenal		0.03
Kidney		0.03
Spleen		0.08
Pancreas		0.04
Stomach		0.18
Intestine		0.01
Bone Marrow (BM)	Cranium (7.6%)*	5.82
	Mandibles (0.8%)*	3.79
	C-spine (3.9%)*	1.39
	Clavicles (0.8%)*	4.69
	Scapulae (2.8%)*	0.51
	Sternum (3.1%)*	12.86
	Ribs (16.1%)*	2.52
	T/L spine (28.4%)*	0.11
	Pelvis (27.4%)*	0.00
	Total BM dose	1.41
Urinary bladder		0.00
Uterus		0.00
Ovaries		0.00
Contralateral breast		18.70

*These percentages represent the portion of bone marrow (BM) in different locations. They were adapted from ICRP report 70 (1995).

Table (A-12) Lists organs radiation dose, other than breast, from one screening visit for FFDM machine 12.

Organ		Absorbed dose (µGy)
Brain		1.33
Salivary glands		2.34
Thyroid		8.20
Oesophagus		0.11
Thymus		1.17
Heart		0.18
Lung		2.30
Liver		0.79
Gall bladder		0.29
Adrenal		0.08
Kidney		0.13
Spleen		0.17
Pancreas		0.13
Stomach		0.52
Intestine		0.08
Bone Marrow (BM)	Cranium (7.6%)*	2.16
	Mandibles (0.8%)*	2.34
	C-spine (3.9%)*	0.45
	Clavicles (0.8%)*	4.77
	Scapulae (2.8%)*	0.02
	Sternum (3.1%)*	12.88
	Ribs (16.1%)*	2.62
	T/L spine (28.4%)*	0.04
	Pelvis (27.4%)*	0.00
	Total BM dose	1.07
Urinary bladder		0.00
Uterus		0.00
Ovaries		0.00
Contralateral breast		26.62

*These percentages represent the portion of bone marrow (BM) in different locations. They were adapted from ICRP report 70 (1995).

Table (A-13) Lists organs radiation dose, other than breast, from one screening visit for FFDM machine 13.

Organ		Absorbed dose (µGy)
Brain		0.17
Salivary glands		1.80
Thyroid		7.00
Oesophagus		0.28
Thymus		1.32
Heart		0.71
Lung		2.64
Liver		0.87
Gall bladder		0.02
Adrenal		0.26
Kidney		0.11
Spleen		0.37
Pancreas		0.13
Stomach		0.50
Intestine		0.05
Bone Marrow (BM)	Cranium (7.6%)*	0.51
	Mandibles (0.8%)*	1.80
	C-spine (3.9%)*	0.24
	Clavicles (0.8%)*	4.54
	Scapulae (2.8%)*	0.28
	Sternum (3.1%)*	15.73
	Ribs (16.1%)*	3.14
	T/L spine (28.4%)*	0.17
	Pelvis (27.4%)*	0.00
	Total BM dose	1.15
Urinary bladder		0.00
Uterus		0.00
Ovaries		0.00
Contralateral breast		24.75

*These percentages represent the portion of bone marrow (BM) in different locations. They were adapted from ICRP report 70 (1995).

Table (A-14) Lists organs radiation dose, other than breast, from one screening visit for FFDM machine 14.

Organ		Absorbed dose (µGy)
Brain		0.63
Salivary glands		2.20
Thyroid		8.43
Oesophagus		0.02
Thymus		1.45
Heart		0.35
Lung		2.62
Liver		0.74
Gall bladder		0.29
Adrenal		0.18
Kidney		0.13
Spleen		0.29
Pancreas		0.18
Stomach		0.51
Intestine		0.00
Bone Marrow (BM)	Cranium (7.6%)*	1.62
	Mandibles (0.8%)*	2.20
	C-spine (3.9%)*	0.38
	Clavicles (0.8%)*	5.44
	Scapulae (2.8%)*	0.20
	Sternum (3.1%)*	17.56
	Ribs (16.1%)*	3.08
	T/L spine (28.4%)*	0.10
	Pelvis (27.4%)*	0.00
	Total BM dose	1.27
Urinary bladder		0.00
Uterus		0.00
Ovaries		0.00
Contralateral breast		25.14

*These percentages represent the portion of bone marrow (BM) in different locations. They were adapted from ICRP report 70 (1995).

Table (A-15) Lists organs radiation dose, other than breast, from one screening visit for FFDM machine 15.

Organ		Absorbed dose (µGy)
Brain		0.13
Salivary glands		2.21
Thyroid		8.60
Oesophagus		0.13
Thymus		2.90
Heart		0.37
Lung		2.46
Liver		0.48
Gall bladder		0.17
Adrenal		0.00
Kidney		0.01
Spleen		0.02
Pancreas		0.00
Stomach		0.31
Intestine		0.01
Bone Marrow (BM)	Cranium (7.6%)*	0.69
	Mandibles (0.8%)*	2.21
	C-spine (3.9%)*	0.05
	Clavicles (0.8%)*	10.06
	Scapulae (2.8%)*	0.10
	Sternum (3.1%)*	17.30
	Ribs (16.1%)*	3.07
	T/L spine (28.4%)*	0.01
	Pelvis (27.4%)*	0.00
	Total BM dose	1.19
Urinary bladder		0.00
Uterus		0.00
Ovaries		0.00
Contralateral breast		28.00

*These percentages represent the portion of bone marrow (BM) in different locations. They were adapted from ICRP report 70 (1995).

Table (A-16) Lists organs radiation dose, other than breast, from one screening visit for FFDM machine 16.

Organ		Absorbed dose (µGy)
Brain		0.33
Salivary glands		1.60
Thyroid		6.21
Oesophagus		0.12
Thymus		2.52
Heart		0.19
Lung		2.44
Liver		0.33
Gall bladder		0.13
Adrenal		0.00
Kidney		0.05
Spleen		0.08
Pancreas		0.03
Stomach		0.17
Intestine		0.02
Bone Marrow (BM)	Cranium (7.6%)*	0.46
	Mandibles (0.8%)*	1.60
	C-spine (3.9%)*	0.05
	Clavicles (0.8%)*	7.74
	Scapulae (2.8%)*	0.00
	Sternum (3.1%)*	18.00
	Ribs (16.1%)*	2.64
	T/L spine (28.4%)*	0.05
	Pelvis (27.4%)*	0.00
	Total BM dose	1.11
Urinary bladder		0.00
Uterus		0.00
Ovaries		0.00
Contralateral breast		19.04

*These percentages represent the portion of bone marrow (BM) in different locations. They were adapted from ICRP report 70 (1995).

Appendix B: Effective risk data for women aged 25 -75 years resulted from the sixteen FFDM machines using LAR extrapolated by the three methods.

Table (B-1) Presents effective risk for women aged 25-75 years resulted from FFDM machine 1 (3 visits).

Age (year)	Effective risk (case/10^6)								
	Visit 1			Visit 2			Visit 3		
	Method 1	Method 2	Method 3	Method 1	Method 2	Method 3	Method 1	Method 2	Method 3
25	83.977	83.977	105.657	84.047	84.047	105.745	83.908	83.908	105.568
26	79.641	79.641	105.657	79.708	79.708	105.745	79.576	79.576	105.568
27	75.305	75.305	105.657	75.368	75.368	105.745	75.243	75.243	105.568
28	70.969	70.969	105.657	71.029	71.029	105.745	70.911	70.911	105.568
29	66.633	66.633	105.657	66.689	66.689	105.745	66.579	66.579	105.568
30	62.297	62.297	62.297	62.349	62.349	62.349	62.247	62.247	62.247
31	58.297	59.542	62.297	58.345	59.592	62.349	58.248	59.494	62.247
32	55.618	56.787	62.297	55.663	56.834	62.349	55.571	56.740	62.247
33	53.003	54.033	62.297	53.046	54.077	62.349	52.959	53.987	62.247
34	50.453	51.278	62.297	50.494	51.319	62.349	50.410	51.234	62.247
35	47.967	48.523	62.297	48.005	48.561	62.349	47.926	48.481	62.247
36	45.546	45.768	62.297	45.581	45.804	62.349	45.506	45.727	62.247
37	43.188	43.013	62.297	43.221	43.046	62.349	43.149	42.974	62.247
38	40.895	40.258	62.297	40.926	40.288	62.349	40.857	40.221	62.247
39	38.665	37.503	62.297	38.694	37.531	62.349	38.629	37.468	62.247
40	36.500	34.749	34.749	36.527	34.773	34.773	36.465	34.714	34.714
41	34.399	33.003	34.749	34.423	33.025	34.773	34.365	32.969	34.714
42	32.362	31.256	34.749	32.384	31.277	34.773	32.329	31.224	34.714
43	30.388	29.510	34.749	30.409	29.530	34.773	30.357	29.479	34.714
44	28.479	27.764	34.749	28.497	27.782	34.773	28.449	27.734	34.714
45	26.634	26.018	34.749	26.650	26.034	34.773	26.605	25.989	34.714
46	24.852	24.272	34.749	24.867	24.286	34.773	24.824	24.244	34.714
47	23.135	22.526	34.749	23.148	22.538	34.773	23.108	22.499	34.714
48	21.481	20.780	34.749	21.493	20.790	34.773	21.455	20.754	34.714
49	19.892	19.034	34.749	19.901	19.043	34.773	19.866	19.009	34.714
50	18.366	17.288	17.288	18.374	17.295	17.295	18.341	17.263	17.263
51	16.904	16.328	17.288	16.911	16.334	17.295	16.880	16.304	17.263
52	15.506	15.368	17.288	15.511	15.373	17.295	15.483	15.345	17.263
53	14.172	14.408	17.288	14.176	14.413	17.295	14.150	14.386	17.263
54	12.901	13.449	17.288	12.904	13.452	17.295	12.880	13.427	17.263
55	11.695	12.489	17.288	11.697	12.491	17.295	11.674	12.468	17.263
56	10.552	11.529	17.288	10.553	11.531	17.295	10.533	11.509	17.263
57	9.474	10.569	17.288	9.473	10.570	17.295	9.455	10.550	17.263
58	8.459	9.609	17.288	8.458	9.610	17.295	8.440	9.591	17.263
59	7.508	8.650	17.288	7.506	8.649	17.295	7.490	8.632	17.263
60	6.620	7.690	7.690	6.618	7.688	7.688	6.604	7.672	7.672
61	5.797	7.221	7.690	5.794	7.219	7.688	5.781	7.204	7.672
62	5.037	6.752	7.690	5.033	6.750	7.688	5.022	6.736	7.672
63	4.342	6.283	7.690	4.337	6.281	7.688	4.327	6.267	7.672
64	3.710	5.814	7.690	3.705	5.812	7.688	3.696	5.799	7.672
65	3.142	5.345	7.690	3.136	5.342	7.688	3.128	5.331	7.672
66	2.637	4.876	7.690	2.632	4.873	7.688	2.624	4.862	7.672
67	2.197	4.407	7.690	2.191	4.404	7.688	2.185	4.394	7.672
68	1.820	3.938	7.690	1.815	3.935	7.688	1.809	3.926	7.672
69	1.508	3.469	7.690	1.502	3.466	7.688	1.496	3.457	7.672
70	1.259	3.000	3.000	1.253	2.997	2.997	1.248	2.989	2.989
71	1.074	2.801	3.000	1.068	2.798	2.997	1.064	2.791	2.989
72	0.952	2.602	3.000	0.947	2.599	2.997	0.943	2.592	2.989
73	0.895	2.403	3.000	0.890	2.400	2.997	0.886	2.394	2.989
74	0.892	2.204	3.000	0.888	2.201	2.997	0.884	2.195	2.989
75	0.890	2.005	3.000	0.885	2.002	2.997	0.882	1.997	2.989

Table (B-2) Presents effective risk for women aged 25-75 years resulted from FFDM machine 2 (3visits).

Age (year)	Effective risk (case/10^6)								
	Visit 1			Visit 2			Visit 3		
	Method 1	Method 2	Method 3	Method 1	Method 2	Method 3	Method 1	Method 2	Method 3
25	80.447	80.444	101.214	80.394	80.392	101.148	80.373	80.371	101.120
26	76.293	76.290	101.214	76.242	76.240	101.148	76.224	76.222	101.120
27	72.140	72.136	101.214	72.091	72.089	101.148	72.074	72.072	101.120
28	67.986	67.982	101.214	67.940	67.938	101.148	67.924	67.922	101.120
29	63.832	63.828	101.214	63.789	63.786	101.148	63.775	63.772	101.120
30	59.678	59.674	59.674	59.637	59.635	59.635	59.625	59.622	59.622
31	55.847	57.036	59.674	55.808	56.998	59.635	55.796	56.986	59.622
32	53.281	54.397	59.674	53.243	54.360	59.635	53.232	54.349	59.622
33	50.777	51.758	59.674	50.740	51.723	59.635	50.731	51.713	59.622
34	48.334	49.119	59.674	48.299	49.086	59.635	48.290	49.076	59.622
35	45.954	46.481	59.674	45.919	46.448	59.635	45.911	46.440	59.622
36	43.634	43.842	59.674	43.601	43.811	59.635	43.594	43.803	59.622
37	41.377	41.203	59.674	41.344	41.174	59.635	41.338	41.167	59.622
38	39.180	38.565	59.674	39.149	38.536	59.635	39.143	38.530	59.622
39	37.045	35.926	59.674	37.015	35.899	59.635	37.010	35.893	59.622
40	34.972	33.287	33.287	34.942	33.262	33.262	34.938	33.257	33.257
41	32.959	31.615	33.287	32.931	31.590	33.262	32.927	31.586	33.257
42	31.008	29.942	33.287	30.981	29.919	33.262	30.977	29.915	33.257
43	29.119	28.270	33.287	29.092	28.247	33.262	29.089	28.244	33.257
44	27.290	26.598	33.287	27.265	26.576	33.262	27.262	26.573	33.257
45	25.523	24.925	33.287	25.498	24.904	33.262	25.496	24.902	33.257
46	23.817	23.253	33.287	23.793	23.233	33.262	23.791	23.230	33.257
47	22.172	21.581	33.287	22.149	21.561	33.262	22.148	21.559	33.257
48	20.589	19.908	33.287	20.567	19.890	33.262	20.565	19.888	33.257
49	19.066	18.236	33.287	19.045	18.219	33.262	19.044	18.217	33.257
50	17.605	16.563	16.563	17.585	16.547	16.547	17.584	16.546	16.546
51	16.205	15.644	16.563	16.185	15.628	16.547	16.185	15.628	16.546
52	14.866	14.725	16.563	14.847	14.710	16.547	14.847	14.709	16.546
53	13.588	13.805	16.563	13.570	13.791	16.547	13.570	13.791	16.546
54	12.372	12.886	16.563	12.354	12.872	16.547	12.354	12.872	16.546
55	11.216	11.967	16.563	11.199	11.954	16.547	11.200	11.953	16.546
56	10.122	11.047	16.563	10.106	11.035	16.547	10.106	11.035	16.546
57	9.089	10.128	16.563	9.073	10.116	16.547	9.074	10.116	16.546
58	8.117	9.209	16.563	8.102	9.197	16.547	8.103	9.198	16.546
59	7.206	8.290	16.563	7.191	8.279	16.547	7.192	8.279	16.546
60	6.356	7.370	7.370	6.342	7.360	7.360	6.343	7.361	7.361
61	5.567	6.921	7.370	5.554	6.911	7.360	5.555	6.912	7.361
62	4.839	6.472	7.370	4.827	6.462	7.360	4.828	6.463	7.361
63	4.173	6.022	7.370	4.161	6.014	7.360	4.162	6.014	7.361
64	3.567	5.573	7.370	3.556	5.565	7.360	3.557	5.565	7.361
65	3.023	5.124	7.370	3.012	5.116	7.360	3.014	5.117	7.361
66	2.540	4.675	7.370	2.529	4.667	7.360	2.531	4.668	7.361
67	2.118	4.225	7.370	2.108	4.218	7.360	2.109	4.219	7.361
68	1.757	3.776	7.370	1.747	3.769	7.360	1.749	3.770	7.361
69	1.457	3.327	7.370	1.448	3.321	7.360	1.449	3.321	7.361
70	1.218	2.877	2.877	1.209	2.872	2.872	1.211	2.873	2.873
71	1.040	2.687	2.877	1.032	2.681	2.872	1.034	2.682	2.873
72	0.924	2.496	2.877	0.916	2.491	2.872	0.917	2.491	2.873
73	0.868	2.305	2.877	0.861	2.300	2.872	0.862	2.301	2.873
74	0.866	2.114	2.877	0.858	2.109	2.872	0.860	2.110	2.873
75	0.863	1.923	2.877	0.856	1.919	2.872	0.857	1.920	2.873

Table (B-3) Presents effective risk for women aged 25-75 years resulted from FFDM machine 3.

Age (year)	Effective risk (case/10^6)		
	Method 1	Method 2	Method 3
25	70.406	70.406	88.586
26	66.770	66.770	88.586
27	63.134	63.134	88.586
28	59.497	59.497	88.586
29	55.861	55.861	88.586
30	52.225	52.225	52.225
31	48.878	49.919	52.225
32	46.634	47.613	52.225
33	44.444	45.306	52.225
34	42.309	43.000	52.225
35	40.227	40.693	52.225
36	38.199	38.387	52.225
37	36.226	36.081	52.225
38	34.306	33.774	52.225
39	32.439	31.468	52.225
40	30.627	29.161	29.161
41	28.868	27.700	29.161
42	27.162	26.238	29.161
43	25.511	24.776	29.161
44	23.912	23.315	29.161
45	22.368	21.853	29.161
46	20.877	20.391	29.161
47	19.439	18.930	29.161
48	18.054	17.468	29.161
49	16.724	16.006	29.161
50	15.446	14.545	14.545
51	14.222	13.741	14.545
52	13.052	12.936	14.545
53	11.934	12.132	14.545
54	10.870	11.328	14.545
55	9.860	10.524	14.545
56	8.903	9.720	14.545
57	7.999	8.916	14.545
58	7.149	8.112	14.545
59	6.352	7.307	14.545
60	5.608	6.503	6.503
61	4.918	6.109	6.503
62	4.281	5.715	6.503
63	3.697	5.321	6.503
64	3.167	4.926	6.503
65	2.690	4.532	6.503
66	2.266	4.138	6.503
67	1.896	3.744	6.503
68	1.579	3.349	6.503
69	1.315	2.955	6.503
70	1.104	2.561	2.561
71	0.947	2.392	2.561
72	0.844	2.223	2.561
73	0.793	2.054	2.561
74	0.789	1.885	2.561
75	0.793	1.716	2.561

Table (B-4) Presents effective risk for women aged 25-75 years resulted from FFDM machine 4.

Age (year)	Effective risk (case/10^6)		
	Method 1	Method 2	Method 3
25	66.023	66.023	83.073
26	62.613	62.613	83.073
27	59.203	59.203	83.073
28	55.793	55.793	83.073
29	52.382	52.382	83.073
30	48.972	48.972	48.972
31	45.831	46.808	48.972
32	43.726	44.644	48.972
33	41.671	42.480	48.972
34	39.667	40.316	48.972
35	37.714	38.152	48.972
36	35.811	35.988	48.972
37	33.959	33.824	48.972
38	32.158	31.660	48.972
39	30.407	29.495	48.972
40	28.706	27.331	27.331
41	27.056	25.960	27.331
42	25.455	24.588	27.331
43	23.906	23.217	27.331
44	22.406	21.846	27.331
45	20.957	20.474	27.331
46	19.558	19.103	27.331
47	18.209	17.731	27.331
48	16.910	16.360	27.331
49	15.661	14.988	27.331
50	14.463	13.617	13.617
51	13.315	12.863	13.617
52	12.217	12.109	13.617
53	11.169	11.355	13.617
54	10.171	10.600	13.617
55	9.223	9.846	13.617
56	8.325	9.092	13.617
57	7.478	8.338	13.617
58	6.680	7.584	13.617
59	5.933	6.829	13.617
60	5.235	6.075	6.075
61	4.588	5.706	6.075
62	3.991	5.337	6.075
63	3.444	4.968	6.075
64	2.947	4.598	6.075
65	2.500	4.229	6.075
66	2.103	3.860	6.075
67	1.756	3.491	6.075
68	1.460	3.122	6.075
69	1.213	2.752	6.075
70	1.016	2.383	2.383
71	0.870	2.226	2.383
72	0.773	2.068	2.383
73	0.727	1.910	2.383
74	0.724	1.753	2.383
75	0.720	1.595	2.383

Table (B-5) Presents effective risk for women aged 25-75 years resulted from FFDM machine 5.

Age (year)	Effective risk (case/10^6)		
	Method 1	Method 2	Method 3
25	69.486	69.486	87.423
26	65.898	65.898	87.423
27	62.311	62.311	87.423
28	58.724	58.724	87.423
29	55.136	55.136	87.423
30	51.549	51.549	51.549
31	48.238	49.269	51.549
32	46.022	46.990	51.549
33	43.859	44.710	51.549
34	41.749	42.431	51.549
35	39.692	40.151	51.549
36	37.688	37.872	51.549
37	35.738	35.593	51.549
38	33.840	33.313	51.549
39	31.995	31.034	51.549
40	30.204	28.754	28.754
41	28.465	27.309	28.754
42	26.779	25.865	28.754
43	25.147	24.420	28.754
44	23.567	22.975	28.754
45	22.040	21.530	28.754
46	20.566	20.085	28.754
47	19.145	18.641	28.754
48	17.776	17.196	28.754
49	16.461	15.751	28.754
50	15.198	14.306	14.306
51	13.989	13.512	14.306
52	12.832	12.718	14.306
53	11.728	11.923	14.306
54	10.677	11.129	14.306
55	9.678	10.335	14.306
56	8.733	9.541	14.306
57	7.840	8.747	14.306
58	7.000	7.952	14.306
59	6.213	7.158	14.306
60	5.479	6.364	6.364
61	4.798	5.976	6.364
62	4.169	5.588	6.364
63	3.593	5.200	6.364
64	3.070	4.812	6.364
65	2.600	4.424	6.364
66	2.183	4.036	6.364
67	1.819	3.648	6.364
68	1.507	3.260	6.364
69	1.248	2.872	6.364
70	1.042	2.483	2.483
71	0.889	2.319	2.483
72	0.789	2.154	2.483
73	0.741	1.989	2.483
74	0.739	1.824	2.483
75	0.737	1.660	2.483

Table (B-6) Presents effective risk for women aged 25-75 years resulted from FFDM machine 6.

Age (year)	Effective risk (case/10^6)		
	Method 1	Method 2	Method 3
25	61.405	61.405	77.258
26	58.235	58.235	77.258
27	55.064	55.064	77.258
28	51.894	51.894	77.258
29	48.723	48.723	77.258
30	45.553	45.553	45.553
31	42.627	43.538	45.553
32	40.668	41.523	45.553
33	38.756	39.509	45.553
34	36.891	37.494	45.553
35	35.073	35.479	45.553
36	33.302	33.464	45.553
37	31.578	31.449	45.553
38	29.900	29.435	45.553
39	28.270	27.420	45.553
40	26.686	25.405	25.405
41	25.150	24.128	25.405
42	23.660	22.851	25.405
43	22.217	21.574	25.405
44	20.820	20.297	25.405
45	19.471	19.020	25.405
46	18.168	17.743	25.405
47	16.912	16.466	25.405
48	15.702	15.189	25.405
49	14.540	13.912	25.405
50	13.424	12.635	12.635
51	12.355	11.933	12.635
52	11.332	11.232	12.635
53	10.357	10.530	12.635
54	9.428	9.828	12.635
55	8.545	9.126	12.635
56	7.710	8.424	12.635
57	6.921	7.722	12.635
58	6.179	7.021	12.635
59	5.483	6.319	12.635
60	4.835	5.617	5.617
61	4.233	5.274	5.617
62	3.677	4.931	5.617
63	3.169	4.589	5.617
64	2.707	4.246	5.617
65	2.291	3.903	5.617
66	1.923	3.560	5.617
67	1.601	3.218	5.617
68	1.326	2.875	5.617
69	1.097	2.532	5.617
70	0.915	2.189	2.189
71	0.780	2.044	2.189
72	0.692	1.899	2.189
73	0.650	1.753	2.189
74	0.649	1.608	2.189
75	0.647	1.463	2.189

Table (B-7) Presents effective risk for women aged 25-75 years resulted from FFDM machine 7.

Age (year)	Effective risk (case/10^6)		
	Method 1	Method 2	Method 3
25	97.492	97.492	122.662
26	92.458	92.458	122.662
27	87.424	87.424	122.662
28	82.390	82.390	122.662
29	77.356	77.356	122.662
30	72.323	72.323	72.323
31	67.680	69.125	72.323
32	64.571	65.928	72.323
33	61.536	62.731	72.323
34	58.577	59.534	72.323
35	55.692	56.337	72.323
36	52.881	53.140	72.323
37	50.145	49.942	72.323
38	47.484	46.745	72.323
39	44.897	43.548	72.323
40	42.384	40.351	40.351
41	39.945	38.325	40.351
42	37.581	36.298	40.351
43	35.291	34.272	40.351
44	33.075	32.246	40.351
45	30.934	30.219	40.351
46	28.866	28.193	40.351
47	26.873	26.167	40.351
48	24.954	24.140	40.351
49	23.109	22.114	40.351
50	21.339	20.088	20.088
51	19.642	18.973	20.088
52	18.019	17.859	20.088
53	16.471	16.745	20.088
54	14.996	15.631	20.088
55	13.596	14.517	20.088
56	12.270	13.403	20.088
57	11.018	12.289	20.088
58	9.840	11.175	20.088
59	8.736	10.061	20.088
60	7.706	8.947	8.947
61	6.750	8.402	8.947
62	5.868	7.857	8.947
63	5.060	7.313	8.947
64	4.326	6.768	8.947
65	3.666	6.223	8.947
66	3.081	5.678	8.947
67	2.569	5.134	8.947
68	2.132	4.589	8.947
69	1.768	4.044	8.947
70	1.478	3.499	3.499
71	1.263	3.267	3.499
72	1.121	3.035	3.499
73	1.054	2.804	3.499
74	1.050	2.572	3.499
75	1.047	2.340	3.499

Table (B-8) Presents effective risk for women aged 25-75 years resulted from FFDM machine 8.

Age (year)	Effective risk (case/10^6)		
	Method 1	Method 2	Method 3
25	76.661	76.661	96.448
26	72.703	72.703	96.448
27	68.746	68.746	96.448
28	64.788	64.788	96.448
29	60.830	60.830	96.448
30	56.873	56.873	56.873
31	53.223	54.360	56.873
32	50.780	51.847	56.873
33	48.395	49.333	56.873
34	46.068	46.820	56.873
35	43.801	44.307	56.873
36	41.591	41.794	56.873
37	39.441	39.281	56.873
38	37.349	36.767	56.873
39	35.315	34.254	56.873
40	33.339	31.741	31.741
41	31.423	30.148	31.741
42	29.564	28.555	31.741
43	27.764	26.962	31.741
44	26.022	25.369	31.741
45	24.338	23.776	31.741
46	22.713	22.183	31.741
47	21.146	20.590	31.741
48	19.637	18.997	31.741
49	18.187	17.404	31.741
50	16.794	15.811	15.811
51	15.460	14.935	15.811
52	14.185	14.059	15.811
53	12.967	13.183	15.811
54	11.808	12.307	15.811
55	10.707	11.430	15.811
56	9.664	10.554	15.811
57	8.679	9.678	15.811
58	7.752	8.802	15.811
59	6.884	7.926	15.811
60	6.074	7.050	7.050
61	5.322	6.621	7.050
62	4.629	6.193	7.050
63	3.993	5.764	7.050
64	3.416	5.335	7.050
65	2.897	4.907	7.050
66	2.436	4.478	7.050
67	2.033	4.049	7.050
68	1.689	3.620	7.050
69	1.402	3.192	7.050
70	1.174	2.763	2.763
71	1.004	2.580	2.763
72	0.893	2.397	2.763
73	0.839	2.214	2.763
74	0.836	2.031	2.763
75	0.832	1.849	2.763

Table (B-9) Presents effective risk for women aged 25-75 years resulted from FFDM machine 9.

Age (year)	Effective risk (case/10^6)		
	Method 1	Method 2	Method 3
25	63.311	63.311	79.655
26	60.042	60.042	79.655
27	56.773	56.773	79.655
28	53.504	53.504	79.655
29	50.235	50.235	79.655
30	46.966	46.966	46.966
31	43.951	44.890	46.966
32	41.931	42.813	46.966
33	39.960	40.736	46.966
34	38.038	38.659	46.966
35	36.164	36.583	46.966
36	34.338	34.506	46.966
37	32.561	32.429	46.966
38	30.832	30.352	46.966
39	29.151	28.275	46.966
40	27.519	26.199	26.199
41	25.935	24.882	26.199
42	24.399	23.566	26.199
43	22.912	22.250	26.199
44	21.472	20.934	26.199
45	20.081	19.617	26.199
46	18.738	18.301	26.199
47	17.444	16.985	26.199
48	16.197	15.668	26.199
49	14.999	14.352	26.199
50	13.848	13.036	13.036
51	12.746	12.312	13.036
52	11.692	11.589	13.036
53	10.687	10.865	13.036
54	9.729	10.141	13.036
55	8.819	9.418	13.036
56	7.958	8.694	13.036
57	7.145	7.971	13.036
58	6.380	7.247	13.036
59	5.663	6.524	13.036
60	4.994	5.800	5.800
61	4.373	5.446	5.800
62	3.800	5.093	5.800
63	3.276	4.739	5.800
64	2.799	4.386	5.800
65	2.371	4.032	5.800
66	1.991	3.678	5.800
67	1.659	3.325	5.800
68	1.375	2.971	5.800
69	1.139	2.618	5.800
70	0.951	2.264	2.264
71	0.812	2.114	2.264
72	0.720	1.964	2.264
73	0.677	1.813	2.264
74	0.675	1.663	2.264
75	0.673	1.513	2.264

Table (B-10) Presents effective risk for women aged 25-75 years resulted from FFDM machine 10.

Age (year)	Effective risk (case/10^6)		
	Method 1	Method 2	Method 3
25	73.697	73.697	92.723
26	69.892	69.892	92.723
27	66.087	66.087	92.723
28	62.282	62.282	92.723
29	58.477	58.477	92.723
30	54.672	54.672	54.672
31	51.160	52.254	54.672
32	48.809	49.836	54.672
33	46.515	47.418	54.672
34	44.277	45.000	54.672
35	42.095	42.582	54.672
36	39.970	40.165	54.672
37	37.900	37.747	54.672
38	35.888	35.329	54.672
39	33.931	32.911	54.672
40	32.031	30.493	30.493
41	30.187	28.961	30.493
42	28.399	27.428	30.493
43	26.667	25.896	30.493
44	24.991	24.363	30.493
45	23.371	22.831	30.493
46	21.808	21.298	30.493
47	20.301	19.766	30.493
48	18.849	18.233	30.493
49	17.454	16.701	30.493
50	16.115	15.169	15.169
51	14.832	14.326	15.169
52	13.605	13.484	15.169
53	12.434	12.642	15.169
54	11.319	11.799	15.169
55	10.260	10.957	15.169
56	9.257	10.115	15.169
57	8.311	9.272	15.169
58	7.420	8.430	15.169
59	6.585	7.588	15.169
60	5.807	6.745	6.745
61	5.084	6.334	6.745
62	4.417	5.922	6.745
63	3.807	5.511	6.745
64	3.252	5.099	6.745
65	2.754	4.688	6.745
66	2.311	4.276	6.745
67	1.925	3.865	6.745
68	1.595	3.453	6.745
69	1.320	3.042	6.745
70	1.102	2.630	2.630
71	0.939	2.456	2.630
72	0.833	2.281	2.630
73	0.783	2.107	2.630
74	0.781	1.932	2.630
75	0.779	1.757	2.630

Table (B-11) Presents effective risk for women aged 25-75 years resulted from FFDM machine 11.

Age (year)	Effective risk (case/10^6)		
	Method 1	Method 2	Method 3
25	57.995	57.995	72.964
26	55.001	55.001	72.964
27	52.007	52.007	72.964
28	49.013	49.013	72.964
29	46.019	46.019	72.964
30	43.026	43.025	43.025
31	40.263	41.124	43.025
32	38.414	39.222	43.025
33	36.610	37.320	43.025
34	34.849	35.418	43.025
35	33.133	33.516	43.025
36	31.461	31.614	43.025
37	29.834	29.712	43.025
38	28.250	27.811	43.025
39	26.711	25.909	43.025
40	25.216	24.007	24.007
41	23.766	22.801	24.007
42	22.359	21.596	24.007
43	20.996	20.390	24.007
44	19.678	19.184	24.007
45	18.404	17.979	24.007
46	17.174	16.773	24.007
47	15.988	15.567	24.007
48	14.846	14.362	24.007
49	13.748	13.156	24.007
50	12.695	11.951	11.951
51	11.685	11.288	11.951
52	10.720	10.625	11.951
53	9.798	9.962	11.951
54	8.921	9.299	11.951
55	8.088	8.636	11.951
56	7.299	7.973	11.951
57	6.554	7.310	11.951
58	5.853	6.647	11.951
59	5.196	5.984	11.951
60	4.583	5.321	5.321
61	4.014	4.997	5.321
62	3.489	4.673	5.321
63	3.009	4.349	5.321
64	2.572	4.025	5.321
65	2.180	3.701	5.321
66	1.831	3.376	5.321
67	1.527	3.052	5.321
68	1.266	2.728	5.321
69	1.050	2.404	5.321
70	0.878	2.080	2.080
71	0.749	1.942	2.080
72	0.665	1.804	2.080
73	0.625	1.666	2.080
74	0.623	1.528	2.080
75	0.621	1.390	2.080

Table (B-12) Presents effective risk for women aged 25-75 years resulted from FFDM machine 12.

Age (year)	Effective risk (case/10^6)		
	Method 1	Method 2	Method 3
25	68.459	68.459	86.133
26	64.925	64.925	86.133
27	61.390	61.390	86.133
28	57.855	57.855	86.133
29	54.320	54.320	86.133
30	50.786	50.786	50.786
31	47.524	48.540	50.786
32	45.340	46.294	50.786
33	43.208	44.048	50.786
34	41.129	41.802	50.786
35	39.103	39.556	50.786
36	37.128	37.310	50.786
37	35.206	35.064	50.786
38	33.337	32.818	50.786
39	31.519	30.572	50.786
40	29.754	28.326	28.326
41	28.041	26.902	28.326
42	26.380	25.479	28.326
43	24.771	24.055	28.326
44	23.214	22.632	28.326
45	21.710	21.208	28.326
46	20.258	19.784	28.326
47	18.857	18.361	28.326
48	17.509	16.937	28.326
49	16.213	15.514	28.326
50	14.969	14.090	14.090
51	13.777	13.308	14.090
52	12.638	12.525	14.090
53	11.550	11.743	14.090
54	10.514	10.960	14.090
55	9.531	10.178	14.090
56	8.599	9.396	14.090
57	7.720	8.613	14.090
58	6.892	7.831	14.090
59	6.117	7.048	14.090
60	5.394	6.266	6.266
61	4.723	5.884	6.266
62	4.103	5.501	6.266
63	3.536	5.119	6.266
64	3.021	4.737	6.266
65	2.558	4.355	6.266
66	2.147	3.972	6.266
67	1.788	3.590	6.266
68	1.481	3.208	6.266
69	1.226	2.826	6.266
70	1.024	2.444	2.444
71	0.873	2.281	2.444
72	0.774	2.119	2.444
73	0.727	1.957	2.444
74	0.725	1.795	2.444
75	0.724	1.633	2.444

Table (B-13) Presents effective risk for women aged 25-75 years resulted from FFDM machine 13.

Age (year)	Effective risk (case/10^6)		
	Method 1	Method 2	Method 3
25	64.392	64.392	81.014
26	61.068	61.068	81.014
27	57.744	57.744	81.014
28	54.419	54.419	81.014
29	51.095	51.095	81.014
30	47.771	47.771	47.771
31	44.703	45.659	47.771
32	42.650	43.547	47.771
33	40.646	41.435	47.771
34	38.691	39.322	47.771
35	36.785	37.210	47.771
36	34.928	35.098	47.771
37	33.121	32.986	47.771
38	31.362	30.874	47.771
39	29.653	28.762	47.771
40	27.993	26.650	26.650
41	26.382	25.311	26.650
42	24.820	23.972	26.650
43	23.307	22.633	26.650
44	21.843	21.295	26.650
45	20.428	19.956	26.650
46	19.062	18.617	26.650
47	17.746	17.278	26.650
48	16.478	15.940	26.650
49	15.259	14.601	26.650
50	14.089	13.262	13.262
51	12.968	12.526	13.262
52	11.896	11.790	13.262
53	10.873	11.054	13.262
54	9.899	10.318	13.262
55	8.973	9.582	13.262
56	8.097	8.846	13.262
57	7.270	8.110	13.262
58	6.492	7.374	13.262
59	5.762	6.638	13.262
60	5.082	5.902	5.902
61	4.451	5.542	5.902
62	3.868	5.183	5.902
63	3.334	4.823	5.902
64	2.850	4.463	5.902
65	2.414	4.104	5.902
66	2.027	3.744	5.902
67	1.689	3.384	5.902
68	1.401	3.024	5.902
69	1.161	2.665	5.902
70	0.970	2.305	2.305
71	0.827	2.152	2.305
72	0.734	1.999	2.305
73	0.690	1.846	2.305
74	0.688	1.694	2.305
75	0.686	1.541	2.305

Table (B-14) Presents effective risk for women aged 25-75 years resulted from FFDM machine 14.

Age (year)	Effective risk (case/10^6)		
	Method 1	Method 2	Method 3
25	65.500	65.500	82.410
26	62.118	62.118	82.410
27	58.736	58.736	82.410
28	55.354	55.354	82.410
29	51.972	51.972	82.410
30	48.590	48.590	48.590
31	45.470	46.442	48.590
32	43.381	44.293	48.590
33	41.342	42.145	48.590
34	39.353	39.996	48.590
35	37.415	37.848	48.590
36	35.526	35.699	48.590
37	33.687	33.551	48.590
38	31.899	31.402	48.590
39	30.160	29.254	48.590
40	28.471	27.105	27.105
41	26.833	25.744	27.105
42	25.244	24.382	27.105
43	23.705	23.020	27.105
44	22.216	21.658	27.105
45	20.777	20.297	27.105
46	19.388	18.935	27.105
47	18.048	17.573	27.105
48	16.759	16.211	27.105
49	15.519	14.850	27.105
50	14.329	13.488	13.488
51	13.189	12.739	13.488
52	12.098	11.991	13.488
53	11.058	11.242	13.488
54	10.067	10.494	13.488
55	9.126	9.745	13.488
56	8.235	8.997	13.488
57	7.393	8.248	13.488
58	6.602	7.499	13.488
59	5.860	6.751	13.488
60	5.168	6.002	6.002
61	4.526	5.636	6.002
62	3.933	5.271	6.002
63	3.391	4.905	6.002
64	2.898	4.539	6.002
65	2.455	4.173	6.002
66	2.061	3.807	6.002
67	1.718	3.441	6.002
68	1.424	3.075	6.002
69	1.180	2.710	6.002
70	0.986	2.344	2.344
71	0.841	2.188	2.344
72	0.746	2.033	2.344
73	0.701	1.877	2.344
74	0.699	1.722	2.344
75	0.697	1.567	2.344

Table (B-15) Presents effective risk for women aged 25-75 years resulted from FFDM machine 15.

Age (year)	Effective risk (case/10^6)		
	Method 1	Method 2	Method 3
25	60.975	60.975	76.718
26	57.827	57.827	76.718
27	54.678	54.678	76.718
28	51.530	51.530	76.718
29	48.381	48.381	76.718
30	45.232	45.232	45.232
31	42.328	43.232	45.232
32	40.383	41.232	45.232
33	38.485	39.232	45.232
34	36.633	37.232	45.232
35	34.828	35.232	45.232
36	33.070	33.232	45.232
37	31.359	31.232	45.232
38	29.694	29.232	45.232
39	28.075	27.232	45.232
40	26.503	25.232	25.232
41	24.978	23.964	25.232
42	23.499	22.697	25.232
43	22.066	21.429	25.232
44	20.680	20.161	25.232
45	19.340	18.894	25.232
46	18.047	17.626	25.232
47	16.800	16.358	25.232
48	15.600	15.091	25.232
49	14.446	13.823	25.232
50	13.338	12.556	12.556
51	12.277	11.859	12.556
52	11.262	11.162	12.556
53	10.293	10.465	12.556
54	9.371	9.768	12.556
55	8.495	9.071	12.556
56	7.666	8.375	12.556
57	6.882	7.678	12.556
58	6.146	6.981	12.556
59	5.455	6.284	12.556
60	4.811	5.587	5.587
61	4.213	5.247	5.587
62	3.662	4.906	5.587
63	3.156	4.566	5.587
64	2.698	4.225	5.587
65	2.285	3.885	5.587
66	1.919	3.544	5.587
67	1.599	3.203	5.587
68	1.326	2.863	5.587
69	1.098	2.522	5.587
70	0.918	2.182	2.182
71	0.783	2.037	2.182
72	0.695	1.892	2.182
73	0.653	1.748	2.182
74	0.651	1.603	2.182
75	0.649	1.458	2.182

Table (B-16) Presents effective risk for women aged 25-75 years resulted from FFDM machine 16.

Age (year)	Effective risk (case/10^6)		
	Method 1	Method 2	Method 3
25	59.777	59.777	75.207
26	56.691	56.691	75.207
27	53.605	53.605	75.207
28	50.519	50.519	75.207
29	47.433	47.433	75.207
30	44.347	44.347	44.347
31	41.500	42.387	44.347
32	39.593	40.426	44.347
33	37.733	38.465	44.347
34	35.918	36.504	44.347
35	34.148	34.543	44.347
36	32.425	32.583	44.347
37	30.747	30.622	44.347
38	29.115	28.661	44.347
39	27.528	26.700	44.347
40	25.987	24.740	24.740
41	24.491	23.497	24.740
42	23.041	22.254	24.740
43	21.636	21.011	24.740
44	20.277	19.768	24.740
45	18.964	18.525	24.740
46	17.696	17.282	24.740
47	16.473	16.039	24.740
48	15.296	14.797	24.740
49	14.165	13.554	24.740
50	13.078	12.311	12.311
51	12.038	11.628	12.311
52	11.043	10.944	12.311
53	10.093	10.261	12.311
54	9.188	9.578	12.311
55	8.330	8.895	12.311
56	7.516	8.211	12.311
57	6.748	7.528	12.311
58	6.026	6.845	12.311
59	5.349	6.162	12.311
60	4.717	5.478	5.478
61	4.131	5.144	5.478
62	3.590	4.811	5.478
63	3.095	4.477	5.478
64	2.645	4.143	5.478
65	2.240	3.809	5.478
66	1.881	3.475	5.478
67	1.568	3.141	5.478
68	1.299	2.807	5.478
69	1.077	2.473	5.478
70	0.899	2.139	2.139
71	0.767	1.997	2.139
72	0.681	1.855	2.139
73	0.640	1.713	2.139
74	0.638	1.572	2.139
75	0.636	1.430	2.139

Appendix C: The proposed 274 screening scenarios used to establish the regression model.

Table (C-1) Lists the proposed 274 screening scenarios used for regression model.

Age range (year)	Screening frequency	Age range (year)	Screening frequency	Age range (year)	Screening frequency
25-55	annual, biennial, triennial	32-67	annual, biennial, triennial	47-69	annual, biennial, triennial
25-60	annual, biennial, triennial	32-68	annual, biennial, triennial	47-73	annual, biennial, triennial
25-65	annual, biennial, triennial	32-70	annual, biennial, triennial	47-75	annual, biennial, triennial
25-70	annual, biennial, triennial	32-74	annual, biennial, triennial	48-68	annual, biennial, triennial
25-75	annual, biennial, triennial	33-73	annual, biennial, triennial	48-70	annual, biennial, triennial
26-50	annual, biennial, triennial	35-45	annual, biennial, triennial	49-55	annual, biennial, triennial
27-34	annual, biennial, triennial	35-50	annual, biennial, triennial	49-59	annual, biennial, triennial
27-37	annual, biennial, triennial	35-55	annual, biennial, triennial	49-62	annual, biennial, triennial
27-40	annual, biennial, triennial	35-70	annual, biennial, triennial	49-65	annual, biennial, triennial
27-43	annual, biennial, triennial	35-75	annual, biennial, triennial	49-68	annual, biennial, triennial
27-46	annual, biennial, triennial	36-72	annual, biennial, triennial	49-70	annual, biennial, triennial
27-49	annual, biennial, triennial	37-58	annual, biennial, triennial	49-72	annual, biennial, triennial
27-52	annual, biennial, triennial	37-61	annual, biennial, triennial	49-75	annual, biennial, triennial
27-55	annual, biennial, triennial	37-65	annual, biennial, triennial	50-64	annual, biennial, triennial
27-58	annual, biennial, triennial	37-67	annual, biennial, triennial	50-67	annual, biennial, triennial
27-61	annual, biennial, triennial	37-72	annual, biennial, triennial	50-73	annual, biennial, triennial
27-64	annual, biennial, triennial	37-75	annual, biennial, triennial	50-75	annual, biennial, triennial
27-67	annual, biennial, triennial	38-65	annual, biennial, triennial	52-72	annual, biennial, triennial
27-70	annual, biennial, triennial	40-60	annual, biennial, triennial	52-75	annual, biennial, triennial
27-72	annual, biennial, triennial	40-69	annual, biennial, triennial	53-70	annual, biennial, triennial
27-75	annual, biennial, triennial	40-74	annual, biennial, triennial	54-63	annual, biennial, triennial
29-62	annual, biennial, triennial	40-75	annual, biennial, triennial	55-75	annual, biennial, triennial
30-75	annual, biennial, triennial	42-65	annual, biennial, triennial	57-75	annual, biennial, triennial
32-45	annual, biennial, triennial	42-70	annual, biennial, triennial	60-73	annual, biennial, triennial
32-48	annual, biennial, triennial	42-72	annual, biennial, triennial	60-75	annual, biennial, triennial
32-50	annual, biennial, triennial	42-75	annual, biennial, triennial	62-75	annual, biennial, triennial
32-52	annual, biennial, triennial	43-71	annual, biennial, triennial	63-75	annual, biennial, triennial
32-55	annual, biennial, triennial	44-65	annual, biennial, triennial	64-75	annual, biennial, triennial
32-58	annual, biennial, triennial	44-70	annual, biennial, triennial	65-75	annual, biennial, triennial
32-61	annual, biennial, triennial	44-75	annual, biennial, triennial	66-75	annual
32-64	annual, biennial, triennial	45-75	annual, biennial, triennial		

Appendix D: Relationship graphs between MGD and total effective risk.

First LAR Extrapolation Method

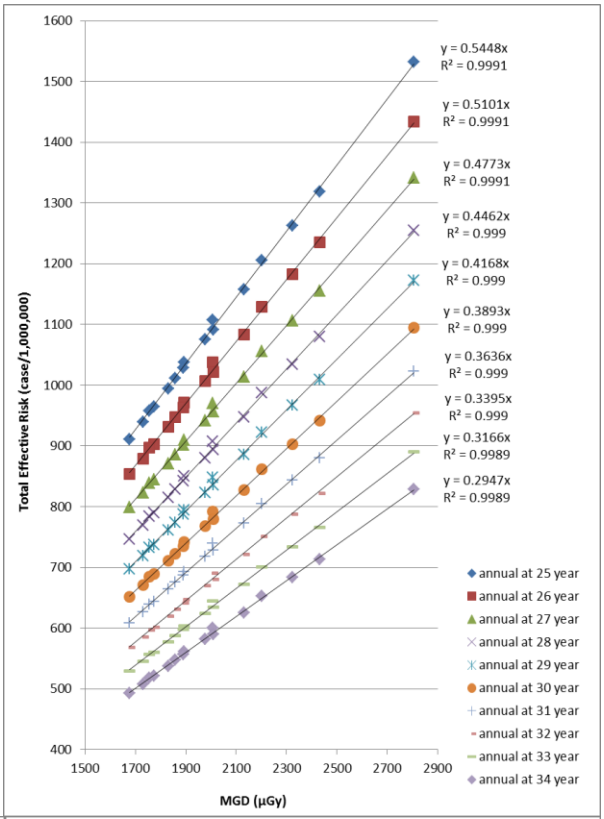

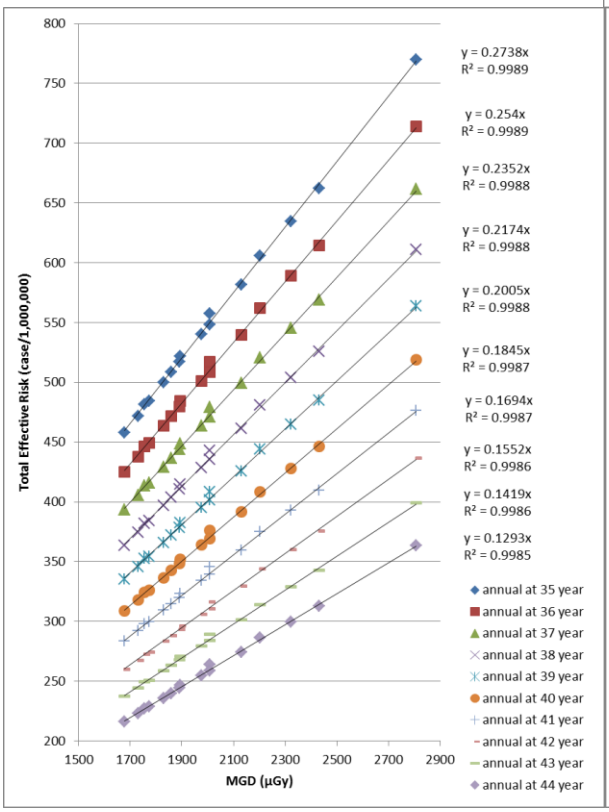

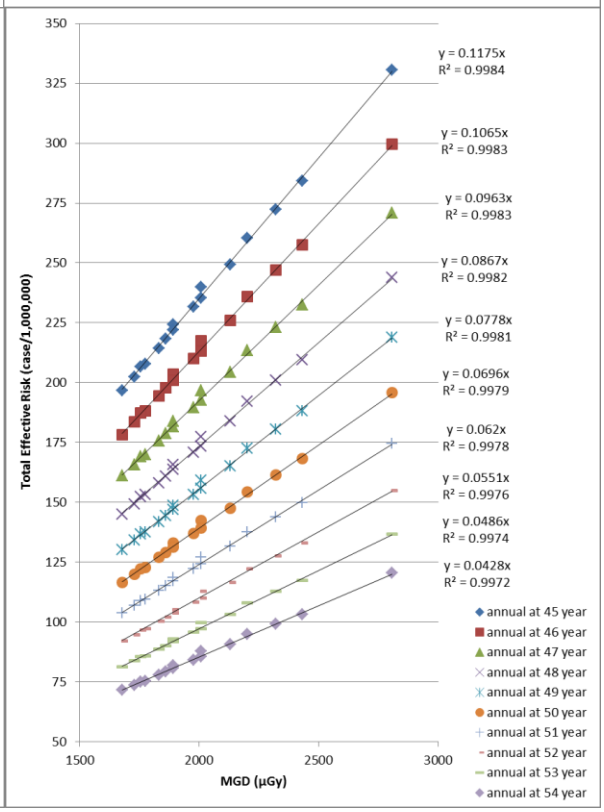

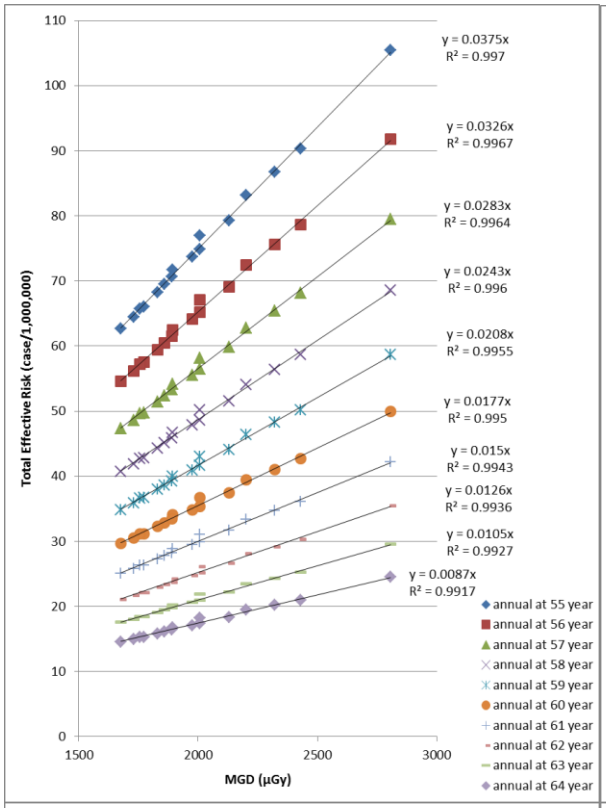
Total Effective Risk (case/1,000,000)
MGD (µGy)
y = 0.0375x R² = 0.997
y = 0.0326x R² = 0.9967
y = 0.0283x R² = 0.9964
y = 0.0243x R² = 0.996
y = 0.0208x R² = 0.9955
y = 0.0177x R² = 0.995
y = 0.015x R² = 0.9943
y = 0.0126x R² = 0.9936
y = 0.0105x R² = 0.9927
y = 0.0087x R² = 0.9917
annual at 55 year
annual at 56 year
annual at 57 year
annual at 58 year
annual at 59 year
annual at 60 year
annual at 61 year
annual at 62 year
annual at 63 year
annual at 64 year

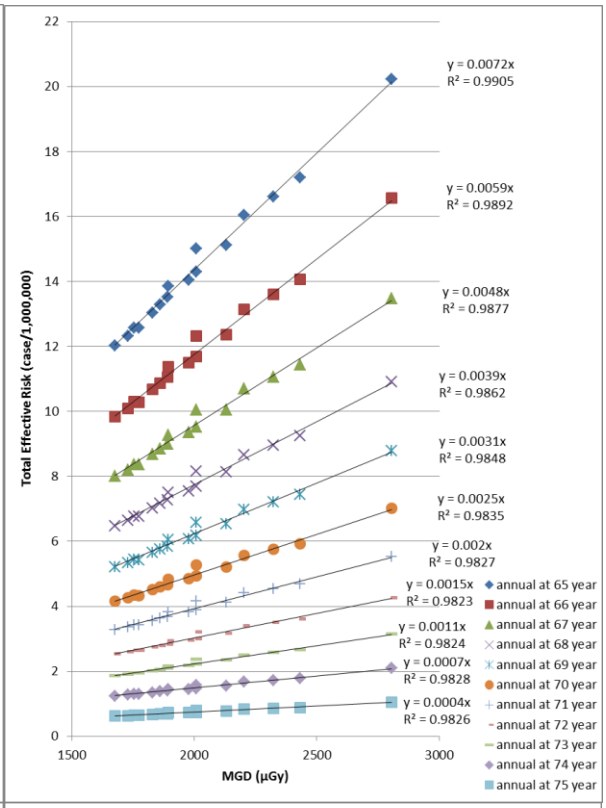
Total Effective Risk (case/1,000,000)
MGD (µGy)
y = 0.0072x R² = 0.9905
y = 0.0059x R² = 0.9892
y = 0.0048x R² = 0.9877
y = 0.0039x R² = 0.9862
y = 0.0031x R² = 0.9848
y = 0.0025x R² = 0.9835
y = 0.002x R² = 0.9827
y = 0.0015x R² = 0.9823
y = 0.0011x R² = 0.9824
y = 0.0007x R² = 0.9828
y = 0.0004x R² = 0.9826
annual at 65 year
annual at 66 year
annual at 67 year
annual at 68 year
annual at 69 year
annual at 70 year
annual at 71 year
annual at 72 year
annual at 73 year
annual at 74 year
annual at 75 year

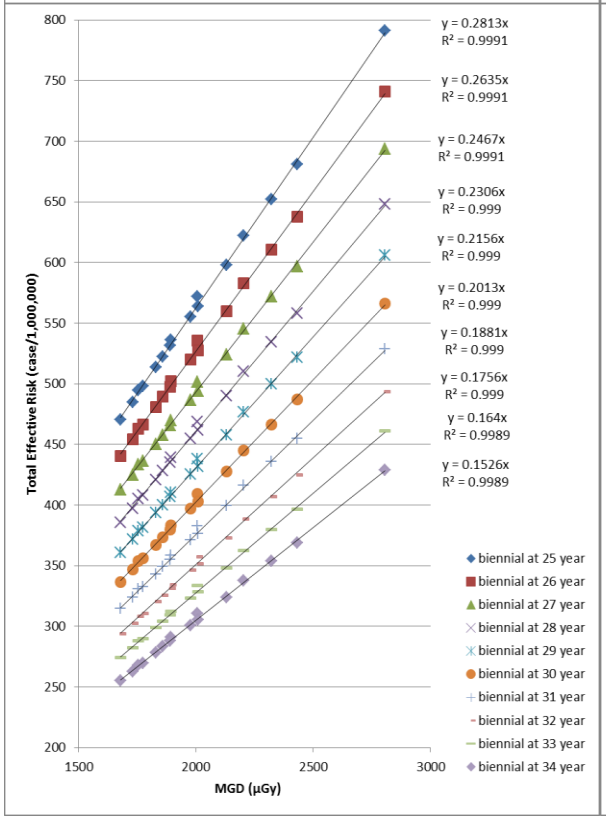
Total Effective Risk (case/1,000,000)
MGD (µGy)
y = 0.2813x R² = 0.9991
y = 0.2635x R² = 0.9991
y = 0.2467x R² = 0.9991
y = 0.2306x R² = 0.999
y = 0.2156x R² = 0.999
y = 0.2013x R² = 0.999
y = 0.1881x R² = 0.999
y = 0.1756x R² = 0.999
y = 0.164x R² = 0.9989
y = 0.1526x R² = 0.9989
biennial at 25 year
biennial at 26 year
biennial at 27 year
biennial at 28 year
biennial at 29 year
biennial at 30 year
biennial at 31 year
biennial at 32 year
biennial at 33 year
biennial at 34 year

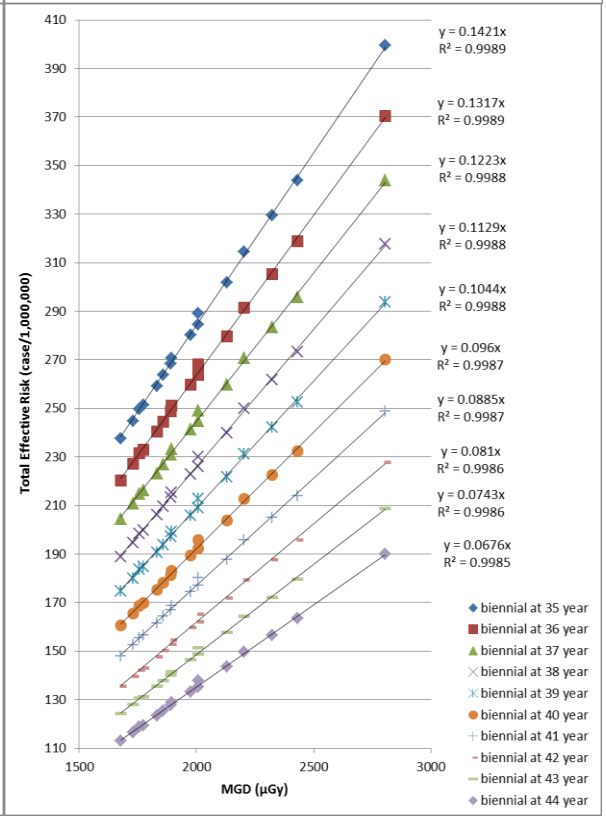
Total Effective Risk (case/1,000,000)
MGD (µGy)
y = 0.1421x R² = 0.9989
y = 0.1317x R² = 0.9989
y = 0.1223x R² = 0.9988
y = 0.1129x R² = 0.9988
y = 0.1044x R² = 0.9988
y = 0.096x R² = 0.9987
y = 0.0885x R² = 0.9987
y = 0.081x R² = 0.9986
y = 0.0743x R² = 0.9986
y = 0.0676x R² = 0.9985
biennial at 35 year
biennial at 36 year
biennial at 37 year
biennial at 38 year
biennial at 39 year
biennial at 40 year
biennial at 41 year
biennial at 42 year
biennial at 43 year
biennial at 44 year

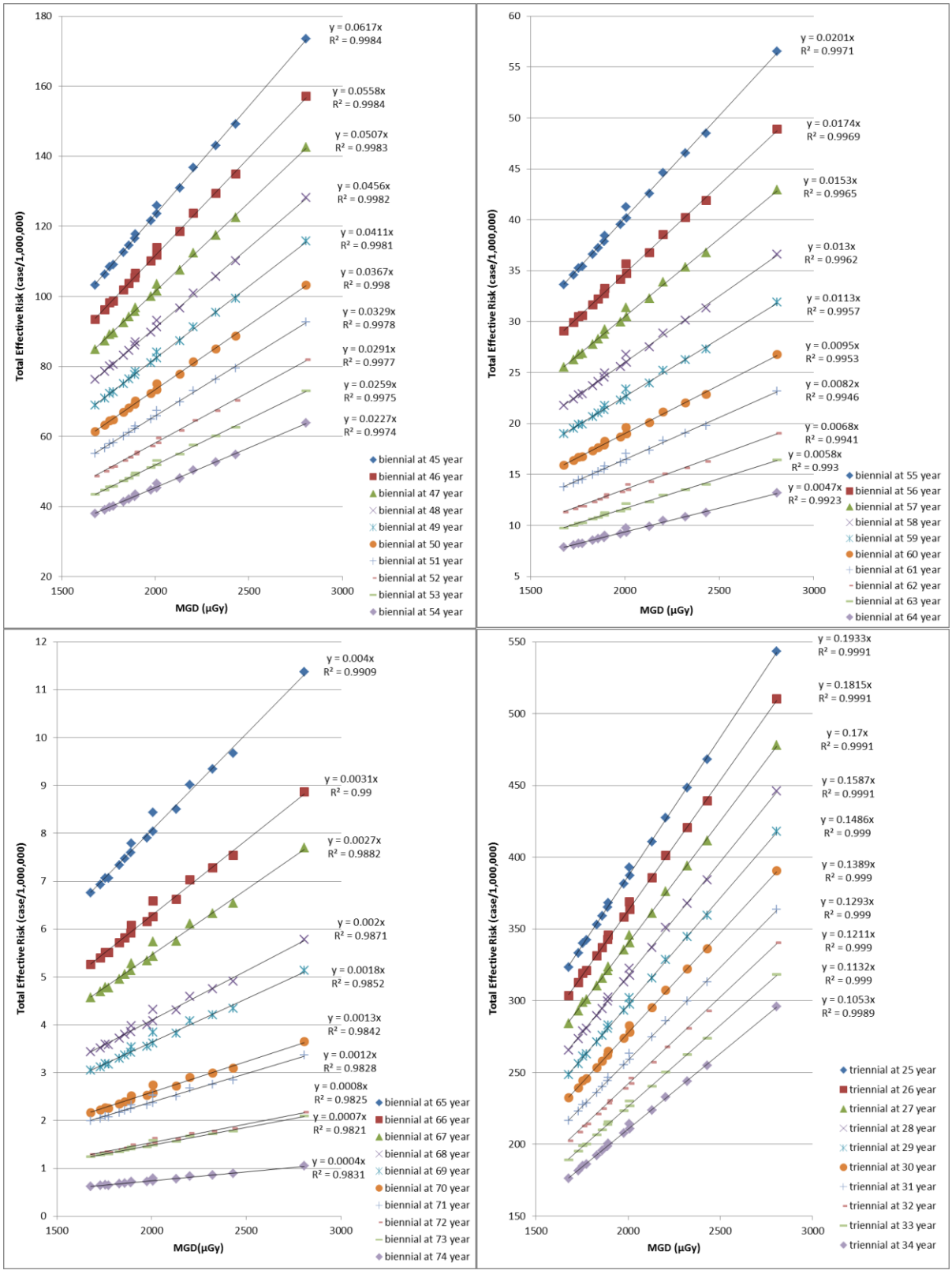
Total Effective Risk (case/1,000,000)
MGD (μGy)
y = 0.0617x R² = 0.9984
y = 0.0558x R² = 0.9984
y = 0.0507x R² = 0.9983
y = 0.0456x R² = 0.9982
y = 0.0411x R² = 0.9981
y = 0.0367x R² = 0.998
y = 0.0329x R² = 0.9978
y = 0.0291x R² = 0.9977
y = 0.0259x R² = 0.9975
y = 0.0227x R² = 0.9974
biennial at 45 year
biennial at 46 year
biennial at 47 year
biennial at 48 year
biennial at 49 year
biennial at 50 year
biennial at 51 year
biennial at 52 year
biennial at 53 year
biennial at 54 year
y = 0.0201x R² = 0.9971
y = 0.0174x R² = 0.9969
y = 0.0153x R² = 0.9965
y = 0.013x R² = 0.9962
y = 0.0113x R² = 0.9957
y = 0.0095x R² = 0.9953
y = 0.0082x R² = 0.9946
y = 0.0068x R² = 0.9941
y = 0.0058x R² = 0.993
y = 0.0047x R² = 0.9923
biennial at 55 year
biennial at 56 year
biennial at 57 year
biennial at 58 year
biennial at 59 year
biennial at 60 year
biennial at 61 year
biennial at 62 year
biennial at 63 year
biennial at 64 year
Total Effective Risk (case/1,000,000)
MGD(μGy)
y = 0.004x R² = 0.9909
y = 0.0031x R² = 0.99
y = 0.0027x R² = 0.9882
y = 0.002x R² = 0.9871
y = 0.0018x R² = 0.9852
y = 0.0013x R² = 0.9842
y = 0.0012x R² = 0.9828
y = 0.0008x R² = 0.9825
y = 0.0007x R² = 0.9821
y = 0.0004x R² = 0.9831
biennial at 65 year
biennial at 66 year
biennial at 67 year
biennial at 68 year
biennial at 69 year
biennial at 70 year
biennial at 71 year
biennial at 72 year
biennial at 73 year
biennial at 74 year
Total Effective Risk (case/1,000,000)
MGD (μGy)
y = 0.1933x R² = 0.9991
y = 0.1815x R² = 0.9991
y = 0.17x R² = 0.9991
y = 0.1587x R² = 0.9991
y = 0.1486x R² = 0.999
y = 0.1389x R² = 0.999
y = 0.1293x R² = 0.999
y = 0.1211x R² = 0.999
y = 0.1132x R² = 0.999
y = 0.1053x R² = 0.9989
triennial at 25 year
triennial at 26 year
triennial at 27 year
triennial at 28 year
triennial at 29 year
triennial at 30 year
triennial at 31 year
triennial at 32 year
triennial at 33 year
triennial at 34 year

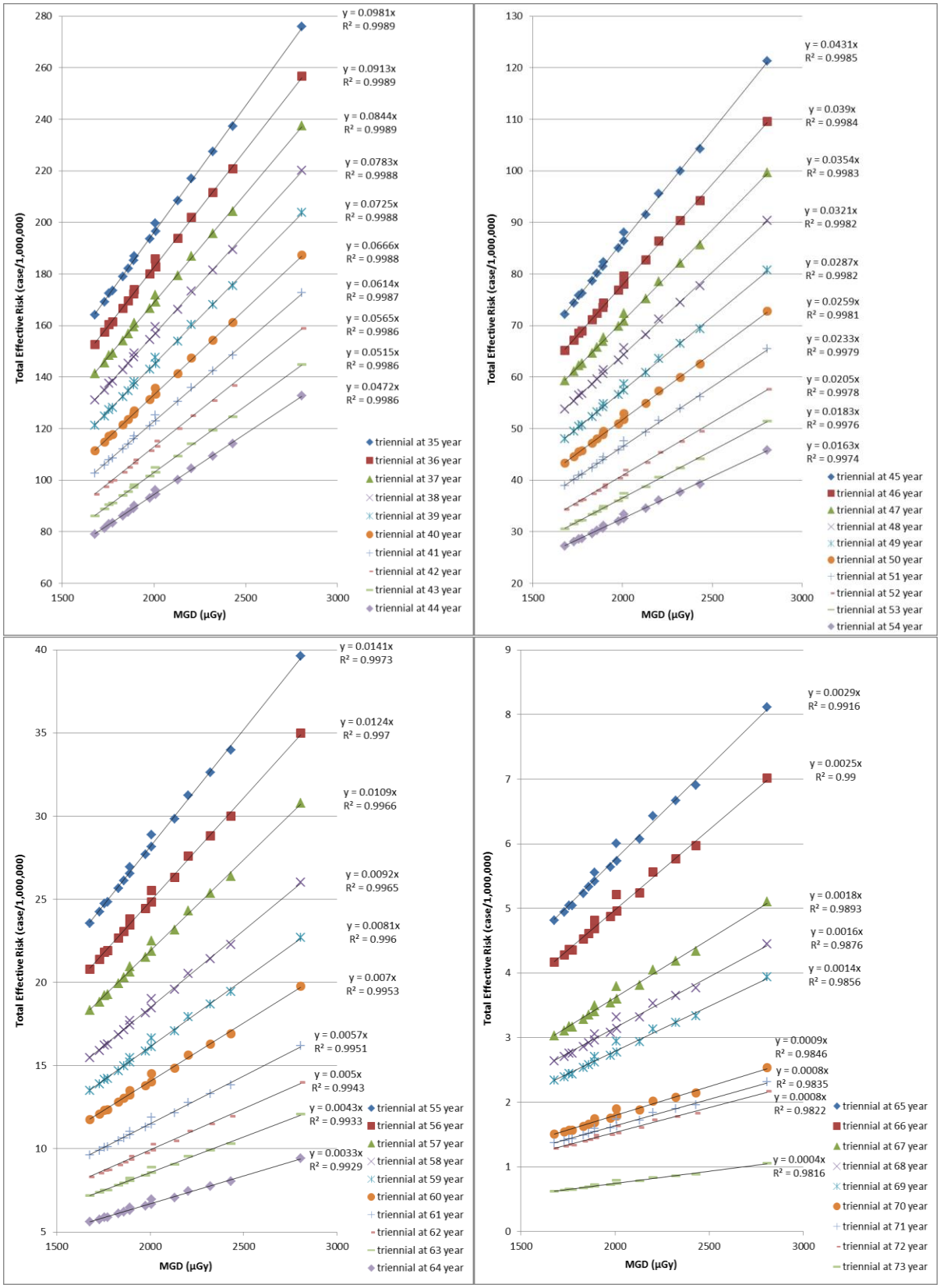
Total Effective Risk (case/1,000,000)
MGD (µGy)
y = 0.0981x R² = 0.9989
y = 0.0913x R² = 0.9989
y = 0.0844x R² = 0.9989
y = 0.0783x R² = 0.9988
y = 0.0725x R² = 0.9988
y = 0.0666x R² = 0.9988
y = 0.0614x R² = 0.9987
y = 0.0565x R² = 0.9986
y = 0.0515x R² = 0.9986
y = 0.0472x R² = 0.9986
triennial at 35 year
triennial at 36 year
triennial at 37 year
triennial at 38 year
triennial at 39 year
triennial at 40 year
triennial at 41 year
triennial at 42 year
triennial at 43 year
triennial at 44 year
y = 0.0431x R² = 0.9985
y = 0.039x R² = 0.9984
y = 0.0354x R² = 0.9983
y = 0.0321x R² = 0.9982
y = 0.0287x R² = 0.9982
y = 0.0259x R² = 0.9981
y = 0.0233x R² = 0.9979
y = 0.0205x R² = 0.9978
y = 0.0183x R² = 0.9976
y = 0.0163x R² = 0.9974
triennial at 45 year
triennial at 46 year
triennial at 47 year
triennial at 48 year
triennial at 49 year
triennial at 50 year
triennial at 51 year
triennial at 52 year
triennial at 53 year
triennial at 54 year
y = 0.0141x R² = 0.9973
y = 0.0124x R² = 0.997
y = 0.0109x R² = 0.9966
y = 0.0092x R² = 0.9965
y = 0.0081x R² = 0.996
y = 0.007x R² = 0.9953
y = 0.0057x R² = 0.9951
y = 0.005x R² = 0.9943
y = 0.0043x R² = 0.9933
y = 0.0033x R² = 0.9929
triennial at 55 year
triennial at 56 year
triennial at 57 year
triennial at 58 year
triennial at 59 year
triennial at 60 year
triennial at 61 year
triennial at 62 year
triennial at 63 year
triennial at 64 year
y = 0.0029x R² = 0.9916
y = 0.0025x R² = 0.99
y = 0.0018x R² = 0.9893
y = 0.0016x R² = 0.9876
y = 0.0014x R² = 0.9856
y = 0.0009x R² = 0.9846
y = 0.0008x R² = 0.9835
y = 0.0008x R² = 0.9822
y = 0.0004x R² = 0.9816
triennial at 65 year
triennial at 66 year
triennial at 67 year
triennial at 68 year
triennial at 69 year
triennial at 70 year
triennial at 71 year
triennial at 72 year
triennial at 73 year

Second LAR Extrapolation Method

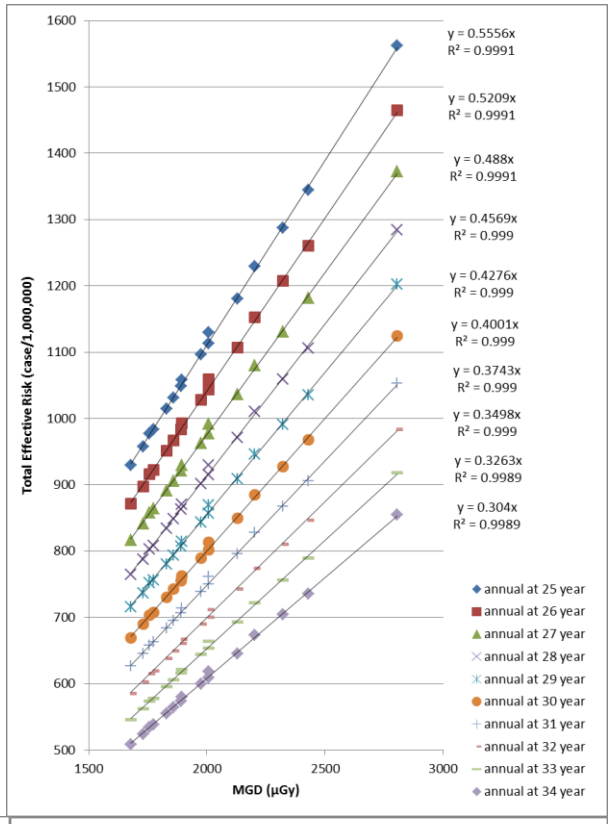

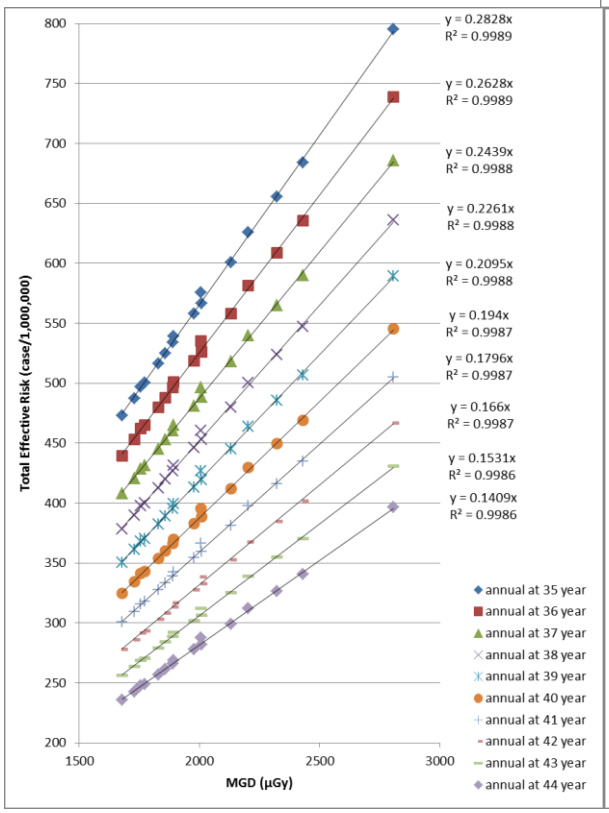

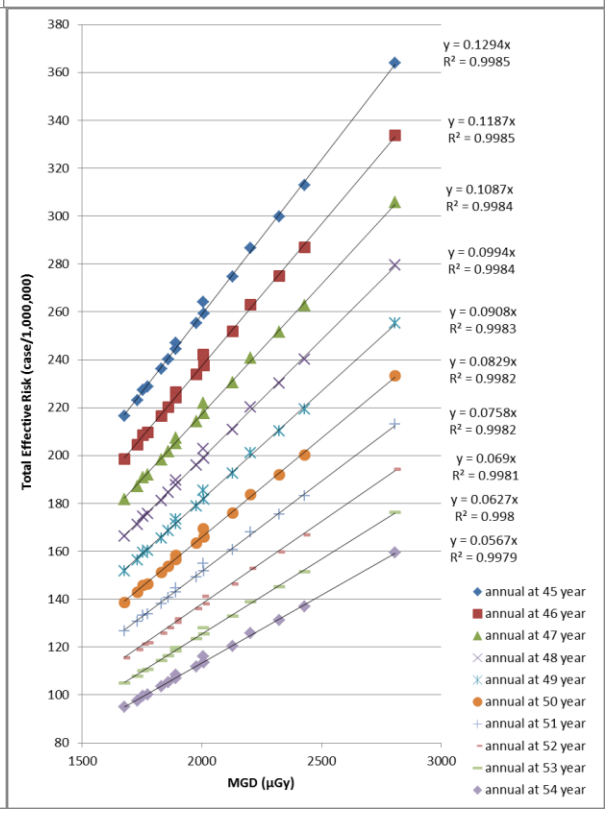

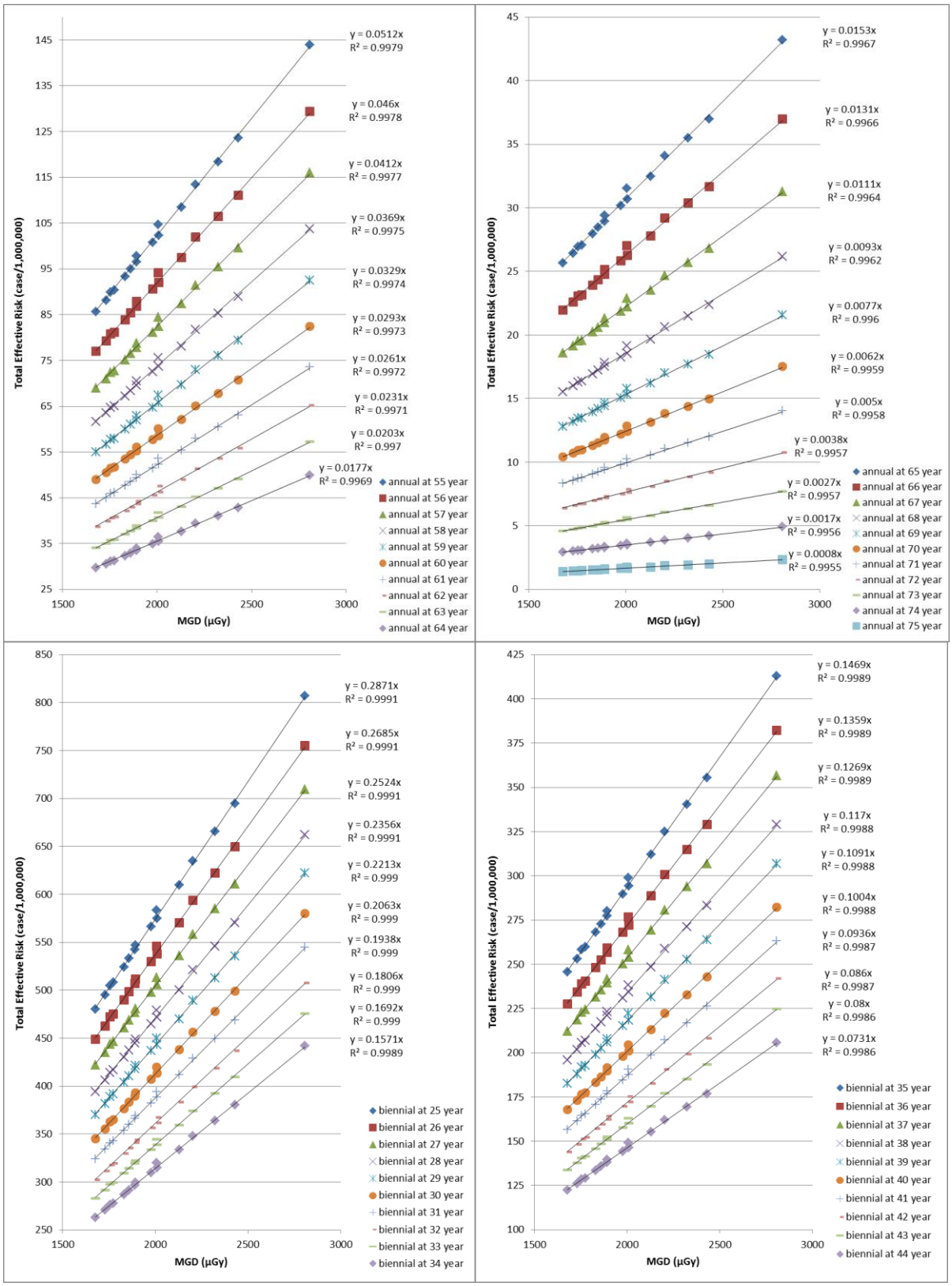
Total Effective Risk (case/1,000,000)
MGD (µGy)
y = 0.0512x R² = 0.9979
y = 0.046x R² = 0.9978
y = 0.0412x R² = 0.9977
y = 0.0369x R² = 0.9975
y = 0.0329x R² = 0.9974
y = 0.0293x R² = 0.9973
y = 0.0261x R² = 0.9972
y = 0.0231x R² = 0.9971
y = 0.0203x R² = 0.997
y = 0.0177x R² = 0.9969
annual at 55 year
annual at 56 year
annual at 57 year
annual at 58 year
annual at 59 year
annual at 60 year
annual at 61 year
annual at 62 year
annual at 63 year
annual at 64 year
y = 0.0153x R² = 0.9967
y = 0.0131x R² = 0.9966
y = 0.0111x R² = 0.9964
y = 0.0093x R² = 0.9962
y = 0.0077x R² = 0.996
y = 0.0062x R² = 0.9959
y = 0.005x R² = 0.9958
y = 0.0038x R² = 0.9957
y = 0.0027x R² = 0.9957
y = 0.0017x R² = 0.9956
y = 0.0008x R² = 0.9955
annual at 65 year
annual at 66 year
annual at 67 year
annual at 68 year
annual at 69 year
annual at 70 year
annual at 71 year
annual at 72 year
annual at 73 year
annual at 74 year
annual at 75 year
y = 0.2871x R² = 0.9991
y = 0.2685x R² = 0.9991
y = 0.2524x R² = 0.9991
y = 0.2356x R² = 0.9991
y = 0.2213x R² = 0.999
y = 0.2063x R² = 0.999
y = 0.1938x R² = 0.999
y = 0.1806x R² = 0.999
y = 0.1692x R² = 0.999
y = 0.1571x R² = 0.9989
biennial at 25 year
biennial at 26 year
biennial at 27 year
biennial at 28 year
biennial at 29 year
biennial at 30 year
biennial at 31 year
biennial at 32 year
biennial at 33 year
biennial at 34 year
y = 0.1469x R² = 0.9989
y = 0.1359x R² = 0.9989
y = 0.1269x R² = 0.9989
y = 0.117x R² = 0.9988
y = 0.1091x R² = 0.9988
y = 0.1004x R² = 0.9988
y = 0.0936x R² = 0.9987
y = 0.086x R² = 0.9987
y = 0.08x R² = 0.9986
y = 0.0731x R² = 0.9986
biennial at 35 year
biennial at 36 year
biennial at 37 year
biennial at 38 year
biennial at 39 year
biennial at 40 year
biennial at 41 year
biennial at 42 year
biennial at 43 year
biennial at 44 year

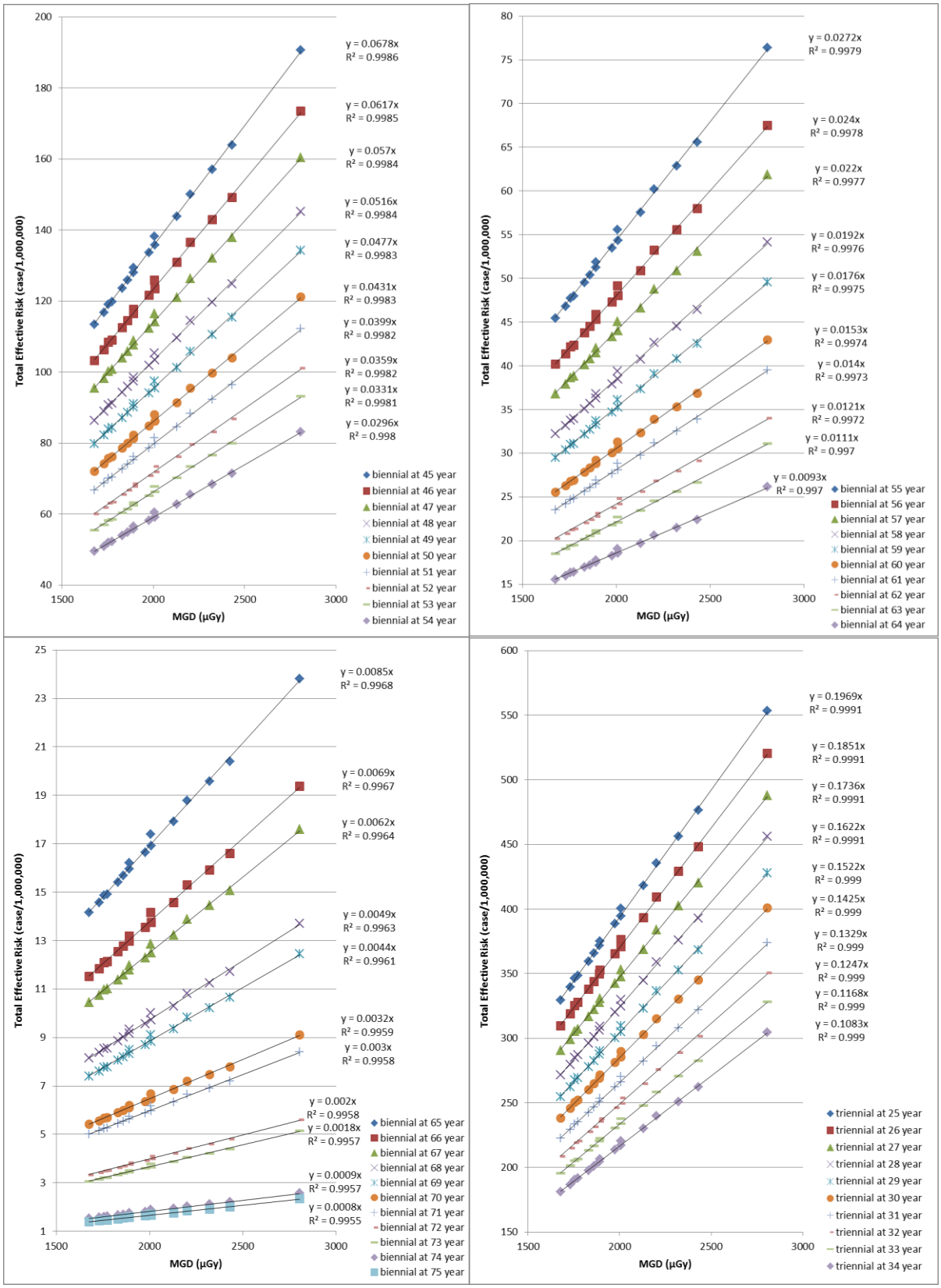
Total Effective Risk (case/1,000,000)
MGD (μGy)
y = 0.0678x R² = 0.9986
y = 0.0617x R² = 0.9985
y = 0.057x R² = 0.9984
y = 0.0516x R² = 0.9984
y = 0.0477x R² = 0.9983
y = 0.0431x R² = 0.9983
y = 0.0399x R² = 0.9982
y = 0.0359x R² = 0.9982
y = 0.0331x R² = 0.9981
y = 0.0296x R² = 0.998
biennial at 45 year
biennial at 46 year
biennial at 47 year
biennial at 48 year
biennial at 49 year
biennial at 50 year
biennial at 51 year
biennial at 52 year
biennial at 53 year
biennial at 54 year
y = 0.0272x R² = 0.9979
y = 0.024x R² = 0.9978
y = 0.022x R² = 0.9977
y = 0.0192x R² = 0.9976
y = 0.0176x R² = 0.9975
y = 0.0153x R² = 0.9974
y = 0.014x R² = 0.9973
y = 0.0121x R² = 0.9972
y = 0.0111x R² = 0.997
y = 0.0093x R² = 0.997
biennial at 55 year
biennial at 56 year
biennial at 57 year
biennial at 58 year
biennial at 59 year
biennial at 60 year
biennial at 61 year
biennial at 62 year
biennial at 63 year
biennial at 64 year
y = 0.0085x R² = 0.9968
y = 0.0069x R² = 0.9967
y = 0.0062x R² = 0.9964
y = 0.0049x R² = 0.9963
y = 0.0044x R² = 0.9961
y = 0.0032x R² = 0.9959
y = 0.003x R² = 0.9958
y = 0.002x R² = 0.9958
y = 0.0018x R² = 0.9957
y = 0.0009x R² = 0.9957
y = 0.0008x R² = 0.9955
biennial at 65 year
biennial at 66 year
biennial at 67 year
biennial at 68 year
biennial at 69 year
biennial at 70 year
biennial at 71 year
biennial at 72 year
biennial at 73 year
biennial at 74 year
biennial at 75 year
y = 0.1969x R² = 0.9991
y = 0.1851x R² = 0.9991
y = 0.1736x R² = 0.9991
y = 0.1622x R² = 0.9991
y = 0.1522x R² = 0.999
y = 0.1425x R² = 0.999
y = 0.1329x R² = 0.999
y = 0.1247x R² = 0.999
y = 0.1168x R² = 0.999
y = 0.1083x R² = 0.999
triennial at 25 year
triennial at 26 year
triennial at 27 year
triennial at 28 year
triennial at 29 year
triennial at 30 year
triennial at 31 year
triennial at 32 year
triennial at 33 year
triennial at 34 year

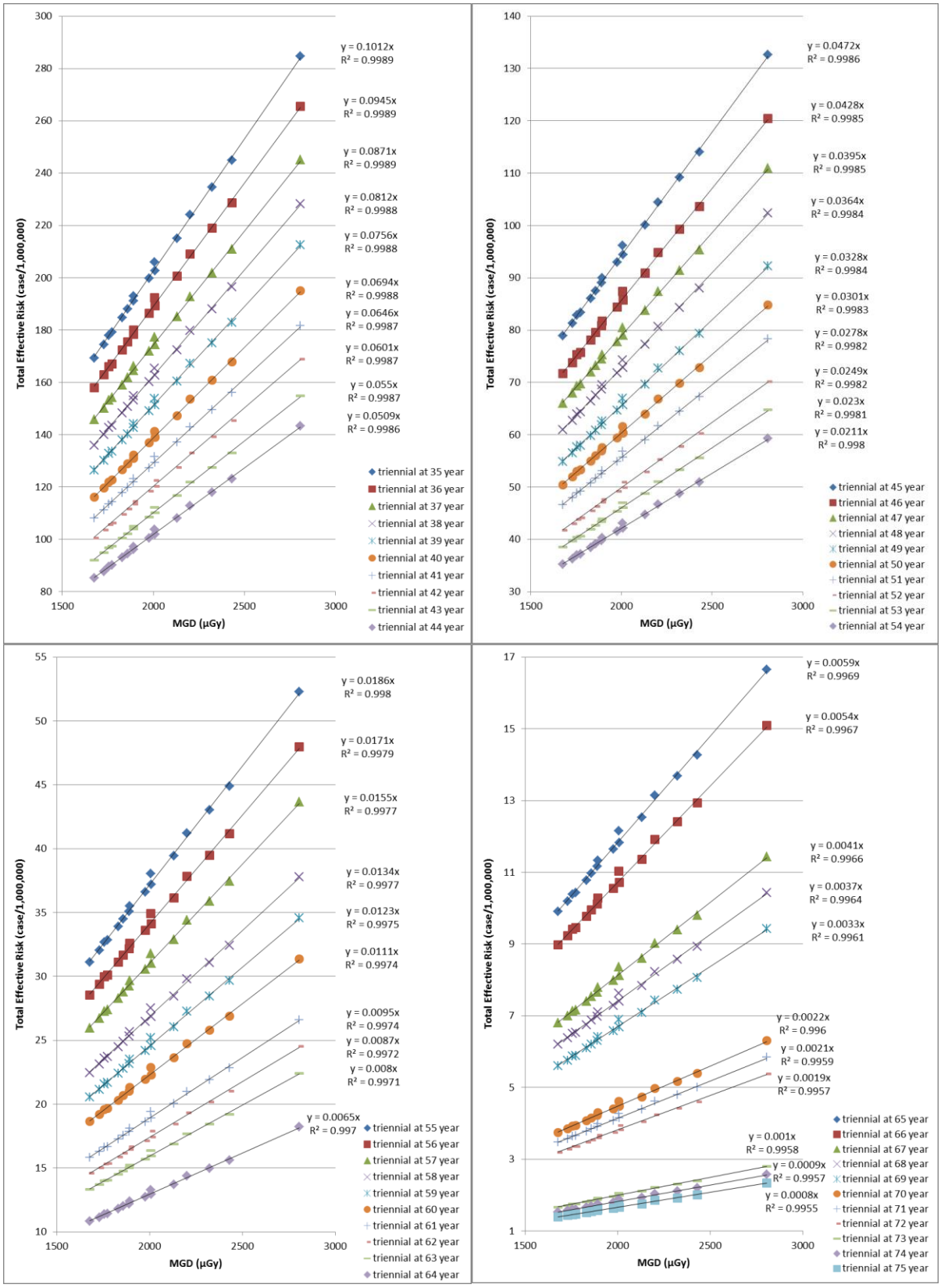
Total Effective Risk (case/1,000,000)
MGD (µGy)
y = 0.1012x R² = 0.9989
y = 0.0945x R² = 0.9989
y = 0.0871x R² = 0.9989
y = 0.0812x R² = 0.9988
y = 0.0756x R² = 0.9988
y = 0.0694x R² = 0.9988
y = 0.0646x R² = 0.9987
y = 0.0601x R² = 0.9987
y = 0.055x R² = 0.9987
y = 0.0509x R² = 0.9986
triennial at 35 year
triennial at 36 year
triennial at 37 year
triennial at 38 year
triennial at 39 year
triennial at 40 year
triennial at 41 year
triennial at 42 year
triennial at 43 year
triennial at 44 year
y = 0.0472x R² = 0.9986
y = 0.0428x R² = 0.9985
y = 0.0395x R² = 0.9985
y = 0.0364x R² = 0.9984
y = 0.0328x R² = 0.9984
y = 0.0301x R² = 0.9983
y = 0.0278x R² = 0.9982
y = 0.0249x R² = 0.9982
y = 0.023x R² = 0.9981
y = 0.0211x R² = 0.998
triennial at 45 year
triennial at 46 year
triennial at 47 year
triennial at 48 year
triennial at 49 year
triennial at 50 year
triennial at 51 year
triennial at 52 year
triennial at 53 year
triennial at 54 year
y = 0.0186x R² = 0.998
y = 0.0171x R² = 0.9979
y = 0.0155x R² = 0.9977
y = 0.0134x R² = 0.9977
y = 0.0123x R² = 0.9975
y = 0.0111x R² = 0.9974
y = 0.0095x R² = 0.9974
y = 0.0087x R² = 0.9972
y = 0.008x R² = 0.9971
y = 0.0065x R² = 0.997
triennial at 55 year
triennial at 56 year
triennial at 57 year
triennial at 58 year
triennial at 59 year
triennial at 60 year
triennial at 61 year
triennial at 62 year
triennial at 63 year
triennial at 64 year
y = 0.0059x R² = 0.9969
y = 0.0054x R² = 0.9967
y = 0.0041x R² = 0.9966
y = 0.0037x R² = 0.9964
y = 0.0033x R² = 0.9961
y = 0.0022x R² = 0.996
y = 0.0021x R² = 0.9959
y = 0.0019x R² = 0.9957
y = 0.001x R² = 0.9958
y = 0.0009x R² = 0.9957
y = 0.0008x R² = 0.9955
triennial at 65 year
triennial at 66 year
triennial at 67 year
triennial at 68 year
triennial at 69 year
triennial at 70 year
triennial at 71 year
triennial at 72 year
triennial at 73 year
triennial at 74 year
triennial at 75 year

Third LAR Extrapolation Method

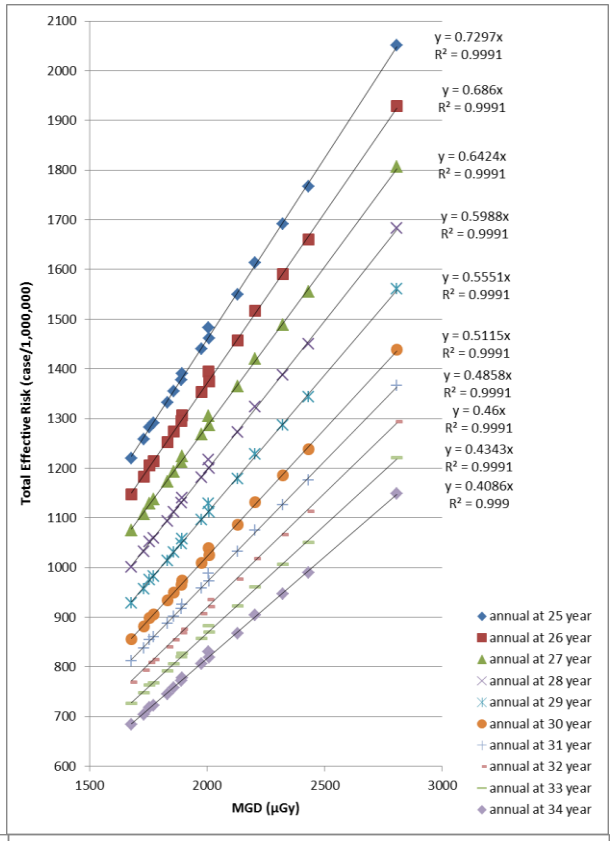

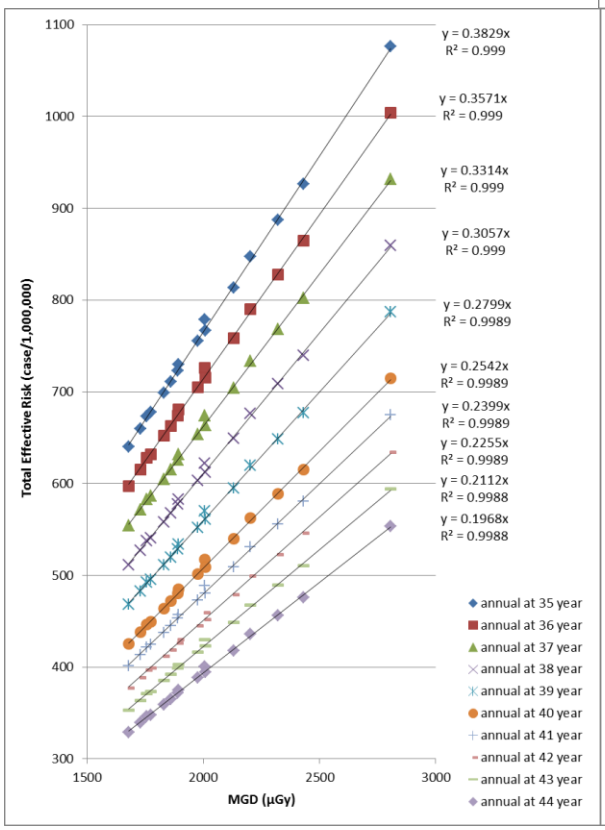

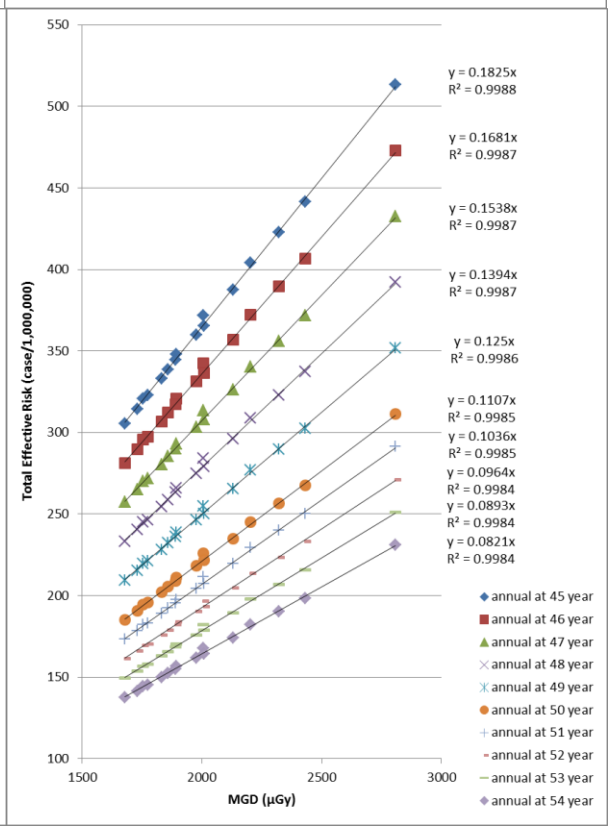

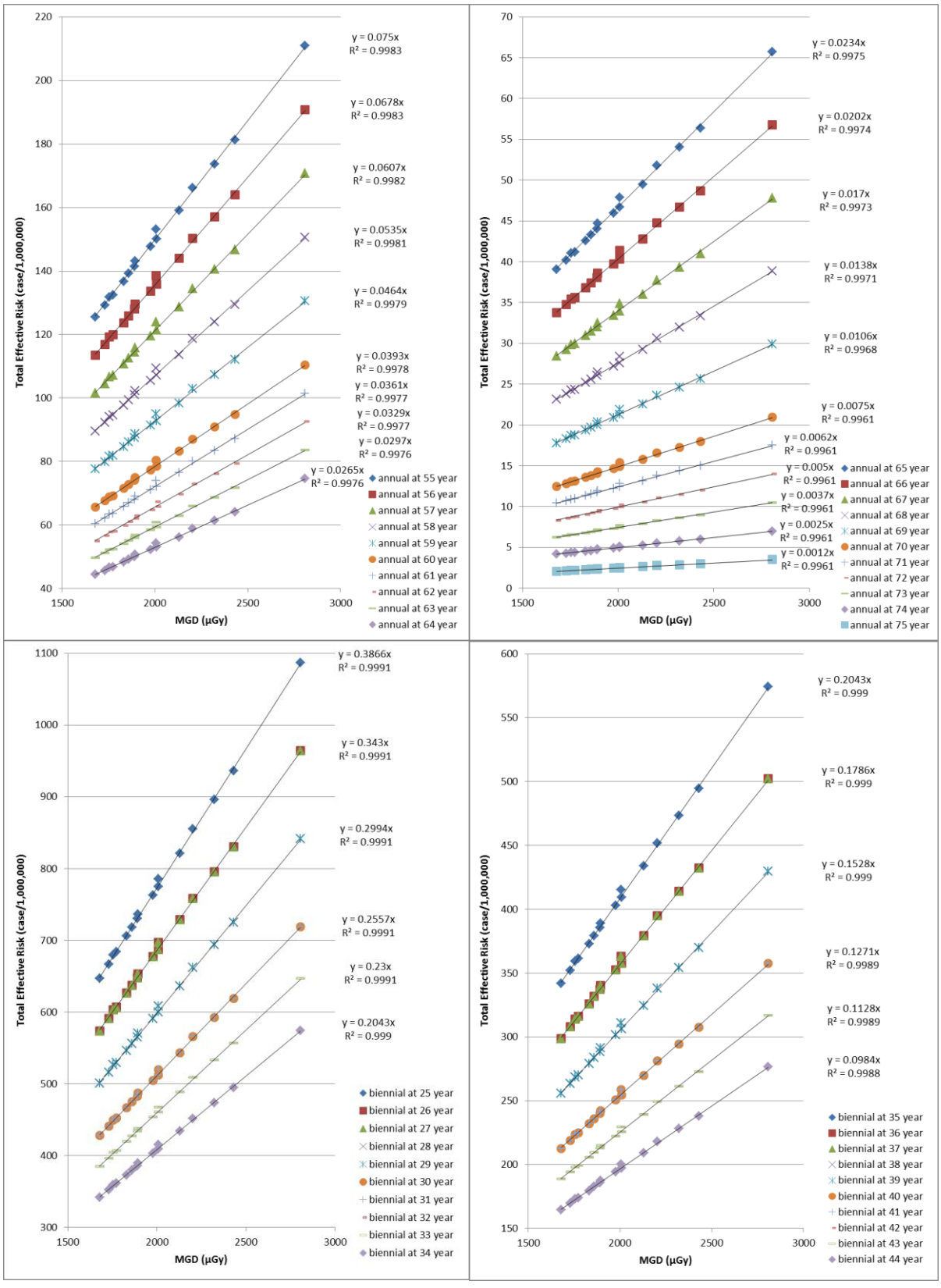
Total Effective Risk (case/1,000,000)
MGD (µGy)
y = 0.075x R² = 0.9983
y = 0.0678x R² = 0.9983
y = 0.0607x R² = 0.9982
y = 0.0535x R² = 0.9981
y = 0.0464x R² = 0.9979
y = 0.0393x R² = 0.9978
y = 0.0361x R² = 0.9977
y = 0.0329x R² = 0.9977
y = 0.0297x R² = 0.9976
y = 0.0265x R² = 0.9976
annual at 55 year
annual at 56 year
annual at 57 year
annual at 58 year
annual at 59 year
annual at 60 year
annual at 61 year
annual at 62 year
annual at 63 year
annual at 64 year
y = 0.0234x R² = 0.9975
y = 0.0202x R² = 0.9974
y = 0.017x R² = 0.9973
y = 0.0138x R² = 0.9971
y = 0.0106x R² = 0.9968
y = 0.0075x R² = 0.9961
y = 0.0062x R² = 0.9961
y = 0.005x R² = 0.9961
y = 0.0037x R² = 0.9961
y = 0.0025x R² = 0.9961
y = 0.0012x R² = 0.9961
annual at 65 year
annual at 66 year
annual at 67 year
annual at 68 year
annual at 69 year
annual at 70 year
annual at 71 year
annual at 72 year
annual at 73 year
annual at 74 year
annual at 75 year
y = 0.3866x R² = 0.9991
y = 0.343x R² = 0.9991
y = 0.2994x R² = 0.9991
y = 0.2557x R² = 0.9991
y = 0.23x R² = 0.9991
y = 0.2043x R² = 0.999
biennial at 25 year
biennial at 26 year
biennial at 27 year
biennial at 28 year
biennial at 29 year
biennial at 30 year
biennial at 31 year
biennial at 32 year
biennial at 33 year
biennial at 34 year
y = 0.2043x R² = 0.999
y = 0.1786x R² = 0.999
y = 0.1528x R² = 0.999
y = 0.1271x R² = 0.9989
y = 0.1128x R² = 0.9989
y = 0.0984x R² = 0.9988
biennial at 35 year
biennial at 36 year
biennial at 37 year
biennial at 38 year
biennial at 39 year
biennial at 40 year
biennial at 41 year
biennial at 42 year
biennial at 43 year
biennial at 44 year

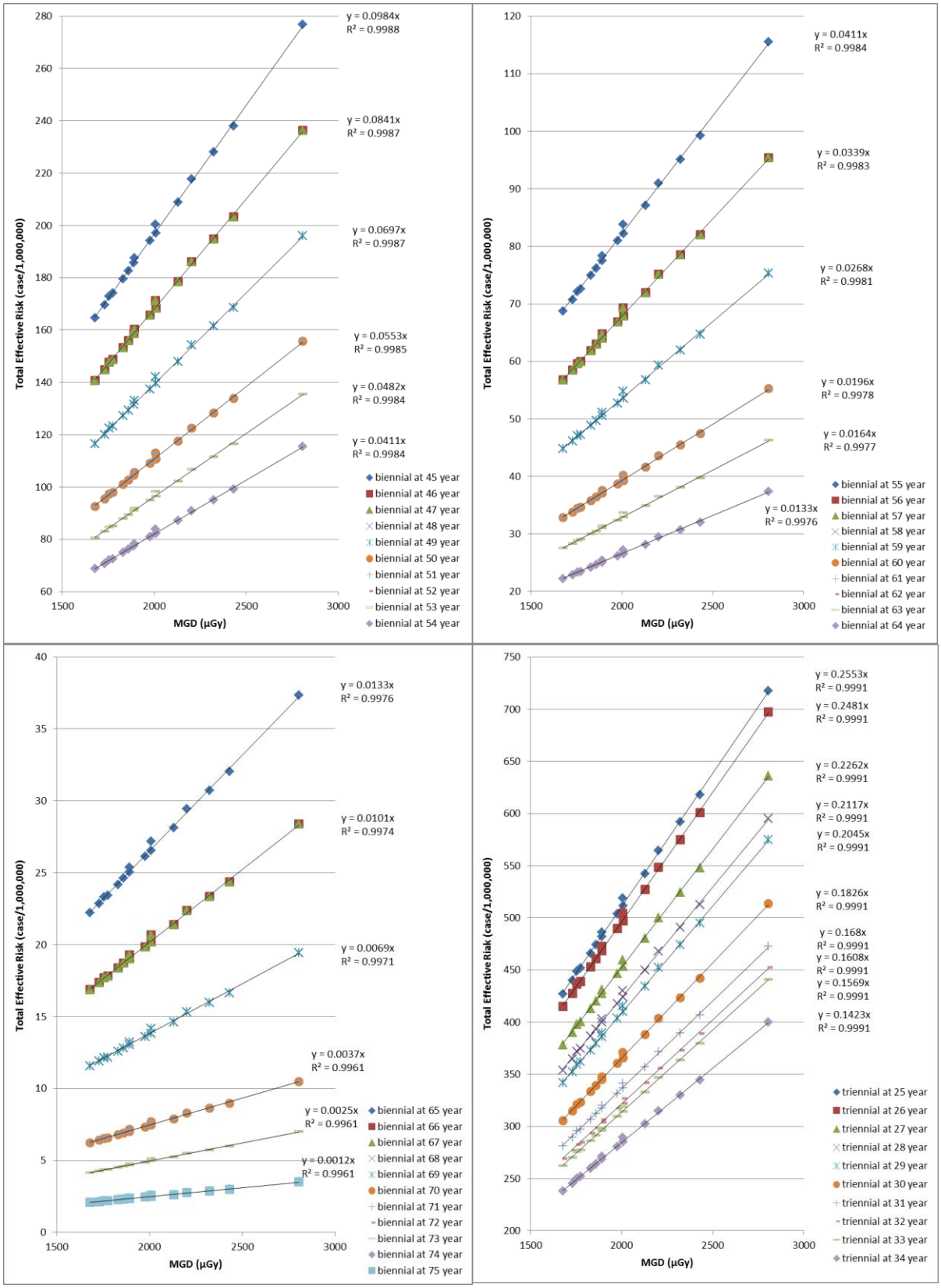
Total Effective Risk (case/1,000,000)
MGD (µGy)
y = 0.0984x R² = 0.9988
y = 0.0841x R² = 0.9987
y = 0.0697x R² = 0.9987
y = 0.0553x R² = 0.9985
y = 0.0482x R² = 0.9984
y = 0.0411x R² = 0.9984
biennial at 45 year
biennial at 46 year
biennial at 47 year
biennial at 48 year
biennial at 49 year
biennial at 50 year
biennial at 51 year
biennial at 52 year
biennial at 53 year
biennial at 54 year
y = 0.0411x R² = 0.9984
y = 0.0339x R² = 0.9983
y = 0.0268x R² = 0.9981
y = 0.0196x R² = 0.9978
y = 0.0164x R² = 0.9977
y = 0.0133x R² = 0.9976
biennial at 55 year
biennial at 56 year
biennial at 57 year
biennial at 58 year
biennial at 59 year
biennial at 60 year
biennial at 61 year
biennial at 62 year
biennial at 63 year
biennial at 64 year
y = 0.0133x R² = 0.9976
y = 0.0101x R² = 0.9974
y = 0.0069x R² = 0.9971
y = 0.0037x R² = 0.9961
y = 0.0025x R² = 0.9961
y = 0.0012x R² = 0.9961
biennial at 65 year
biennial at 66 year
biennial at 67 year
biennial at 68 year
biennial at 69 year
biennial at 70 year
biennial at 71 year
biennial at 72 year
biennial at 73 year
biennial at 74 year
biennial at 75 year
y = 0.2553x R² = 0.9991
y = 0.2481x R² = 0.9991
y = 0.2262x R² = 0.9991
y = 0.2117x R² = 0.9991
y = 0.2045x R² = 0.9991
y = 0.1826x R² = 0.9991
y = 0.168x R² = 0.9991
y = 0.1608x R² = 0.9991
y = 0.1569x R² = 0.9991
y = 0.1423x R² = 0.9991
triennial at 25 year
triennial at 26 year
triennial at 27 year
triennial at 28 year
triennial at 29 year
triennial at 30 year
triennial at 31 year
triennial at 32 year
triennial at 33 year
triennial at 34 year

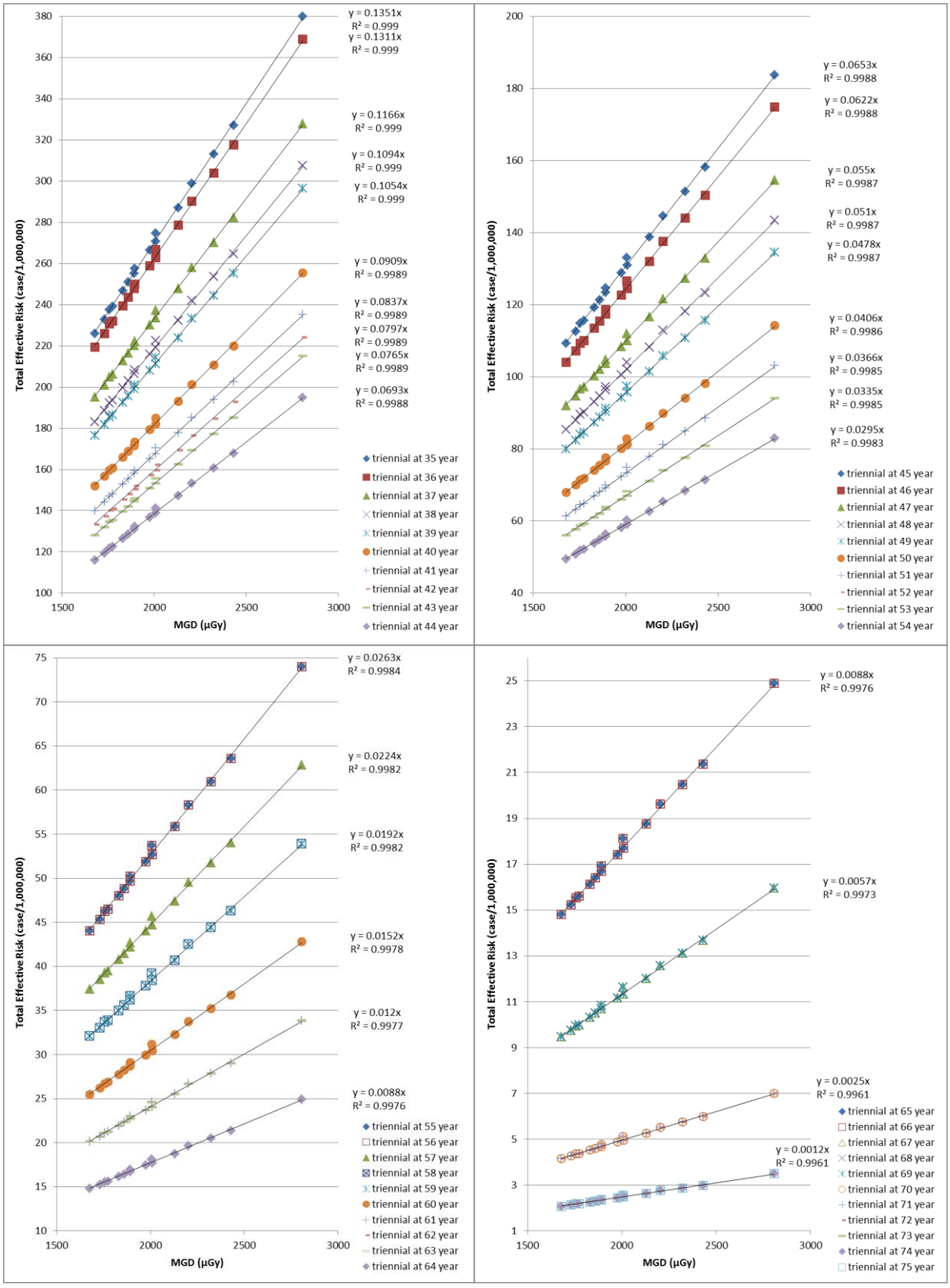
Total Effective Risk (case/1,000,000)
MGD (μGy)
y = 0.1351x R² = 0.999
y = 0.1311x R² = 0.999
y = 0.1166x R² = 0.999
y = 0.1094x R² = 0.999
y = 0.1054x R² = 0.999
y = 0.0909x R² = 0.9989
y = 0.0837x R² = 0.9989
y = 0.0797x R² = 0.9989
y = 0.0765x R² = 0.9989
y = 0.0693x R² = 0.9988
triennial at 35 year
triennial at 36 year
triennial at 37 year
triennial at 38 year
triennial at 39 year
triennial at 40 year
triennial at 41 year
triennial at 42 year
triennial at 43 year
triennial at 44 year
y = 0.0653x R² = 0.9988
y = 0.0622x R² = 0.9988
y = 0.055x R² = 0.9987
y = 0.051x R² = 0.9987
y = 0.0478x R² = 0.9987
y = 0.0406x R² = 0.9986
y = 0.0366x R² = 0.9985
y = 0.0335x R² = 0.9985
y = 0.0295x R² = 0.9983
triennial at 45 year
triennial at 46 year
triennial at 47 year
triennial at 48 year
triennial at 49 year
triennial at 50 year
triennial at 51 year
triennial at 52 year
triennial at 53 year
triennial at 54 year
y = 0.0263x R² = 0.9984
y = 0.0224x R² = 0.9982
y = 0.0192x R² = 0.9982
y = 0.0152x R² = 0.9978
y = 0.012x R² = 0.9977
y = 0.0088x R² = 0.9976
triennial at 55 year
triennial at 56 year
triennial at 57 year
triennial at 58 year
triennial at 59 year
triennial at 60 year
triennial at 61 year
triennial at 62 year
triennial at 63 year
triennial at 64 year
y = 0.0088x R² = 0.9976
y = 0.0057x R² = 0.9973
y = 0.0025x R² = 0.9961
y = 0.0012x R² = 0.9961
triennial at 65 year
triennial at 66 year
triennial at 67 year
triennial at 68 year
triennial at 69 year
triennial at 70 year
triennial at 71 year
triennial at 72 year
triennial at 73 year
triennial at 74 year
triennial at 75 year

<u>Appendix E:</u> Total effective risk of worldwide screening programmes resulted from the sixteen FFDM machines for the three LAR extrapolation methods.

Table (E-1) Presents the total effective risk of worldwide screening programmes resulted from FFDM machine 1 (visit 1) using the LAR extrapolated by the three methods.

Programme	Total effective risk (case/10^6)		
	Method 1	Method 2	Method 3
Australia, Japan, Korea, United State (AAFP, NCI, and USPSTF)	232.39	242.94	307.63
Belgium, Croatia, Cyprus, Denmark, Finland, Germany, Italy, Latvia, Lithuania, Luxembourg, Norway, Poland, Slovenia, Spain (Catalonia), Switzerland	85.61	96.31	124.89
Canada , France, Israel, Netherlands	88.71	104.12	133.89
China	147.29	145.03	190.86
Czech	163.53	176.93	238.13
Estonia	77.44	81.68	101.82
Hungary	142.69	148.87	213.75
Iceland	229.28	235.13	298.63
India	366.83	373.03	481.37
Ireland	81.15	87.50	109.51
Malta	50.60	51.87	69.15
New Zealand, Portugal, Spain (Navarra)	146.40	156.75	229.13
Nigeria	230.54	238.13	301.63
Sweden	270.81	279.99	374.13
United Kingdom	84.81	93.24	129.97
United State (ACOG)	311.98	339.32	441.52
United State (ACS, ACR, and NCCN)	446.43	469.41	615.26
Uruguay	306.02	324.30	423.52
Canada	366.83	373.03	481.37
United Kingdom	444.65	465.20	609.26
United State (ACS)	942.36	968.41	1238.23
United State (NCCN)	1318.88	1344.94	1766.52

Screening programmes designed for high breast cancer risk women are highlighted in grey.

Table (E-2) Presents the total effective risk of worldwide screening programmes resulted from FFDM machine 1 (visit 2) using the LAR extrapolated by the three methods.

Programme	Total effective risk (case/10^6)		
	Method 1	Method 2	Method 3
Australia, Japan, Korea, United State (AAFP, NCI, and USPSTF)	232.46	243.02	307.77
Belgium, Croatia, Cyprus, Denmark, Finland, Germany, Italy, Latvia, Lithuania, Luxembourg, Norway, Poland, Slovenia, Spain (Catalonia), Switzerland	85.60	96.32	124.91
Canada , France, Israel, Netherlands	88.69	104.11	133.90
China	147.37	145.11	190.98
Czech	163.55	176.97	238.22
Estonia	77.45	81.70	101.85
Hungary	142.73	148.91	213.86
Iceland	229.37	235.23	298.78
India	366.99	373.19	481.64
Ireland	81.16	87.51	109.54
Malta	50.61	51.89	69.18
New Zealand, Portugal, Spain (Navarra)	146.42	156.78	229.23
Nigeria	230.62	238.22	301.78
Sweden	270.91	280.10	374.32
United Kingdom	84.81	93.25	130.01
United State (ACOG)	312.02	339.39	441.67
United State (ACS, ACR, and NCCN)	446.56	469.56	615.54
Uruguay	306.09	324.40	423.69
Canada	366.99	373.19	481.64
United Kingdom	444.78	465.36	609.55
United State (ACS)	942.88	968.96	1239.03
United State (NCCN)	1319.72	1345.80	1767.76

Screening programmes designed for high breast cancer risk women are highlighted in grey.

Table (E-3) Presents the total effective risk of worldwide screening programmes resulted from FFDM machine 1 (visit 3) using the LAR extrapolated by the three methods.

Programme	Total effective risk (case/10^6)		
	Method 1	Method 2	Method 3
Australia, Japan, Korea, United State (AAFP, NCI, and USPSTF)	232.03	242.58	307.22
Belgium, Croatia, Cyprus, Denmark, Finland, Germany, Italy, Latvia, Lithuania, Luxembourg, Norway, Poland, Slovenia, Spain (Catalonia), Switzerland	85.43	96.13	124.68
Canada , France, Israel, Netherlands	88.51	103.91	133.65
China	147.11	144.85	190.65
Czech	163.23	176.64	237.79
Estonia	77.30	81.54	101.66
Hungary	142.46	148.64	213.48
Iceland	228.95	234.80	298.25
India	366.33	372.52	480.79
Ireland	81.00	87.34	109.33
Malta	50.51	51.79	69.05
New Zealand, Portugal, Spain (Navarra)	146.14	156.49	228.82
Nigeria	230.20	237.79	301.24
Sweden	270.42	279.59	373.66
United Kingdom	84.64	93.07	129.77
United State (ACOG)	311.43	338.75	440.87
United State (ACS, ACR, and NCCN)	445.73	468.70	614.44
Uruguay	305.52	323.79	422.93
Canada	366.33	372.52	480.79
United Kingdom	443.96	464.50	608.46
United State (ACS)	941.23	967.27	1236.91
United State (NCCN)	1317.45	1343.49	1764.75

Screening programmes designed for high breast cancer risk women are highlighted in grey.

Table (E-4) Presents the total effective risk of worldwide screening programmes resulted from FFDM machine 2 (visit 1) using the LAR extrapolated by the three methods.

Programme	Total effective risk (case/10^6)		
	Method 1	Method 2	Method 3
Australia, Japan, Korea, United State (AAFP, NCI, and USPSTF)	222.83	232.77	294.74
Belgium, Croatia, Cyprus, Denmark, Finland, Germany, Italy, Latvia, Lithuania, Luxembourg, Norway, Poland, Slovenia, Spain (Catalonia), Switzerland	82.14	92.30	119.67
Canada , France, Israel, Netherlands	85.15	99.78	128.30
China	141.17	138.95	182.84
Czech	156.84	169.54	228.16
Estonia	74.28	78.27	97.56
Hungary	136.83	142.64	204.79
Iceland	219.82	225.28	286.10
India	351.67	357.40	461.17
Ireland	77.84	83.85	104.93
Malta	48.52	49.71	66.25
New Zealand, Portugal, Spain (Navarra)	140.40	150.19	219.53
Nigeria	221.04	228.16	288.98
Sweden	259.65	268.27	358.43
United Kingdom	81.35	89.34	124.53
United State (ACOG)	299.24	325.14	423.04
United State (ACS, ACR, and NCCN)	428.08	449.77	589.47
Uruguay	293.46	310.74	405.77
Canada	351.67	357.40	461.17
United Kingdom	426.35	445.73	583.72
United State (ACS)	903.19	927.77	1186.22
United State (NCCN)	1263.88	1288.45	1692.29

Screening programmes designed for high breast cancer risk women are highlighted in grey.

Table (E-5) Presents the total effective risk of worldwide screening programmes resulted from FFDM machine 2 (visit 2) using the LAR extrapolated by the three methods.

Programme	Total effective risk (case/10^6)		
	Method 1	Method 2	Method 3
Australia, Japan, Korea, United State (AAFP, NCI, and USPSTF)	222.53	232.54	294.46
Belgium, Croatia, Cyprus, Denmark, Finland, Germany, Italy, Latvia, Lithuania, Luxembourg, Norway, Poland, Slovenia, Spain (Catalonia), Switzerland	81.99	92.18	119.54
Canada , France, Israel, Netherlands	84.98	99.66	128.15
China	141.02	138.82	182.69
Czech	156.60	169.36	227.94
Estonia	74.16	78.18	97.46
Hungary	136.64	142.49	204.60
Iceland	219.54	225.06	285.84
India	351.24	357.06	460.77
Ireland	77.72	83.75	104.82
Malta	48.45	49.65	66.19
New Zealand, Portugal, Spain (Navarra)	140.19	150.03	219.32
Nigeria	220.75	227.94	288.72
Sweden	259.31	268.00	358.11
United Kingdom	81.22	89.24	124.40
United State (ACOG)	298.78	324.78	422.61
United State (ACS, ACR, and NCCN)	427.49	449.30	588.92
Uruguay	293.04	310.41	405.38
Canada	351.24	357.06	460.77
United Kingdom	425.78	445.28	583.17
United State (ACS)	902.25	926.98	1185.27
United State (NCCN)	1262.71	1287.42	1691.01

Screening programmes designed for high breast cancer risk women are highlighted in grey.

Table (E-6) Presents the total effective risk of worldwide screening programmes resulted from FFDM machine 2 (visit 3) using the LAR extrapolated by the three methods.

Programme	Total effective risk (case/10^6)		
	Method 1	Method 2	Method 3
Australia, Japan, Korea, United State (AAFP, NCI, and USPSTF)	222.52	232.52	294.44
Belgium, Croatia, Cyprus, Denmark, Finland, Germany, Italy, Latvia, Lithuania, Luxembourg, Norway, Poland, Slovenia, Spain (Catalonia), Switzerland	82.00	92.19	119.53
Canada , France, Israel, Netherlands	84.99	99.66	128.15
China	141.01	138.81	182.67
Czech	156.61	169.35	227.92
Estonia	74.17	78.18	97.45
Hungary	136.64	142.49	204.58
Iceland	219.54	225.05	285.82
India	351.23	357.03	460.72
Ireland	77.72	83.75	104.81
Malta	48.45	49.65	66.18
New Zealand, Portugal, Spain (Navarra)	140.20	150.03	219.30
Nigeria	220.75	227.92	288.69
Sweden	259.31	267.99	358.08
United Kingdom	81.22	89.24	124.40
United State (ACOG)	298.79	324.78	422.59
United State (ACS, ACR, and NCCN)	427.49	449.28	588.87
Uruguay	293.05	310.40	405.35
Canada	351.23	357.03	460.72
United Kingdom	425.78	445.25	583.13
United State (ACS)	902.16	926.86	1185.10
United State (NCCN)	1262.53	1287.22	1690.70

Screening programmes designed for high breast cancer risk women are highlighted in grey.

Table (E-7) Presents the total effective risk of worldwide screening programmes resulted from FFDM machine 3 using the LAR extrapolated by the three methods.

Programme	Total effective risk (case/10^6)		
	Method 1	Method 2	Method 3
Australia, Japan, Korea, United State (AAFP, NCI, and USPSTF)	195.69	204.51	258.73
Belgium, Croatia, Cyprus, Denmark, Finland, Germany, Italy, Latvia, Lithuania, Luxembourg, Norway, Poland, Slovenia, Spain (Catalonia), Switzerland	72.32	81.27	105.24
Canada , France, Israel, Netherlands	75.06	87.94	112.92
China	123.80	121.91	160.28
Czech	137.90	149.11	200.41
Estonia	65.31	68.86	85.73
Hungary	120.20	125.37	179.72
Iceland	192.95	197.85	251.05
India	308.60	313.78	404.54
Ireland	68.47	73.78	92.23
Malta	42.63	43.70	58.18
New Zealand, Portugal, Spain (Navarra)	123.41	132.07	192.72
Nigeria	194.06	200.41	253.61
Sweden	227.94	235.62	314.49
United Kingdom	71.57	78.62	109.41
United State (ACOG)	263.10	285.96	371.65
United State (ACS, ACR, and NCCN)	376.01	395.22	517.46
Uruguay	257.83	273.13	356.29
Canada	308.60	313.78	404.54
United Kingdom	374.43	391.62	512.34
United State (ACS)	791.90	813.69	1039.71
United State (NCCN)	1107.57	1129.35	1482.64

Screening programmes designed for high breast cancer risk women are highlighted in grey.

Table (E-8) Presents the total effective risk of worldwide screening programmes resulted from FFDM machine 4 using the LAR extrapolated by the three methods.

Programme	Total effective risk (case/10^6)		
	Method 1	Method 2	Method 3
Australia, Japan, Korea, United State (AAFP, NCI, and USPSTF)	183.14	191.43	242.27
Belgium, Croatia, Cyprus, Denmark, Finland, Germany, Italy, Latvia, Lithuania, Luxembourg, Norway, Poland, Slovenia, Spain (Catalonia), Switzerland	67.59	75.99	98.46
Canada , France, Israel, Netherlands	70.11	82.20	105.61
China	115.95	114.18	150.18
Czech	128.98	139.51	187.61
Estonia	61.08	64.41	80.24
Hungary	112.48	117.33	168.30
Iceland	180.63	185.22	235.12
India	288.93	293.80	378.92
Ireland	64.03	69.01	86.31
Malta	39.89	40.89	54.47
New Zealand, Portugal, Spain (Navarra)	115.45	123.57	180.46
Nigeria	181.64	191.43	237.50
Sweden	213.37	220.57	294.55
United Kingdom	66.92	73.54	102.41
United State (ACOG)	246.08	267.53	347.88
United State (ACS, ACR, and NCCN)	351.86	369.90	484.54
Uruguay	241.25	255.60	333.58
Canada	288.93	293.80	378.92
United Kingdom	350.42	366.56	479.77
United State (ACS)	741.78	762.24	974.26
United State (NCCN)	1037.79	1058.26	1389.62

Screening programmes designed for high breast cancer risk women are highlighted in grey.

Table (E-9) Presents the total effective risk of worldwide screening programmes resulted from FFDM machine 5 using the LAR extrapolated by the three methods.

Programme	Total effective risk (case/10^6)		
	Method 1	Method 2	Method 3
Australia, Japan, Korea, United State (AAFP, NCI, and USPSTF)	192.31	201.04	254.57
Belgium, Croatia, Cyprus, Denmark, Finland, Germany, Italy, Latvia, Lithuania, Luxembourg, Norway, Poland, Slovenia, Spain (Catalonia), Switzerland	70.85	79.71	103.35
Canada , France, Israel, Netherlands	73.42	86.17	110.80
China	121.89	120.02	157.93
Czech	135.33	146.42	197.06
Estonia	64.09	67.60	84.26
Hungary	118.08	123.20	176.89
Iceland	189.74	194.58	247.12
India	303.57	308.69	398.34
Ireland	67.16	72.41	90.62
Malta	41.87	42.93	57.22
New Zealand, Portugal, Spain (Navarra)	121.15	129.72	189.61
Nigeria	190.78	197.06	249.61
Sweden	224.11	231.70	309.60
United Kingdom	70.18	77.16	107.55
United State (ACOG)	258.18	280.80	365.37
United State (ACS, ACR, and NCCN)	369.44	388.45	509.14
Uruguay	253.25	268.37	350.47
Canada	303.57	308.69	398.34
United Kingdom	367.97	384.97	504.18
United State (ACS)	779.81	801.37	1024.63
United State (NCCN)	1091.37	1112.92	1461.75

Screening programmes designed for high breast cancer risk women are highlighted in grey.

Table (E-10) Presents the total effective risk of worldwide screening programmes resulted from FFDM machine 6 using the LAR extrapolated by the three methods.

Programme	Total effective risk (case/10^6)		
	Method 1	Method 2	Method 3
Australia, Japan, Korea, United State (AAFP, NCI, and USPSTF)	169.83	177.55	224.85
Belgium, Croatia, Cyprus, Denmark, Finland, Germany, Italy, Latvia, Lithuania, Luxembourg, Norway, Poland, Slovenia, Spain (Catalonia), Switzerland	62.54	70.37	91.26
Canada , France, Israel, Netherlands	64.80	76.07	97.83
China	107.67	106.01	139.53
Czech	119.49	129.30	174.04
Estonia	56.59	59.69	74.41
Hungary	104.28	108.80	156.24
Iceland	167.58	171.86	218.29
India	268.12	272.65	351.88
Ireland	59.29	63.93	80.03
Malta	36.97	37.91	50.54
New Zealand, Portugal, Spain (Navarra)	106.97	114.55	167.48
Nigeria	168.49	174.04	220.48
Sweden	197.93	204.64	273.48
United Kingdom	61.96	68.13	94.99
United State (ACOG)	227.96	247.96	322.68
United State (ACS, ACR, and NCCN)	326.25	343.06	449.71
Uruguay	223.63	237.00	309.55
Canada	268.12	272.65	351.88
United Kingdom	324.96	339.99	445.33
United State (ACS)	688.87	707.92	905.24
United State (NCCN)	964.19	983.25	1291.53

Screening programmes designed for high breast cancer risk women are highlighted in grey.

Table (E-11) Presents the total effective risk of worldwide screening programmes resulted from FFDM machine 7 using the LAR extrapolated by the three methods.

Programme	Total effective risk (case/10^6)		
	Method 1	Method 2	Method 3
Australia, Japan, Korea, United State (AAFP, NCI, and USPSTF)	270.09	282.33	357.43
Belgium, Croatia, Cyprus, Denmark, Finland, Germany, Italy, Latvia, Lithuania, Luxembourg, Norway, Poland, Slovenia, Spain (Catalonia), Switzerland	99.58	112.00	145.17
Canada , France, Israel, Netherlands	103.23	121.10	155.67
China	171.11	168.48	221.67
Czech	190.12	205.68	276.72
Estonia	90.04	94.96	118.33
Hungary	165.85	173.02	248.33
Iceland	266.44	273.22	346.93
India	426.24	433.43	559.18
Ireland	94.36	101.73	127.28
Malta	58.81	60.30	80.35
New Zealand, Portugal, Spain (Navarra)	170.19	182.20	266.23
Nigeria	267.92	276.72	350.43
Sweden	314.71	325.36	434.63
United Kingdom	98.62	108.40	151.04
United State (ACOG)	362.73	394.44	513.10
United State (ACS, ACR, and NCCN)	518.88	545.54	714.85
Uruguay	355.71	376.93	492.10
Canada	426.24	433.43	559.18
United Kingdom	516.78	540.63	707.85
United State (ACS)	1094.66	1124.89	1438.08
United State (NCCN)	1531.78	1562.01	2051.38

Screening programmes designed for high breast cancer risk women are highlighted in grey.

Table (E-12) Presents the total effective risk of worldwide screening programmes resulted from FFDM machine 8 using the LAR extrapolated by the three methods.

Programme	Total effective risk (case/10^6)		
	Method 1	Method 2	Method 3
Australia, Japan, Korea, United State (AAFP, NCI, and USPSTF)	212.62	222.25	281.30
Belgium, Croatia, Cyprus, Denmark, Finland, Germany, Italy, Latvia, Lithuania, Luxembourg, Norway, Poland, Slovenia, Spain (Catalonia), Switzerland	78.45	88.21	114.30
Canada , France, Israel, Netherlands	81.35	95.40	122.59
China	134.65	132.58	174.40
Czech	149.72	161.95	217.82
Estonia	70.91	74.78	93.15
Hungary	130.58	136.21	195.43
Iceland	209.72	215.05	273.01
India	335.48	341.12	440.00
Ireland	74.32	80.11	100.20
Malta	46.31	47.47	63.24
New Zealand, Portugal, Spain (Navarra)	134.02	143.45	209.53
Nigeria	210.90	217.82	275.77
Sweden	247.73	256.10	342.02
United Kingdom	77.67	85.36	118.90
United State (ACOG)	285.64	310.57	403.89
United State (ACS, ACR, and NCCN)	408.50	429.45	562.60
Uruguay	280.07	296.74	387.32
Canada	335.48	341.12	440.00
United Kingdom	406.83	425.57	557.07
United State (ACS)	861.33	885.09	1131.33
United State (NCCN)	1205.06	1228.82	1613.57

Screening programmes designed for high breast cancer risk women are highlighted in grey.

Table (E-13) Presents the total effective risk of worldwide screening programmes resulted from FFDM machine 9 using the LAR extrapolated by the three methods.

Programme	Total effective risk (case/10^6)		
	Method 1	Method 2	Method 3
Australia, Japan, Korea, United State (AAFP, NCI, and USPSTF)	175.24	183.19	231.96
Belgium, Croatia, Cyprus, Denmark, Finland, Germany, Italy, Latvia, Lithuania, Luxembourg, Norway, Poland, Slovenia, Spain (Catalonia), Switzerland	64.57	72.64	94.18
Canada , France, Israel, Netherlands	66.91	78.53	100.97
China	111.06	109.36	143.90
Czech	123.32	133.43	179.57
Estonia	58.40	61.60	76.78
Hungary	107.60	112.26	161.17
Iceland	172.89	177.30	225.17
India	276.61	281.28	362.96
Ireland	61.20	65.99	82.58
Malta	38.16	39.12	52.14
New Zealand, Portugal, Spain (Navarra)	110.40	118.20	172.77
Nigeria	173.84	179.57	227.44
Sweden	204.21	211.13	282.10
United Kingdom	63.96	70.31	98.01
United State (ACOG)	235.28	255.88	332.94
United State (ACS, ACR, and NCCN)	336.65	353.97	463.93
Uruguay	230.77	244.55	319.35
Canada	276.61	281.28	362.96
United Kingdom	335.30	350.79	459.40
United State (ACS)	710.54	730.18	933.59
United State (NCCN)	994.41	1014.04	1331.87

Screening programmes designed for high breast cancer risk women are highlighted in grey.

Table (E-14) Presents the total effective risk of worldwide screening programmes resulted from FFDM machine 10 using the LAR extrapolated by the three methods.

Programme	Total effective risk (case/10^6)		
	Method 1	Method 2	Method 3
Australia, Japan, Korea, United State (AAFP, NCI, and USPSTF)	203.89	213.15	269.93
Belgium, Croatia, Cyprus, Denmark, Finland, Germany, Italy, Latvia, Lithuania, Luxembourg, Norway, Poland, Slovenia, Spain (Catalonia), Switzerland	75.10	84.49	109.57
Canada , France, Israel, Netherlands	77.81	91.34	117.46
China	129.24	127.26	167.48
Czech	143.46	155.23	208.94
Estonia	67.94	71.66	89.33
Hungary	125.19	130.61	187.56
Iceland	201.18	206.31	262.04
India	321.87	327.31	422.39
Ireland	71.19	76.76	96.08
Malta	44.39	45.51	60.67
New Zealand, Portugal, Spain (Navarra)	128.44	137.52	201.05
Nigeria	202.28	208.94	264.67
Sweden	237.61	245.67	328.28
United Kingdom	74.40	81.80	114.03
United State (ACOG)	273.70	297.70	387.39
United State (ACS, ACR, and NCCN)	391.68	411.85	539.85
Uruguay	268.49	284.53	371.60
Canada	321.87	327.31	422.39
United Kingdom	390.12	408.16	534.59
United State (ACS)	826.90	849.76	1086.57
United State (NCCN)	1157.33	1180.20	1550.18

Screening programmes designed for high breast cancer risk women are highlighted in grey.

Table (E-15) Presents the total effective risk of worldwide screening programmes resulted from FFDM machine 11 using the LAR extrapolated by the three methods.

Programme	Total effective risk (case/10^6)		
	Method 1	Method 2	Method 3
Australia, Japan, Korea, United State (AAFP, NCI, and USPSTF)	160.67	167.95	212.63
Belgium, Croatia, Cyprus, Denmark, Finland, Germany, Italy, Latvia, Lithuania, Luxembourg, Norway, Poland, Slovenia, Spain (Catalonia), Switzerland	59.23	66.62	86.36
Canada , France, Israel, Netherlands	61.40	72.03	92.60
China	101.80	100.23	131.88
Czech	113.09	122.35	164.62
Estonia	53.56	56.49	70.40
Hungary	98.66	102.93	147.74
Iceland	158.50	162.54	206.39
India	253.57	257.84	332.67
Ireland	56.13	60.51	75.72
Malta	34.99	35.87	47.80
New Zealand, Portugal, Spain (Navarra)	101.24	108.38	158.38
Nigeria	159.38	164.62	208.47
Sweden	187.22	193.55	258.57
United Kingdom	58.66	64.48	89.85
United State (ACOG)	215.76	234.63	305.23
United State (ACS, ACR, and NCCN)	308.67	324.53	425.27
Uruguay	211.60	224.22	292.75
Canada	253.57	257.84	332.67
United Kingdom	307.42	321.61	421.11
United State (ACS)	651.22	669.20	855.52
United State (NCCN)	911.25	929.23	1220.34

Screening programmes designed for high breast cancer risk women are highlighted in grey.

Table (E-16) Presents the total effective risk of worldwide screening programmes resulted from FFDM machine 12 using the LAR extrapolated by the three methods.

Programme	Total effective risk (case/10^6)		
	Method 1	Method 2	Method 3
Australia, Japan, Korea, United State (AAFP, NCI, and USPSTF)	189.40	198.00	250.74
Belgium, Croatia, Cyprus, Denmark, Finland, Germany, Italy, Latvia, Lithuania, Luxembourg, Norway, Poland, Slovenia, Spain (Catalonia), Switzerland	69.76	78.49	101.78
Canada , France, Israel, Netherlands	72.28	84.84	109.11
China	120.06	118.21	155.57
Czech	133.26	144.20	194.09
Estonia	63.11	66.57	82.98
Hungary	116.29	121.33	174.23
Iceland	186.88	191.64	243.41
India	298.99	304.04	392.37
Ireland	66.13	71.31	89.25
Malta	41.24	42.28	56.36
New Zealand, Portugal, Spain (Navarra)	119.31	127.75	186.76
Nigeria	187.90	194.09	245.85
Sweden	220.72	228.21	304.95
United Kingdom	69.11	75.98	105.93
United State (ACOG)	254.25	276.54	359.85
United State (ACS, ACR, and NCCN)	363.84	382.58	501.48
Uruguay	249.40	264.31	345.19
Canada	298.99	304.04	392.37
United Kingdom	362.39	379.15	496.59
United State (ACS)	768.12	789.36	1009.34
United State (NCCN)	1075.07	1096.31	1440.00

Screening programmes designed for high breast cancer risk women are highlighted in grey.

Table (E-17) Presents the total effective risk of worldwide screening programmes resulted from FFDM machine 13 using the LAR extrapolated by the three methods.

Programme	Total effective risk (case/10^6)		
	Method 1	Method 2	Method 3
Australia, Japan, Korea, United State (AAFP, NCI, and USPSTF)	178.29	186.38	235.98
Belgium, Croatia, Cyprus, Denmark, Finland, Germany, Italy, Latvia, Lithuania, Luxembourg, Norway, Poland, Slovenia, Spain (Catalonia), Switzerland	65.70	73.91	95.82
Canada , France, Israel, Netherlands	68.09	79.90	102.74
China	112.98	111.25	146.38
Czech	125.47	135.76	182.68
Estonia	59.42	62.68	78.11
Hungary	109.48	114.21	163.97
Iceland	175.90	180.38	229.07
India	281.41	286.16	369.23
Ireland	62.27	67.14	84.02
Malta	38.82	39.80	53.05
New Zealand, Portugal, Spain (Navarra)	112.33	120.26	175.77
Nigeria	176.87	182.68	231.37
Sweden	207.76	214.80	286.98
United Kingdom	65.08	71.54	99.71
United State (ACOG)	239.39	260.35	338.72
United State (ACS, ACR, and NCCN)	342.51	360.12	471.97
Uruguay	234.79	248.81	324.89
Canada	281.41	286.16	369.23
United Kingdom	341.13	356.89	467.36
United State (ACS)	722.82	742.79	949.68
United State (NCCN)	1011.54	1031.51	1354.75

Screening programmes designed for high breast cancer risk women are highlighted in grey.

Table (E-18) Presents the total effective risk of worldwide screening programmes resulted from FFDM machine 14 using the LAR extrapolated by the three methods.

Programme	Total effective risk (case/10^6)		
	Method 1	Method 2	Method 3
Australia, Japan, Korea, United State (AAFP, NCI, and USPSTF)	181.32	189.55	240.01
Belgium, Croatia, Cyprus, Denmark, Finland, Germany, Italy, Latvia, Lithuania, Luxembourg, Norway, Poland, Slovenia, Spain (Catalonia), Switzerland	66.82	75.16	97.45
Canada , France, Israel, Netherlands	69.25	81.26	104.48
China	114.91	113.15	148.89
Czech	127.61	138.07	185.80
Estonia	60.43	63.74	79.44
Hungary	111.34	116.16	166.76
Iceland	178.89	183.45	232.98
India	286.21	291.04	375.54
Ireland	63.33	68.28	85.45
Malta	39.48	40.48	53.95
New Zealand, Portugal, Spain (Navarra)	114.24	122.31	178.77
Nigeria	179.88	185.80	235.32
Sweden	211.30	218.46	291.88
United Kingdom	66.18	72.76	101.41
United State (ACOG)	243.46	264.78	344.49
United State (ACS, ACR, and NCCN)	348.34	366.26	480.02
Uruguay	238.79	253.04	330.43
Canada	286.21	291.04	375.54
United Kingdom	346.94	362.97	475.33
United State (ACS)	735.16	755.48	965.92
United State (NCCN)	1028.84	1049.16	1377.97

Screening programmes designed for high breast cancer risk women are highlighted in grey.

Table (E-19) Presents the total effective risk of worldwide screening programmes resulted from FFDM machine 15 using the LAR extrapolated by the three methods.

Programme	Total effective risk (case/10^6)		
	Method 1	Method 2	Method 3
Australia, Japan, Korea, United State (AAFP, NCI, and USPSTF)	168.79	176.45	223.42
Belgium, Croatia, Cyprus, Denmark, Finland, Germany, Italy, Latvia, Lithuania, Luxembourg, Norway, Poland, Slovenia, Spain (Catalonia), Switzerland	62.20	69.97	90.71
Canada , France, Israel, Netherlands	64.46	75.64	97.26
China	106.97	105.32	138.59
Czech	118.79	128.52	172.96
Estonia	56.25	59.33	73.95
Hungary	103.64	108.13	155.24
Iceland	166.53	170.77	216.87
India	266.42	270.92	349.58
Ireland	58.95	63.56	79.54
Malta	36.75	37.68	50.22
New Zealand, Portugal, Spain (Navarra)	106.34	113.86	166.41
Nigeria	167.44	172.96	219.06
Sweden	196.69	203.36	271.70
United Kingdom	61.61	67.73	94.40
United State (ACOG)	226.63	246.47	320.68
United State (ACS, ACR, and NCCN)	324.26	340.94	446.84
Uruguay	222.28	235.55	307.59
Canada	266.42	270.92	349.58
United Kingdom	322.96	337.88	442.47
United State (ACS)	684.35	703.26	899.16
United State (NCCN)	957.74	976.65	1282.75

Screening programmes designed for high breast cancer risk women are highlighted in grey.

Table (E-20) Presents the total effective risk of worldwide screening programmes resulted from FFDM machine 16 using the LAR extrapolated by the three methods.

Programme	Total effective risk (case/10^6)		
	Method 1	Method 2	Method 3
Australia, Japan, Korea, United State (AAFP, NCI, and USPSTF)	165.50	173.01	219.06
Belgium, Croatia, Cyprus, Denmark, Finland, Germany, Italy, Latvia, Lithuania, Luxembourg, Norway, Poland, Slovenia, Spain (Catalonia), Switzerland	60.98	68.60	88.95
Canada , France, Israel, Netherlands	63.20	74.17	95.36
China	104.88	103.27	135.89
Czech	116.47	126.02	169.58
Estonia	55.16	58.18	72.51
Hungary	101.62	106.02	152.21
Iceland	163.28	167.44	212.64
India	261.23	265.63	342.76
Ireland	57.80	62.32	77.99
Malta	36.04	36.94	49.24
New Zealand, Portugal, Spain (Navarra)	104.27	111.64	163.16
Nigeria	164.18	169.58	214.78
Sweden	192.86	199.39	266.40
United Kingdom	60.41	66.41	92.56
United State (ACOG)	222.21	241.67	314.42
United State (ACS, ACR, and NCCN)	317.94	334.29	438.12
Uruguay	217.95	230.96	301.59
Canada	261.23	265.63	342.76
United Kingdom	316.66	331.29	433.84
United State (ACS)	670.99	689.53	881.60
United State (NCCN)	939.02	957.56	1257.63

Screening programmes designed for high breast cancer risk women are highlighted in grey.

Appendix F: Proposed phantom structure to simulate breast of different thicknesses.

Table (F-1) Lists proposed thickness of PMMA and PE required to simulate breast of 20-100 mm thickness (Bouwman et al., 2013)

Breast thickness (mm)	PMMA thickness (mm)	PE thickness (mm)
20	20.0	0.0
30	27.5	2.5
40	30.0	10.0
50	32.5	17.5
60	32.5	27.5
70	32.5	37.5
80	32.5	47.5
90	35.0	55.0
100	37.5	62.5

References

Abuidris, D. O., Elsheikh, A., Ali, M., Musa, H., Elgaili, E., Ahmed, A. O., . . . Mohammed, S. I. (2013). Breast-cancer screening with trained volunteers in a rural area of Sudan: a pilot study. *The Lancet Oncology, 14*(4), 363-370. doi: 10.1016/s1470-2045(12)70583-1.

Agt, H. v., Fracheboud, J., Steen, A. v. d., & Koning, H. d. (2012). Do women make an informed choice about participating in breast cancer screening? A survey among women invited for a first mammography screening examination. *Patient Education and Counselimg, 89*(2), 353-359. doi: 10.1016/j.pec.2012.08.003.

Alexander, F. E., Anderson, T. J., Brown, H. K., Forrest, A. P., Hepburn, W., Kirkpatrick, A. E., . . . Shepherd, S. M. (1994). The Edinburgh randomised trial of breast cancer screening: results after 10 years of follow-up. *British Journal of Cancer, 70*(3), 542-548.

Allen, S. D. (2012). The breast. In P. Butler, A. Mitchell & J. C. Healy (Eds.), Applied Radiological Anatomy (pp. 126-133): Cambridge University Press. doi: 10.1017/cbo9780511977930.008.

ALMousa, D. S., Ryan, E. A., Mello-Thoms, C., & Brennan, P. C. (2014). What effect does mammographic breast density have on lesion detection in digital mammography? *Clinical Radiology, 69*(4), 333-341. doi: 10.1016/j.crad.2013.11.014.

Alonzo-Proulx, O., Jong, R. A., & Yaffe, M. J. (2012). Volumetric breast density characteristics as determined from digital mammograms. *Physics in Medicine and Biology, 57*(1), 7443–7457. doi: 10.1088/0031-9155/57/22/7443.

Alonzo-Proulx, O., Packard, N., Boone, J. M., Al-Mayah, A., Brock, K. K., Shen, S. Z., & Yaffe, M. J. (2010). Validation of a method for measuring the volumetric breast density from digital mammograms. *Physics in Medicine and Biology, 55*(11), 3027-3044. doi: 10.1088/0031-9155/55/11/003.

Alsager, A. A., & Spyrou, N. M. (2007). Evaluation of image performance of CZT detector for digital mammography: Monte Carlo simulation. *Nuclear Instruments and Methods in Physics Research Section A: Accelerators, Spectrometers, Detectors and Associated Equipment, 580*(1), 462-465. doi: 10.1016/j.nima.2007.05.128.

American Cancer Society (ACS). (2011a). *Breast cancer facts & figures 2011-2012*. Atlanta: American Cancer Society, Inc.

American Cancer Society (ACS). (2011b). *Cancer facts and figures 2011*. Atlanta: American Cancer Society, Inc.

American Cancer Society (ACS). (2013a). Breast cancer facts & figures 2013-2014. Atlanta: American Cancer Society, Inc.

American Cancer Society (ACS). (2013b). Mammograms and other breast imaging tests. from: http://www.cancer.org/healthy/findcancerearly/examandtestdescriptions/mammogramsandotherbreastimagingprocedures/mammograms-and-other-breast-imaging-procedures-toc.

American Cancer Society (ACS). (2014). Breast cancer. Retrieved 19-04-2016, from: http://www.cancer.org/acs/groups/cid/documents/webcontent/003090-pdf.pdf.

American Cancer Society (ACS). (2015a). Breast cancer prevention and early detection. Retrieved 24-4-2016, from: http://www.cancer.org/acs/groups/cid/documents/webcontent/003165-pdf.pdf.

American Cancer Society (ACS). (2015b). Breast density and your mammogram report. Retrieved 19-04-2016, from: http://www.cancer.org/acs/groups/content/@editorial/documents/document/acspc-039989.pdf.

American Cancer Society (ACS). (2015c). Global cancer facts & figures (3rd ed.). Atlanta: American Cancer Society, Inc.

American Congress of Obstetricians and Gynecologists (ACOG). (2015). ACOG Committee Opinion no.625: Management of women with dense breasts diagnosed by mammography. *Obstetrics and Gynecology, 125*, 750-751.

Anderson, W. F., Jatoi, I., Tse, J., & Rosenberg, P. S. (2010). Male breast cancer: a population-based comparison with female breast cancer. *Journal of Clinical Oncology, 28*(2), 232-239. doi: 10.1200/jco.2009.23.8162.

Andersson, I., Aspegren, K., Janzon, L., Landberg, T., Lindholm, K., Linell, F., . . . Sigfússon, B. (1988). Mammographic screening and mortality from breast cancer: the Malmö mammographic screening trial. *BMJ : British Medical Journal, 297*(6654), 943-948.

Argo, W. P., Hintenlang, K., & Hintenlang, D. E. (2004). A tissue-equivalent phantom series for mammography dosimetry. *Journal of Applied Clinical Medical Physics, 5*(4), 112-119.

Assiamah , M. (2004). *Dosimetric techniques for mammography mass screening programs.* (Ph.D.), Witwatersrand, South Africa.

Assiamah, M., Nam, T. L., & Keddy, R. J. (2005). Comparison of mammography radiation dose values obtained from direct incident air kerma measurements with values from measured X-ray spectral data. *Applied Radiation and Isotopes, 62*(4), 551-560. doi: 10.1016/j.apradiso.2004.09.010.

Aznar, M. C., Hemdal, B., Medin, J., Marckmann, C. J., Andersen, C. E., Botter-Jensen, L., . . . Mattsson, S. (2005). In vivo absorbed dose measurements in mammography using a new real-time luminescence technique. *British Journal of Radiology, 78*(928), 328-334. doi: 10.1259/bjr/22554286.

Baines, C. J. (2011). Rational and irrational issues in breast cancer screening. *Cancers (Basel), 3*(1), 252-266. doi: 10.3390/cancers3010252.

Balonov, M. I., & Shrimpton, P. C. (2012). Effective dose and risks from medical X-ray procedures. *Annals of the ICRP, 41*(3-4), 129-141. doi: 10.1016/j.icrp.2012.06.002.

Baptista, M., Di Maria, S., Barros, S., Figueira, C., Sarmento, M., Orvalho, L., & Vaz, P. (2015). Dosimetric characterization and organ dose assessment in digital breast tomosynthesis: Measurements and Monte Carlo simulations using voxel phantoms. *Medical Physics, 42*(7), 3788-3800. doi: 10.1118/1.4921362.

Baptista, M., Di Maria, S., Oliveira, N., Matela, N., Janeiro, L., Almeida, P., & Vaz, P. (2014). Image quality and dose assessment in digital breast tomosynthesis: A Monte Carlo study. *Radiation Physics and Chemistry, 104*, 158-162. doi: 10.1016/j.radphyschem.2013.12.036.

BC Centre for Disease Control. (2016). Proper Selection, Care, Quality Control and Disposal of Lead Aprons. Retrieved 28-07-2016, from http://www.bccdc.ca/health-info/health-your-environment/radiation/radiation-issue-notes-x-ray-shielding-guidelines-and-other-useful-documents.

Beckett, J. R., & Kotre, C. J. (2000). Dosimetric implications of age related glandular changes in screening mammography. *Physics in Medicine and Biology, 45*(3), 801-813.

Beemsterboer, P. M. M., Warmerdam, P. G., Boer, R., & de Koning, H. J. (1998). Radiation risk of mammography related to benefit in screening programmes: a favourable balance? *Journal of Medical Screening, 5*(2), 81-87. doi: 10.1136/jms.5.2.81.

Benevides , L. A., Hintenlang, D. E., Rosenfeld, A., Kron, T., d'Errico, F., & Moscovitch, M. (2011). Dosimetry in Mammography: Average Glandular Dose Based on Homogeneous Phantom. 231-248. doi: 10.1063/1.3576170.

Benevides, L. A. (2005). *Breast dosimetry in clinical mammography.* (Ph.D.), Florida.

Bentley, K., Poulos, A., & Rickard, M. (2008). Mammography image quality: Analysis of evaluation criteria using pectoral muscle presentation. *Radiography, 14*(3), 189-194. doi: 10.1016/j.radi.2007.02.002.

Bernardi, D., Ciatto, S., Pellegrini, M., Anesi, V., Burlon, S., Cauli, E., . . . Houssami, N. (2012). Application of breast tomosynthesis in screening: incremental effect on mammography acquisition and reading time. *British Journal of Radiology, 85*(1020), e1174-e1178. doi: 10.1259/bjr/19385909.

Berrington de Gonzalez, A., & Reeves, G. (2005). Mammographic screening before age 50 years in the UK: comparison of the radiation risks with the mortality benefits. *British Journal of Cancer, 93*(5), 590-596. doi: 10.1038/sj.bjc.6602683.

Berrington de Gonzalez, A., Berg, C. D., Visvanathan, K., & Robson, M. (2009). Estimated risk of radiation-induced breast cancer from mammographic screening for young BRCA mutation carriers. *Journal of the National Cancer Institute, 101*(3), 205-209. doi: 10.1093/jnci/djn440.

Bjurstam, N., Bjorneld, L., Warwick, J., Sala, E., Duffy, S. W., Nystrom, L., . . . Wahlin, T. (2003). The Gothenburg Breast Screening Trial. *Cancer, 97*(10), 2387-2396. doi: 10.1002/cncr.11361.

Bliznakova , K., Speller, R., Horrocks, J., Liaparinos, P., Kolitsi, Z., & Pallikarakis, N. (2010). Experimental validation of a radiographic simulation code using breast phantom for X-ray imaging. *Computers in Biology and Medicine, 40*(2), 208-214. doi: 10.1016/j.compbiomed.2009.11.017.

Bliznakova, K., Sechopoulos, I., Buliev, I., & Pallikarakis, N. (2012). BreastSimulator: A software platform for breast x-ray imaging research. *Journal of Biomedical Graphics and Computing, 2*(1). doi: 10.5430/jbgc.v2n1p1.

Blue Cross and Blue Shield Association, Kaiser Foundation Health Plan, & Southern California Permanente Medical Group. (2014). Use of digital breast tomosynthesis with mammography for breast cancer screening or diagnosis. *Technolology Evaluation Centre Assessment Programme Executive Summary, 28*(6), 1-6.

Bluekens, A. M., Veldkamp, W. J., Schuur, K. H., Karssemeijer, N., Broeders, M. J., & den Heeten, G. J. (2015). The potential use of ultra-low radiation dose images in digital mammography--a clinical proof-of-concept study in craniocaudal views. *British Journal of Radiology, 88*(1047), 20140626. doi: 10.1259/bjr.20140626.

Boone, J. M. (1999). Glandular Breast Dose for Monoenergetic and High-Energy X-ray Beams: Monte Carlo Assessment. *Radiology, 213*(1), 23-37. doi: doi:10.1148/radiology.213.1.r99oc3923.

Boone, J. M., Lindfors, K. K., Cooper, V. N., 3rd, & Seibert, J. A. (2000). Scatter/primary in mammography: comprehensive results. *Medical Physics, 27*(10), 2408-2416. doi: 10.1118/1.1312812.

Bos, A. J. J. (2001a). High senstivity thermoluminescene dosimetry. Nuclear Instruments and Methods in Physics Research B, 184(1), 3-28.

Bos, A. J. J. (2001b). On the energy conversion in thermoluminescece dosimetry material. Radiation Measurements, 33(1), 737-744.

Bos, A. J. J. (2007). Theory of thermoluminescence. *Radiation Measurements, 41*, S45-S56. doi: 10.1016/j.radmeas.2007.01.003.

Bosmans, H., & Marshall, N. (2013). Radiation Doses and Risks Associated with Mammographic Screening. *Current Radiology Reports, 1*(1), 30-38. doi: 10.1007/s40134-013-0008-x.

Bouwman, R. W., Diaz, O., van Engen, R. E., Young, K. C., den Heeten, G. J., Broeders, M. J., . . . Dance, D. R. (2013). Phantoms for quality control procedures in digital breast tomosynthesis: dose assessment. *Physics in Medicine and Biology, 58*(13), 4423-4438. doi: 10.1088/0031-9155/58/13/4423.

Boyd , N. F., Guo , H., Martin , L. J., Sun , L., Stone , J., Fishell , E., . . . Yaffe , M. J. (2007). Mammographic Density and the Risk and Detection of Breast Cancer. *New England Journal of Medicine, 356*(3), 227-236. doi: doi:10.1056/NEJMoa062790.

Boyd, N. F., Jensen, H. M., Cooke, G., & Han, H. L. (1992). Relationship between mammographic and histological risk factors for breast cancer. *Journal of the National Cancer Institute, 84*(15), 1170-1179.

Boyd, N. F., Martin, L. J., Bronskill, M., Yaffe, M. J., Duric, N., & Minkin, S. (2010). Breast tissue composition and susceptibility to breast cancer. *Journal of the National Cancer Institute, 102*(16), 1224-1237. doi: 10.1093/jnci/djq239.

Boyd, N. F., Martin, L. J., Yaffe, M. J., & Minkin, S. (2011). Mammographic density and breast cancer risk: current understanding and future prospects. *Breast Cancer Research, 13*(6), 223. doi: 10.1186/bcr2942.

Boyle, P. (2003). Screening. *European Respiratory Journal, 21*(Supplement 39), 3S-15s. doi: 10.1183/09031936.03.00406003.

Brady, Z. (2012). *Radiation doses and risks from paediatric computed tomography.* (Ph.D.), RMIT University, Melbourne.

Brandt, S. S., Karemore, G., Karssemeijer, N., & Nielsen, M. (2011). An Anatomically Oriented Breast Coordinate System for Mammogram Analysis. *IEEE Transections on Medical Imaging, 30*(10).

Brenner , D., & Huda, W. (2008). Effective dose: a useful concept in diagnostic radiology. *Radiation Protection Dosimetry, 128*(4), 503-508. doi: 10.1093/rpd/ncn056.

Brenner, D. J. (2008). Effective dose: a flawed concept that could and should be replaced. *British Journal of Radiology, 81*(967), 521-523. doi: 10.1259/bjr/22942198.

Brenner, D. J. (2012). We can do better than effective dose for estimating or comparing low-dose radiation risks. *Annals of the ICRP, 41*(3-4), 124-128. doi: 10.1016/j.icrp.2012.07.001.

Brenner, D. J. (2014). What we know and what we don't know about cancer risks associated with radiation doses from radiological imaging. *British Journal of Radiology, 87*(1035), 20130629. doi: 10.1259/bjr.20130629.

Brenner, D. J., Sawant, S. G., Hande, M. P., Miller, R. C., Elliston, C. D., Fu, Z., . . . Marino, S. A. (2002). Routine screening mammography: how important is the radiation-risk side of the benefit-risk equation? *International Journal of Radiation Biology, 78*(12), 1065-1067. doi: 10.1080/0955300021000016576.

Brnic , Z., & Hebrang , A. (2001). Breast compression and radiation dose in two different mammographic oblique projections: 45 and 60 degrees. *European Journal of Radiology, 40*(1), 10-15.

Bushberg, J. T., Seibert, J. A., Leidholdt, E. M., & Boone, J. M. (2002). *The essential physics of medical imaging* (2nd ed.). Philadelphia: Lippincott Williams & Wilkins.

Bushong, S. C. (2013). *Radiologic science for technologists : physics, biology, and protection* (10th ed.). Missouri: Mosby.

Byng, J. W., Mainprize, J. G., & Yaffe, M. J. (1998). X-ray characterization of breast phantom materials. *Physics in Medicine and Biology, 43*(5), 1367.

Caldwell, C. B., & Yaffe, M. J. (1990). Development of an anthropomorphic breast phantom. *Medical Physics, 17*(2), 273-280. doi: doi:http://dx.doi.org/10.1118/1.596506.

Camargo-Mendoza, R. E., Poletti, M. E., Costa, A. M., & Caldas, L. V. E. (2011). Measurement of some dosimetric parameters for two mammography systems using thermoluminescent dosimetry. *Radiation Measurements, 46*(12), 2086-2089. doi: 10.1016/j.radmeas.2011.06.019.

Cancer Australia. (2014). Breast screen and you: information about mammography screening. from from: http://www.cancerscreening.gov.au/internet/screening/publishing.nsf/Content/breastscreen-n-you-html.

Cardinal Health. (2003). Mammographic Accreditation Phantom Nuclear Associates Model 18-220. from: http://www.elimpex.com/companies/victoreen/Catalog/DI5.pdf.

Cassola, V. F., & Hoff, G. (2010). Comparative study of computational dosimetry involving homogeneous phantoms and a voxel phantom in mammography: a discussion on applications in constancy tests and calculation of glandular dose in patient. *Radiologia Brasileira, 43*, 395-400.

Chelliah, K. K., Voon, N. M. F., & Ahamad, H. (2013). Breast Density: Does It Vary among the Main Ethnic Groups in Malaysia? *Open Journal of Medical Imaging, 03*(04), 105-109. doi: 10.4236/ojmi.2013.34017.

Chen, B., Wang, Y., Sun, X., Guo, W., Zhao, M., Cui, G., . . . Yu, J. (2012). Analysis of patient dose in full field digital mammography. *European Journal of Radiology, 81*(5), 868-872. doi: 10.1016/j.ejrad.2011.02.027.

Chiarelli, A. M., Edwards, S. A., Prummel, M. V., Muradali, D., Majpruz, V., Done, S. J., . . . Yaffe, M. J. (2013). Digital compared with screen-film mammography: performance measures in concurrent cohorts within an organized breast screening program. *Radiology, 268*(3), 684-693. doi: 10.1148/radiol.13122567.

Ciatto, S., Houssami, N., Bernardi, D., Caumo, F., Pellegrini, M., Brunelli, S., . . . Macaskill, P. (2013). Integration of 3D digital mammography with tomosynthesis for population breast-cancer screening (STORM): a prospective comparison study. The *Lancet Oncology, 14*(7), 583-589. doi: 10.1016/s1470-2045(13)70134-7.

Ciraj-Bjelac, O., Avramova-Cholakova, S., Beganovic, A., Economides, S., Faj, D., Gershan, V., . . . Rehani, M. M. (2012). Image quality and dose in mammography in 17 countries in Africa, Asia and Eastern Europe: results from IAEA projects. *European Journal of Radiology, 81*(9), 2161-2168. doi: 10.1016/j.ejrad.2011.05.026.

Coldman, A. J., Phillips, N., Olivotto, I. A., Gordon, P., Warren, L., & Kan, L. (2008). Impact of changing from annual to biennial mammographic screening on breast cancer outcomes in women aged 50-79 in British Columbia. *Journal of Medical Screening, 15*(4), 182-187. doi: 10.1258/jms.2008.008064.

Collins, P. (2005). *Assessment of effective dose in computed tomography using an anthropomorphic phantom.* (M.Sc.), National University of Irland, Galway.

Computerized Imaging Reference Systems (CIRS). (2013). Mammography Phototimer Consistency Testing Slabs. from: http://www.cirsinc.com/products/all/45/mammography-phototimer-consistency-testing-slabs/.

Computerized Imaging Reference System (CIRS), Tissue Simulation and Phantom Technology. (2012). ATOM dosimetry phantoms models 701-706. Virginia: CIRS, Inc.

Costa, A. M., Barbi, G. L., Bertucci, E. C., Ferreira, H., Sansavino, S. Z., Colenci, B., & Caldas, L. V. (2010). In vivo dosimetry with thermoluminescent dosimeters in external photon beam radiotherapy. *Applied Radiation and Isotopes, 68*(4-5), 760-762. doi: 10.1016/j.apradiso.2009.09.039.

Cowen, A. R., Kengyelics, S. M., & Davies, A. G. (2008). Solid-state, flat-panel, digital radiography detectors and their physical imaging characteristics. *Clinical Radiology, 63*(5), 487-498. doi: 10.1016/j.crad.2007.10.014.

Cristy, M. (1981). Active bone marrow distribution as a function of age in humans. *Physics in Medicine and Biology, 26*(3), 389.

Cunha, D. M., Tomal, A., & Poletti, M. E. (2012). Optimization of x-ray spectra in digital mammography through Monte Carlo simulations. *Physics in Medicine and Biology, 57*(7), 1919-1935. doi: 10.1088/0031-9155/57/7/1919.

Cunha, D. M., Tomal, A., & Poletti, M. E. (2013). Monte Carlo Simulation of X-Ray Spectra in Mammography and Contrast-Enhanced Digital Mammography Using the Code PENELOPE. *IEEE Transactions on Nuclear Science, 60*(2), 495-502. doi: 10.1109/TNS.2012.2226750.

D'Orsi, C. J., Bassett, L. W., Appleton, C. M., Berg, W. A., Burnside, E. S., Feig, S. A., . . . Trinh, M. M. (2013). Breast Imaging Reporting and Data SystemACR BI-RADS® Atlas. Reston: American College of Radiology.

Dance, D. R. (1990). Monte Carlo calculation of conversion factors for the estimation of mean glandular breast dose. *Physics in Medicine and Biology, 35*(9), 1211-1219.

Dance, D. R., & Young, K. C. (2014). Estimation of mean glandular dose for contrast enhanced digital mammography: factors for use with the UK, European and IAEA breast dosimetry protocols. *Physics in Medicine and Biology, 59*(9), 2127-2137. doi: 10.1088/0031-9155/59/9/2127.

Dance, D. R., Hunt, R. A., Bakic, P. R., Maidment, A. D., Sandborg, M., Ullman, G., & Alm Carlsson, G. (2005). Breast dosimetry using high-resolution voxel phantoms. *Radiation Protection Dosimetry, 114*(1-3), 359-363. doi: 10.1093/rpd/nch510.

Dance, D. R., Persliden, J., & Carlsson, G. A. (1992). Calculation of dose and contrast for two mammographic grids. *Physics in Medicine and Biology, 37*(1), 235.

Dance, D. R., Skinner, C. L., & Carlsson, G. A. (1999). Breast dosimetry. *Applied Radiation and Isotopes, 50*(1), 185-203.

Dance, D. R., Skinner, C. L., Young, K. C., Beckett, J. R., & Kotre, C. J. (2000a). Additional factors for the estimation of mean glandular breast dose using the UK mammography dosimetry protocol. *Physics in Medicine and Biology, 45*, 3225–3240.

Dance, D. R., Thilander, A. K., Sandborg, M., Skinner, C. L., Castellano, I. A., & Carlsson, G. A. (2000b). Influence of anode/filter material and tube potential on contrast, signal-to-noise ratio and average absorbed dose in mammography: a Monte Carlo study. *British Journal of Radiology, 73*(874), 1056-1067. doi:10.1259/bjr.73.874.11271898.

Dance, D. R., Young, K. C., & van Engen, R. E. (2009). Further factors for the estimation of mean glandular dose using the United Kingdom, European and IAEA breast dosimetry protocols. *Physics in Medicine and Biology, 54*(14), 4361-4372. doi: 10.1088/0031-9155/54/14/002.

Dance, D. R., Young, K. C., & van Engen, R. E. (2011). Estimation of mean glandular dose for breast tomosynthesis: factors for use with the UK, European and IAEA breast dosimetry protocols. *Physics in Medicine and Biology, 56*(2), 453-471. doi: 10.1088/0031-9155/56/2/011.

Dang, P. A., Freer, P. E., Humphrey, K. L., Halpern, E. F., & Rafferty, E. A. (2014). Addition of tomosynthesis to conventional digital mammography: effect on image interpretation time of screening examinations. *Radiology, 270*(1), 49-56. doi: 10.1148/radiol.13130765.

Darlington, A. J. (2015). Anatomy of the breast. In P. Hogg, J. Kelly & C. Mercer (Eds.), *Digital mammography: A holistic approach*. Cham: Springer.

de González, A. B., & Darby, S. (2004). Risk of cancer from diagnostic X-rays: estimates for the UK and 14 other countries. *The Lancet, 363*(9406), 345-351. doi: 10.1016/s0140-6736(04)15433-0.

Del Turco, M. R., Mantellini, P., Ciatto, S., Bonardi, R., Martinelli, F., Lazzari, B., & Houssami, N. (2007). Full-field digital versus screen-film mammography: comparative accuracy in concurrent screening cohorts. *American Journal of Roentgenology, 189*(4), 860-866. doi: 10.2214/AJR.07.2303.

Delis, H., Spyrou, G., Costaridou, L., Tzanakos, G., & Panayiotakis, G. (2007). Evaluating the Figure of Merit in mammography utilizing Monte Carlo simulation. *Nuclear Instruments and Methods in Physics Research Section A: Accelerators, Spectrometers, Detectors and Associated Equipment, 580*(1), 493-496. doi: 10.1016/j.nima.2007.05.197.

Delis, H., Spyrou, G., Panayiotakis, G., & Tzanakos, G. (2005). DOSIS: a Monte Carlo simulation program for dose related studies in mammography. *European Journal of Radiology, 54*(3), 371-376. doi: 10.1016/j.ejrad.2004.07.014.

Dellie, S. T., Rao, A. D. P., Admassie, D., & Meshesha, A. Z. (2013). Evaluation of Mean Glandular Dose during Diagnostic Mammography Examination for Detection of

Breast Pathology, in Ethiopia. *OMICS Journal of Radiology, 01*(04). doi: 10.4172/2167-7964.1000109.

Destounis, S., & Gruttadauria, J. L. (2015). An Overview of Digital Breast Tomosynthesis. *Journal of Radiology Nursing, 34*(3), 131-136. doi: 10.1016/j.jradnu.2014.10.004.

Di Maria, S., Barros, S., Bento, J., Teles, P., Figueira, C., Pereira, M., . . . Paulo, G. (2011). TLD measurements and Monte Carlo simulations for glandular dose and scatter fraction assessment in mammography: A comparative study. *Radiation Measurements, 46*(10), 1103-1108. doi: 10.1016/j.radmeas.2011.06.072.

Diaz, O., Dance, D. R., Young, K. C., Elangovan, P., Bakic, P. R., & Wells, K. (2014). Estimation of scattered radiation in digital breast tomosynthesis. *Physics in Medicine and Biology, 59*(15), 4375-4390. doi: 10.1088/0031-9155/59/15/4375.

Diekmann, F., & Bick, U. (2011). Breast tomosynthesis. *Seminars in Ultrasound, CT and MRI, 32*(4), 281-287. doi: 10.1053/j.sult.2011.03.002.

Dietze, G., Harrison, J. D., & Menzel, H. G. (2009). Effective dose: a flawed concept that could and should be replaced. Comments on a paper by D J Brenner (British Journal of Radiology 2008;81:521-3). *British Journal of Radiology, 82*(976), 348-350; author reply 350-341. doi: 10.1259/bjr/91937653.

Diffey, J. L. (2012). *Development and Evaluation of a Method for Measuring Breast Density.* (PhD), University of Manchester, Manchester.

Diffey, J., Hufton, A., Beeston, C., Smith, J., Marchant, T., & Astley, S. (2008). Quantifying Breast Thickness for Density Measurement. In E. A. Krupinski (Ed.), *Digital Mammography: 9th International Workshop, IWDM 2008 Tucson, AZ, USA, July 20-23, 2008 Proceedings* (pp. 651-658). Berlin, Heidelberg: Springer Berlin Heidelberg.

Ding, H., & Molloi, S. (2012). Quantification of breast density with spectral mammography based on a scanned multi-slit photon-counting detector: a feasibility study. *Physics in Medicine and Biology, 57*(15), 4719-4738. doi: 10.1088/0031-9155/57/15/4719.

Djulbegovic, B., & Lyman, G. H. (2006). Screening mammography at 40–49 years: regret or no regret? *The Lancet, 368*(9552), 2035-2037. doi: 10.1016/s0140-6736(06)69816-4.

Dobrzynski, L., Fornalski, K. W., & Feinendegen, L. E. (2015). Cancer Mortality Among People Living in Areas With Various Levels of Natural Background Radiation. *Dose-Response, 13*(3), 1559325815592391. doi: 10.1177/1559325815592391.

Lerda, D., Deandrea, S., Freeman, C., López-Alcalde, J., Neamtiu, L., Nicholl, C., . . . Villanueva, S. (2014). *Report of a European survey on the organisation of breast cancer care services* Retrieved from: http://publications.jrc.ec.europa.eu/repository/bitstream/JRC89731/lbna26593enn_002.pdf doi:10.2788/51070.

Dong, S. L., Chu, T. C., Lan, G. Y., Lin, Y. C., Yeh, Y. H., & Chuang, K. S. (2011). Development of an adjustable model breast for mammographic dosimetry assessment in Taiwanese women. *American Journal of Roentgenology, 196*(4), W476-481. doi: 10.2214/AJR.09.3700.

Drake, R. L., Vogl, W., & Mitchell, A. W. M. (2015). *Gray's anatomy for students* (3rd ed.). Edinburgh: Churchill Livingstone.

Duarte, I. C., Caldeira, L., Soares, F., Silva, J. S., & Janela, F. (2010). GATE Mammogram Simulation of NCAT Breast Phantom. In O. Dössel & W. C. Schlegel (Eds.), *World Congress on Medical Physics and Biomedical Engineering, September 7 - 12, 2009, Munich, Germany: Vol. 25/4 Image Processing, Biosignal Processing, Modelling and Simulation, Biomechanics* (pp. 1482-1485). Berlin, Heidelberg: Springer Berlin Heidelberg.

Egan, R. L. (1960). Experience with mammography in Tumour institution : evaluation of 1000 studies. *Radiology, 75*(6), 894-900.

Ekpo, E. U., & McEntee, M. F. (2014). Measurement of breast density with digital breast tomosynthesis--a systematic review. *British Journal of Radiology, 87*(1043), 20140460. doi: 10.1259/bjr.20140460.

Ekpo, E. U., Hogg, P., Highnam, R., & McEntee, M. F. (2015). Breast composition: Measurement and clinical use. *Radiography, 21*(4), 324-333. doi: 10.1016/j.radi.2015.06.006.

Ellis, H. (2004). Anatomy of the breast. *Surgery (Oxford), 22*(7), 145-147. doi: 10.1383/surg.22.7.145.38357.

European Commission. (1996). European protocol on dosimetry in mammography (pp. 70).

European Commission. (2006). European guidelines for quality assurance in breast cancer screening and diagnosis. Belgium: European Communities.

European Commission. (2008). European Guidance on Estimating Population Doses from Medical X-Ray Procedures. Luxembourg.

European Commission. (2013). European guidline for quality assurance in breast cancer screening and diagnosis : fourth edition supplements. Belgium: European Communities.

European Commission. (2014). Council Directive 2013/59/Euratom. *Official Journal of the European Union, 57*.

Farquharson, M. J., Spyrou, N. M., al-Bahri, J., & Highgate, D. J. (1995). Low energy photon attenuation measurements of hydrophilic materials for tissue equivalent phantoms. *Applied Radiation and Isotopes, 46*(8), 783-790.

Feng , S. S., Patel, B., & Sechopoulos, I. (2013). Objective models of compressed breast shapes undergoing mammography. *Medical Physics, 40*(3), 031902. doi: 10.1118/1.4789579.

Feng, S. S. J., & Sechopoulos, I. (2012). Clinical Digital Breast Tomosynthesis System: Dosimetric Characterization. *Radiology, 263*(1), 35-42.

Ferlay, J., Soerjomataram, I., Ervik, M., Dikshit, R., Eser, S., Mathers, C., . . . Bray, F. (2013). Cancer Incidence and Mortality Worldwide. *GLOBOCAN 2012 v1.0.* Retrieved 4-20, 2016, from: http://globocan.iarc.fr.

Field, A. P. (2013). *Discovering statistics using IBM SPSS statistics : and sex and drugs and rock 'n' roll* (4th ed.). London: SAGE Publications.

Finkel, M. L. (2005). *Understanding the mammography controversy: science, politics, and breast cancer screening*. United State of America: Praeger Publishers.

Fischmann, A., Siegmann, K. C., Wersebe, A., Claussen, C. D., & Muller-Schimpfle, M. (2005). Comparison of full-field digital mammography and film-screen mammography: image quality and lesion detection. *British Journal of Radiology, 78*(928), 312-315. doi: 10.1259/bjr/33317317.

Ford, K., Marcus, E., & Lum, B. (1999). Breast cancer screening, diagnosis,and treatment. *Disease-a-Month, 45*(9), 337-394.

Förnvik, D., Andersson, I., Svahn, T., Timberg, P., Zackrisson, S., & Tingberg, A. (2010). *The effect of reduced breast compression in breast tomosynthesis: An observer study using clinical cases*. Paper presented at the European congress of radiology 2010, Vienna.

Forrest, S. P. (1986). *Breast cancer screening: report to the health ministers of England, Wales, Scotland, and Northern Ireland*. London: Her Majestry's Stationery Office.

Freed, M., Badal, A., Jennings, R. J., de las Heras, H., Myers, K. J., & Badano, A. (2011). X-ray properties of an anthropomorphic breast phantom for MRI and x-ray imaging. *Physics in Medicine and Biology, 56*(12), 3513-3533. doi: 10.1088/0031-9155/56/12/005.

Freitas-Junior, R., Correa, R., Peixoto, J.-E., Ferreira, R., & Tanaka, R. (2012). Abstract P3-01-07: Estimated risk of radiation-induced breast cancer from mammographic screening . *Cancer Research, 72*(24 Supplement), P3-01-07. doi: 10.1158/0008-5472.sabcs12-p3-01-07.

Friedewald, S. M., Rafferty, E. A., Rose, S. L., Durand, M. A., Plecha, D. M., Greenberg, J. S., . . . Conant, E. F. (2014). Breast cancer screening using tomosynthesis in combination with digital mammography. *Journal of the American Medical Association, 311*(24), 2499-2507. doi: 10.1001/jama.2014.6095.

Frisell, J., Lidbrink, E., Hellstrom, L., & Rutqvist, L. E. (1997). Followup after 11 years--update of mortality results in the Stockholm mammographic screening trial. *Breast Cancer Research and Treatment, 45*(3), 263-270.

Fulea, D., Cosma, C., & Pop, I. G. (2009). Monte Carlo method for radiological X-ray examinations. *Romanian Journal of Physics, 54*(7-8), 629-639.

Furetta, C., & Weng, P. S. (1998). *Operational Thermoluminescence Dosimetry*. Singapore: World Scientific.

Gaona, E., Nieto, J. A., Góngora, J. A. I. D., Arreola, M., & Enríquez, J. G. F. (2007). TL dosimetry for quality control of CR mammography imaging systems. Radiation Effects and Defects in Solids, 162(10-11), 759-763. doi: 10.1080/10420150701482170

Gareen, I. F., & Gatsonis, C. (2003). Primer on Multiple Regression Models for Diagnostic Imaging Research. *Radiology, 229*(2), 305-310. doi: doi:10.1148/radiol.2292030324.

Gastrin, G., Miller, A. B., To, T., Aronson, K. J., Wall, C., Hakama, M., . . . Pukkala, E. (1994). Incidence and mortality from breast cancer in the Mama Program for Breast Screening in Finland, 1973-1986. *Cancer, 73*(8), 2168-2174.

Geeraert, N., Klausz, R., Muller, S., Bloch, I., & Bosmans, H. (2012). *Breast characteristics and dosimetric data in X-ray mammography - a large sample worldwide survey* Paper presented at the International Conference on Radiation Protection in Medicine, Germany.

Geeraert, N., Klausz, R., Muller, S., Bloch, I., & Bosmans, H. (2015). Evaluation of exposure in mammography: limitations of average glandular dose and proposal of a new quantity. *Radiation Protection Dosimetry, 165*(1-4), 342-345. doi: 10.1093/rpd/ncv069.

Gennaro, G., & di Maggio, C. (2006). Dose comparison between screen/film and full-field digital mammography. *European Radiology, 16*(11), 2559-2566. doi: 10.1007/s00330-006-0314-2.

Gershon-Cohen , J., & Strickler , A. (1938). Roentgenologic examination of the normal breast : its evaluation in demonstrating early neoplastic changes. *American Journal of Roentgenology, 40*(2), 189-201.

Gilbert, F. J., Tucker, L., Gillan, M. G., Willsher, P., Cooke, J., Duncan, K. A., . . . Duffy, S. W. (2015). The TOMMY trial: a comparison of TOMosynthesis with digital MammographY in the UK NHS Breast Screening Programme--a multicentre retrospective reading study comparing the diagnostic performance of digital breast tomosynthesis and digital mammography with digital mammography alone. *Health Technology Assessment, 19*(4), i-xxv, 1-136. doi: 10.3310/hta19040.

Gilbert, F. J., Young, K. C., Astley, S. M., Whelehan, P., & Gillan, M. G. C. (2010). Digital breast tomosynthesis. *NHSBSP Publication no. 69*. Sheffield: NHSBSP.

Gingold, E. L., Wu, X., & Barnes, G. T. (1995). Contrast and dose with Mo-Mo, Mo-Rh, and Rh-Rh target-filter combinations in mammography. *Radiology, 195*(3), 639-644. doi: doi:10.1148/radiology.195.3.7753987.

Gold, R. H., Bassett, L. W., & Widoff, B. E. (1990). Highlights from the history of mammography. *RadioGraphics, 10*(6), 1111-1131.

Gomes, D. S., Rezende, A. M. L., Barragan, C. V. M., Costa, K. C., Donato, S., Castro, W. J., . . . Nogueira1, M. S. (2011). *Average glandular dose in patients submitted to mammography exams*. Paper presented at the International Nuclear Atomic Conference, Brazil.

Gotzsche, P. C., & Jorgensen, K. J. (2013). Screening for breast cancer with mammography. Cochrane *Database Syst Rev, 6*, CD001877. doi: 10.1002/14651858.CD001877.pub5.

Gøtzsche, P. C., & Jørgensen, K. J. (2013). The benefits and harms of breast cancer screening. *The Lancet, 381*(9869), 799. doi: 10.1016/s0140-6736(13)60618-2.

Gøtzsche, P. C., Hartling, O. J., Nielsen, M., & Brodersen, J. (2012). Screening for breast cancer with mammography.

Gould, H. R., Ruzicka, F. F., Sanchez-Ubeda, R., & Perez, J. (1960). Xeroradiography of the breast. *American Journal of Roentgenology, 84*(2), 220-223.

Gram, I. T., Funkhouser, E., & Tabar, L. (1997). The Tabar classification of mammographic parenchymal patterns. *European Journal of Radiology, 24*(2), 131-136.

Green, S., Palethorpe, J. E., Peach, D., & Bradley, D. A. (1999). Performance assessment of patient dosimetry services and X-ray quality assurance instruments used in diagnostic radiology. *Applied Radiation and Isotopes, 50*(1), 137-152.

Griffey, R. T., & Sodickson, A. (2009). Cumulative radiation exposure and cancer risk estimates in emergency department patients undergoing repeat or multiple CT. *American Journal of Roentgenology, 192*(4), 887-892. doi: 10.2214/AJR.08.1351.

Groves, A. M., Owen, K. E., Courtney, H. M., Yates, S. J., Goldstone, K. E., Blake, G. M., & Dixon, A. K. (2004). 16-detector multislice CT: dosimetry estimation by TLD measurement compared with Monte Carlo simulation. *British Journal of Radiology, 77*(920), 662-665. doi: 10.1259/bjr/48307881.

Guimarães , C. C., Moralles, M., & Okuno, E. (2007). GEANT4 simulation of the angular dependence of TLD-based monitor response. *Nuclear Instruments and Methods in Physics Research Section A: Accelerators, Spectrometers, Detectors and Associated Equipment, 580*(1), 514-517. doi: 10.1016/j.nima.2007.05.218.

Guimarães, C. C., Moralles, M., & Okuno, E. (2008). Performance of GEANT4 in dosimetry applications: Calculation of X-ray spectra and kerma-to-dose equivalent conversion coefficients. *Radiation Measurements, 43*(9-10), 1525-1531. doi: 10.1016/j.radmeas.2008.07.001.

Gur, D., Abrams, G. S., Chough, D. M., Ganott, M. A., Hakim, C. M., Perrin, R. L., . . . Bandos, A. I. (2009). Digital breast tomosynthesis: observer performance study. *American Journal of Roentgenology, 193*(2), 586-591. doi: 10.2214/AJR.08.2031.

Haas, B. M., Kalra, V., Geisel, J., Raghu, M., Durand, M., & Philpotts, L. E. (2013). Comparison of tomosynthesis plus digital mammography and digital mammography alone for breast cancer screening. *Radiology, 269*(3), 694-700. doi: 10.1148/radiol.13130307.

Hackney, L. (2015). Etiology and epidemiology of breast cancer. In P. Hogg, J. Kelly & C. Mercer (Eds.), *Digital Mammography: A holistic approach*. Cham: Springer.

Hambly, N. M., McNicholas, M. M., Phelan, N., Hargaden, G. C., O'Doherty, A., & Flanagan, F. L. (2009). Comparison of digital mammography and screen-film mammography in breast cancer screening: a review in the Irish breast screening program. *American Journal of Roentgenology, 193*(4), 1010-1018. doi: 10.2214/AJR.08.2157.

Hammerstein, G. R., Miller, D. W., White, D. R., Masterson, M. E., Woodard, H. Q., & Laughlin, J. S. (1979). Absorbed Radiation Dose in Mammography. *Radiology, 130*(2), 485-491. doi: doi:10.1148/130.2.485.

Harding, C., Pompei, F., Burmistrov, D., Welch, H. G., Abebe, R., & Wilson, R. (2015). Breast Cancer Screening, Incidence, and Mortality Across US Counties. *Journal of the American Medical Association (Internal Medicine), 175*(9), 1483-1489. doi: 10.1001/jamainternmed.2015.3043.

Hart, D., Wall, B. F., Hillier, M. C., & Shrimpton, P. C. (2010). Frequency and collective dose for medical and dental x-ray examinations in the UK, 2008.

Hatziioannou, K. A., Psarrakos, K., Molyvda-Athanasopoulou, E., Kitis, G., Papanastassiou, E., Sofroniadis, I., & Kimoundri, O. (2000). Dosimetric considerations in mammography. *European Radiology, 10*(7), 1193-1196.

Hauge, I. H., Hogg, P., Szczepura, K., Connolly, P., McGill, G., & Mercer, C. (2012). The readout thickness versus the measured thickness for a range of screen film mammography and full-field digital mammography units. *Medical Physics, 39*(1), 263-271. doi: 10.1118/1.3663579.

Hauge, I. H., Pedersen, K., Sanderud, A., Hofvind, S., & Olerud, H. M. (2012). Patient doses from screen-film and full-field digital mammography in a population-based screening programme. *Radiation Protection Dosimetry, 148*(1), 65-73. doi: 10.1093/rpd/ncq598.

Health Protection Agency (HPA). (2011). *Risk of solid cancers following radiation Exposure: estimates for the UK population*. Oxfordshire: Health Protection Agency.

Heddson, B., Ronnow, K., Olsson, M., & Miller, D. (2007). Digital versus screen-film mammography: a retrospective comparison in a population-based screening program. *European Journal of Radiology, 64*(3), 419-425. doi: 10.1016/j.ejrad.2007.02.030.

Helvie, M. A., Chan, H.-P., Adler, D. D., & Boyd, P. G. (1994). Breast Thickness in Routine Mammograms: Effect on Image Quality and Radiation Dose. *American Journal of Roentgenology, 163*(1), 1371-1374.

Helvie, M., & Rosen, E. (2011). Mammographic Breast Density and Ultrasound Breast Screening. In Society of Breast Imaging (SBI)(Ed.), *SBI Summer Newsletter*.

Hendee, W. R., & Ritenour, E. R. (2002). *Medical imaging physics* (4th ed.). New York: Wiley-Liss.

Hendrick, R. E. (2010). Radiation doses and cancer risks from breast imaging studies. *Radiology, 257*(1), 246-253.

Hendrick, R. E., Pisano, E. D., Averbukh, A., Moran, C., Berns, E. A., Yaffe, M. J., . . . Gatsonis, C. (2010). Comparison of acquisition parameters and breast dose in digital mammography and screen-film mammography in the American College of Radiology Imaging Network digital mammographic imaging screening trial. *American Journal of Roentgenology, 194*(2), 362-369. doi: 10.2214/AJR.08.2114.

Hobbie, R. K., & Roth, B. J. (2007). *Intermediate Physics for Medicine and Biology* (4th Ed.). New York: Springer Science & Business Media.

Hogg, P., Szczepura, K., Darlington, A., & Maxwell, A. (2013). A method to measure paddle and detector pressures and footprints in mammography. *Medical Physics, 40*(4), 041907. doi: 10.1118/1.4792720.

Hourdakis, C. J., Boziari, A., & Koumbouli, E. (2009). The effect of a compression paddle on energy response, calibration and measurement with mammographic dosimeters using ionization chambers and solid-state detectors. *Physics in Medicine and Biology, 54*(4), 1047-1059. doi: 10.1088/0031-9155/54/4/015.

Huang , B., Li, J., Law, M. W., Zhang, J., Shen, Y., & Khong, P. L. (2010). Radiation dose and cancer risk in retrospectively and prospectively ECG-gated coronary angiography using 64-slice multidetector CT. *British Journal of Radiology, 83*(986), 152-158. doi: 10.1259/bjr/29879495.

Huang, B., Law, M. W.-M., & Khong, P.-L. (2009). Whole-Body PET/CT Scanning: Estimation of Radiation Dose and Cancer Risk. *Radiology, 251*(1), 166-174. doi: doi:10.1148/radiol.2511081300.

Hubbell, J. H., & Seltzer, S. M. (1996). Tables of X-Ray Mass Attenuation Coefficients and Mass Energy-Absorption Coefficients from 1 keV to 20 MeV for Elements Z = 1 to 92 and 48 Additional Substances of Dosimetric Interest. (NISTIR 5632 NIST). Retrieved 28-07-2016. from: http://www.nist.gov/pml/data/xraycoef/index.cfm.

Huda, W., Nickoloff, E. L., & Boone, J. M. (2008). Overview of patient dosimetry in diagnostic radiology in the USA for the past 50 years. *Medical Physics, 35*(12), 5713. doi: 10.1118/1.3013604.

International Atomic Energy Agency (IAEA). (2005). Optimization of the radiological protection of patients: Image quality and dose in mammography (coordinated research in Europe). Austria.

Internation Atomic Energy Agency (IAEA). (2011). Quality Assurance Programme for Digital Mammography. In IAEA (Ed.), *IAEA Human Health Series* (pp. 140). Austria: IAEA in Austria.

International Agency for Research on Cancer (IARC). (2015). *IARC Handbooks of Cancer Prevention: Benefits of mammography screening outweigh adverse effects for women aged 50–69 years* IARC (Ed.) Retrieved from: http://www.iarc.fr/en/media-centre/pr/2015/pdfs/pr234_E.pdf

Iball, G. R., & Brettle, D. S. (2011). Organ and effective dose reduction in adult chest CT using abdominal lead shielding. *British Journal of Radiology, 84*(1007), 1020-1026. doi: doi:10.1259/bjr/53865832.

International Commission on Radiological Protection (ICRP). (1995). Basic anatomical and physiological data: The skeleton (publication 70). *Annals of the ICRP, 25*(2), 1-80.

International Commission on Radiological Protection (ICRP). (2007). The 2007 Recommendations of the International Commission on Radiological Protection. ICRP publication 103. *Annals of the ICRP, 37*(2-4), 1-332. doi: 10.1016/j.icrp.2007.10.003.

International Cancer Screening Network (ICSN). (2015). Breast Cancer Screening Programs in 26 ICSN Countries, 2012: Organization, Policies, and Program Reach. 2015, from: http://healthcaredelivery.cancer.gov/icsn/breast/screening.html.

Independent UK Panel on Breast Cancer Screening. (2013). The benefits and harms of breast cancer screening – Authors' reply. *The Lancet, 381*(9869), 803-804. doi: 10.1016/s0140-6736(13)60628-5.

Ingleby , H., & Gershon-Cohen , J. (1960). *Comparative anatomy, pathology, and roentgenology of the breast*. Philadelphia: University of Pennsylvania Press.

Institute of Physics and Engineering in medicine (IPEM). (2005). *The commissioning and routine testing of mammographic X-ray systems*. (report 89). York: IPEM.

Izewska, J., & Rajan, G. (2005). Radiation dosimeters. In E. B. Podgorsak (Ed.), *Radiation oncology physics: A handbook for teachers and students*. Vienna: IAEA.

Jacobson, D. (2001). *Rad Tech's Guide to Mammography: Physics, Instrumentation, and Quality Control*. Malden Blackwell Science.

Jakubiak, R. R., Gamba, H. R., Neves, E. B., & Peixoto, J. E. (2013). Image quality, threshold contrast and mean glandular dose in CR mammography. *Physics in Medicine and Biology, 58*(18), 6565-6583. doi: 10.1088/0031-9155/58/18/6565.

James, J. J. (2004). The current status of digital mammography. *Clinical Radiology, 59*(1), 1-10. doi: 10.1016/j.crad.2003.08.011.

Jan, M., Mattoo, J. A., Salroo, N. A., & Ahangar, S. (2010). Triple assessment in the diagnosis of breast cancer in Kashmir. *Indian Journal of Surgery, 72*(2), 97-103. doi: 10.1007/s12262-010-0030-7.

Jansen, J. T., & Zoetelief, J. (1995). MBS: a model for risk benefit analysis of breast cancer screening. *British Journal of Radiology, 68*(806), 141-149. doi: 10.1259/0007-1285-68-813-h141.

Jansen, J. T., & Zoetelief, J. (1997a). Assessment of lifetime gained as a result of mammographic breast cancer screening using a computer model. *British Journal of Radiology, 70*(834), 619-628. doi: 10.1259/bjr.70.834.9227256.

Jansen, J. T., & Zoetelief, J. (1997b). Optimisation of mammographic breast cancer screening using a computer simulation model. *European Journal of Radiology, 24*(2), 137-144.

Jansen-van der Weide, M. C., Greuter, M. J., Jansen, L., Oosterwijk, J. C., Pijnappel, R. M., & de Bock, G. H. (2010). Exposure to low-dose radiation and the risk of breast cancer among women with a familial or genetic predisposition: a meta-analysis. *European Radiology, 20*(11), 2547-2556. doi: 10.1007/s00330-010-1839-y.

Jin, J. (2014). Breast Cancer Screening: Benefits and Harms. *Journal of the American Medical Association, 312*(23), 2585.

Johnson, J. N., Hornik, C. P., Li, J. S., Benjamin, D. K., Jr., Yoshizumi, T. T., Reiman, R. E., . . . Hill, K. D. (2014). Cumulative radiation exposure and cancer risk estimation in children with heart disease. *Circulation, 130*(2), 161-167. doi: 10.1161/CIRCULATIONAHA.113.005425.

Kalager, M., Zelen, M., Langmark, F., & Adami, H. O. (2010). Effect of screening mammography on breast-cancer mortality in Norway. The *New England Journal of Medicine, 363*(13), 1203-1210. doi: 10.1056/NEJMoa1000727.

Karlsson, M., Nygren, K., Wickman, G., & Hettinger, G. (1976). Absorbed dose in mammary radiography. *Acta Radiologica: Therapy, Physics, Biology, 15*(3), 252-258.

Kelly, J. (2015). Supplementary mammographic projections. In P. Hogg, J. Kelly & C. Mercer (Eds.), *Digital mammography: A holistic approach*. Cham: Springer.

KIRAN. (2010). Lead equivalence test procedure. Retrieved 28-07-2016, from: http://www.kiranxray.com/lead-equivalence.asp

Kita, Y., Highnam, R., & Brady, M. (1998). *Correspondence between different view breast X-rays using a simulation of breast deformation*. Paper presented at the IEEE Conference on Computer Vision and Pattern Recognition.

Kitis, G., Furetta, C., Prokic, M., & Prokic, V. (2000). Kinetic parameters of some tissue equivalent thermoluminescence materials. *Journal of Physics D: Applied Physics, 33*(11), 1252.

Kleinerman, R. A. (2006). Cancer risks following diagnostic and therapeutic radiation exposure in children. *Pediatric Radiology, 36 Suppl 2*, 121-125. doi: 10.1007/s00247-006-0191-5.

Kontos, D., Ikejimba, L. C., Bakic, P. R., Troxel, A. B., Conant, E. F., & Maidment, A. D. (2011). Analysis of parenchymal texture with digital breast tomosynthesis: comparison with digital mammography and implications for cancer risk assessment. *Radiology, 261*(1), 80-91. doi: 10.1148/radiol.11100966.

Kopans , D. B. (2007). *Breast imaging* (3rd ed.). Philadelphia: Lippincott Williams & Wilkin.

Kopans, D., Gavenonis, S., Halpern, E., & Moore, R. (2011). Calcifications in the breast and digital breast tomosynthesis. *Breast Journal, 17*(6), 638-644. doi: 10.1111/j.1524-4741.2011.01152.x.

Kortov, V. (2007). Materials for thermoluminescent dosimetry: Current status and future trends. Radiation Measurements, 42(4-5), 576-581. doi: 10.1016/j.radmeas.2007.02.067

Kotre, C. J., & Reis, C. S. d. (2015). Mammography Equipment. In P. Hogg, J. Kelly & C. Mercer (Eds.), *Digital Mammography: A holistic approach*. Cham: Springer.

Koukou, V., Martini, N., Velissarakos, K., Gkremos, D., Fountzoula, C., Bakas, A., . . . Fountos, G. (2015). PVAL breast phantom for dual energy calcification detection. *Journal of Physics: Conference Series, 637*, 012013. doi: 10.1088/1742-6596/637/1/012013.

Kramer, R., Khoury, H. J., Vieira, J. W., Loureiro, E. C. M., Lima, V. J. M., Lima, F. R. A., & Hoff, G. (2004). All about FAX: a Female Adult voXel phantom for Monte Carlo calculation in radiation protection dosimetry. *Physics in Medicine and Biology, 49*(23), 5203.

Kunosic, S. (2012). An Analysis of Application of Mean Glandular Dose and Factors on Which It Depends to Patients of Various Age Groups. In N. Uchiyama (Ed.), *Mammography - Recent Advances*: InTech. Retrieved from: http://www.intechopen.com/books/mammography-recentadvances/an-analysis-of-application-of-mean-glandular-dose-and-factors-on-which-it-depends-to-patients-ofvar.

Lança, L., & Silva, A. (2009a). Digital radiography detectors – A technical overview: Part 1. *Radiography, 15*(1), 58-62. doi: 10.1016/j.radi.2008.02.004.

Lança, L., & Silva, A. (2009b). Digital radiography detectors – A technical overview: Part 2. *Radiography, 15*(2), 134-138. doi: 10.1016/j.radi.2008.02.005.

Lane, D. L., Stafford, R. J., & Whitman, G. J. (2013). Breast MRI. In M. K. Markey (Ed.), *Physics of mammographic imaging*. Boca Raton: Taylor & Francis Group.

Lang, K., Andersson, I., Rosso, A., Tingberg, A., Timberg, P., & Zackrisson, S. (2016). Performance of one-view breast tomosynthesis as a stand-alone breast cancer screening modality: results from the Malmo Breast Tomosynthesis Screening Trial, a population-based study. *European Radiology, 26*(1), 184-190. doi: 10.1007/s00330-015-3803-3.

Law, J. (2006). The development of mammography. *Physics in Medicine and Biology, 51*(13), R155-167. doi: 10.1088/0031-9155/51/13/R10.

Law, M., Ma, W. K., Lau, D., Chan, E., Yip, L., & Lam, W. (2016). Cumulative radiation exposure and associated cancer risk estimates for scoliosis patients: Impact of repetitive full spine radiography. *European Journal of Radiology, 85*(3), 625-628. doi: 10.1016/j.ejrad.2015.12.032.

Leborgne, R. (1951). Diagnosis of tumour of the breast by simple roentgenography. *American Journal of Roentgenology, 65*(1), 1-11.

Lee, L., Stickland, V., Wilson, A. R. M., & Evans, A. (2003). *Fundamentals of mammography* (2nd ed.). London: Churchill Livingstone.

Leidens, M., Goes, E., & Nicolluci, P. (2013). Use of Monte Carlo method to determine radiation dose to organs and tissues from mammography. *Medical Physics, 40*(6), 139.

Lewin, J. M., D'Orsi, C. J., Hendrick, R. E., Moss, L. J., Isaacs, P. K., Karellas, A., & Cutter, G. R. (2002). Clinical comparison of full-field digital mammography and screen-film mammography for detection of breast cancer. *American Journal of Roentgenology, 179*(3), 671-677. doi: 10.2214/ajr.179.3.1790671.

Li, X., Samei, E., Segars, W. P., Sturgeon, G. M., Colsher, J. G., & Frush, D. P. (2011). Patient-specific Radiation Dose and Cancer Risk for Pediatric Chest CT. *Radiology, 259*(3), 862-874. doi: doi:10.1148/radiol.11101900.

Lim, Y. Y., & Maxwell, A. J. (2015). Digital breast tomosynthesis. In P. Hogg, J. Kelly & C. Mercer (Eds.), *Digital mammography: A holistic approach*. Cham: Springer.

Lin , E. C. (2010). Radiation risk from medical imaging. *Mayo Clinic Proceedings, 85*(12), 1142-1146; quiz 1146. doi: 10.4065/mcp.2010.0260.

Lin, M. T., Tung, C. J., & Tsai, H. Y. (2011). Scatter and energy dependence of thermoluminescent dosimeter to determine half-value layer in digital mammography: Monte Carlo results. *Radiation Measurements, 46*(12), 2090-2093. doi: 10.1016/j.radmeas.2011.08.010.

Lind, H., Svane, G., Kemetli, L., & Tornberg, S. (2010). Breast Cancer Screening Program in Stockholm County, Sweden - Aspects of Organization and Quality Assurance. *Breast Care (Basel), 5*(5), 353-357. doi: 10.1159/000321255.

Linet, M. S., Kim, K. P., & Rajaraman, P. (2009). Children's exposure to diagnostic medical radiation and cancer risk: epidemiologic and dosimetric considerations. *Pediatric Radiology, 39 Suppl 1*, S4-26. doi: 10.1007/s00247-008-1026-3.

Linet, M. S., Slovis, T. L., Miller, D. L., Kleinerman, R., Lee, C., Rajaraman, P., & Berrington de Gonzalez, A. (2012). Cancer risks associated with external radiation from diagnostic imaging procedures. *CA: A Cancer Journal for Clinicians, 62*(2), 75-100. doi: 10.3322/caac.21132.

Lisa, D., Claire, H., Helen, W.-F., Mamoon, H., & Tomas, K. (2004). Variations in dose response with x-ray energy of LiF:Mg,Cu,P thermoluminescence dosimeters: implications for clinical dosimetry. *Physics in Medicine and Biology, 49*(17), 3831.

Little, M. P., Wakeford, R., Tawn, E. J., Bouffler, S. D., & Gonzalez, A. B. d. (2009). Risks Associated with Low Doses and Low Dose Rates of Ionizing Radiation: Why Linearity May Be (Almost) the Best We Can Do. *Radiology, 251*(1), 6-12. doi: doi:10.1148/radiol.2511081686.

Lundgren, B. (1977). The oblique view at mammography. *British Journal of Radiology, 50*(597), 626-628. doi: doi:10.1259/0007-1285-50-597-626.

Luo, L. Z. (2008). Extensive fade study of Harshaw LiF TLD materials. Radiation Measurements, 43(2-6), 365-370. doi: 10.1016/j.radmeas.2007.11.069

M. Ali, R., England, A., & Hogg, P. (2015). *Lifetime risk of radiation-induced cancer from screening mammography*. Paper presented at the United Kingdom Radiology Congress, Liverpool.

M. Ali, R., England, A., McEntee, M. F., & Hogg, P. (2015). A method for calculating effective lifetime risk of radiation-induced cancer from screening mammography. *Radiography, 21*(4), 298-303. doi: 10.1016/j.radi.2015.07.008.

Ma, A. K. W., & Alghamdi, A. A. (2011). Development of a Realistic Computational Breast Phantom for Dosimetric Simulations. *Progress in Nuclear Science and Technology, 2*(1), 147-152. doi: 10.15669/pnst.2.147.

Ma, C. M., Coffey, C. W., DeWerd, L. A., Liu, C., Nath, R., Seltzer, S. M., & Seuntjens, J. P. (2001). AAPM protocol for 40–300 kV x-ray beam dosimetry in radiotherapy and radiobiology. *Medical Physics, 28*(6), 868. doi: 10.1118/1.1374247.

Magnus, A. L. (1995). *Three dimensional localization of lesions from digitized mammograms (Unpublished Master Thesis)*. (Master), Air University.

Malmgren, J. A., Parikh, J., Atwood, M. K., & Kaplan, H. G. (2014). Improved Prognosis of Women Aged 75 and Older with Mammography-detected Breast Cancer. *Radiology, 273*(3), 686-694. doi: doi:10.1148/radiol.14140209.

Marmot , M. G., Altman, D. G., Cameron, D. A., Dewar, J. A., Thompson, S. G., & Wilcox, M. (2012). The benefits and harms of breast cancer screening: an independent review. *The Lancet, 380*(9855), 1778-1786. doi: 10.1016/s0140-6736(12)61611-0.

Marmot, M. G., Altman, D. G., Cameron, D. A., Dewar, J. A., Thompson, S. G., & Wilcox, M. (2013). The benefits and harms of breast cancer screening: an independent review: A report jointly commissioned by Cancer Research UK and the Department of Health (England) October 2012. *British Journal of Cancer, 108*(11), 2205-2240. doi: 10.1038/bjc.2013.177.

Mathews, J. D., Forsythe, A. V., Brady, Z., Butler, M. W., Goergen, S. K., Byrnes, G. B., . . . Darby, S. C. (2013). Cancer risk in 680,000 people exposed to computed tomography scans in childhood or adolescence: data linkage study of 11 million Australians. *BMJ, 346*, f2360. doi: 10.1136/bmj.f2360.

McCullagh, J. B., Baldelli, P., & Phelan, N. (2011). Clinical dose performance of full field digital mammography in a breast screening programme. *British Journal of Radiology, 84*(1007), 1027-1033. doi: 10.1259/bjr/83821596.

Meghzifene, A., Dance, D. R., McLean, D., & Kramer, H. M. (2010). Dosimetry in diagnostic radiology. *European Journal of Radiology, 76*(1), 11-14. doi: 10.1016/j.ejrad.2010.06.032.

Mekasut, N. (2011). Mammography : from past to present. *The Bangkok Medical Journal, 1*(1), 71-84.

Mercer , C. E., Hill, C. A., Kelly, A., & Smith, H. L. (2015). Practical mammography. In P. Hogg, J. Kelly & C. Mercer (Eds.), *Digital Mammography: A holistic approach*. Cham: Springer.

Mercer, C. E., Hogg, P., Cassidy, S., & Denton, E. R. E. (2013). Does an increase in compression force really improve visual image quality in mammography? – An initial investigation. *Radiography, 19*(4), 363-365. doi: 10.1016/j.radi.2013.07.002.

Mercer, C. E., Hogg, P., Lawson, R., Diffey, J., & Denton, E. R. (2013). Practitioner compression force variability in mammography: a preliminary study. *British Journal of Radiology, 86*(1022), 20110596. doi: 10.1259/bjr.20110596.

Mercer, C. E., Hogg, P., Szczepura, K., & Denton, E. R. E. (2013). Practitioner compression force variation in mammography: A 6-year study. *Radiography, 19*(3), 200-206. doi: 10.1016/j.radi.2013.06.001.

Mercer, C. E., Szczepura, K., Kelly, J., Millington, S. R., Denton, E. R. E., Borgen, R., . . . Hogg, P. (2015). A 6-year study of mammographic compression force: Practitioner variability within and between screening sites. *Radiography, 21*(1), 68-73. doi: 10.1016/j.radi.2014.07.004.

Mertelmeier, T., Speitel, J., & Frumento, C. (2012). 3D breast tomosynthesis – intelligent technology for clear clinical benefits white paper. Muenchen: Siemens Healthcare.

Michell, M. J., Iqbal, A., Wasan, R. K., Evans, D. R., Peacock, C., Lawinski, C. P., . . . Whelehan, P. (2012). A comparison of the accuracy of film-screen mammography, full-field digital mammography, and digital breast tomosynthesis. *Clinical Radiology, 67*(10), 976-981. doi: 10.1016/j.crad.2012.03.009.

Miller, A. B., Wall, C., Baines, C. J., Sun, P., To, T., & Narod, S. A. (2014). Twenty five year follow-up for breast cancer incidence and mortality of the Canadian National Breast Screening Study: randomised screening trial. *BMJ, 348*, g366. doi: 10.1136/bmj.g366.

Montesdeoca, O. D. ı. (2013). *Scattered radiation in projection X-ray mammography and digital breast tomosynthesis.* (Ph.D.), University of Surry, Surry.

Mori, H., Koshida, K., Ishigamori, O., & Matsubara, K. (2014). Evaluation of the effectiveness of X-ray protective aprons in experimental and practical fields. *Radiological Physics and Technology, 7*(1), 158-166. doi: 10.1007/s12194-013-0246-x.

Moscovitch, M., & Horowitz, Y. S. (2007). Thermoluminescent materials for medical applications: LiF:Mg,Ti and LiF:Mg,Cu,P. Radiation Measurements, 41, S71-S77. doi: 10.1016/j.radmeas.2007.01.008

Moss, S. M., Wale, C., Smith, R., Evans, A., Cuckle, H., & Duffy, S. W. (2015). Effect of mammographic screening from age 40 years on breast cancer mortality in the UK Age trial at 17 years' follow-up: a randomised controlled trial. *The Lancet Oncology, 16*(9), 1123-1132. doi: 10.1016/s1470-2045(15)00128-x.

Mothiram, U., Brennan, P. C., Lewis, S. J., Moran, B., & Robinson, J. (2014). Digital radiography exposure indices: A review. *Journal of Medical Radiation Sciences, 61*(2), 112-118. doi: 10.1002/jmrs.49.

Mun, H. S., Kim, H. H., Shin, H. J., Cha, J. H., Ruppel, P. L., Oh, H. Y., & Chae, E. Y. (2013). Assessment of extent of breast cancer: comparison between digital breast tomosynthesis and full-field digital mammography. *Clinical Radiology, 68*(12), 1254-1259. doi: 10.1016/j.crad.2013.07.006.

Myronakis, M. E., Zvelebil, M., & Darambara, D. G. (2013). Normalized mean glandular dose computation from mammography using GATE: a validation study. *Physics in Medicine and Biology, 58*(7), 2247-2265. doi: 10.1088/0031-9155/58/7/2247.

National Academy of Sciences (NAS). (2006). *Health Risks from Exposure to Low Levels of Ionizing Radiation: BEIR VII – Phase 2*. Washington: National Academies Press.

Nass, S. J., Henderson, I. C., & Lashof, J. C. (2001). *Mammography and beyond: Developing technologies for the early detection of breast cancer*. Washington: Nationa academy press.

Nelson, H. D., Cantor, A., Humphrey, L., Fu, R., Pappas, M., Daeges, M., & Griffin, J. (2016). Screening for Breast Cancer: A Systematic Review to Update the 2009 U.S. Preventive Services Task Force Recommendation. *Evidence Synthesis No. 124*. Rockville: Agency for Healthcare Research and Quality.

Nelson, H. D., Tyne, K., Naik, A., Bougatsos, C., Chan, B., Nygren, P., & Humphrey, L. (2009). Screening for breast cancer: systematic evidence review update for the U.S. Preventive Services Task Force. *Evidence review update No. 74*. Rockville: Agency for Healthcare Research and Quality (US).

Nelson, V. K., & Hill, R. F. (2011). Backscatter factor measurements for kilovoltage X-ray beams using thermoluminescent dosimeters (TLDs). *Radiation Measurements, 46*(12), 2097-2099. doi: 10.1016/j.radmeas.2011.08.019.

National Health Services Breast Screening Programme (NHSBSP). (2013a). *NHS breast screening helping you decide*. London: King's Health Partners Retrieved from: http://www.cancerscreening.nhs.uk/breastscreen/publications/nhsbsp.pdf.

National Health Services Breast Screening Programme (NHSBSP). (2003). Review of radiation risk in breast screening. NHSBSP publication No. 54. Sheffield.

National Health Services Breast Screening Programme (NHSBSP). (2006). *Screening for breast cancer in England: past and future*. (61). Sheffield: NHS Cancer Screening Programmes.

National Health Services Breast Screening Programme (NHSBSP). (2009). *Commissioning and routine testing of full field digital mammography systems. NHSBSP Equipment report 0604. Version* 3. Sheffield: NHS Cancer Screening Programmes.

National Health Services Breast Screening Programme (NHSBSP). (2013b). *Protocols for the surveillance of women at higher risk of developing breast cancer Version 4*. (74). Kiera Chapman (ed.).

National Health Services Breast Screening Programme (NHSBSP). (2014). NHS breast screening programme extending the screening age range. Retrieved 03-09-2014, from: http://www.cancerscreening.nhs.uk/breastscreen/rollout-age-extension-leaflet.pdf.

Niklason, L. T., Christian, B. T., Niklason, L. E., Kopans, D. B., Castleberry, D. E., Opsahl-Ong, B. H., . . . Wirth, R. F. (1997). Digital tomosynthesis in breast imaging. *Radiology, 205*(2), 399-406. doi: doi:10.1148/radiology.205.2.9356620.

Noroozian, M., Hadjiiski, L., Rahnama-Moghadam, S., Klein, K. A., Jeffries, D. O., Pinsky, R. W., . . . Roubidoux, M. A. (2012). Digital breast tomosynthesis is comparable to

mammographic spot views for mass characterization. *Radiology, 262*(1), 61-68. doi: 10.1148/radiol.11101763.

Nsiah-Akoto, I., Andam, A. B., Adisson, E. K., & Forson, A. J. (2011). Preliminary studies into the determination of mean glandular dose during diagnostic mammography procedure in Ghana. *Research Journal of Applied Sciences, Engineering and Technology, 3*(8), 720-724.

Nuclear Energy Agency (NEA). (2011). Evolution of ICRP Recommendations 1977, 1990 and 2007. Retrieved on 15-10-2014, from: http://www.oecd-nea.org/rp/reports/2011/nea6920-ICRP-recommendations.pdf.

Obenauer, S., Hermann, K. P., & Grabbe, E. (2003). Dose reduction in full-field digital mammography: an anthropomorphic breast phantom study. *British Journal of Radiology, 76*(907), 478-482. doi: 10.1259/bjr/67597156.

Odle, T. G. (2004). Radiation dose in mammography. *Radiologic Technology, 75*(4), 297M-313M.

Olarinoye, I. O., & Sharifat, I. (2010). A protocol for setting dose reference level for medical radiography in Nigeria: a review. *Bayero Journal of Pure and Applied Sciences, 3*(1), 138-141.

Olgar, T., Bor, D., Berkmen, G., & Yazar, T. (2009). Patient and staff doses for some complex x-ray examinations. *Journal of Radiological Protection, 29*(3), 393.

Oliveira , M. A., Dantas, M. V. A., Santana, P. C., Squair, P. L., Gomes, D. S., & Nogueira, M. S. (2011). Assessment of glandular dose and image quality in mammography using computerised radiography employing a polymethylmethacrylate breast simulator. *Radiation Measurements, 46*(12), 2081-2085. doi: 10.1016/j.radmeas.2011.06.015.

Oliveira, M., Nogueira, M. S., Guedes, E., Andrade, M. C., Peixoto, J. E., Joana, G. S., & Castro, J. G. (2007). Average glandular dose and phantom image quality in mammography. *Nuclear Instruments and Methods in Physics Research Section A: Accelerators, Spectrometers, Detectors and Associated Equipment, 580*(1), 574-577. doi: 10.1016/j.nima.2007.05.228.

Olko, P. (2010). Advantages and disadvantages of luminescence dosimetry. Radiation Measurements, 45(3-6), 506-511. doi: 10.1016/j.radmeas.2010.01.016

Olsson, S., Andersson, I., Karlberg, I., Bjurstam, N., Frodis, E., & Hakansson, S. (2000). Implementation of service screening with mammography in Sweden: from pilot study to nationwide programme. *Journal of Medical Screening, 7*(1), 14-18.

Ongeval, C. V. (2007). Digital mammography for screening and diagnosis of breast cancer : An overview. *Journal of the Belgian Society of Radiology (JBR–BTR), 90*(3), 163-166.

Office for National Statistics (ONS). (2012). *Breast cancer: incidence, mortality and survival, 2010.* Retrieved from: www.ons.gov.uk.

Ossati, M. S. (2015). *Design, development and use of a deformable breast phantom to assess the relationship between thickness and lesion visibility in full field digital mammography.* (Ph.D.), University of Salford, Salford.

Oyar, O., & Kislalioglu, A. (2012). How protective are the lead aprons we use against ionizing radiation? *Diagnostic and Interventional Radiology, 18*(2), 147-152. doi: 10.4261/1305-3825.DIR.4526-11.1.

Ozasa, K., Shimizu, Y., Suyama, A., Kasagi, F., Soda, M., Grant, E. J., . . . Kodama, K. (2012). Studies of the mortality of atomic bomb survivors, Report 14, 1950-2003: an overview of cancer and noncancer diseases. *Radiation Research, 177*(3), 229-243.

Pagliari, C. M., Hoang, T., Reddy, M., Wilkinson, L. S., Poloniecki, J. D., & Given-Wilson, R. M. (2012). Diagnostic quality of 50 and 100 mum computed radiography compared with screen-film mammography in operative breast specimens. *British Journal of Radiology, 85*(1015), 910-916. doi: 10.1259/bjr/74825285.

Palazuelos, G., Trujillo, S., & Romero, J. (2014). Breast tomosynthesis : the new age of mammography. *Revista Colombiana de Radiologia, 25*(2), 3926-3933.

Pandya, S., & Moore, R. G. (2011). Breast Development and Anatomy. *Clinical Obstetrics and Gynecology, 54*(1), 91-95.

Park, H.-S., Kim, H.-J., Choi, Y.-N., Oh, Y., & Kim, S. T. (2011). Optimization of the Imaging Parameters in Clinical Digital Mammography. *Journal of the Korean Physical Society, 59*(1), 176. doi: 10.3938/jkps.59.176.

Parker, M. S., Kelleher, N. M., Hoots, J. A., Chung, J. K., Fatouros, P. P., & Benedict, S. H. (2008). Absorbed radiation dose of the female breast during diagnostic multidetector chest CT and dose reduction with a tungsten-antimony composite breast shield: preliminary results. *Clinical Radiology, 63*(3), 278-288. doi: 10.1016/j.crad.2007.07.029.

Pearce, M. S., Salotti, J. A., Little, M. P., McHugh, K., Lee, C., Kim, K. P., . . . Berrington de González, A. (2012). Radiation exposure from CT scans in childhood and subsequent risk of leukaemia and brain tumours: a retrospective cohort study. *The Lancet, 380*(9840), 499-505. doi: 10.1016/s0140-6736(12)60815-0.

Peart, O. (2005). *Mammography and breast imaging : just the facts*. New York: McGraw-Hill Medical.

Perisinakis, K., Damilakis, J., Theocharopoulos, N., Manios, E., Vardas, P., & Gourtsoyiannis, N. (2001). Accurate Assessment of Patient Effective Radiation Dose and Associated Detriment Risk From Radiofrequency Catheter Ablation Procedures. *Circulation, 104*(1), 58-62. doi: 10.1161/hc2601.091710.

Pisano , E. D., Gatsonis, C., Hendrick, E., Yaffe, M., Baum, J. K., Acharyya, S., . . . Rebner, M. (2005). Diagnostic performance of digital versus film mammography for breast-cancer screening. The *New England Journal of Medicine, 353*(17), 1773-1783. doi: 10.1056/NEJMoa052911.

Pisano, E. D., & Yaffe, M. J. (2005). Digital Mammography. *Radiology, 234*(2), 353-362.

Poletti, M. E., Goncalves, O. D., & Mazzaro, I. (2002). X-ray scattering from human breast tissues and breast-equivalent materials. *Physics in Medicine and Biology, 47*(1), 47-63.

Pozuelo, F., Gallardo, S., Querol, A., Verdu, G., & Rodenas, J. (2012). *X-ray simulation with the Monte Carlo code PENELOPE. Application to Quality Control.* Paper presented at the 34th Annual International Conference of the IEEE Engineering in Medicine and Biology Society, San Diego, California USA.

Prasad, K. N., Cole, W. C., & Hasse, G. M. (2004). Health risks of low dose ionizing radiation in humans: a review. *Experimental Biology and Medicine, 229*(5), 378-382.

Price, B. D., Gibson, A. P., Tan, L. T., & Royle, G. J. (2010). An elastically compressible phantom material with mechanical and x-ray attenuation properties equivalent to breast tissue. *Physics in Medicine and Biology, 55*(4), 1177-1188. doi: 10.1088/0031-9155/55/4/018.

Qian, X. (2013). Fundamentals of digital mammography. In M. K. Markey (Ed.), Physics of mammographic imaging. Boca Raton: Taylor & Francis Group.

Rafferty, E. A., Park, J. M., Philpotts, L. E., Poplack, S. P., Sumkin, J. H., Halpern, E. F., & Niklason, L. T. (2013). Assessing radiologist performance using combined digital mammography and breast tomosynthesis compared with digital mammography alone: results of a multicenter, multireader trial. *Radiology, 266*(1), 104-113. doi: 10.1148/radiol.12120674.

Rezaei, F. S., Feghhi, S. A. H., Aghamiri, S. M. R., Rezaei, A. S., & Ebrahimi, A. (2011). *Using Monte Carlo Method for Evaluation of kVp & mAs variation effect on Absorbed Dose in Mammography*. Paper presented at the European Congress of Radiology (ECR), Vienna. http://dx.doi.org/10.1594/ecr2011/C-2078.

Rivera, T. (2012). Thermoluminescence in medical dosimetry. *Applied Radiation and Isotopes, 71 Suppl*, 30-34. doi: 10.1016/j.apradiso.2012.04.018.

Romano, S., & McFetridge, E. (1938). The limitations and dangers of mammography by contrast mediums. *Journal of the American Medical Association, 110*(23), 1905-1910. doi: 10.1001/jama.1938.02790230021009.

Rose, S. L., Tidwell, A. L., Bujnoch, L. J., Kushwaha, A. C., Nordmann, A. S., & Sexton, R., Jr. (2013). Implementation of breast tomosynthesis in a routine screening practice: an observational study. *American Journal of Roentgenology, 200*(6), 1401-1408. doi: 10.2214/AJR.12.9672.

Russo, P., Coppola, T., Mettivier, G., Montesi, M. C., & Lauria, A. (2009, Oct. 24 2009-Nov. 1 2009). *Distribution of absorbed dose in cone-beam breast computed tomography: A phantom study with radiochromic films.* Paper presented at the 2009 IEEE Nuclear Science Symposium Conference Record (NSS/MIC).

Säbel, M., & Aichinger, H. (1996). Recent development in breast imaging. *Physics in Medicine and Biology, 41*(3), 315–368.

Saito, M. (2007). Dual-energy approach to contrast-enhanced mammography using the balanced filter method: Spectral optimization and preliminary phantom measurement. *Medical Physics, 34*(11), 4236-4246. doi: doi:http://dx.doi.org/10.1118/1.2790841.

Salehi, Z., Ya Ali, N. K., & Yusoff, A. L. (2012). X-ray spectra and quality parameters from Monte Carlo simulation and analytical filters. *Applied Radiation and Isotopes, 70*(11), 2586-2589. doi: 10.1016/j.apradiso.2011.12.007.

Salvat, F., & Fernández-Varea, J. M. (2009). Overview of physical interaction models for photon and electron transport used in Monte Carlo codes. *Metrologia, 46*(2), S112-S138. doi: 10.1088/0026-1394/46/2/s08.

Salvat, F., Fernández-Varea, J. M., & Sempau, J. (2011). *PENELOPE-2011: A code system for Monte Carlo simulation of electron and photon transport.* Paper presented at the Workshop Proceedings.

Salvatore, M., Margolies, L., Kale, M., Wisnivesky, J., Kotkin, S., Henschke, C. I., & Yankelevitz, D. F. (2014). Breast Density: Comparison of Chest CT with Mammography. *Radiology, 270*(1), 67-73. doi: doi:10.1148/radiol.13130733.

Samei, E., Saunders, R. S., Jr., Baker, J. A., & Delong, D. M. (2007). Digital mammography: effects of reduced radiation dose on diagnostic performance. *Radiology, 243*(2), 396-404. doi: 10.1148/radiol.2432061065.

Saslow, D., Boetes, C., Burke, W., Harms, S., Leach, M. O., Lehman, C. D., . . . Russell, C. A. (2007). American Cancer Society guidelines for breast screening with MRI as an adjunct to mammography. *CA: A Cancer Journal for Clinicians, 57*(2), 75-89.

Saunders, R. S., Samei, E., Lo, J. Y., & Baker, J. A. (2009). Can Compression Be Reduced for Breast Tomosynthesis? Monte Carlo Study on Mass and Microcalcification Conspicuity in Tomosynthesis. *Radiology, 251*(3), 673-682. doi: doi:10.1148/radiol.2521081278.

Savva, A. (2010). *Personnel TLD monitors, their calibration and response.* (M.Sc.), University of Surrey, Surry.

Schmitzberger, F. F., Fallenberg, E. M., Lawaczeck, R., Hemmendorff, M., Moa, E., Danielsson, M., . . . Diekmann, F. (2011). Development of low-dose photon-counting contrast-enhanced tomosynthesis with spectral imaging. *Radiology, 259*(2), 558-564. doi: 10.1148/radiol.11101682.

Schueller, G., Riedl, C. C., Mallek, R., Eibenberger, K., Langenberger, H., Kaindl, E., . . . Helbich, T. H. (2008). Image quality, lesion detection, and diagnostic efficacy in digital mammography: full-field digital mammography versus computed radiography-based mammography using digital storage phosphor plates. *European Journal of Radiology, 67*(3), 487-496. doi: 10.1016/j.ejrad.2007.08.016.

Schulz-Wendtland, R., Fuchsjager, M., Wacker, T., & Hermann, K. P. (2009). Digital mammography: an update. *European Journal of Radiology, 72*(2), 258-265. doi: 10.1016/j.ejrad.2009.05.052.

Seabold, P. S. (1931). Roentgenographic diagnosis of diseases of the breast. *Surgery, gynecology and obstetrics, 53*, 461-468.

Sechopoulos , I., Suryanarayanan , S., Vedantham , S., D'Orsi, C. J., & Karellas, A. (2008). Radiation dose to organs and tissues from mammography: Monte Carlo and phantom study. *Radiology, 246*(2), 434-443.

Sechopoulos, I. (2013a). A review of breast tomosynthesis. Part I. The image acquisition process. *Medical Physics, 40*(1), 014301. doi: 10.1118/1.4770279.

Sechopoulos, I. (2013b). A review of breast tomosynthesis. Part II. Image reconstruction, processing and analysis, and advanced applications. *Medical Physics, 40*(1), 014302. doi: 10.1118/1.4770281.

Sechopoulos, I., & Hendrick, R. E. (2012). Mammography and the risk of thyroid cancer. *American Journal of Roentgenology, 198*(3), 705-707. doi: 10.2214/AJR.11.7225.

Sechopoulos, I., Bliznakova, K., Qin, X., Fei, B., & Feng, S. S. (2012). Characterization of the homogeneous tissue mixture approximation in breast imaging dosimetry. *Medical Physics, 39*(8), 5050-5059. doi: 10.1118/1.4737025.

Sechopoulos, I., Vedantham, S., Suryanarayanan, S., D'Orsi, C. J., & Karellas, A. (2008). Monte Carlo and phantom study of the radiation dose to the body from dedicated CT of the breast. *Radiology, 247*(1), 98-105. doi: 10.1148/radiol.2471071080.

Seo, D., Han, S., Kim, K. H., Kim, J., Park, K., Lim, H., & Kim, J. (2015). Evaluation based on Monte Carlo simulation of lifetime attributable risk of cancer after neck X-ray radiography. *La Radiologia Medica (Radiol Med), 120*(11), 1043-1049. doi: 10.1007/s11547-015-0543-z.

Servomaa, A., & Tapiovaara, M. (1998). Organ Dose Calculation in Medical X-Ray Examinations by the Program PCXMC. *Radiation Protection Dosimetry, 80*(1-3), 213-219.

Shapiro, S. (1997). Periodic screening for breast cancer: the HIP Randomized Controlled Trial. Health Insurance Plan. *Journal of the National Cancer Institute Monogr*(22), 27-30.

Shaw, C. C., & Whitman, G. J. (2013). Breast CT. In M. K. Markey (Ed.), *Physics of mammographic imaging*. Boca Raton: Taylor & Francis Group.

Shen, S.-W., Wang, Y.-F., Shu, H., Tang, X., Wei, C.-F., Song, Y.-S., . . . Wei, L. (2014). Experimental measurement of radiation dose in a dedicated breast CT system. *Chinese Physics C, 38*(3), 038201.

Shepherd, J. A., Kerlikowske, K., Ma, L., Duewer, F., Fan, B., Wang, J., . . . Cummings, S. R. (2011). Volume of mammographic density and risk of breast cancer. *Cancer Epidemiology, Biomarkers and Prevention, 20*(7), 1473-1482. doi: 10.1158/1055-9965.epi-10-1150.

Shirazi, A., Mahdavi, S. R., Khodadadee, A., Ghaffory, M., & Mesbahi, A. (2008). Monte Carlo simulation of TLD response function: Scattered radiation field application. *Reports of Practical Oncology & Radiotherapy, 13*(1), 23-28.

Silverstein, M. J., Recht, A., Lagios, M. D., Bleiweiss, I. J., Blumencranz, P. W., Gizienski, T., . . . Willey, S. C. (2009). Special report: Consensus conference III. Image-detected breast cancer: state-of-the-art diagnosis and treatment. *Journal of the American College of Surgeons, 209*(4), 504-520. doi: 10.1016/j.jamcollsurg.2009.07.006.

Skaane , P., & Skjennald, A. (2004). Screen-film mammography versus full-field digital mammography with soft-copy reading: randomized trial in a population-based screening program--the Oslo II Study. *Radiology, 232*(1), 197-204. doi: 10.1148/radiol.2321031624.

Skaane , P., Bandos, A. I., Gullien, R., Eben, E. B., Ekseth, U., Haakenaasen, U., . . . Gur, D. (2013). Comparison of digital mammography alone and digital mammography plus tomosynthesis in a population-based screening program. *Radiology, 267*(1), 47-56. doi: 10.1148/radiol.12121373.

Skaane , P., Hofvind, S., & Skjennald, A. (2007). Randomized trial of screen-film versus full-field digital mammography with soft-copy reading in population-based screening program: follow-up and final results of Oslo II study. *Radiology, 244*(3), 708-717. doi: 10.1148/radiol.2443061478.

Skaane, P. (2012). Tomosynthesis in X-ray: proven additional value? *European Journal of Radiology, 81*, S156-S157. doi: 10.1016/s0720-048x(12)70065-7.

Skaane, P., Young, K., & Skjennald, A. (2003). Population-based Mammography Screening: Comparison of Screen-Film and Full-Field Digital Mammography with Soft-Copy Reading—Oslo I Study. *Radiology, 229*(3), 877-884. doi: doi:10.1148/radiol.2293021171.

Smith , N. B., & Webb, A. (2011). *Introduction to medical imaging : physics, engineering and clinical applications*. New York: Cambridge University Press.

Smith , R. A., Saslow, D., Sawyer, K. A., Burke, W., Costanza, M. E., Evans, W. P., . . . Sener, S. (2003). American Cancer Society guidelines for breast cancer screening: update 2003. *CA: A Cancer Journal for Clinicians, 53*(3), 141-169.

Smith, H., Szczepura, K., Mercer, C., Maxwell, A., & Hogg, P. (2015). Does elevating image receptor increase breast receptor footprint and improve pressure balance? *Radiography, 21*(4), 359-363. doi: http://dx.doi.org/10.1016/j.radi.2015.02.001.

Smith, A. (2005). Fundamentals of digital mammography : physics, technology and practical considerations. From: https://www.mmhospital.org/upload/docs/pdf/Fundamentals%20of%20DM.pdf.

Smith, A. (2012). Breast tomosynthesis considerations for routine clinical use. Hologic white paper. From: http://www.wishmd.com/wp-content/uploads/2016/04/tomo-white-paper.pdf.

Sobotka, P. K., Chelminski, K., Bulski, W., Kacperski, K., Dziukowa, J., Wesolowska, E., . . . Domanski, A. W. (2012). Breast phantom for comparison X-ray and polarimetric optical tomography imaging. *Photonics Letters of Poland, 4*(1). doi: 10.4302/plp.2012.1.14.

Sookpeng, S., & Ketted, P. (2006). Mean glandular dose from routine mammography. *Naresuan University Journal, 14*(3), 19-26.

Spuur, K., Poulos, A., Currie, G., & Rickard, M. (2010). Mammography: Correlation of pectoral muscle width and the length in the mediolateral oblique view of the breast. *Radiography, 16*(4), 286-291. doi: 10.1016/j.radi.2010.05.008.

Standring, S., & Gray, H. (2008). *Gray's anatomy : The anatomical basis of clinical practice* (40th, anniversary ed.). Edinburgh: Churchill Livingstone/Elsevier.

Statkiewicz-Sherer, M. A., Visconti, P. J., & Ritenour, E. R. (2010). *Radiation protection in medical radiography* (6th ed.). London: Mosby.

Steen, A. V., & Tiggelen, R. V. (2007). Short history of mammography : a Belgian perspective. *Journal of the Belgian Society of Radiology (JBR–BTR), 90*(3), 151-153.

Stone, J., Ding, J., Warren, R. M., Duffy, S. W., & Hopper, J. L. (2010). Using mammographic density to predict breast cancer risk: dense area or percentage dense area. *Breast Cancer Research, 12*(6), R97. doi: 10.1186/bcr2778.

Strudley, C. J., Looney, P., & Young, K. C. (2014). *Technical evaluation of Hologic Selenia Dimensions digital breast tomosynthesis system. NHSBSP Equipment Report 1307. Version 2*. NHSBSP.

Suad, K., Suada, K., Samek, D., Amila, H., & Samir, K. (2013). Analysis of application of mean glandular dose and factors on which it depends to patients aged 65 to 80. *Journal of Physical Science and Application, 3*(6), 387-391.

Suhaimi, S. A. A., Mohamed, A., & Ahmad, M. (2015). Effects of reduced compression in digital breast tomosynthesis on pain, anxiety, and image quality. *Malaysian Journal of Medical Sciences, 22*(6).

Sulieman, A., Theodorou, K., Vlychou, M., Topaltzikis, T., Kanavou, D., Fezoulidis, I., & Kappas, C. (2007). Radiation dose measurement and risk estimation for paediatric patients undergoing micturating cystourethrography. *British Journal of Radiology, 80*(957), 731-737. doi: 10.1259/bjr/16010686.

Suzuki, K., & Yamashita, S. (2012). Low-dose radiation exposure and carcinogenesis. *Japanese Journal of Clinical Oncology, 42*(7), 563-568. doi: 10.1093/jjco/hys078.

Svahn, T. M., Chakraborty, D. P., Ikeda, D., Zackrisson, S., Do, Y., Mattsson, S., & Andersson, I. (2012). Breast tomosynthesis and digital mammography: a comparison of diagnostic accuracy. *British Journal of Radiology, 85*(1019), e1074-1082. doi: 10.1259/bjr/53282892.

Tabár, L., Vitak, B., Chen, T. H.-H., Yen, A. M.-F., Cohen, A., Tot, T., . . . Duffy, S. W. (2011). Swedish two-county trial: impact of mammographic screening on breast cancer mortality during 3 decades. *Radiology, 260*(3), 658-663.

Tagliafico, A., Tagliafico, G., & Houssami, N. (2013). Differences in breast density assessment using mammography, tomosynthesis and MRI and their implications for practice. *British Journal of Radiology, 86*(1032), 20130528. doi: 10.1259/bjr.20130528.

Tagliafico, A., Tagliafico, G., Astengo, D., Airaldi, S., Calabrese, M., & Houssami, N. (2013). Comparative estimation of percentage breast tissue density for digital mammography, digital breast tomosynthesis, and magnetic resonance imaging. *Breast Cancer Research and Treatment, 138*(1), 311-317. doi: 10.1007/s10549-013-2419-z.

Taleei, R., & Shahriari, M. (2009). Monte Carlo simulation of X-ray spectra and evaluation of filter effect using MCNP4C and FLUKA code. *Applied Radiation and Isotopes, 67*(2), 266-271. doi: 10.1016/j.apradiso.2008.10.007.

Testagrossa, B., Acri, G., Causa, F., Novario, R., Giulia, M., & Vermiglio, G. (2012). Unified Procedures for Quality Controls in Analogue and Digital Mammography. In D. I. Akyar (Ed.), Latest Research into Quality Control. Rijeka: InTech. Retrieved from http://www.intechopen.com/books/latest-research-into-quality-control/unified-procedures-for-quality-controls-in-analogue-and-digital-mammography. doi: 10.5772/51349.

Thermo Scientific. (2015). High Sensitivity LIF: Mg, Cu, P Thermoluminescent Dosimetry Materials, Chips. Retrieved 07-28, 2016, from: https://www.thermofisher.com/order/catalog/product/SCP18815#%2Flegacy=thermoscientific.com.

Thierens, H., Bosmans, H., Buls, N., De Hauwere, A., Bacher, K., Jacobs, J., & Clerinx, P. (2009). Typetesting of physical characteristics of digital mammography systems for screening within the Flemish breast cancer screening programme. *European Journal of Radiology, 70*(3), 539-548. doi: 10.1016/j.ejrad.2008.01.046.

Thomassin-Naggara, I., Perrot, N., Dechoux, S., Ribeiro, C., Chopier, J., & de Bazelaire, C. (2015). Added value of one-view breast tomosynthesis combined with digital mammography according to reader experience. *European Journal of Radiology, 84*(2), 235-241. doi: 10.1016/j.ejrad.2014.10.022.

Tirona, M. T. (2013). Breast cancer screening update. *American family physician, 87*(4), 274-278.

Tootell, A. K., Szczepura, K. R., & Hogg, P. (2013). Optimising the number of thermoluminescent dosimeters required for the measurement of effective dose for computed tomography attenuation correction data in SPECT/CT myocardial perfusion imaging. *Radiography, 19*(1), 42-47. doi: 10.1016/j.radi.2012.11.001.

Tootell, A., Szczepura, K., & Hogg, P. (2014). An overview of measuring and modelling dose and risk from ionising radiation for medical exposures. *Radiography, 20*(4), 323-332. doi: http://dx.doi.org/10.1016/j.radi.2014.05.002.

Toward Optimized Practice (TOP) Working Group forBreast Cancer Screening. (2013). *Breast cancer screening: clinical practice guideline*. Edmonton: AB: Toward Optimized Practice Retrieved 28-04-2016 from http://www.topalbertadoctors.org.

Tria Tirona, M. (2013). Breast cancer screening update. *American Family Physician, 87*(4), 274-278.

Triolo, A., Brai, M., Bartolotta, A., & Marrale, M. (2006). Glow curve analysis of TLD-100H irradiated with radiation of different LET: Comparison between two theoretical method. *Nuclear Instruments and Methods in Physics Research Section A: Accelerators, Spectrometers, Detectors and Associated Equipment, 560*(2), 413-417. doi: 10.1016/j.nima.2006.01.030.

Tsai, H. Y., Chong, N. S., Ho, Y. J., & Tyan, Y. S. (2010). Evaluation of depth dose and glandular dose for digital mammography. *Radiation Measurements, 45*(3-6), 726-728. doi: 10.1016/j.radmeas.2010.02.005.

Tubiana, M., Feinendegen, L. E., Yang, C., & Kaminski, J. M. (2009). The Linear No-Threshold Relationship Is Inconsistent with Radiation Biologic and Experimental Data. *Radiology, 251*(1), 13-22. doi: doi:10.1148/radiol.2511080671.

Tung, C. J., Lin, M. T., Hsu, F. Y., Lee, J. H., Chu, C. H., & Tsai, H. Y. (2010). Half-value layer determination using thermoluminescent dosimeters for digital mammography. *Radiation Measurements, 45*(3-6), 729-732. doi: 10.1016/j.radmeas.2010.02.015.

Tyler, N. J., Strudley, C., Hollaway, P., & Peet, D. J. (2009). *Patient dose measurements in full field digital mammography and comparison with dose to the standard breast. Paper presented at the World Congress on Medical Physics and Biomedical Engineering, Munich.*

Uffmann, M., & Schaefer-Prokop, C. (2009). Digital radiography: the balance between image quality and required radiation dose. *European Journal of Radiology, 72*(2), 202-208. doi: 10.1016/j.ejrad.2009.05.060.

United Nations Scientific Committee on the Effect of Atomic Energy (UNSCEAR). (2008). *UNSCEAR 2006 report vol. I . Annex A: Epidemiological studies of radiation and cancer*. Retrieved from: http://www.unscear.org/docs/reports/2006/07-82087_Report_Annex_A_2006_Web_corr.pdf.

Vachon, C. M., van Gils, C. H., Sellers, T. A., Ghosh, K., Pruthi, S., Brandt, K. R., & Pankratz, V. S. (2007). Mammographic density, breast cancer risk and risk prediction. *Breast Cancer Research, 9*(6), 217. doi: 10.1186/bcr1829.

Vaiserman, A. M. (2010). Radiation hormesis: historical perspective and implications for low-dose cancer risk assessment. *Dose-Response, 8*(2), 172-191. doi: 10.2203/dose-response.09-037.Vaiserman.

Veitch, D., Burford, K., Dench, P., Dean, N., & Griffin, P. (2012). Measurement of breast volume using body scan technology(computer-aided anthropometry). *Work, 41 Suppl 1*, 4038-4045. doi: 10.3233/WOR-2012-0068-4038.

Venables, K., Miles, E. A., Aird, E. G., Hoskin, P. J., & Group, S. T. M. (2004). The use of in vivo thermoluminescent dosimeters in the quality assurance programme for the START breast fractionation trial. Radiother Oncol, 71(3), 303-310. doi: 10.1016/j.radonc.2004.02.008

Vetto, J. T., Luoh, S. W., & Naik, A. (2009). Breast cancer in premenopausal women. *Current Problems in Surgery, 46*(12), 944-1004. doi: 10.1067/j.cpsurg.2009.07.002.

Vigeland, E., Klaasen, H., Klingen, T. A., Hofvind, S., & Skaane, P. (2008). Full-field digital mammography compared to screen film mammography in the prevalent round of a population-based screening programme: the Vestfold County Study. *European Radiology, 18*(1), 183-191. doi: 10.1007/s00330-007-0730-y.

Vyborny, C. J., & Schmidt, R. A. (1989). Mammography as a radiographic examination: An overview. *RadioGraphics, 9*(4), 723-764.

Wall, B. F., Kendall, G. M., Edwards, A. A., Bouffler, S., Muirhead, C. R., & Meara, J. R. (2006). What are the risks from medical X-rays and other low dose radiation? *British Journal of Radiology, 79*(940), 285-294. doi: 10.1259/bjr/55733882.

Wang, F.-L., Chen, F., Yin, H., Xu, N., Wu, X.-X., Ma, J.-J., . . . Lu, C. (2013). Effects of Age, Breast Density and Volume on Breast Cancer Diagnosis: A Retrospective Comparison of Sensitivity of Mammography and Ultrasonography in China's Rural Areas. *Asian Pacific Journal of Cancer Prevention, 14*(4), 2277-2282. doi: 10.7314/apjcp.2013.14.4.2277.

Wang, J., & Geiser, W. R. (2013). Image display and visualization in digital mammography. In G. J. Whitman & T. M. Haygood (Eds.), Digital mammography: a practical approach. New York: Cambridge University Press.

Warren, L. M., Dance, D. R., & Young, K. C. (2016). Radiation risk of breast screening in England with digital mammography. *British Journal of Radiology*, 20150897. doi: 10.1259/bjr.20150897.

Warren, S. L. (1930). A roentgenologic study of the breast. *American Journal of Roentgenology, 24*(2), 113-124.

Wentz, G., & Parsons, W. C. (1997). *Mammography for radiologic technologists* (n. ed. Ed.). New York: The McGraw-Hill Companies.

Whelan, C., McLean, D., & Poulos, A. (1999). Investigation of thyroid dose due to mammography. *Australasian Radiology, 43*(3), 307-310.

Whitman, G. J., Khisty, R., & Stafford, R. J. (2013). Breast ultrasound. In M. K. Markey (Ed.), *Physics of mammographic imaging*. Boca Raton: Taylor & Francis Group.

Williams, M. B., Judy, P. G., Gunn, S., & Majewski, S. (2010). Dual-modality breast tomosynthesis. *Radiology, 255*(1), 191-198. doi: 10.1148/radiol.09091160.

Winslow, J. F., Hyer, D. E., Fisher, R. F., Tien, C. J., & Hintenlang, D. E. (2009). Construction of anthropomorphic phantoms for use in dosimetry studies. *Journal of Applied Clinical Medical Physics, 10*(3).

Wu, X., Gingold, E. L., Barnes, G. T., & Tucker, D. M. (1994). Normalized average glandular dose in molybdenum target-rhodium filter and rhodium target-rhodium filter mammography. *Radiology, 193*(1), 83-89.

Yaffe , M. J. (2010). Basic physics of digital mammography. In U. Bick & F. Diekmann (Eds.), *Digital mammography*. Berlin: Springer Science & Business Media.

Yaffe , M. J., Boone, J. M., Packard, N., Alonzo-Proulx, O., Huang, S. Y., Peressotti, C. L., . . . Brock, K. (2009). The myth of the 50-50 breast. *Medical Physics, 36*(12), 5437. doi: 10.1118/1.3250863.

Yaffe , M. J., Byng, J. W., Caldwell, C. B., & Bennett, N. R. (1993). Anthropomorphic radiological phantoms for mammography. *Medical Progress through Technology, 19*(1), 23-30.

Yaffe, M. J., & Maidment, A. D. A. (2014). Mammography. In D. R. Dance, S. Christofides, A. D. A. Maidment, I. D. McLean & K. H. Ng (Eds.), Diagnostic radiology physics : A handbook for teachers and students. Vienna: International Atomic Energy Agency.

Yaffe, M. J., & Mainprize, J. G. (2011). Risk of radiation-induced breast cancer from mammographic screening. *Radiology, 258*(1), 98-105. doi: 10.1148/radiol.10100655/-/DC1.

Yankaskas, B. C., & Gill, K. S. (2005). Diagnostic mammography performance and race: outcomes in Black and White women. *Cancer, 104*(12), 2671-2681. doi: 10.1002/cncr.21550.

Ye, S.-J., Brezovich, I. A., Pareek, P., & Naqvi, S. A. (2004). Benchmark of PENELOPE code for low-energy photon transport: dose comparisons with MCNP4 and EGS4. *Physics in Medicine and Biology, 49*(3), 387-397. doi: 10.1088/0031-9155/49/3/003.

Yoshinaga, S., Mabuchi, K., Sigurdson, A. J., Doody, M. M., & Ron, E. (2004). Cancer Risks among Radiologists and Radiologic Technologists: Review of Epidemiologic Studies. *Radiology, 233*(2), 313-321. doi: doi:10.1148/radiol.2332031119.

Young, K. C. (2006). Recent developments in digital mammography. *Imaging, 18*(2), 68-74. doi: doi:10.1259/imaging/24202756.

Young, K. C., Ramsdale, M. L., & Rust, A. (1996). Dose and image quality in mammography with an automatic beam quality system. *British Journal of Radiology, 69*(822), 555-562. doi: 10.1259/0007-1285-69-822-555.

Young, K. C., Ramsdale, M. L., Rust, A., & Cooke, J. (1997). Effect of automatic kV selection on dose and contrast for a mammographic X-ray system. *British Journal of Radiology, 70*(838), 1036-1042. doi: 10.1259/bjr.70.838.9404208.

Zeidan, M. (2009). *Assessment of Mean Glandular Dose in Mammography.* (Master of Science in Medical Physics), University of Canterbury.

Zenone, F., Aimonetto, S., Catuzzo, P., Peruzzo Cornetto, A., Marchisio, P., Natrella, M., . . . Tofani, S. (2012). Effective dose delivered by conventional radiology to Aosta Valley population between 2002 and 2009. *British Journal of Radiology, 85*(1015), e330-338. doi: 10.1259/bjr/19099861.

Zou, K. H., Tuncali, K., & Silverman, S. G. (2003). Correlation and Simple Linear Regression. Radiology, 227(3), 617-628. doi: doi:10.1148/radiol.2273011499.

Zuley, M. L., Bandos, A. I., Ganott, M. A., Sumkin, J. H., Kelly, A. E., Catullo, V. J., . . . Gur, D. (2013). Digital breast tomosynthesis versus supplemental diagnostic

mammographic views for evaluation of noncalcified breast lesions. *Radiology, 266*(1), 89-95. doi: 10.1148/radiol.12120552.